Investigating the dynamic nature of supramolecular cyclic peptide polymer nanotubes

Julia Yu-jung Rho

A thesis submitted in partial fulfilment of the requirements for the degree of

Doctor of Philosophy in Chemistry

Department of Chemistry

University of Warwick

May 2019

Table of Contents

List of Figures ..... **vi**

List of Tables ..... **xii**

List of Schemes ..... **xiii**

Abbreviations ..... **xv**

Acknowledgements ..... **xviii**

Declaration **xxii**

Chapter 1 Introduction **1**

1.1 Supramolecular polymers 1

1.1.1 Non-covalent interactions in supramolecular polymers 1

1.1.2 Mechanism of growth 2

1.1.3 Living supramolecular polymers 3

1.2 Self-assembling peptide 7

1.2.1 ß-Sheet (hydrogen bond) self-assembly 7

1.3 Self-assembling cyclic peptides 9

1.3.1 History and Design 9

1.3.2 Self-assembling cyclic peptide-polymer conjugates 10

1.3.3 Applications 12

1.4 Characterisation of self-assembled nanostructures 16

1.4.1 Fluorescence probes 16

1.4.2 Light scattering 17

1.5 Scope and motivation of this thesis 19

1.6 References 21

Chapter 2 Design and synthesis of cyclic peptide-polymer-dye conjugates to probe their dynamics. **24**

2.4 Introduction 25

2.5 Results and Discussion 26

2.5.1 Synthesis of asymmetric orthogonal cyclic peptide 26
2.5.2 Synthesis of the cyclic peptide-pyrene/napthalimide conjugates 30
2.5.3 Synthesis of the cyclic peptide-pyrene/napthalimide-polymer conjugates 32
2.5.4 Dynamics of the cyclic peptide-pyrene/napthalimide-polymer conjugates 36
2.5.5 Synthesis of Cyclic Peptide-Cyanine Dye-Polymer Conjugates 38
2.6 Conclusion 44
2.7 Experimental 45
2.7.1 Material 45
2.7.2 Characterisation 45
2.7.3 Peptide Synthesis 47
2.7.4 Cyclisation 49
2.7.5 Deprotection of the cyclic peptide 50
2.7.6 *N*-hydroxysuccinimide (NHS) functionalisation of the napthalimide (NTI) dye 51
2.7.7 Dye conjugation 52
2.7.8 Polymer conjugation 54
2.8 Appendix 61
2.9 References 65
Chapter 3 Investigating the Dynamic Behaviour of Self-Assembling Cyclic Peptide - Polymer Nanotubes in Solution and in Mammalian Cells 66
3.4 Introduction 67
3.5 Results and Discussion 68
3.5.1 Characterisation of the self-assembling cyclic peptide conjugates 68
3.5.2 Spectrochemical properties of dye conjugated cyclic peptides 71
3.5.3 Solvent dependent dynamic unimer exchange of CPNT 72
3.5.4 Concentration dependency of CPNT self-assembly 75

3.5.5 *In vitro* dynamic of cyclic peptide nanotubes 76
3.6 Conclusion 80
3.7 Experimental 81
3.7.1 Materials 81
3.7.2 Characterisation 81
3.8 Appendix 92
3.9 References 97
Chapter 4 Dual self-assembly of cyclic peptide nanotubes to provide stabilisation in water 99
4.1 Introduction 100
4.2 Synthesis and Characterisation. 101
4.2.1 Design and synthesis of CP-diblock polymer conjugates. 101
4.2.2 Characterisation of the diblock and control conjugates 104
4.3 Dynamics of diblock conjugated cyclic peptide nanotubes 105
4.4 Composition of supramolecular diblock conjugates 108
4.5 Conclusion 110
4.6 Experimental 111
4.6.1 Materials 111
4.6.2 Methods 111
4.6.3 Synthesis and Characterisation 113
4.6.4 1,6-diphenylhexatriene (DPH) dye experiment 121
4.6.5 Static Light Scattering (SLS) 122
4.6.6 Single-Angle Neutron Scattering (SANS) 124
4.6.7 Transmission Electron Microscopy (TEM) 127
4.6.8 Toxicity 128
4.6.10 UV-vis spectroscopy 130
4.6.11 Fluorescence emission spectroscopy 130

4.6.12 FRET exchange study 131

4.6.13 Particle tracking and Stochastic Optical Reconstruction Microscopy (STORM) 132

4.6.14 Stochastic Optical Reconstruction Microscopy (STORM) Imaging . 135

4.7 Appendix 137

4.9 References 143

Chapter 5 Conclusion and Outlook 145

List of publications 147

List of Figures

Figure 1.1 Living supramolecular polymerisation of metastable cage-like species. a) General mechanism of step-growth and chain-growth polymerisation. b) Chemical structure of the metastable cage-like monomer, c) Schematic representation of the open 'initiator', caged 'monomer' species and d) growing polymer. Reproduced from Kang *et al.* [12] 5

Figure 1.2 a) Chemical structures of a zinc-porphyrin complex (unimer). Schematic representation of living supramolecular assembly of porphyrin derivatives *via* b) heating (adapted from Ogi *et al*)[13] and c) seeded growth (Reproduced from Jung *et al*)[14].....6

Figure 1.3 a) The chemical structure and b) transmission electron microscopy (TEM) of self-assembling cyclic peptide nanotubes. Reproduced from Ghadiri *et al.*[3] 9

Figure 1.4. RAPTA-C functionalised cyclic peptide polymers. Reproduced from Blunden *et al.* [43] 13

Figure 1.5. a. Structure of cyclic peptides conjugated with poly (N-(2-Hydroxypropyl) methacrylamide (pHPMA) and anti-cancer iridium complex. b. IC50 of the free drug, polymer and conjugate. c. The mass of iridium found in the membrane, cytosol, cytoskeleton and nucleus of the cells. Reproduced from Larnaudie *et al.* [44].....14

Figure 1.6 a) Tubisomes formed via a two-fold self-assembly of amphiphilic cyclic peptide nanotubes using β–sheet hydrogen bonding and hydrophobic interactions. Calcein release study to observe lysosomal escape. b-d) Artistic representation of the dye leaking into the cytosol through the tubisomes. e) Calcein escape from the lysosome in HEK293 cells, f) pre-treated with pBA_{27}-b-$pPEGA_{45}$ (polymer) or g) pBA_{27}-CP-$pPEGA_{45}$ (CP conjugate). Scale bar set to 200µm. Reproduced from Brendel *et al.*[45] 15

Figure 1.7 Illustrating the scattering angle of the detector in relation to the incident beam. 17

Figure 2.1 Chemical structures of asymmetric cyclic peptide for orthogonal conjugation. 26

Figure 2.2 Electron Spray Ionisation – Time of Flight (ESI-ToF) mass spectra of the linear peptide (1), protected cyclic peptide (2) and deprotected cyclic peptide (3). ..29

Figure 2.3 Synthetic route to NHS-functionalised napthalimide (NTI) dye. 30

F**igure 2.4** ESI-ToF Mass spectra of the deprotected cyclic peptide (3), the pyrene conjugated cyclic peptide (4) and the napthalimide conjugated cyclic peptide (5). ..32
Figure 2.5 SEC chromatograph in DMF with 0.1% LiBr comparing the cyclic peptide (CP), polymer (PEG-NH_2 20kDa), cyclic peptide-napthalimide (CP-NTI) conjugate and the reaction mixture of CP-NTI and PEG using the first approach (pre-functionalisation).....34
Figure 2.6 SEC chromatograph comparing the cyclic peptide (CP), polymer (PEG-NH_2 20kDa), cyclic peptide-dye conjugate and the reaction mixture of CP-NTI and PEG using the second approach (post-functionalisation). 35
Figure 2.7 Normalised HPLC of PEG-cyclic peptide-dyes (PEG-CP-NTI). UV detector set to 280nm (tryptophan in the CP) and the fluorescence set to emission of the dyes.....36
Figure 2.8 Normalised absorption and fluorescence spectra of the pyrene and napthalimide conjugate (PEG-CP-PYR, 6 and PEG-CP-NTI, 7). The emission spectra of the donor (PEG-CP-PYR) overlaps with the excitation of the acceptor (PEG-CP-NTI).....37
Figure 2.9 High performance liquid chromatographs (HPLC) of the a) donor conjugates and b) acceptor conjugates. Cyanine 3 and 5 were also measured to compare the polarity of the conjugates to the free dyes.....40
Figure 2.10 Electron spray – Time of Flight (ESI-ToF) mass spectra of the a) asymmetric cyclic peptide, cyclic peptide-Cy3 conjugate (CP-Cy3) and NHS-functionalised cyclic peptide-Cy3 conjugate (NHS-CP-Cy3). b) ESI-ToF spectra of the equivalent Cy5 conjugates. 40
Figure 2.11 Electron spray ionisation – Time of Flight (ESI-ToF) mass spectrometry of the asymmetric cyclic peptide and cyclic peptide with the control alkyl chain without the dye (CP-Alkyl). The NHS-functionalised CP-Alkyl conjugate was not soluble to perform ESI-ToF. 41
Figure 2.12 High performance liquid chromatographs (HPLC) of the asymmetric cyclic peptide, poly (ethylene glycol) (PEG 20kDa) polymer and the control conjugate with the absence of a FRET dye. 43
Figure 2.13 Synthetic route to NHS-functionalised napthalimide (NTI) dye.....51
Figure 2.14 ^{1}H NMR of linear peptide (1). See experimental for assignment.....61
Figure 2.15 ^{1}H NMR of protected cyclic peptide (2). See experimental for assignment. 61

Figure 2.16 ^{1}H NMR of deprotected cyclic peptide (3). See experimental for assignment. 62
Figure 2.17 ^{1}H NMR of NHS-functionalised NTI dye (NTI). See experimental for assignment. 62
Figure 2.18 ^{1}H NMR of cyclic peptide-pyrene (CP-PYR, 4). 63
Figure 2.19 ^{1}H NMR of cyclic peptide-napthalimide (CP-NTI, 5). 63
Figure 2.20 ^{1}H NMR of PEG-cyclic peptide-pyrene (PEG-CP-PYR, 6). Due to the size of the PEG (20kDa) assignment of peak was not possible. 64
Figure 2.21 ^{1}H NMR of PEG-cyclic peptide-napthalimide (PEG-CP-NTI, 7). Due to the size of the PEG (20kDa) assignment of peak was not possible. 64
Figure 3.1 Schematic representation of the cyclic peptide-dye-polymer conjugates. 67
Figure 3.2 a) Reduced SANS scattering data for the PEG-CP-Alkyl (Control) and (Premixed) PEG-CP-Cy3 and PEG-CP-Cy5 system. The lines correspond to a fit to the hairy cylinder model. b) TEM image of cyclic peptide-polymer-dye conjugate (PEG-CP-Cy3) stained with UOAc. Distribution of nanotubular c) lengths and d) diameters extracted from TEM. 69
Figure 3.3 a) Schematic depiction of the FRET occurring in cyclic peptide nanotubes containing donor (Cy3) as well as acceptor (Cy5) dye molecules. b) Fluorescence donor and acceptor emission upon mixing the free dyes (Cy3 and Cy5) and the self-assembling dye conjugates (PEG-CP-Cy3 and PEG-CP-Cy5) in water. 72
Figure 3.4 a) Schematic depiction of the FRET studies. Preassembled individual cyclic peptide-dye-polymer conjugates in water (left) and a 1:1 mixture of both conjugates after the assemblies are left to dynamically exchange (right). b) Fluorescence emission spectra of PEG-CP-Cy3 and PEG-CP-Cy5 upon mixing in water and c) Normalised FRET ratio of the mixed system in DMF, water and toluene. Toluene plateau was reached after 6 days (see Appendix Figure 3.17). 73
Figure 3.5 a) Fluorescence emission concentration dependent study of the mixed nanotubes. The concentration dependence on the cyclic peptide (premixed PEG-CP-Cy3 and PEG-CP-Cy5) stacking measured *via* b) fluorescence emission of the premixed dye conjugates and c) SLS of the control conjugates. 76
Figure 3.6 Confocal microscopy imaging of MDA-231 cells incubated in the presence of either A) PEG-CP-Cy5 alone (4 μM); B) PEG-CP-Cy3 alone (12 μM); C) premixed PEG-CP-Cy5 (4 μM) and PEG-CP-Cy3 (12 μM); D) co-injected PEG-CP-Cy5 (4 μM)

and PEG-CP-Cy3 (12 µM); E) PEG-CP-Cy5 (4 µM) for 30 minutes, washed and PEG-CP-Cy3 (12 µM) for 120 minutes. Unless indicated otherwise, incubation proceeded for 150 min. Nucleus fluorescence was obtained using Hoechst 33342. Excitation/Emission used for measurement are as follow, nucleus channel (405 / 406-459 nm), donor channel (517 / 540-577 nm), acceptor channel (633 / 670-724 nm), FRET (496 / 675-800 nm).....78
Figure 3.7 Average intensity of intracellular fluorescence associated with FRET, as calculated using the mean of fluorescence in each cells for a minimum of 15 cells. 79
Figure 3.8 Reduced scattering data and fit to a hairy cylinder model for the premixed PEG-CP-Cy3 and PEG-CP-Cy5. 84
Figure 3.9 Reduced scattering data and fit to a hairy cylinder model for the control PEG conjugated cyclic peptide (PEG-CP-Alkyl). 85
Figure 3.10 Evolution of KC/R of PEG-CP-Alkyl in water as a function of q^2 obtained by static light scattering. 87
Figure 3.11 Evolution of $1/M_a$ of PEG-CP-Alkyl in water as a function of concentration obtained by static light scattering. 88
Figure 3.12 TEM images of PEG-CP-Cy5 (17). 90
Figure 3.13 TEM of PEG-CP-Alkyl (18). 91
Figure 3.14 Ultraviolet (UV) spectra of PEG-CP-Cy3 and PEG-CP-Cy5 in a) dimethylformamide, b) water and c) toluene at 17.5µM. 92
Figure 3.15 Fluorescence emission spectra of PEG-CP-Cy3 and PEG-CP-Cy5 in a) dimethylformamide, b) water and c) toluene at 17.5µM. 93
Figure 3.16 Fluorescence emission spectra of the FRET mixing study in a) dimethylformamide, b) water and c) toluene. 94
Figure 3.17 The kinetic exchange of PEG-CP-Cy3 and PEG-CP-Cy5 upon mixing in toluene. 95
Figure 3.18 Normalised SEC trace of the initial PEG polymer before conjugation and the fully functionalised PEG-CP-Alkyl control conjugate.....96
Figure 4.1 Self-assembling cyclic peptide-diblock polymer conjugates. In aqueous conditions, the diblock copolymers conjugated onto the cyclic peptide (CP-(pBA-*b*-pDMA)$_2$) self-assembles to form a hydrophobic region around the peptide and a hydrophilic corona. 102
Figure 4.2 SEC traces of the polymers: a) pBA and pBA-block-pDMA in THF and b) pDMA in DMF + 0.1% NH_4BF_4.....102

Figure 4.3 SEC traces of the polymer before conjugation and after conjugation. a) pBA-*b*-pDMA and CP-(pBA-*b*-pDMA)$_2$ and b) pDMA and CP-(pDMA)$_2$ in DMF +0.1% LiBr.....103
Figure 4.4 Characterisation of cyclic peptide-polymer nanotubes. a) TEM image of the diblock conjugates prepared in water. b) SANS profiles of the diblock and control conjugates fitted to a cylindrical micelle model using SASfit software. c) Table of the average length of the nanotubes measured *via* TEM, SANS and SLS respectively. 104
Figure 4.5 Dynamics of cyclic peptide-polymer nanotubes. The calculated length of the nanotubes from SLS over a range of concentrations (0.1 – 3.0 mg mL^{-1}) before and after sonication. 106
Figure 4.6 Kinetics of cyclic peptide-polymer nanotubes. a) The orthogonal functionalization of cyclic peptide (CP) with two polymer arms and a donor or acceptor FRET dye. b) Schematic of stable non-exchanging CP-polymer nanotubes. c) Scheme of dynamically exchanging mixed CP-polymer nanotubes. d) Rate constants for FRET exchange, final and maximum FRET ratio and degree of mixing for the free dye, diblock and control conjugates. Rate constants were determined by fitting to a second order decay function, see experimental section 4.6.11. Final FRET ratio was reached for the diblock and control conjugates after 7 days and 60 minutes respectively e) Graph to show the change in FRET ratio over time measured using fluorescence spectroscopy.....107
Figure 4.7 Composition of cyclic peptide-polymer nanotubes. Schematic and stochastic optical reconstruction microscopy (STORM) of a) co-injected and b) premixed cyclic peptide-polymer-dye conjugates. 110
Figure 4.8 Images of cyclic peptide polymer conjugates with the addition of DPH dye. Upon dye addition, fluorescence was observed in the case of the diblock conjugate solution. No visible fluorescence was observed for the control conjugate, absence of the hydrophobic core.....121
Figure 4.9 Evolution of KC/R of diblock conjugate (CP-(pBA-pDMA)$_2$) in water as a function of q² obtained by static light scattering. a) Before sonication, b) 1 hour after sonication and c) 3 days after sonication. d) Evolution of 1/Ma of diblock conjugate in water as a function of concentration before sonication, 1 hour after and 3 days after sonication obtained by static light scattering. 122

Figure 4.10 Evolution of KC/R of control conjugate (CP-$(pDMA)_2$) in water as a function of q^2 obtained by static light scattering. a) Before sonication, b) 1 hour after sonication and c) 3 days after sonication. d) Evolution of 1/Ma of control conjugate in water as a function of concentration before sonication, 1 hour after and 3 days after sonication obtained by static light scattering. 123
Figure 4.11 TEM images of diblock conjugated cyclic peptides (CP-$(pBA\text{-}pDMA)_2$) prepared in water (1 mg/mL). 127
Figure 4.12 Toxicity profile for diblock (CP-$(pBA\text{-}pDMA)_2$) and control (CP-$(pDMA)_2$) conjugates. 129
Figure 4.13 UV absorption spectra of Cy3-CP-Diblock and Cy5-CP-Diblock conjugates in water at 35 μM. 130
Figure 4.14 Fluorescence emission spectra of Cy3-CP-Diblock and Cy5-CP-Diblock conjugates in water at 35 μM. 130
Figure 4.15 FRET exchange study of cyclic peptide dye conjugates with two polymer arms of a) diblock copolymer pBA_{10}-*b*-$pDMA_{40}$ or b) homopolymer $pDMA_{50}$. 131
Figure 4.16 The MSD as a function of lag time for the experimental data (filled circles) and the fit to each data set (solid line).. 134
Figure 4.17 A STORM image of the premixed sample, the scale bar is 10 μm (left). 135
Figure 4.18 A STORM image of the sample 1 day after co-injection of Cy3 and Cy5 diblock conjugate, the scale bar is 5 μm long.. 136
Figure 4.19 ^{1}H NMR of pBA (19) polymer 137
Figure 4.20 ^{1}H NMR of pBA-pDMA (20) polymer.....137
Figure 4.21 ^{1}H NMR of pDMA (21).....138
Figure 4.22 High Performance Liquid Chromatography (HPLC) spectra of the CP-Cy3-Protected (24) and CP-Cy3-Deprotected (26). Detector set to 280 nm (tryptophan of cyclic peptide) and 563 nm (Cyanine 3 emission).....140
Figure 4.23 High Performance Liquid Chromatography (HPLC) spectra of the Cy5-CP-Boc Protected (25) and CP-Cy5-Boc Deprotected (27). Detector set to 280 nm (tryptophan of cyclic peptide) and 662 nm (Cyanine 5 emission). 141
Figure 4.24 Size exclusion chromatography of the free polymer and the cyclic peptide-polymer dye conjugates in DMF + 0.1% LiBr. a) Cy3-CP-$(pBA\text{-}pDMA)_2$ (28), b) Cy5-CP-$(pBA\text{-}pDMA)_2$ (29), c) Cy3-CP-$(pDMA)_2$ (30) and d) Cy5-CP-$(pDMA)_2$ (31). 142

List of Tables

Table 3.1 Summary on the characterisation of CPNTs using SANS and TEM. TEM values are represented as mean lengths and diameters ± standard deviation of 37 individual nanotubes. 70

Table 3.2 The rate kinetics of the exchanging donor and acceptor conjugated cyclic peptide-polymer nanotubes. The final FRET ratio was the value at which the plateaux was reached. 75

Table 3.3 Parameters and results from fitting the SANS scattering data to a hairy-cylinder model. 83

Table 3.4 HPLC gradient method 86

Table 4.1 Electrospray ionisation (ESI) - Mass spectrometry (MS) characterisation of cyclic peptide and dye conjugates carried out on the Agilent 6130B single Quad. . 120

Table 4.2 Length of the nanotubes calculated from static light scattering over a range of concentrations (0.1 – 3.0 mg mL^{-1}) before and after sonication. 123

Table 4.3 Parameters and results from fitting the SANS scattering data to a hairy-cylinder model 125

Table 4.4 Tabular results of the particle tracking experiments. The fit was performed on the ensemble averaged MSD which was calculated from the average of many MSDs calculated from each individual track and the number in each sample is greater than 1,000 as shown. The power law fit exponent is shown and is close to 1 as expected. A control experiment was also performed using fluorescent beads with a radius of 50 nm. Our results agreed with the manufactures specification of the size. 134

List of Schemes

Scheme 1.1. The self-assembly process in an isodesmic and cooperative mechanism.....3

Scheme 1.2. Simplified route to uniform cylindrical micelles *via* crystallization driven self-assembly. a) block co-polymer unimer with a crystallisable PFS core (orange) and phosphine containing polysiloxane corona (purple). Adapted from Lunn *et al.*[11].....4

Scheme 1.3. Parallel and Anti-parallel β–sheet formation. 7

Scheme 1.4. Examples and general design features of self-assembling a) dipeptides and b) peptide amphiphiles. 8

Scheme 1.5. Cyclic peptides laterally aggregate to form long nanotubular bundles. Upon polymer conjugation the polymer arms help solubilise the CPNT and prevent lateral aggregation. 11

Scheme 1.6. Different modes of action a) intramolecular pore, b) barrel stave and c) carpet-like of self-assembling cyclic peptide nanotubes in lipid bilayer membranes. Reproduced from Fernandez-Lopez *et al.*[32] 12

Scheme 2.1 Simplified scheme to make alternating D- and L- linear octa-peptide using solid phase peptide synthesis (SPPS). 27

Scheme 2.2 Cyclisation of linear octa-peptide (1) to form protected cyclic peptide (2). Boc deprotection of the cyclic peptide using TFA, TIPS and H_2O to give the asymmetric azide amine cyclic peptide (3). 28

Scheme 2.3 Schematic representation of the synthetic route to the cyclic peptide-dyes. 31

Scheme 2.4 a) Pre-functionalisation and b) Post-functionalisation methods to attaching the polymer to the CP-dye conjugates. 33

Scheme 2.5 Schematic representation of the synthesis of cyclic peptide-dye-polymer conjugates. 38

Scheme 2.6 Simplified scheme to make alternating D- and L- linear octa-peptide using solid phase peptide synthesis (SPPS). 47

Scheme 2.7 Cyclisation of linear octa-peptide (1) to form protected cyclic peptide (2). 49

Scheme 2.8 Boc deprotection of cyclic peptide. 50

Scheme 2.9 Synthetic route to the cyclic peptide-pyrene conjugate (CP-PYR). 52

Scheme 2.10 Synthetic route to the cyclic peptide-napthalimide conjugate (5). 53

Scheme 2.11 NHS-coupling of the strained alkyne (BCN-NHS) and linear PEG-amine (PEG-NH_2) to form linear PEG with strained alkyne (PEG-BCN). 54
Scheme 2.12 Strained alkyne-azide coupling reaction to form the PEG-CP-PYR via the pre-functionalisation strategy 54
Scheme 2.13 Strained alkyne-azide coupling to form the NHS-functionalised cyclic peptide-pyrene conjugate (NHS-CP-PYR). 55
Scheme 2.14 NHS-amine coupling reaction to form the cyclic peptide-polymer-dye conjugate (PEG-CP-PYR, 6). 56
Scheme 4.1 Preparation of diblock co-polymer of butyl acrylate (BA) and dimethyl acrylamide (DMA). 113
Scheme 4.2 Preparation of homopolymer of dimethylacrylamide (DMA). 114
Scheme 4.3 Preparation of cyclic peptide-diblock conjugates 115
Scheme 4.4 Preparation of cyclic peptide-pDMA conjugates 115
Scheme 4.5. Preparation of Cyannine3 conjugated cyclic peptide-polymer conjugates 116
Scheme 4.6 Deprotection of Boc groups on the cyclic peptide-dye conjugates 117
Scheme 4.7 Preparation of Cy5 conjugated cyclic peptides. 117
Scheme 4.8 Preparation of cyclic peptide-dye-diblock polymer conjugates 118
Scheme 4.9 Preparation of cyclic peptide-dye-homopolymer conjugates 119
Scheme 4.10 Preparation of the linear and cyclic peptide. See literature procedure for details.[21] 138
Scheme 4.11 Preparation of the linear and cyclic peptide with orthogonal amine protection chemistry. See literature procedure for details.[3] 139

Abbreviations

^{1}H	Proton
AFM	Atomic force microscopy
ATR	Attenuated total refection
ATRP	Atom transfer radical polymerization
BA	Butyl acrylate
BCN	Strained alkyne
BCN-NHS	(1R,8S,9s)-Bicyclo[6.1.0]non-4-yn-9-ylmethyl N-succinimidyl carbonate
BTA	Benzene 1,3,5, tricarboxamides
CDSA	Crystallisation-driven self-assembly
CEMA	2-Chloroethyl methacrylate
CP	Cyclic peptide
CPNT	Cyclic peptide nanotubes
Cy	Cyanine
DCM	Dichloromethane
DIPEA	*N*,*N*-Diisopropylethylamine
DMA	Dimethyl acrylamide
DMF	Dimethylformamide
DMSO	Dimethyl sulfoxide
DMTMM·BF4	4-(4,6-dimethoxy-1,3,5-triazin-2-yl)–4–methylmorpholiniumtetra fluoroborate
DOX	Doxorubicin
DP	Degree of polymerisation
DPH	1,6-Diphenylhexatriene
DRI	Differential refractive index
EDC	1-Ethyl-3- (3-dimethylaminopropyl) carbodiimide
ESI-ToF	Electrospray ionisation time-of-flight
FRET	Förster/Fluorescence resonance energy transfer
FTIR	Fourier transform infrared
GPC	Gel permeation chromatography
H_2O	Water

HATU	1- [Bis (dimethyl amino) methylene] -1H -1,2,3 - triazolo [4,5-b] pyridinium 3-oxid hexa fluoro phosphate
H-bond	Hydrogen bonding
HBTU	2-(1H-benzotriazol-1-yl)-1,1,3,3–tetra methyluraniumhexafluorophosphate
HEA	Hydroxyl ethyl acrylate
HFIP	Hexafluoroisopropanol
HPLC	High performance liquid chromatography
k	Rate constant
LiBr	Lithium Bromide
MDA-231	Human breast adenocarcinoma cells
MS	Mass spectrometry
MSD	Mean square displacement
N_{agg}	Number of aggregation
NHS	N-hydroxysuccinimide
NMR	Nuclear magnetic resonance
NTI	Napthalimide
NTI-NHS	2,5-dioxopyrrolidin-1-yl 6-(6-morpholino-1,3-dioxo-1H-benzo[de]isoquinolin-2(3H)-yl)hexanoate
PA	Peptide amphiphiles
pAA	Poly (acrylic acid)
PABTC	(Propanoic acid)yl butyl trithiocarbonate
PBS	Phosphate-buffered saline
PC-3	Epithelial prostate cancer cells
pDMAEMA	Poly (2-dimethylamino) ethyl methacrylate
PEG	Poly (ethylene glycol)
pEtOx	Poly(2-ethyl-2-oxazoline)
PFS	Polyferrocenylsilane
pMMA	Poly (methyl methacrylate)
PMS	N-methyl dibenzopyrazine methyl sulfate
PTFE	Polytetrafluoroethylene
PYR	Pyrene
PYR-NHS	1-Pyrenebutyric acid N-hydroxysuccinimide ester

RAFT	Reversible addition − fragmentation chain-transfer polymerization
SANS	Small angle neutron scattering
SEC	Size exclusion chromatography
SLD	Scattering length density
SLS	Static Light Scattering
SPPS	Solid phase peptide synthesis
STORM	Stochastic optical reconstruction microscopy
TEM	Transmission electron microscopy
TFA	Trifluoroacetic acid
THF	Tetrahydrofuran
TIPS	Triisopropylsilane
UPy	Ureido-pyrimidinone
UV	Ultraviolet
XTT	2,3-Bis-(2-methoxy-4-nitro-5-sulfophenyl)-2H-tetrazolium-5-carboxanilide

Acknowledgements

I have so many people to thank, I will try not to forget anyone.

First, I would like to thank my PhD supervisor, *Prof. Sebastien Perrier*, for allowing me to work in this amazing group and institution. Thank you for all the times you asked me if I need a meeting - the stress on my face probably said it all. Your advice always helped me to put things into perceptive; it is normal to be nervous before your first ACS talk and we can't do everything in one PhD.

I will like to thank *Prof. Rachel O'Reilly* for allowing me to join her group for the summer for my first exposure to research and polymer chemistry. My first lab supervisor, *Dr. Helen Willcock* who had the patience to teach a 2nd year undergraduate how to work in a real research lab for the first time. After my time here, with the help of Warwick Chemistry and *Rachel*, the international placement coordinator at the time, I had my chance to escape the world of polymers to work on organic optoelectronics in Singapore. Coming back, I asked my wonderfully supportive personal tutor *Prof. Giovanni Costantini* what I should do for my Masters year if I wanted to re-join polymer chemistry. To which he replied, there is a new polymer chemist called Seb and I think he would be a good choice. The rest is history.

To my postdoc and mentors. Thank you *Ming* for teaching me how to make a cyclic peptide by hand, an experience I will never forget. I still degas my cyclisations as an omen. To my first mentor, *Johannes*, I don't think it would be fair to write all the ways you have helped me be a better chemist and researcher. I have learnt towards the end of my PhD just how much you have taught me and that the best way to thank you is by teaching others who have come after me. To *Matthias*, thank you for teaching me in the most German way, to just get on with it. Thank you for the sea of red corrections every time I send you something to read. To *Kristian*, for being an awesome therapist to a nervous 1st year, a job you so rightly said comes with being a post-doc. To *Sylvain*, for being an inspiration to us all, work hard nap harder. Thank you for teaching me how to hike and I apologies, your nickname from the beam time has stuck - most of the group think you are Sylvia. To *Raoul*, I will remember you always for your insane peptide wisdom and our hilarious conversations about many things - including yoga pants.

Sophie, the first of her name, thank you all your amazing baking, motherly guidance and advice. I will never forget your expression when you saw my lab bench clean for the first time. *Tammie*, my first Aussie friend, we have discussed in length so much; skincare, bullet journals and on a rare occasion some science. You have taught me so much, I think back to my first PowerPoint slides. *Liam* 'LiLi', my first northern friend, your humour is much missed in the lab since you left. *Ximo*, I have never known someone so happy, enthusiastic and it is always a joy to be around. I am sorry I never made it to Melbourne but I know I will come a visit you some day. *Ed*, thank you for talking to me before Seb forced us to be friends, apparently our friendship had to be. *Carlos*, all I remember of our conversations are good food and coffee, I am hungry just thinking about the Spanish pork and seabass you describe so eloquently. *Qiao and Jie*, it has been lovely to have supramolecular polymer friends – I have learnt so much.

Alex 'Cookie' I feel more prepared to enter the world outside of our group with a small snippet of your academic knowledge sitting the same office, you kept us connected to a world outside of Warwick. Also, your lab singing is sorely missed. *Junliang*, I have learnt to trust nobody with your smile, beware of the delicious plate of dumplings! Thank you *Pratik* for showing us how to be an awesome PhD without working late. I think we could talk for England. I think we literally talked our way over country boarders on the way to Grenoble and Edinburgh. *Joji*, for showing us we don't have to sleep to get work done. *Moriceau*, the most French person I know, hopefully someone will continue our breakdancing/yoga lessons at the Sebinar. *Caro* for being such an amazing conference buddy, nothing could have prepared us for our first ACS. *Robert* for always being there to nerd out about RAFT or plants. *Majda*, for being such as strong example for us all. I still think of you getting mad, when I have a haircut.

To my cohort. *Agnes* I can't believe we are at the end, I really didn't think it would ever come. Thank you for always being there, I have enjoyed all our food evening, will need to make new Raclette friends to get my cheese fix. Thinking of food I need to make some doriyaki asap. *Andy L*, thank you for answering all my random pharmacy/health questions and chairing that second day at the Sebinar on my behalf. *Andy K*, I won't forget the run we did for the last bus, after eating a whole lamb shank and a fair bit of wine. We had no idea what we got ourselves in for – first beam time memories. *Ji* thank you so much for all the lovely conversations and pancakes, I have really enjoyed making a new Korean friend.

To the students who remain. *Sean,* I think have shared a lot of solubility trauma, I am glad you did not leave. All I can say is that your time will come to leave the nest. Your Taylor Swift memes will never be forgotten. *Tom,* aka 'T-money', the group is in good hands. The job of group mum is not a voluntary one, but one of unwilling inheritance use your power wisely. My last year in the group would not have been the same without you to reminisce about the old days – like true Brits. *Satu,* it has been really nice to get to know you this year. Thank you for helping me bring back the coffee group even though most days it's just us. Your sheer drive and enthusiasm for your work is so nice to see. *Maria K* 'Mariah Carey' I will never forget the first time you joined us, you have come so far in your chemistry journey. The next time someone spoils the end to something, I will think of you. *Sophie*, thank you for joining the CP team. I know exactly how you feel as everyone is planning to leave, I just want to say it will be fine in the end. *Ramon,* I hope we can look back at this time and say we all have gym habits for life but I am doubtful. It's been great fun to escape thesis writing to the first office. I will always call it 'rice with things' from now on. *Fannie* for always teaching us we are do it wrong – the French way or the highway, vive la France!

To the incredible students I have had the pleasure to supervise and meet during my time here. *Huda,* the face of innocence, thank you for being such an amazing student, I will remember standing side-by-side in the lab with you trying to make gels and me trying to break them. *Tobi, Tim, Lucas and Sophie* 'The Rock' Laroque for showing us that the German undergraduates seem light years ahead. *Leila V,* I wish you all the best in whatever you do, just know I think you should do a PhD instead, I will miss our Thursday gym sessions. *Ting,* I have never met a Masters student quite like you, I will miss your Tom takedowns. *Vito,* thanks for being great company whilst I write this never ending thesis.

To the newest members of the Perrier group, it has been a pleasure to get to meet you before I leave *Steve and Alexia*. We would all have to stay another 10 years to get all our crazy ideas to work but it has been so much fun coming up with you.

To the corridor family, and extended Warwick polymer community. Thank you, *Prof. David Haddleton (Dave),* it's been so much fun working on this corridor with your lovely group and all the amazing equipment you have amassed. I have thoroughly enjoyed your stories of the people who have passed through these doors, especially

the ones about Seb as a PhD student. The corridor would not have been the same without you all, thank you *Paul, Simula, Chongyu, Rachel, GPC Dan, James, Atty, Mohammed, Chris, Nutt, Lawton, Glen, Patrick, Evelina, Vasiliki, both Georges, Congkai and Spyros*. *Prof. Stefan Bon*, and his awesome group, *Sam, Matt, Andrea, Josh, Brooke, Corina and Ross*. Friends from the other building, *Lewis, Anne, Panos, Chris and Benoit*. Thank you for my much needed supportive chats, *Athina, Richard and Tara.*

To my awesome collaborators. *Liam MacFarlane*, thank you for all your support with both TEM and navigating the Singaporean paper work maze. *Henry and Tom* for the amazing opportunity to image my compounds on their incredible build. *Mitch*, I don't think snapchat will exist in 10 year time but I am thoroughly enjoy yours.

To my time in the States. Thank you *Prof. Brent Sumerlin* for the opportunity to work in Florida with his amazing group. *Becky and Gabe* for feeding my delicious food. *Georg* for teaching me the difference between Austrians and Germans. Thank you to my extended UF family *Emma, Suby, Charlie, John, Sofia, Kabb, Sims, Angie, Jake, Digvi and Dan*.

Lastly, I would like to thank my family and friends.

Friends to escape the chemistry world on occasion, I would not here without your help and motivation. *Dash, Minnie, Fred, Nirupa, Penny, Tahira, Sophie, Gaya, Grace, Haena, Yena and especially Jaeyoung.*

Thank you *Caz, William, Alex and Pam* I will never forget your kind words of support, amazing Christmas dinners and escapes to the Cape.

Thank you *Louis*, without whom these last 8 years would not have meant so much.

Thank you *Mum, Dad and Jeff* for everything.

Declaration

Experimental work contained in this thesis is original research carried out by the author, in the Department of Chemistry at the University of Warwick between October 2015 and May 2019. No material contained here has been submitted for any other degree or at any other institution.

Results from others are referenced throughout the text in the usual manner.

The work presented was carried out by the author with the following exceptions:

Chapter 3: The transmission electron microscopy was performed by Liam MacFarlane (University of Bristol, Department of Chemistry).

Chapter 3: The in vitro dynamic study was performed by Raoul Peltier (University of Warwick, School of Life Sciences)

Chapter 4: The XTT assay was performed by Sean Ellacott (University of Warwick, School of Life Sciences).

Chapter 4: The stochastic optical reconstruction microscopy and particle tracking was performed by Henry Cox (University of Manchester, Department of Physics).

Date: _____ _____

Julia Yu-jung Rho

Chapter 1 Introduction

1.1 Supramolecular polymers

Supramolecular interactions can be found throughout nature and are essential to most biological functions. The fundamental concept of molecules interacting with one another, covalently or non-covalently, is used to explain what is happening on a chemical level. For a long time, the assumption was that the properties of a molecule were governed primarily by the properties of the single molecule. With our growing understanding of chemistry it became harder to ignore the effect environment played on a system; therefore giving rise to the new idea that molecular interactions could not be ignored. Key concepts, such as coordination chemistry, the lock-and-key model and host-guest binding all elude to this notion of molecular interactions. The prefix 'supra' means 'beyond the limits' of or 'outside of' and from this the term 'supramolecular' has been used to denote the interactions outside the limits of the molecule. The distinction between 'intra' and 'inter' molecular is made by differentiating how the atoms are bonded together, either covalently or non-covalently.

Supramolecular polymers consist of molecules that spontaneously self-assemble with one another *via* non-covalent interactions. These structures can form a range of different morphologies on the nanoscale, such as nanofibers,[1] nanoribbons[2] and nanotubes.[3] Examples of these systems can also be found in nature, such as actin and tubulin.[4] Making synthetic supramolecular polymers *via* a 'bottom up' approach is a very appealing proposition for chemists.[5] Using well-established organic chemistry we can manipulate the functionality of these unimers to systemically promote assembly, introduce secondary interactions and provide attachment sites for post-modification. This gives us endless possibility to design and tailor these materials for a wide range of applications.

1.1.1 Non-covalent interactions in supramolecular polymers

In classical polymerisation monomers are covalently linked together to form a long polymer chain; in supramolecular polymerisation a long chain of unimers is linked by non-covalent interactions. The range of non-covalent bonds between molecules include hydrogen bonding, hydrophobic interactions, π-π stacking and van der Waals.

Due to non-covalent bonds being much weaker than covalent bonds they are usually reversible with temperature and concentration.

Importantly, in supramolecular polymers the bonding arrangements are most commonly both, multivalent and directional. Multivalency is crucial for the continued growth of the polymer passed two units. Additionally, the bond strength scales with the number of bonds between two monomers. Due to the directionality of the bond being maintained over a long range, the assembled aggregates typically adopt an elongated morphology such as a nanotube or nanofiber.

1.1.2 Mechanism of growth

Depending on the unimer the self-assembly of the supramolecular polymerisation should proceed *via* one of two prominent mechanisms; isodesmic or cooperative.[6, 7] See Scheme 1.1.

In an isodesmic polymerization the reactivity of the unimer and the growing chain are equal; as a result the polymerisation occurs in a way comparable to step-growth polymerization. This happens when there are no neighbouring group effects. The decrease in free energy with each successive monomer attachment to the growing polymer remains constant throughout the polymerisation. The aggregation number is dependent on temperature and concentration, increasing the temperature or decreasing the concentration will lead to disassembly and *vice versa*. Most notably, there is no critical concentration and temperature.

When proceeding by a cooperative mechanism the polymerisation occurs in a non-linear fashion, in two stages, a nucleation stage followed by an elongation stage. For the formation of a nucleus a critical concentration/temperature must be reached (nucleation stage). After this point, further increases in concentration or decreases in temperature leads to the growth of the polymer chain from the nucleus (elongation stage). Notably, the change in rate of polymerisation between the nucleation and elongation stages can be represented by two different rate constants. In a cooperative mechanism the rate constant for nucleation is smaller than of the elongation. This chain-growth polymerisation, whereby the monomers can only react to the ‘active’ growing chain, makes it possible to control the dispersity of the polymer *via* living polymerisation techniques.

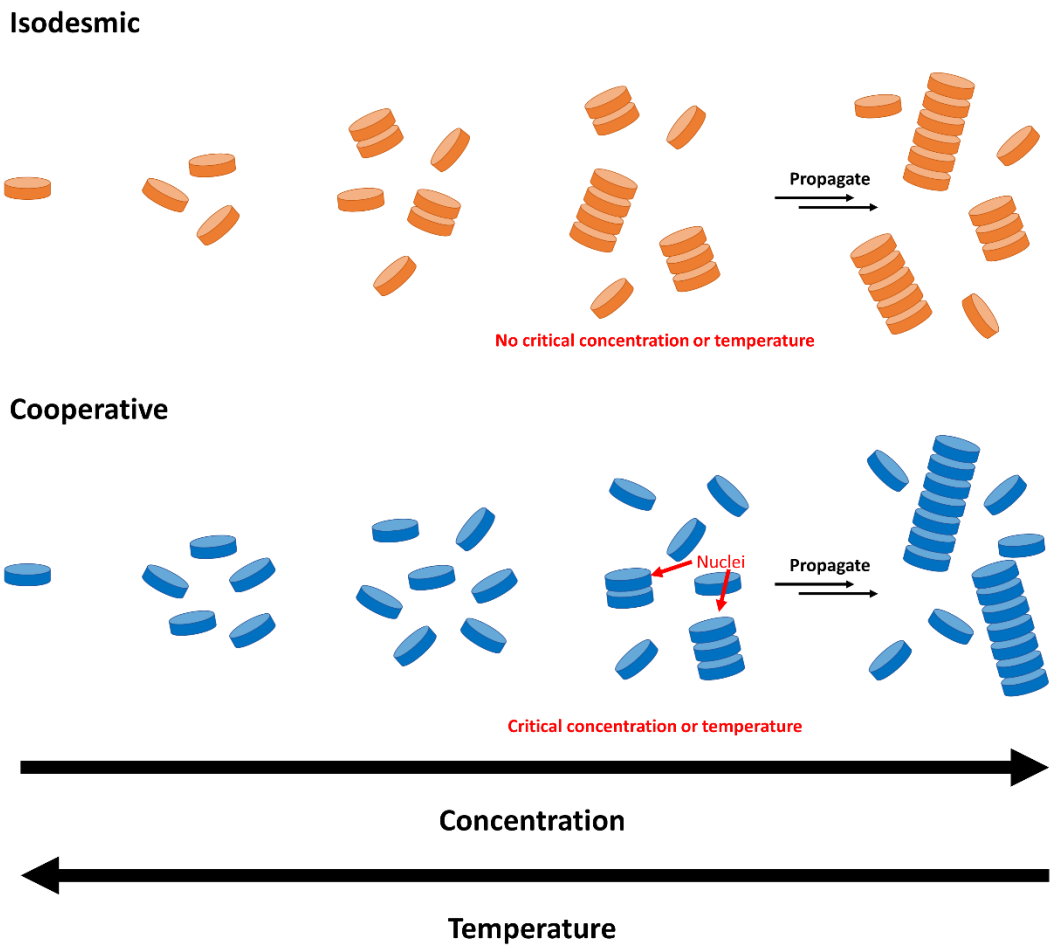

Scheme 1.1. The self-assembly process in an isodesmic and cooperative mechanism.

1.1.3 Living supramolecular polymers

Nature produces mono-disperse polymers, such as proteins, to carry out vital living processes. However, achieving this for synthetic polymers has been far more challenging. Dispersity is the measure of the heterogeneity of polymers, the larger the length distribution of chains the higher the dispersity. Conventional polymers, where the monomers are linked covalently, have used living polymerisation techniques to better control the length and distribution of polymers. This principle has also been adopted to control the dispersity of supramolecular polymers. During polymerisation, an initiator can react with another monomer to generate a new active centre on the monomer. With each successive monomer addition the polymer propagates and the last monomer to react importantly retain the active group. In a living system, where the initiation is faster than propagation and there are no side reactions *via* termination

or chain transfer, all the active chain end can be nucleated before growing uniformly – this results in a much lower dispersity polymer. Controlling the dispersity of the polymers is vital as the degree of polymerisation (DP) i.e. the polymer chain length, can drastically effect the properties of the material. Lower dispersity polymers will enables us to better target, tune and reproduce the polymers for their desired applications. Using the concept of 'living' supramolecular polymerization we can synthesise uniform self-assembled structures.

The first approach leading to a living supramolecular polymerization established and developed by Manners, Winnik and co-workers utilises crystallisation-driven self-assembly (CDSA). In CDSA, a block co-polymer is self-assembled as one block is solvophobic and the other is solvophillic. Importantly the solvophobic block, most commonly polyferrocenylsilane (PFS), forms a semi-crystalline core. This crystallinity generates directionality and kinetically traps the self-assembled structures preventing them from dynamically disassembling and re-assembling. Upon sonication these self-assembled structures can be broken up into uniform 'seed micelles'. In the presence of additional unimers the seed micelles behave as nuclei from which they can propagate to produce uniform elongated supramolecular polymers. More recently, work has been focused on using this method to create aqueous monodispersed micelles and 2D-platelet morphologies using polylactides are the core-forming block. [8-10]

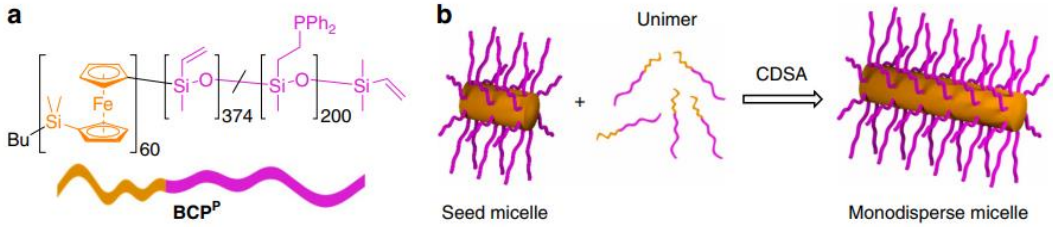

Scheme 1.2. Simplified route to uniform cylindrical micelles *via* crystallization driven self-assembly. a) block co-polymer unimer with a crystallisable PFS core (orange) and phosphine containing polysiloxane corona (purple). Adapted from Lunn *et al.*[11]

Aida and co-workers also developed a method to forming living supramolecular polymers using a metastable cage-like structures. The initiator and monomer species consist of a concave structure of aromatic rings functionalised with a range of different R-groups on the periphery. Once assembled, the phenyl groups take part in π-π stacking, but crucially, the R-groups contain amide bonds which can hydrogen bond to each other. The carboxylic acid group on the initiator can be used to spring open

the metastable cage monomer; this hydrogen bond reorganisation initiates the polymerisation and the resultant initiator-monomer complex can further propagate with more monomers during the chain growth stage. The subsequent polymers were shown to be well controlled *via* size exclusion chromatography (SEC) and atomic force microscopy (AFM). In addition, both SEC and AFM also showed size or length of the polymers could be tuned by increasing the monomer to initiator ratio, as expected in a living polymerisation.

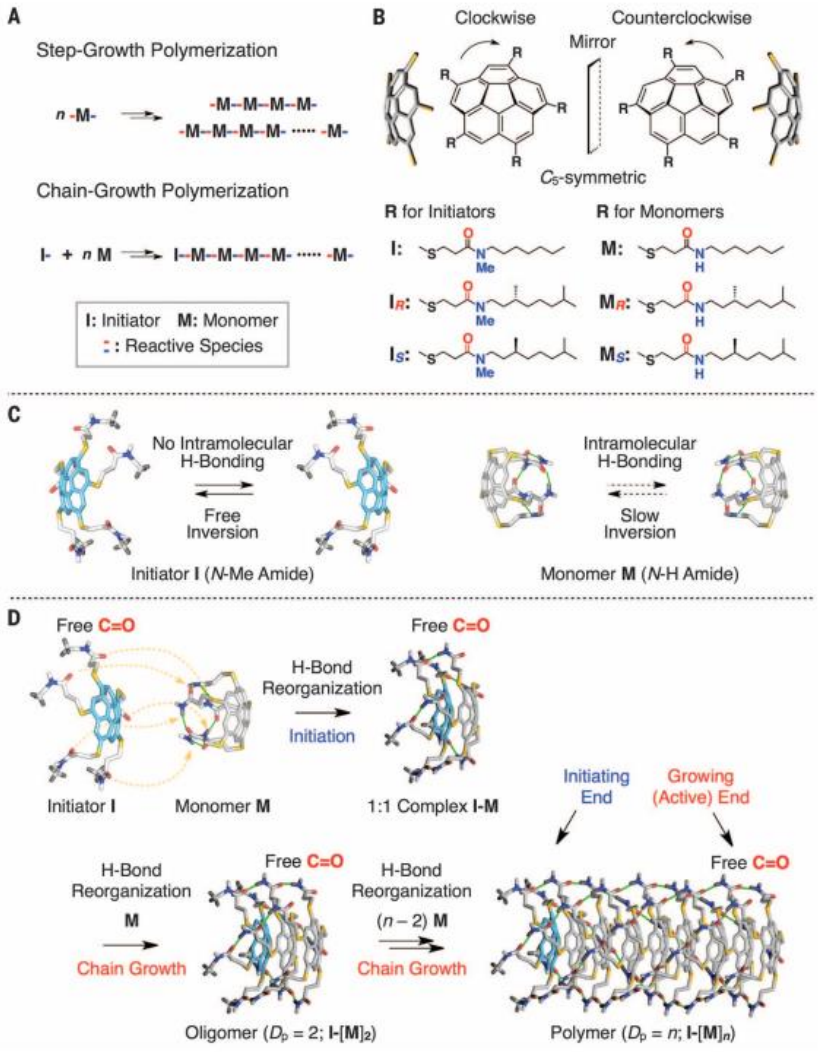

Figure 1.1 Living supramolecular polymerisation of metastable cage-like species. a) General mechanism of step-growth and chain-growth polymerisation. b) Chemical structure of the metastable cage-like monomer, c) Schematic representation of the open 'initiator', caged 'monomer' species and d) growing polymer. Reproduced from Kang *et al.* [12]

Subsequently, a third way to produce defined supramolecular polymers was developed by Sugiyasu, Takeushi and co-workers, using the formation of stabilised aggregates of zinc or copper complexed porphyrin derivatives. As the zinc porphyrin-based molecules were heated they preferential disassembled to their unimeric state. Upon cooling they stacked to form *J*-aggregated nanoparticles however given a few days to equilibrate the system could rearrange to form *H*-aggregated nanofibers. This phenomenon can be seen to take place much faster (in a few hours) if the *H*-aggregates are put in the presence of the some *J*-aggregates. This suggests the transformation into *H*-aggregates can be initiated by 'seeding'. By introducing 'nuclei' or 'seeds' the polymerization can proceed *via* a controlled pathway, resulting in the formation of uniform fibres, see Figure 1.1 a and b.[13] More recently these porphyrins have also been shown to form uniform assemblies *via* CDSA approach, see Figure 1.1c.

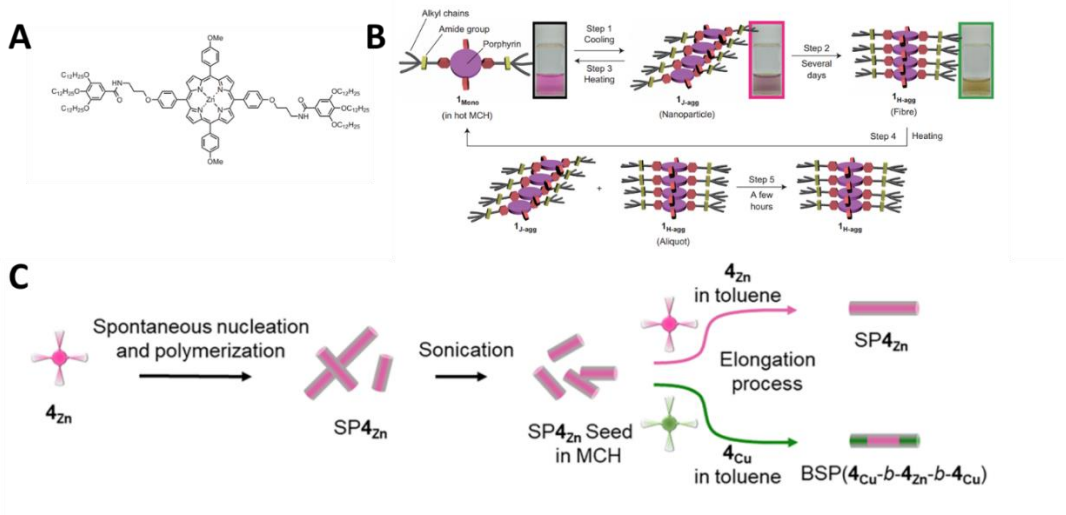

Figure 1.2 a) Chemical structures of a zinc-porphyrin complex (unimer). Schematic representation of living supramolecular assembly of porphyrin derivatives *via* b) heating (adapted from Ogi *et al*)[13] and c) seeded growth (Reproduced from Jung *et al*)[14].

All these approaches illustrate remarkable control over the supramolecular polymerisation, however require highly specialised unimers and conditions. Despite these advances, designing controlled self-assembly systems for biological relevant systems in aqueous conditions has been much more challenging.

1.2 Self-assembling peptide

Hydrogen bonds can be found everywhere in the natural world. For this reason, when designing supramolecular polymers for biological applications, many systems use hydrogen bonds to recreate their desired nanostructures. In particular, the self-assembling peptides, which have the ability to spontaneously aggregate to form long ordered structures have been widely exploited to form β-sheets and α-helixes assemblies.

By using amino acids which are naturally occurring in the body, the aim is to minimise their potential biological side effects. These systems have garnered much attention for their potential biological applications in drug delivery[15, 16] and tissue engineering.[17] Additionally, the amino acid building blocks of peptides provide an extensive library of functional groups with their own in-built self-assembly motif in the form of amide bonds. The amide bonds on the peptides can take part in hydrogen bonding to form directional β-sheet arrays.

1.2.1 ß-Sheet (hydrogen bond) self-assembly

The amide bonds perpendicular to the peptide backbone can take part in hydrogen bonding to form supramolecular structures. Due to hydrogen bonds being directional, peptides have a tendency to form one-dimensional elongated structures, typically nanofibers. The β-sheet formation of the peptide can occur in a parallel or anti-parallel fashion, scheme 1.3.

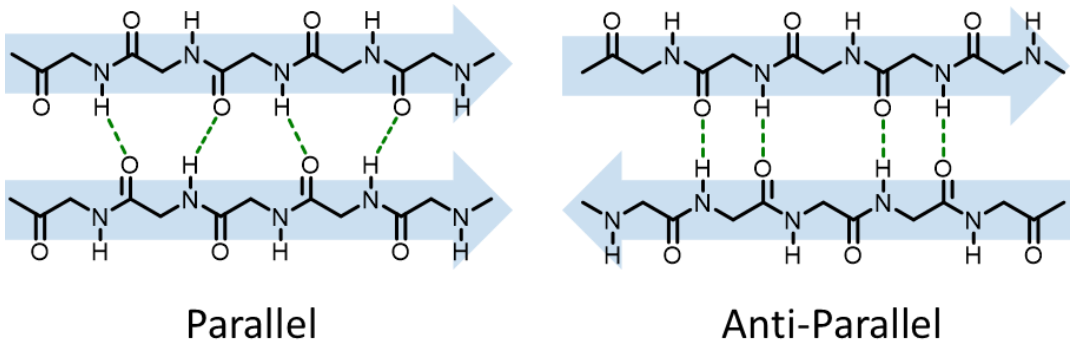

Scheme 1.3. Parallel and Anti-parallel β–sheet formation.

The simplest example of self-assembling peptides are the dipeptide systems.[18, 19] The general design of these dipeptides consist of two amino acids, typically aromatic, attached to an hydrophobic R group on the *N*-terminus *via* a linker (i.e. –O-CH_2- or –

CH_2-), see Scheme 1.4a. The interplay of hydrophobicity and hydrophilicity between these exchangeable groups make this system very versatile. The design of the dipeptides are optimised to self-assemble in water and as a result they form extremely long nanofibers, which in turn entangle to produce gel networks. Using their simple design and ability to form hydrogels in water, these peptides have been studied for their applications as 3D cell culture supports[17] and energy transfer systems for use in bioelectronics[20].

Another key example of supramolecular peptide polymers are peptide amphiphiles (PA). PAs contain an alkyl hydrophobic tail, β-sheet forming middle segment and outer charged groups for stabilisation, see Scheme 1.4.[21] The hydrophobic tail and hydrophilic charged surface groups allow them to behave as surfactants in aqueous media. However, unlikely typical surfactants which self-assemble into spheres to form micelles, the directional hydrogen bonding β-sheet motif forces the peptides into a nanofibillar conformation. This two-fold self-assembly system has been used to develop bio-mimetic self-assembled nanofibers to aid bone mineralisation and targeted cell-signalling.[15, 22]

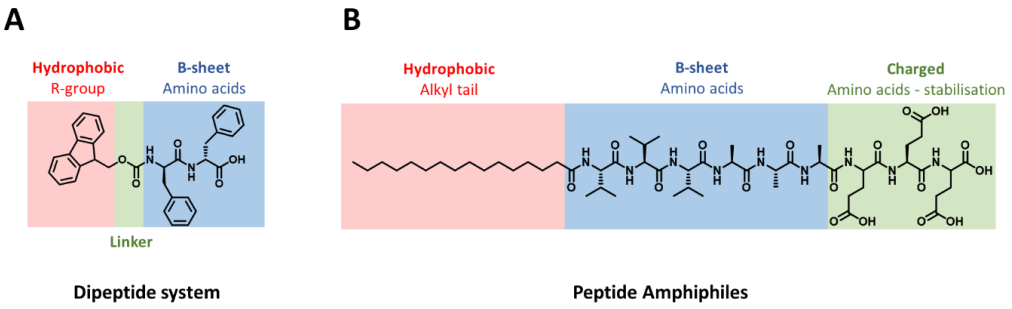

Scheme 1.4. Examples and general design features of self-assembling a) dipeptides and b) peptide amphiphiles.

Non-peptide self-assembly systems which use amide bonds such as the bis-urea,[23] benzene 1,3,5, tricarboxamides (BTA)[24, 25] and ureido-pyrimidinone (UPy)[26-28] motifs have also been shown to self-assemble into β-sheet stacking elongated nanostructures.

1.3 Self-assembling cyclic peptides

1.3.1 History and Design

Naturally occurring cyclic peptides have been found to possess remarkable toxicity and antimicrobial activity.[29] For this reason, cyclic peptides have been synthetically reproduced in the lab in order to study their potential as antibiotics or therapeutic drugs. To give an example, Cyclosporin A has become a pharmaceutical success as an immunosuppressive drug. 56e

In 1974, De Santis *et al.* first proposed that cyclic peptides with a specific conformation could stack on top of each other to form nanotubes.[30] He hypothesised that a linear peptide with an even number of α alternating D- and L- amino acids could from a flat ring like structure upon cyclisation. With this configuration the amide bonds on the cyclic peptide would be perpendicular to the ring enabling them hydrogen bond with each other, see Figure 1.3a. In 1993, with increasing methods to make and characterise synthetic peptides, Ghadiri and co-workers were able to observe these self-assembling cyclic peptide nanotubes by transmission electron microscopy (TEM) (Figure 1.3b).[3]

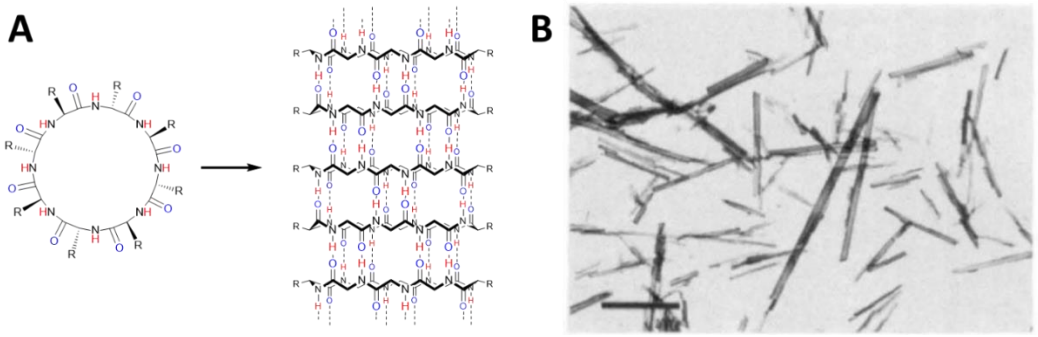

Figure 1.3 a) The chemical structure and b) transmission electron microscopy (TEM) of self-assembling cyclic peptide nanotubes. Reproduced from Ghadiri *et al.*[3]

These cyclic peptide nanotubes (CPNT) have a number of desirable design features. Using a 'bottom up' approach the sequence of the amino acids in the peptide can be altered to provide solubility and site specific functionality. The functional R group of the amino acid protrude out of the nanotube assembly – therefore decorating the periphery of the peptide, see Figure 1.3a. The functional groups on the CPNT are chosen carefully to promote assembly and provide handles for post-modification. Due to the self-assembly process, the peptide can readily precipitate in most solvents, other

than trifluoroacetic acid (TFA), dimethyl sulfoxide (DMSO) and dimethylformamide (DMF), significantly improving the yields during the purification steps.[3, 31, 32]

The amino acid composition of self-assembling cyclic peptides has been reviewed in detailed by Ghadiri, Granja and co-workers.[3, 31-35] The study established that the octa-peptide structure provided plenty of nodes for functionality whilst still mainly the planar ring-structure for self-assembly. The internal diameter and distance between two cyclic octa-peptides was found to be about 7.5 Å and 4.5 Å respectively - determined by X-ray crystallography, electron diffraction and mathematical modelling. Further advances have been made in orthogonal conjugation chemistry, including in this thesis, to provide a library of different CPNT conjugates.

1.3.2 Self-assembling cyclic peptide-polymer conjugates

A major advantage of self-assembling cyclic peptides has been the ease in post-modification using the in-built functionality of the peptide. Most significantly, the attachment of polymers to the outside of the peptide ring has dramatically improved the solubility of these nanostructures. Biesalski and coworkers were first to report the attachment of polymers to cyclic peptide nanotubes using pNIPAM synthesised *via* atom transfer radical polymerisation (ATRP).[36] The introduction of the polymer not only changes the solubility of the unimer but also effects the self-assembly of the nanotube. The sterically bulky polymers on the side of the peptide also prevented lateral aggregation of the peptide and therefore lead to the formation of single nanotubes. The same group went on to study this steric behaviour on the self-assembly and showed by increase the size of the polymer chain they observed a decrease in the overall size of aggregates.

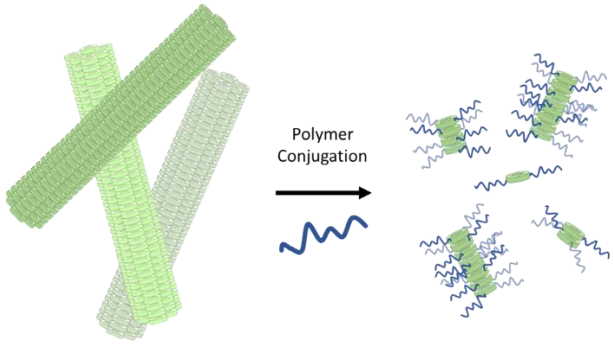

Scheme 1.5. Cyclic peptides laterally aggregate to form long nanotubular bundles. Upon polymer conjugation the polymer arms help solubilise the CPNT and prevent lateral aggregation.

Our group has gone on to attach a wide range of polymers such as polyethylene glycol (PEG), poly(2-ethyl-2-oxazoline) (pEtOx)[37, 38] and polymers synthesised *via* reversible addition − fragmentation chain-transfer polymerization (RAFT) to the CPNT.[39] The attachment of hydrophilic polymers to the periphery of CPNT has allowed them to be studied for a host of bio-therapeutic applications, see section 1.3.3.

Much of the focus has been on attaching highly functional polymers with low dispersities to the cyclic peptide to study their potential bio-therapeutic applications. For this reason many of the conjugates were designed to be stable in aqueous systems. Early examples of these systems looked at the responsive behaviour of CP-polymers in water to stimuli such as temperature and pH. Chapman *et al.* showed that the conjugates could be thermo-responsive. Above the cloud point temperature, the cyclic peptides decorated with poly (2-ethyl-2-oxazoline) (pEtOx) were shown to form large micrometre particles.[37]

The supramolecular nature of the peptide assembly has also been exploited to form pH responsive self-assemblies. Previously poly (acrylic acid) (pAA) conjugated nanotubes were reported to be shorter at high pH upon deprotonation of the carboxylic acid group.[40] This behaviour was explored further by Catrouillet *et al.* to show using poly (2-dimethylamino) ethyl methacrylate (pDMAEMA) the nanotubular length could be tuned at different pHs.[41] By tuning the pH and therefore the amount of charge on the polymer arms, the self-assembly could be disrupted to different degrees.

1.3.3 Applications

Before the attachment of polymers, these cyclic peptides were shown to have interesting antimicrobial activity. In 2001, Fernandez-Lopez and co-workers showed that these peptides were selectively membrane active against bacterial strains, including *Escherichia coli* and *Staphylococcus aureus*.[32] The studies showed the 'carpet-like' self-assembly of the peptide in the membrane lead to fast cell death and avoided receptor interactions, which in turn helps prevent anti-bacterial resistance.

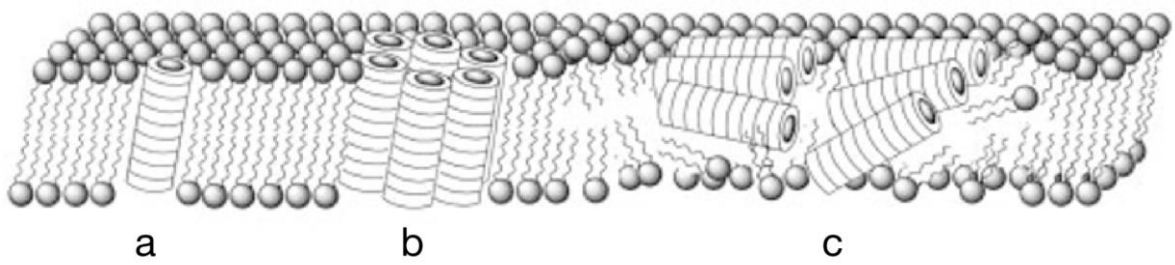

Scheme 1.6. Different modes of action a) intramolecular pore, b) barrel stave and c) carpet-like of self-assembling cyclic peptide nanotubes in lipid bilayer membranes. Reproduced from Fernandez-Lopez *et al.*[32]

Wang *et al.* reported the use of PEGylated CPNT bundles to deliver the model anticancer drug doxorubicin (DOX).[42] The DOX was mixed with cyclic peptide decorated with PEG, cysteine and glutamic acid residues. They hypothesised the charge residues could form ion-pairs which could lead to the nanotubular bundling. Increase activity of the drug was observed with the carrier and the carrier showed no toxicity with the absence of the drug.

Following on, Blunden *et al.* showed the delivery of the ruthenium-based anticancer drug RAPTA-C.[43] A hydrophilic co-polymer of hydroxyl ethyl acrylate (HEA) and 2-chloroethyl methacrylate (CEMA) was synthesised to not only solubilise the CPNT in aqueous conditions but also provide the attachment point for the drug.

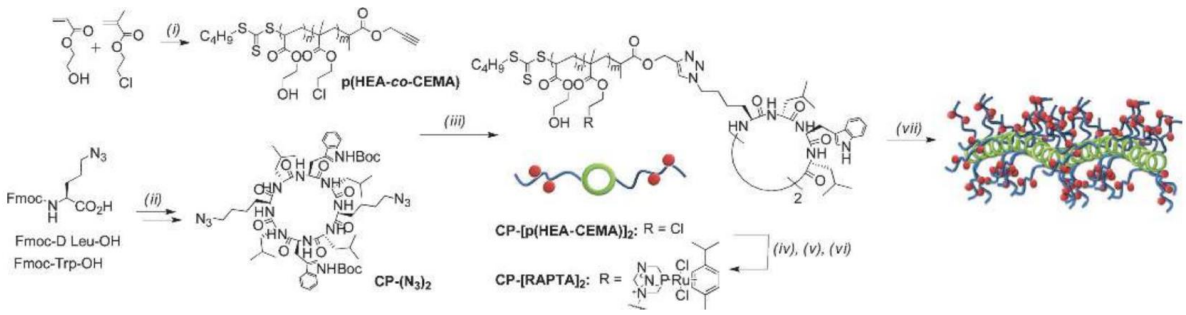

Figure 1.4. RAPTA-C functionalised cyclic peptide polymers. Reproduced from Blunden *et al.* [43]

More recently, Larnaudie *et al.* used a more potent Iridium-based anticancer drug, see Figure 1.5. The IC50 of the drug-conjugated polymer-CPNT was lower than that of the free polymer or drug.[16, 44] The CPNT conjugates produced better specificity with a six-fold decrease in toxicity on the ovarian cancer cell line (A2780). Interestingly, this did not correlate with a higher content of the Iridium in the cells, which implies the drug carrier provides a more efficient mode of action in comparison to its controls.

In a biological setting, many of these dynamic systems are injected or delivered at low concentrations, where they are likely disassemble. If the assemblies are highly dynamic, this could explains why many of these systems are very short in length, typically around 10 nm, at the biologically relevant concentrations. Stabilising the self-assembled nanostructures would enable us to better control the benefits we receive from the supramolecular nature of these systems.

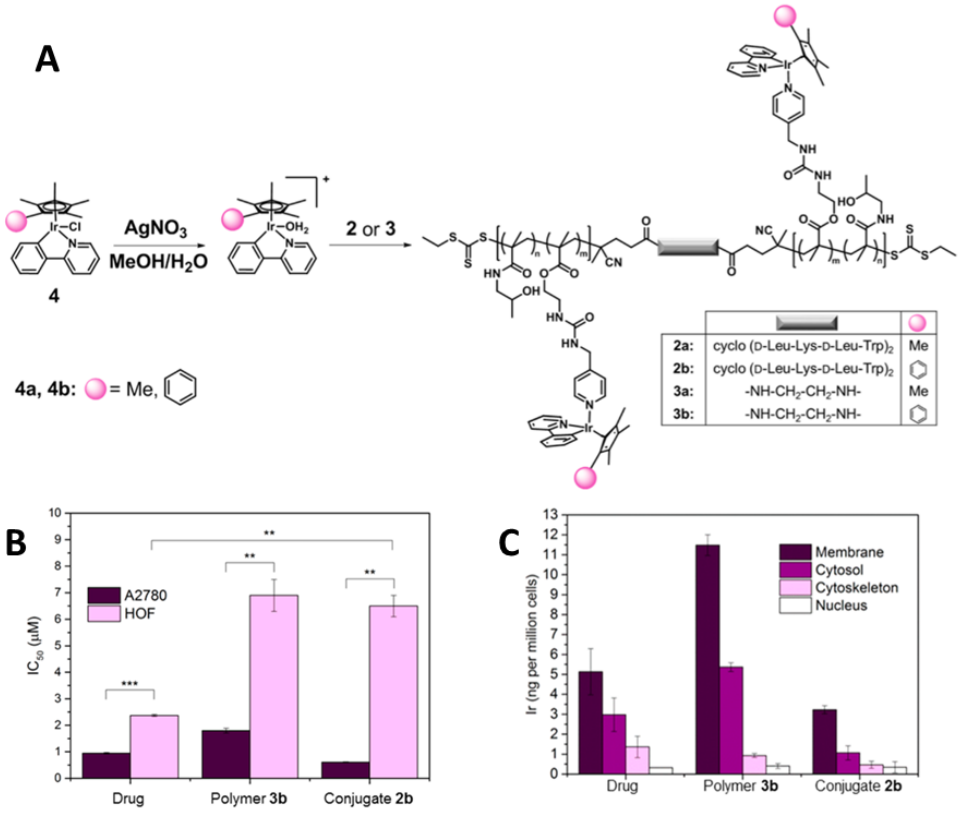

Figure 1.5. a. Structure of cyclic peptides conjugated with poly (N-(2-Hydroxypropyl) methacrylamide (pHPMA) and anti-cancer iridium complex. **b.** IC50 of the free drug, polymer and conjugate. **c.** The mass of iridium found in the membrane, cytosol, cytoskeleton and nucleus of the cells. Reproduced from Larnaudie *et al.* [44]

In recent years, the study of amphiphilic cyclic peptide-polymers have given rise to a secondary self-assembly of individual nanotubes into tubisomes.[45] This secondary assembly is facilitated by attaching a hydrophilic polymer to one side of the cyclic peptide and a hydrophobic polymer to the other. The cyclic peptides not only hydrogen bond to form peptide nanotubes, the hydrophobic polymer chains additional aggregate with one another to hold a secondary tubular structure, see Figure 1.6. In aqueous conditions, this two-fold self-assembly can be observed using small angle neutron scattering (SANS). The secondary structure afforded by the tubisome system provides a much larger pore cavity (diameter 16 nm) in comparison to the single nanotubes (diameter 0.7 nm). This larger cavity was shown to perforate the lysosomal membrane to release calcein into the cytosol.[45]

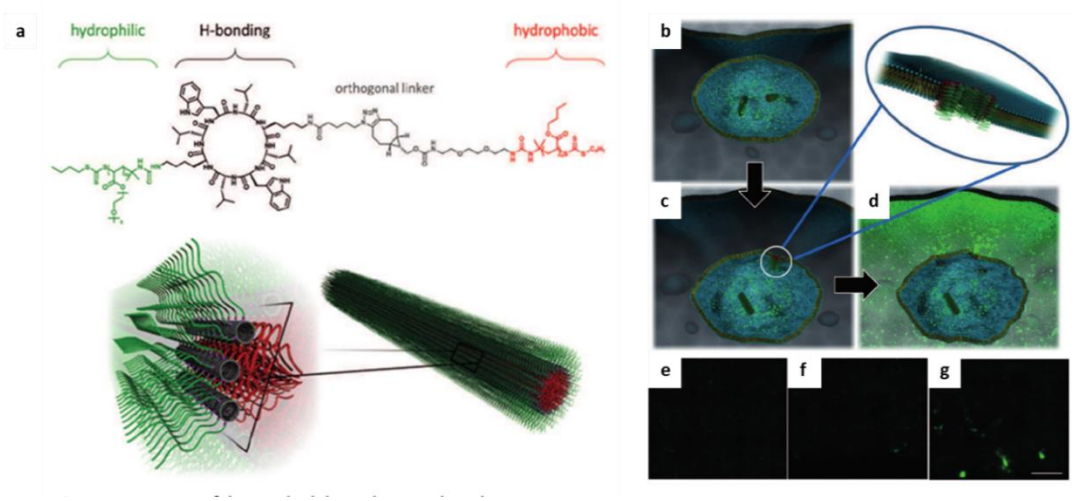

Figure 1.6 a) Tubisomes formed via a two-fold self-assembly of amphiphilic cyclic peptide nanotubes using β–sheet hydrogen bonding and hydrophobic interactions. Calcein release study to observe lysosomal escape. b-d) Artistic representation of the dye leaking into the cytosol through the tubisomes. e) Calcein escape from the lysosome in HEK293 cells, f) pre-treated with pBA_{27}-b-$pPEGA_{45}$ (polymer) or g) pBA_{27}-CP-$pPEGA_{45}$ (CP conjugate). Scale bar set to 200µm. Reproduced from Brendel *et al.*[45]

1.4 Characterisation of self-assembled nanostructures

1.4.1 Fluorescence probes

Many living systems are governed by molecular interactions which take part on the nanoscale. Fluorescent molecules (i.e. fluorophores) can be especially useful in biology to investigate molecular interactions *in situ* in complex biological environments, such as inside cells.

For a compound to fluoresce it needs to emit light upon excitation. This emission of light occurs when the compound relaxes back to the ground state and in the process emits a photon. The energy of the photon released is equal to $h\nu$ where h = Plank's constant and ν= frequency of light.

Förster resonance energy transfer (FRET) is a fluorescence phenomenon that is often utilised in biology to observe the interaction of two different molecules. If the two different species are labelled with FRET dyes, one with a donor and the other with an acceptor, it is possible for the electronic excited state of the donor to transfer energy *via* non-radiative dipole-dipole coupling. This energy transfer can be monitor by the measuring the fluorescence emission of the acceptor upon excitation of the donor. For this energy transfer to take place two conditions must be met. First, the emission of the donor and the excitation of the acceptor must overlap. Second, the donor and acceptor must be close enough in proximity for the dipole-dipole coupling to take place, typically within 10-100 nm.

For this thesis, FRET has been extensively used to monitor the dynamic exchange of cyclic peptides between nanotubes in solution. If the donor and acceptor dye labelled cyclic peptide-polymer unimers are self-assembled in the same nanotube, after dynamically exchanging, this proximity dependent energy transfer should be observed.

1.4.2 Light scattering

Light scattering is a powerful method to characterise nanoscale self-assemblies in solution. In particular, techniques such as static light scattering (SLS) and small angle neutron scattering (SANS) are frequently used to measure the size of self-assembled structures which are not spherical, like nanotubes.

These methods rely on measuring the scattering intensity at various different angles in relation to the incident beam. Using the equation:

$$q = \frac{4\pi}{\lambda_0} sin\frac{\theta}{2}\ (SANS) \quad or \quad q = \frac{4\pi n}{\lambda_0} sin\frac{\theta}{2}\ (SLS) \qquad (1)$$

where q = wave vector, λ_0= wavelength of the incident beam, n = refractive index of the solvent and θ is the angle of the detector from the incident beam, a range of q values can be obtained by varying the angle.

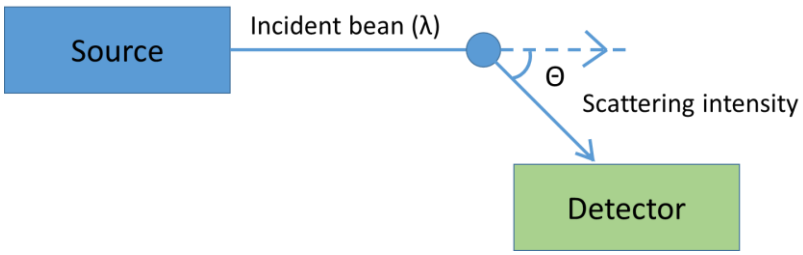

Figure 1.7 Illustrating the scattering angle of the detector in relation to the incident beam.

The wave vector q is also inversely proportional to the window of observation. Therefore the smaller your wave vector q, the larger your window of observation for a fixed wavelength of light, λ_0.

In SANS, using the fact that the scattering length density between deuterium and hydrogen is significantly different, the contrast between deuterated solvents and the hydrogen containing molecules, is used to measure a scattering profile of the aggregates in solution. The scattering profile can be measured and fitted to a range of different models to obtain information about the size and shape of the assemblies.

In SLS, the aggregates are prepared in a range of different concentrations and measure at various different angles.

$$R_\theta = \frac{I_{solution}(\theta) - I_{solvent}(\theta)}{I_{toluene}(\theta)} \cdot \left(\frac{n_{solvent}}{n_{toluene}}\right)^2 \cdot R_{toluene} \qquad (2)$$

I = scattering intensity, n= refractive index, R = Rayleigh ratio.

This equation calculates the Rayleigh ratio at a given angle of the solution after taking into account the solvent and toluene reference.

$$K = \frac{4\pi^2 {n_{solvent}}^2}{\lambda^4 N_a} \cdot \left(\frac{dn}{dc}\right)^2 \qquad (3)$$

K = optical constant, N_a= Avogadro constant, dn/dc = the change in refractive index over the change in concentration.

$$\frac{KC}{R_\theta} = \frac{1}{M_a} \cdot \left(1 + \frac{q^2 \cdot {R_g}^2}{3}\right) \qquad (4)$$

R_g = radius of gyration.

The average molecular weight of the aggregate M_a can be obtained by plotting the KC/R_Θ versus q^2 in a linear regression in accordance with equation (4). At infinite dilution, where there are no inter-particle interactions average molecular weight of the aggregates should be constant. If the molecular weight of the aggregate M_a is the same over infinite dilutions, the average number of aggregation can be calculated from the following equation (6):

$$Number\ of\ aggreation = \frac{Molecular\ weight\ of\ the\ aggreate}{Molecular\ weight\ of\ the\ unimer} \qquad (5)$$

These scattering techniques have been utilised throughout this thesis to characterise the aggregates in solution.

1.5 Scope and motivation of this thesis

Self-assembling cyclic peptide nanotubes have gained considerable interest due to their promising biological applications in drug delivery and as anti-microbials. This can be attributed to their wide range of design features including their ease of functionalisation and reversible supramolecular assembly. The host of functionalities on the peptide can also be used as handles for post-modification. A major step towards using these systems *in vitro* and *in vivo* has been the conjugation of water-soluble polymers to the cyclic peptides which have shown to significantly improve the solubility CPNTs in water.

Our group has looked at using the non-covalent supramolecular nature of the cyclic peptides for drug delivery systems. In an ideal case, a supramolecular drug carrier should show an enhanced therapeutic response compared to its unimeric counterpart but once delivered, be able to depolymerise to its non-assembled state - making it easier to be cleared from the body. This could help prevent accumulation in organs, which can lead to future complications.

It remains unclear whether these self-assembled nanotubes are kinetically stable or are constantly exchanging between nanotubes in a thermodynamic equilibrium. As this behaviour is of paramount importance to predict their performance in future biological studies, an in-depth study of the dynamic nature of supramolecular drug conjugates is critical.

For our supramolecular system, we designed CP–polymer conjugates modified with fluorescent dyes and used Förster resonance energy transfer (FRET) to probe the dynamic nature of the resulting nanotubes. Fluorescence is a powerful tool to study close intramolecular interactions and investigate the dynamic behaviour of supramolecular systems. In the context of cyclic peptides, Granja and co-workers previously employed FRET to study the hydrogen-bonding interaction of small dimeric cyclic peptides.[46] Here, we propose to use FRET to gain an insight into the stacking of cyclic peptide nanotubes (CPNTs) *in situ* and provide vital information about the dynamics of these one-dimensional supramolecular structures. In addition, the use of FRET allowed us to observe the behaviour of these nanotubes in mammalian cells in vitro, thus providing essential information about their dynamics in a complex biological environment.

With our growing mechanistic understanding of supramolecular chemistry from model self-assembling systems, the next important step will be to tailor their behaviour to their intended applications. In a biological setting, many of these dynamic systems will be injected or delivered at low concentrations, where they are likely to disassemble.

Inspired by the hierarchical design and structure of proteins, a two-fold self-assembly approach was developed to help stabilise the elongated peptide nanostructure. The hydrogen bond stacking of the cyclic peptides provides the primary structure and overall cylindrical morphology of the self-assembled aggregates. Here we introduce a secondary structural driving force in the form of a hydrophobic region around the peptide to stabilise the single cyclic peptide nanotubes. The individual nanotubes remain independent due to the hydrophilic corona stabilising the nanostructures in water. This hierarchical approach offers a method to stabilise, not only cyclic peptide assemblies, but also other β-sheet forming self-assembled architectures.

This thesis aims to highlight the importance of understanding the supramolecular behaviour and how armed with this information we can better design these promising synthetic supramolecular polymers.

1.6 References

1. S. Onogi, H. Shigemitsu, T. Yoshii, T. Tanida, M. Ikeda, R. Kubota and I. Hamachi, *Nature Chemistry*, 2016, **8**, 743-752.
2. S. Yagai, Y. Monma, N. Kawauchi, T. Karatsu and A. Kitamura, *Organic letters*, 2007, **9**, 1137-1140.
3. M. R. Ghadiri, J. R. Granja, R. A. Milligan, D. E. McRee and N. Khazanovich, *Nature*, 1993, **366**, 324-327.
4. B. J. G. E. Pieters, M. B. van Eldijk, R. J. M. Nolte and J. Mecinović, *Chemical Society Reviews*, 2016, **45**, 24-39.
5. H. Shaikh, J. Y. Rho, L. J. Macdougall, P. Gurnani, A. M. Lunn, J. Yang, S. Huband, E. D. H. Mansfield, R. Peltier and S. Perrier, *Chemistry – A European Journal*, 2018, **24**, 19066-19074.
6. L. Brunsveld, B. J. B. Folmer, E. W. Meijer and R. P. Sijbesma, *Chemical Reviews*, 2001, **101**, 4071-4098.
7. M. M. J. Smulders, M. M. L. Nieuwenhuizen, T. F. A. de Greef, P. van der Schoot, A. P. H. J. Schenning and E. W. Meijer, *Chemistry – A European Journal*, 2010, **16**, 362-367.
8. J. B. Gilroy, T. Gädt, G. R. Whittell, L. Chabanne, J. M. Mitchels, R. M. Richardson, M. A. Winnik and I. Manners, *Nature Chemistry*, 2010, **2**, 566.
9. J. Qian, X. Li, D. J. Lunn, J. Gwyther, Z. M. Hudson, E. Kynaston, P. A. Rupar, M. A. Winnik and I. Manners, *Journal of the American Chemical Society*, 2014, **136**, 4121-4124.
10. X. Wang, G. Guerin, H. Wang, Y. Wang, I. Manners and M. A. Winnik, *Science*, 2007, **317**, 644-647.
11. D. J. Lunn, O. E. C. Gould, G. R. Whittell, D. P. Armstrong, K. P. Mineart, M. A. Winnik, R. J. Spontak, P. G. Pringle and I. Manners, *Nature Communications*, 2016, **7**, 12371.
12. J. Kang, D. Miyajima, T. Mori, Y. Inoue, Y. Itoh and T. Aida, 2015, **347**, 646-651.
13. S. Ogi, K. Sugiyasu, S. Manna, S. Samitsu and M. Takeuchi, *Nature Chemistry*, 2014, **6**, 188.
14. S. H. Jung, D. Bochicchio, G. M. Pavan, M. Takeuchi and K. Sugiyasu, *Journal of the American Chemical Society*, 2018, **140**, 10570-10577.
15. H. Cui, M. J. Webber and S. I. Stupp, 2010, **94**, 1-18.

16. S. C. Larnaudie, J. Sanchis, T.-H. Nguyen, R. Peltier, S. Catrouillet, J. C. Brendel, C. J. H. Porter, K. A. Jolliffe and S. Perrier, *Biomaterials*, 2018, **178**, 570-582.
17. D. M. Ryan and B. L. Nilsson, *Polymer Chemistry*, 2012, **3**, 18-33.
18. D. J. J. M. b. Adams, 2011, **11**, 160-173.
19. J. Raeburn, T. O. McDonald and D. J. J. C. C. Adams, 2012, **48**, 9355-9357.
20. H. A. M. Ardoña, E. R. Draper, F. Citossi, M. Wallace, L. C. Serpell, D. J. Adams and J. D. Tovar, *Journal of the American Chemical Society*, 2017, **139**, 8685-8692.
21. O.-S. Lee, S. I. Stupp and G. C. Schatz, *Journal of the American Chemical Society*, 2011, **133**, 3677-3683.
22. E. D. Spoerke, S. G. Anthony and S. I. Stupp, *Advanced Materials*, 2009, **21**, 425-430.
23. M. Bellot and L. Bouteiller, *Langmuir*, 2008, **24**, 14176-14182.
24. M. García-Iglesias, B. F. M. de Waal, I. de Feijter, A. R. A. Palmans and E. W. Meijer, 2015, **21**, 377-385.
25. T. F. A. De Greef, M. M. J. Smulders, M. Wolffs, A. P. H. J. Schenning, R. P. Sijbesma and E. W. Meijer, *Chemical Reviews*, 2009, **109**, 5687-5754.
26. J. K. Hirschberg, R. A. Koevoets, R. P. Sijbesma and E. J. C. A. E. J. Meijer, 2003, **9**, 4222-4231.
27. Henk M. Keizer, Rint P. Sijbesma and E. W. Meijer, 2004, **2004**, 2553-2555.
28. B. B. Mollet, Y. Nakano, P. C. M. M. Magusin, A. J. H. Spiering, J. A. J. M. Vekemans, P. Y. W. Dankers and E. W. Meijer, 2016, **54**, 81-90.
29. K. Jensen, *Peptide and Protein Design for Biopharmaceutical Applications*, Wiley, 2009.
30. P. De Santis, S. Morosetti and R. Rizzo, *Macromolecules*, 1974, **7**, 52-58.
31. T. D. Clark, L. K. Buehler and M. R. Ghadiri, *Journal of the American Chemical Society*, 1998, **120**, 651-656.
32. S. Fernandez-Lopez, H.-S. Kim, E. C. Choi, M. Delgado, J. R. Granja, A. Khasanov, K. Kraehenbuehl, G. Long, D. A. Weinberger and K. M. Wilcoxen, *Nature*, 2001, **412**, 452-455.
33. R. Chapman, M. Danial, M. L. Koh, K. A. Jolliffe and S. Perrier, *Chemical Society Reviews*, 2012, **41**, 6023-6041.
34. M. R. Ghadiri, J. R. Granja and L. K. Buehler, *Nature*, 1994, **369**, 301.

35. D. T. Bong, T. D. Clark, J. R. Granja and M. R. Ghadiri, *Angewandte Chemie International Edition*, 2001, **40**, 988-1011.
36. J. Couet, J. D. J. S. Samuel, A. Kopyshev, S. Santer and M. Biesalski, *Angewandte Chemie International Edition*, 2005, **44**, 3297-3301.
37. R. Chapman, P. J. Bouten, R. Hoogenboom, K. A. Jolliffe and S. Perrier, *Chemical Communications*, 2013, **49**, 6522-6524.
38. M. Hartlieb, S. Catrouillet, A. Kuroki, C. Sanchez-Cano, R. Peltier and S. Perrier, *Stimuli-Responsive Membrane Activity of Cyclic-Peptide-Polymer Conjugates*, 2019.
39. S. C. Larnaudie, J. C. Brendel, K. A. Jolliffe and S. Perrier, *Journal of Polymer Science Part A: Polymer Chemistry*, 2016, **54**, 1003-1011.
40. R. Chapman, K. A. Jolliffe and S. Perrier, *Polymer Chemistry*, 2011, **2**, 1956-1963.
41. S. Catrouillet, J. C. Brendel, S. Larnaudie, T. Barlow, K. A. Jolliffe and S. Perrier, *ACS Macro Letters*, 2016, **5**, 1119-1123.
42. Y. Wang, S. Yi, L. Sun, Y. Huang, S. C. Lenaghan and M. Zhang, *Journal of biomedical nanotechnology*, 2014, **10**, 445-454.
43. B. M. Blunden, R. Chapman, M. Danial, H. Lu, K. A. Jolliffe, S. Perrier and M. H. Stenzel, *Chemistry - A European Journal*, 2014, **20**, 12745-12749.
44. S. C. Larnaudie, J. C. Brendel, I. Romero-Canelón, C. Sanchez-Cano, S. Catrouillet, J. Sanchis, J. P. C. Coverdale, J.-I. Song, A. Habtemariam, P. J. Sadler, K. A. Jolliffe and S. Perrier, *Biomacromolecules*, 2018, **19**, 239-247.
45. J. C. Brendel, J. Sanchis, S. Catrouillet, E. Czuba, M. Z. Chen, B. M. Long, C. Nowell, A. Johnston, K. A. Jolliffe and S. Perrier, *Angewandte Chemie International Edition*, 2018, **57**, 16678-16682.
46. R. J. Brea, M. E. Vázquez, M. Mosquera, L. Castedo and J. R. Granja, *Journal of the American Chemical Society*, 2007, **129**, 1653-1657.

Chapter 2 Design and synthesis of cyclic peptide-polymer-dye conjugates to probe their dynamics.

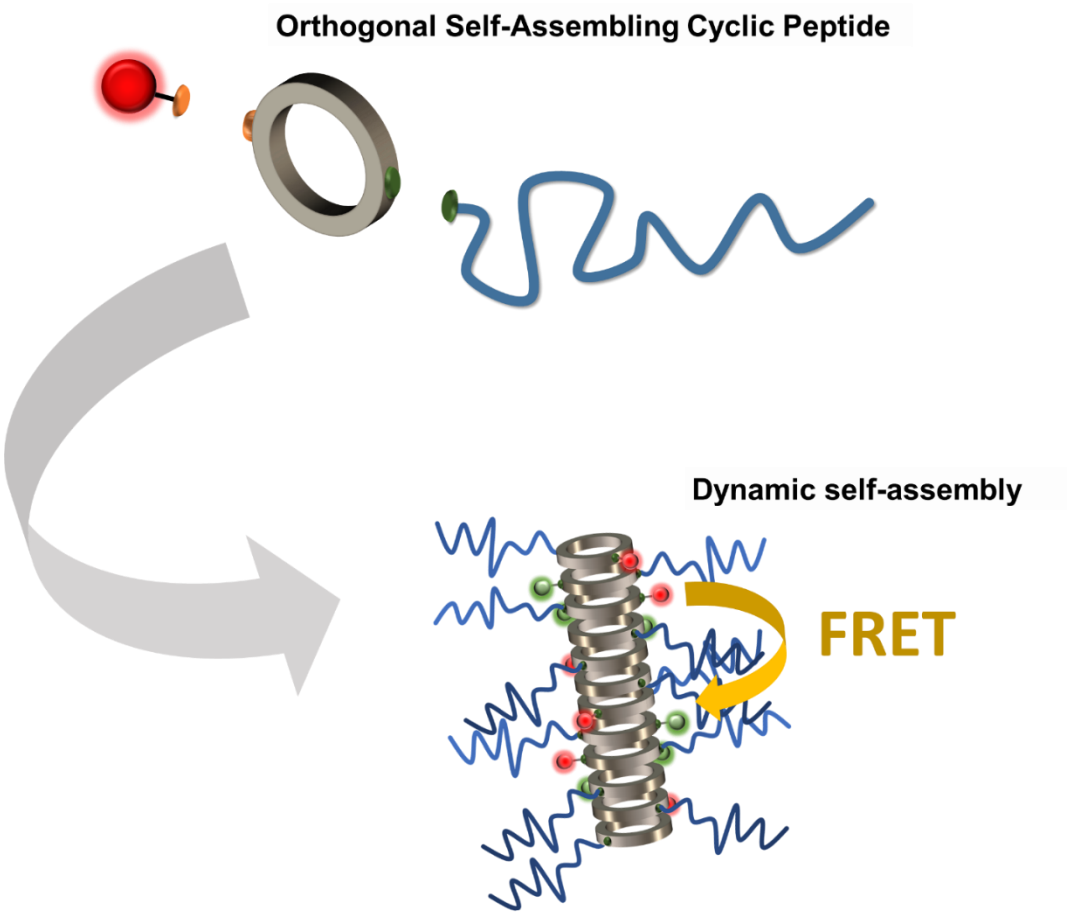

2.4 Introduction

Recently, attention has been focused on designing supramolecular systems that are increasingly relevant for biomedical applications.[1-3] Self-assembling cyclic peptide nanotubes in particular have garnered interest in this field, as they can be easily modified for range of therapeutics. A key advantage of these systems is their built in functionality, the R-group of the amino acids can either contain functionality itself, such as a charge, but equally be used as a conjugation site for post-modification. Our group have previously used both convergent and divergent methods to create cyclic peptide-polymer conjugations.[4]

As for these and other similar supramolecular structures, it remains unclear whether the self-assembled aggregates remain kinetically stable or dynamic in biological environments. Understanding the self-assembly behaviour is of paramount importance to explain and predict their performance *in vitro* and *in vivo* studies; and why an in-depth study into the dynamic nature of CP-polymer conjugates is imperative.

Herein, we designed CP-polymer conjugates modified with fluorescent dyes and used Förster resonance energy transfer (FRET) to probe the dynamic nature of the resulting nanotubes. Fluorescence is a powerful tool to study close intramolecular interactions and investigate the dynamic behaviour of supramolecular systems. [5,6] In the context of cyclic peptides, Granja *et al.* previously employed FRET to study the hydrogen-bonding interaction of small dimeric cyclic peptides.[7] Herein, we propose to use FRET to gain an insight into the stacking of cyclic peptide nanotubes (CPNTs) *in situ* and provide vital information about the dynamics of these one-dimensional supramolecular structures. To gain a detailed understanding, key parameters such as solvent and concentration were varied, and their influence on the assembly process was studied.

We know the conjugation of water-soluble polymers was vital to improve their solubility, therefore new water-soluble FRET dye conjugates were built to study the effect of environment on supramolecular dynamics. In this chapter, using a ‘bottom up’ approach, the design, synthesis and characterisation of asymmetric model conjugates, which contain both a dye and polymer, were established.

2.5 Results and Discussion

2.5.1 Synthesis of asymmetric orthogonal cyclic peptide

In order to investigate the dynamics of self-assembled cyclic peptide–polymer nanotubes, a new class of dye-conjugated peptides was synthesized. To infer information about the kinetic exchange of these systems, each cyclic peptide required the conjugation of a single FRET dye to its periphery. Using a "bottom up" approach, a sequence of amino acids was designed to yield an asymmetric cyclic peptide, which could be used to conjugate both a dye and polymer in an orthogonal manner.[8] The bespoke asymmetric cyclic peptide **3** was used in this study, contained both an azide and amine moiety on its periphery.

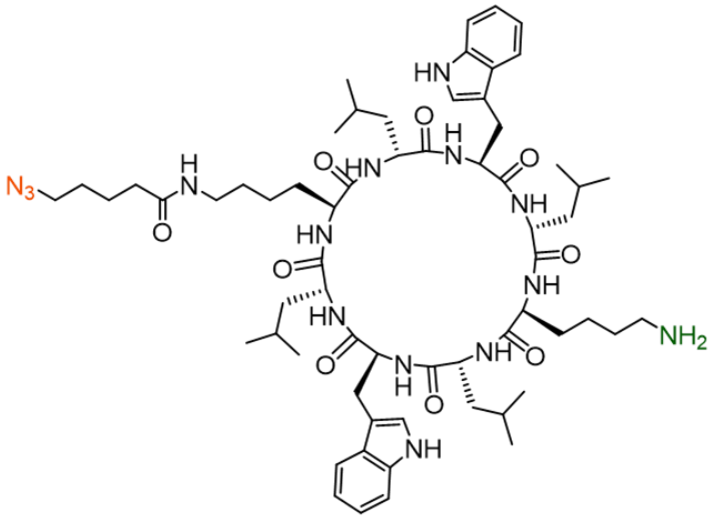

3

Figure 2.1 Chemical structures of asymmetric cyclic peptide for orthogonal conjugation.

The linear octa-peptide was synthesised using solid phase peptide synthesis from the 2-chlorotrityl resin. With the exception of the azide containing amino acid synthesised in our group according to the literature,[8] all other amino acids were purchased from Iris Biotech GmbH. The linear octa-peptide (**1**) was grown in a stepwise fashion *via* solid phase peptide synthesis (SPPS), see Scheme 2.1. The Fmoc procted amino acids were sequentially deprotected and reacted to the growing peptide chain on the resin. 1- [Bis (dimethyl amino) methylene] -1H -1,2,3 - triazolo [4,5-b] pyridinium 3-oxid hexa fluoro phosphate (HATU) and 2- (1H - benzotriazol-1-yl) - 1,1,3,3 – tetra methyl

uranium hexa fluoro phosphate (HBTU) was used to activate the peptide coupling. Detailed synthetic procedure can be found in the experimental.

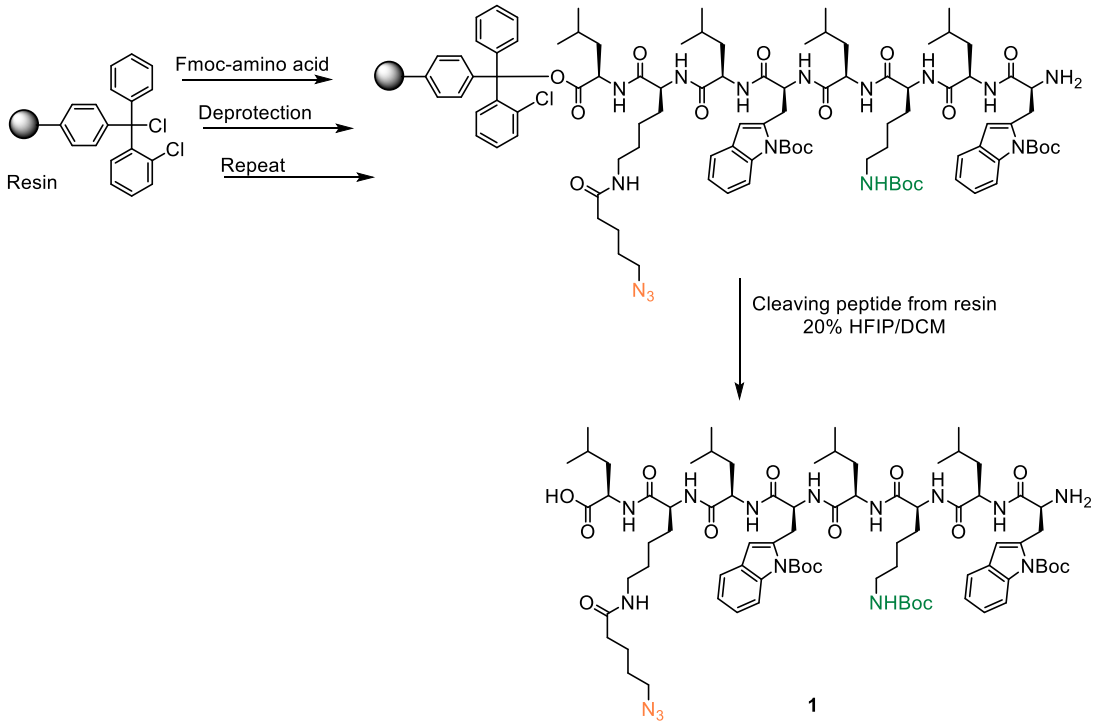

Scheme 2.1 Simplified scheme to make alternating D- and L- linear octa-peptide using solid phase peptide synthesis (SPPS).

This resin releases the peptide in the presence of a mild acid selectively without disturbing the Boc groups on the peptide. The linear peptide (**1**) was collected, purified and analysed *via* proton nuclear magnetic resonance (^{1}H NMR), high performance liquid chromatography (HPLC) and electrospray ionisation time-of-flight (ESI-ToF) mass spectrometry – see experimental and appendix for spectra. Proton NMR of the compound was assigned fully, notably the spectra showed the target compound with some residual hexafluoroisopropanol (HFIP) and DMF. ESI-ToF mass spectroscopy qualitatively confirmed the formation of the linear peptide exclusively, see (Figure 2.2).

The coupling agent 4- (4,6- dimethoxy - 1,3,5 - triazin-2-yl) – 4 – methyl morpholinium tetra fluoroborate (DMTMM · BF_4) was used for the cyclisation, see Scheme 2.2. During the activation of the C-terminus on the peptide, the base 4-methylmorpholine (NMM) was produced causing the reaction to auto-accelerate without the need of additional base. This reduces the concentration of base in the

system which can scramble the stereochemistry of terminal amino acids. For this reason, DMTMM · BF_4 was used to reduce the chance of epimerization and maximise the formation of the desired flat ring-like cyclic peptide.[9] The cyclisation was also performed at high dilution to avoid intermolecular coupling and promote intramolecular cyclisation. The orthogonal Boc protection groups enable the coupling to only take place at the ends of the peptide. In order to purify the peptide, precipitation in ice-cold methanol was used to remove impurities. As racemised or truncated linear peptide will not form the planar cyclic structure needed for self-assembly, these peptides remain in solution whilst the CPs with the correct conformation form aggregates and precipitate. NMR and ESI-ToF analysis show the Boc protected cyclic peptide (**2**) – see appendix and Figure 2.2, respectively.

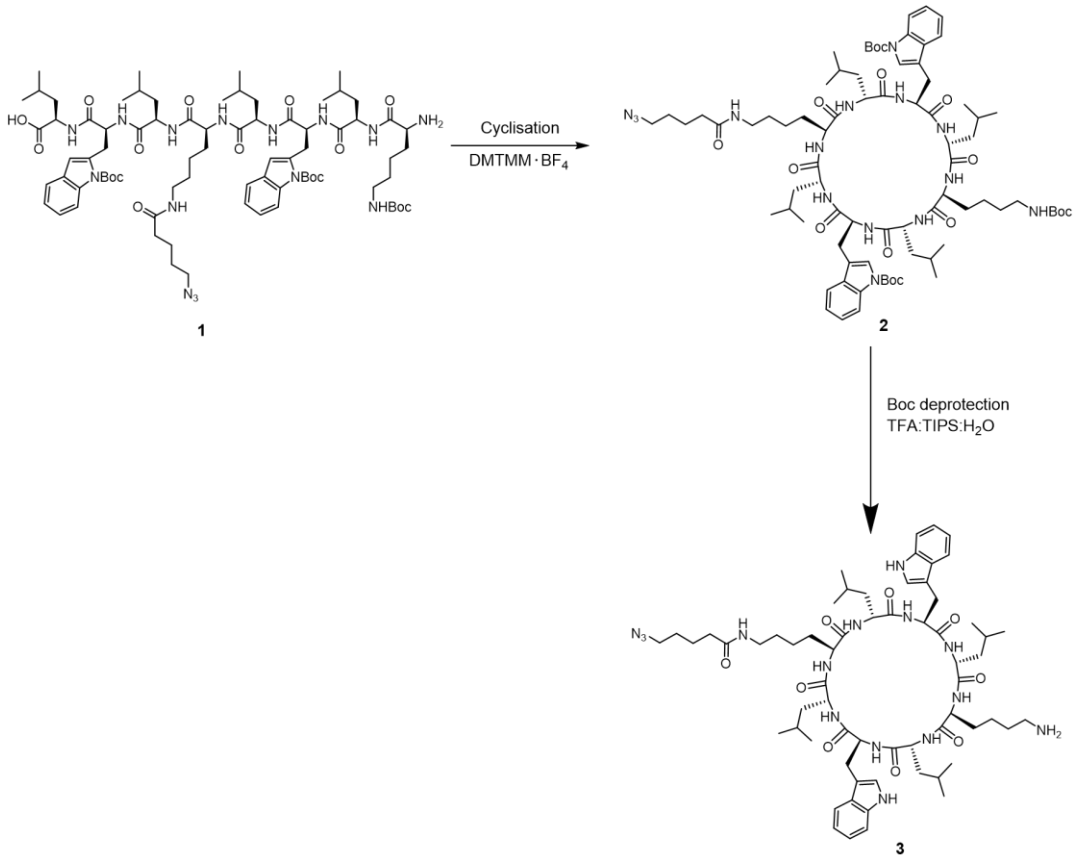

Scheme 2.2 Cyclisation of linear octa-peptide (**1**) to form protected cyclic peptide (**2**). Boc deprotection of the cyclic peptide using TFA, TIPS and H_2O to give the asymmetric azide amine cyclic peptide (**3**).

A mixture of trifluoroacetic acid (TFA), triisopropylsilane (TIPS) and H_2O (18:1:1 vol ratio) was used to deprotect the Boc groups from the cyclic peptide, see Scheme 2.2.

The reaction was followed by ESI-ToF mass spectrometry. After 3 hours the peak associated with the protected cyclic peptide disappeared. The reaction mixture was precipitated in diethyl ether to give a pure product characterised by ESI-ToF mass spectra and ^{1}H NMR – see Figure 2.2 and Appendix, respectively. As purification was completed *via* precipitation, no preparative HPLC was needed for this step.

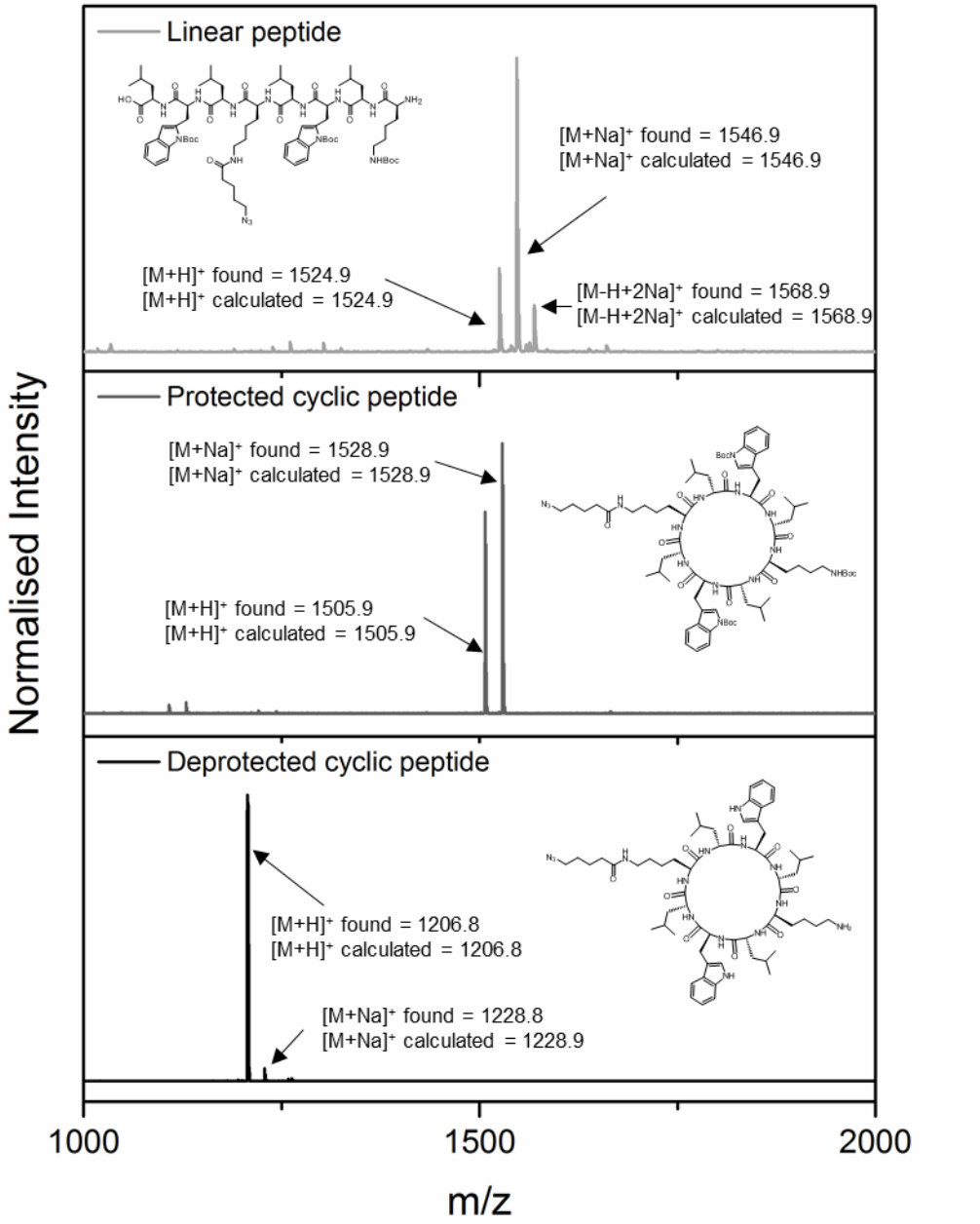

Figure 2.2 Electron Spray Ionisation – Time of Flight (ESI-ToF) mass spectra of the linear peptide (**1**), protected cyclic peptide (**2**) and deprotected cyclic peptide (**3**).

2.5.2 Synthesis of the cyclic peptide-pyrene/napthalimide conjugates

The first FRET pair attached on the cyclic peptide was the pyrene (PYR) donor and napthalimide (NTI) acceptor. These dyes are relatively inexpensive compared to other commercially available FRET pairs, making them more suitable for the development and optimisation of these systems. The coupling of the dye to the cyclic peptide required an efficient chemistry to yield only the conjugate and excess dye, importantly leaving no unmodified cyclic peptide which would be difficult to purify. For this reason, our group has utilised amide bond forming coupling chemistry, which not only efficiently functionalises the CP but result in a stable bond which is not disturbed once formed. One method to activating the carboxylic acid group to reaction with the amide moiety on the CP, is by functionalising it with a good leaving group such as *N*-hydroxysuccinimide (NHS). The coupling agent 1-ethyl-3- (3-dimethylaminopropyl) carbodiimide (EDC) was used to attach the NHS group onto the carboxylic acid on the dye (Figure 2.3).

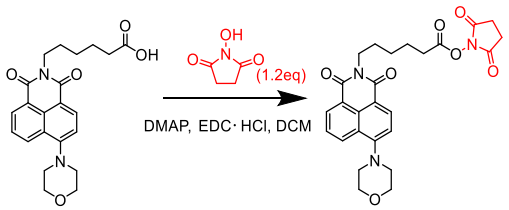

Figure 2.3 Synthetic route to NHS-functionalised napthalimide (NTI) dye.

Using the amine group on the asymmetric cyclic peptide, we can selectively attach the dye to a specific site on the molecule. Independently, the NHS-functionalised pyrene or napthalimide was reacted with the peptide to yield the cyclic peptide-pyrene (CP-PYR) or cyclic peptide-napthalimide (CP-NTI) conjugates respectively.

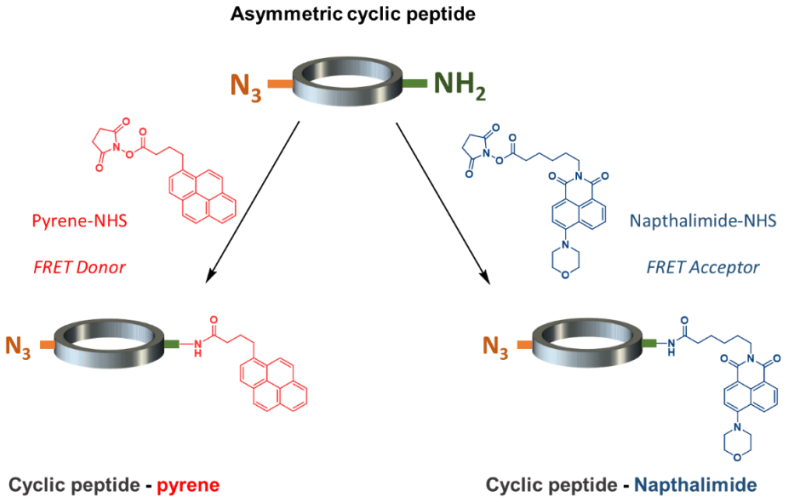

Scheme 2.3 Schematic representation of the synthetic route to the cyclic peptide-dyes.

Due to the strong hydrogen bonds between the CPs, which cause the formation of the nanotubular assemblies, strong hydrogen bond competitive solvents were needed to break up these aggregates to perform the conjugation reactions.[10] Therefore, either DMSO or DMF were used to ensure the cyclic peptides remained in solution during the coupling reaction. A base was also introduced to ensure the amine group of the lysine was deprotonated and able to couple with the dye.

After verifying the product qualitatively *via* ESI-ToF mass spectrometry, the purification was attempted using a number of different precipitation solvents such as ice-cold acetone, methanol and THF. Purification of this reaction proved to be extremely difficult because of the similarity in solubility of dye and CP-dye conjugate in most solvents. Under these conditions both the dye and CP-dyes remained in solution and no precipitate was formed. Finally, ice-cold toluene was used to precipitate the CP-dyes whilst the dye remained in supernatant.

HPLC analysis of these compounds were attempted, however, the CP-dye conjugates were insoluble in the solvents needed to run the samples, such as acetonitrile and methanol, due to their hydrophobicity. The signals obtained were therefore weak and inconclusive. ESI mass spectrometry and proton NMR of the CP-PYR (**4**) and CP-NTI (**5**) conjugates were therefore used to confirm the product, this can be found in Figure 2.4 and experimental.

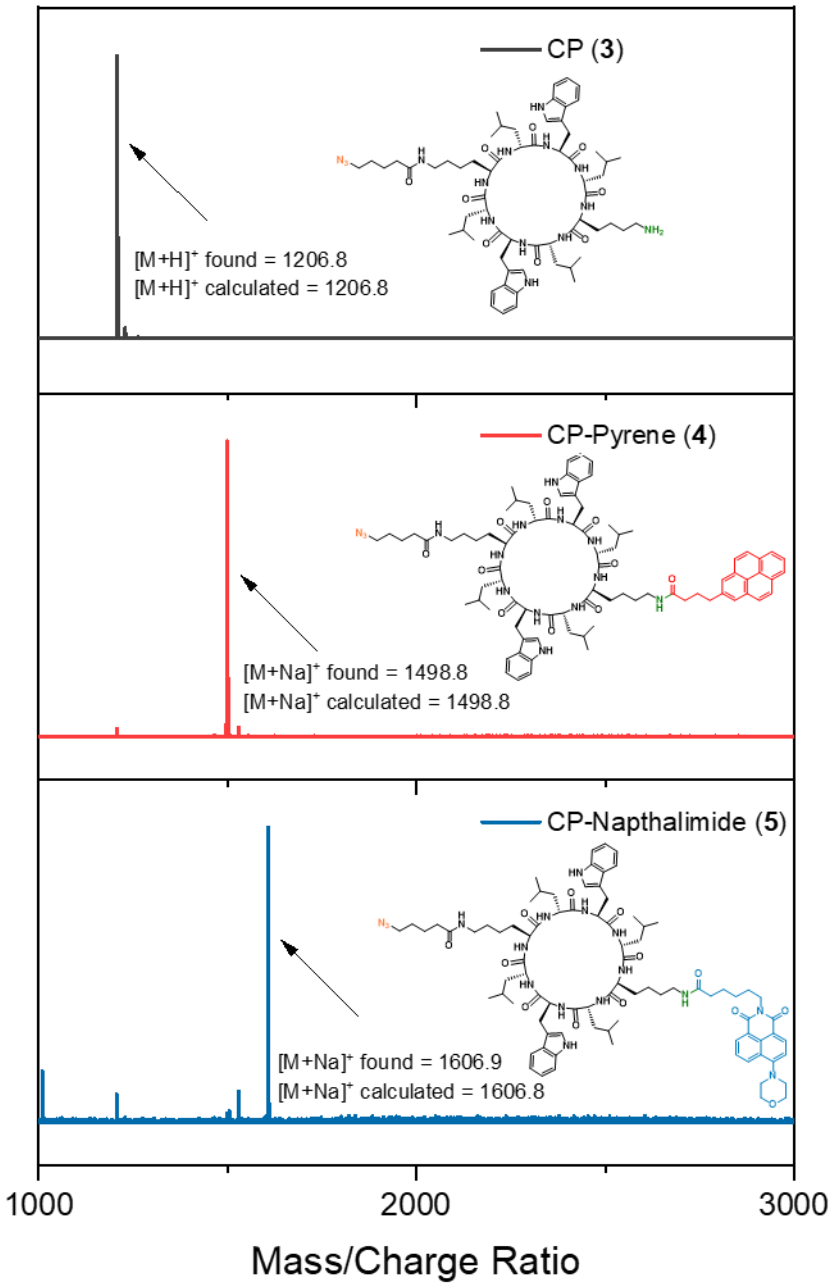

Figure 2.4 ESI-ToF Mass spectra of the deprotected cyclic peptide (**3**), the pyrene conjugated cyclic peptide (**4**) and the napthalimide conjugated cyclic peptide (**5**).

2.5.3 Synthesis of the cyclic peptide-pyrene/napthalimide-polymer conjugates

To provide solubility in water these conjugates were modified with a poly (ethylene glycol) (PEG) polymer. PEGylation not only improved the solubility of the CPs in a

range of solvents, but also prevents the nanotubes from laterally aggregating and precipitating. The orthogonality of the peptide enables us to attach the polymer on the peptide using the azide group. Importantly, to study the mixing of these conjugates in solution each peptide must contain a dye and polymer.

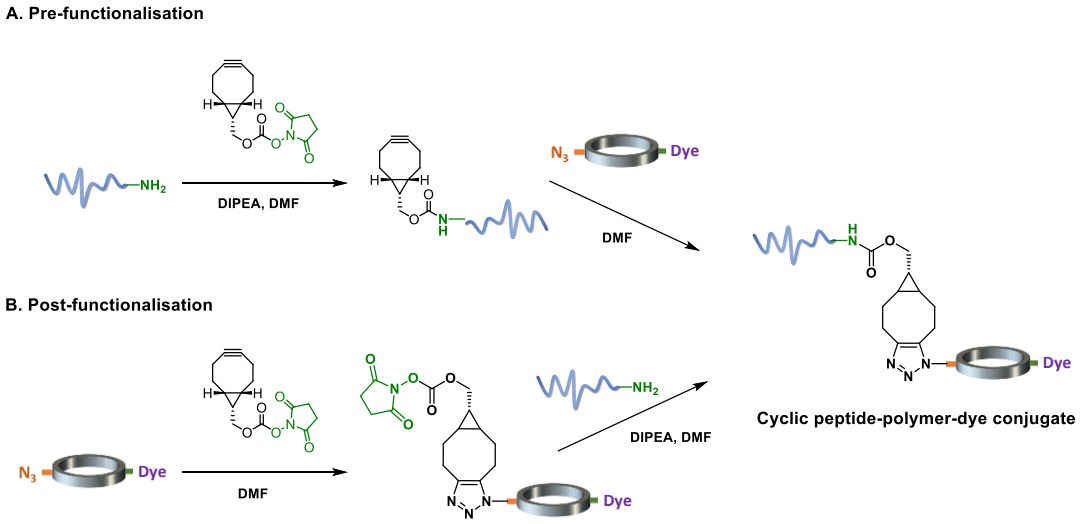

Scheme 2.4 a) Pre-functionalisation and b) Post-functionalisation methods to attaching the polymer to the CP-dye conjugates.

The pre-functionalisation method required first modifying the polymer with a strained alkyne. This was done using an NHS-amine coupling reaction (Scheme 2.5a). As a result, the PEG was modified with a strained alkyne, ready to react with the azide on the peptide. Due to the highly insoluble cyclic peptide-dye compounds, size exclusion chromatography in DMF was used to observe the disappearance of the cyclic peptide upon conjugation. DMF is a good solvent for cyclic peptides as the solvent can compete with the hydrogen bonding sites of the cyclic peptide, therefore disrupting the self-assembly between the CPs. After 3 days mixing the azide functionalised cyclic peptide-napthalimide (CP-NTI, **5**) and strained alkyne modified PEG (20kDa), two distributions could be observed in the SEC trace, see Figure 2.5. The first lower molecular weight distribution is similar to the cyclic peptide or cyclic peptide-dye, the second larger molecular weight distribution is close that of the free polymer. This suggests that there was still a lot of unreacted cyclic peptide-dye in the reaction mixture.

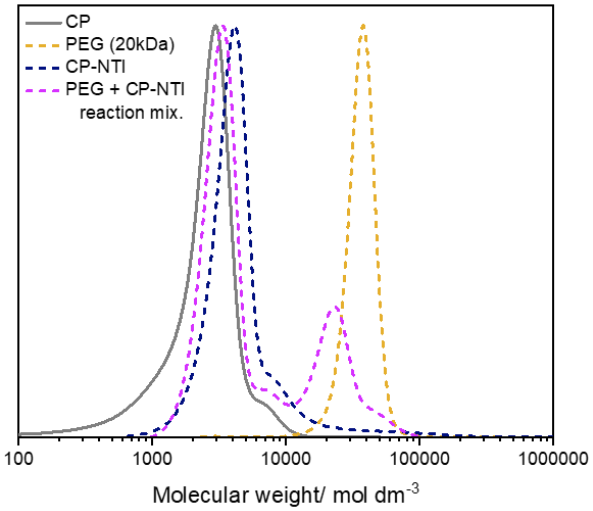

Figure 2.5 SEC chromatograph in DMF with 0.1% LiBr comparing the cyclic peptide (CP), polymer (PEG-NH_2 20kDa), cyclic peptide-napthalimide (CP-NTI) conjugate and the reaction mixture of CP-NTI and PEG using the first approach (pre-functionalisation).

Next, the post-functionalisation method was attempted, see Scheme 2.5b. Using the same chemistry in the reverse order, the azide functionalised CP-dye is reacted with a strained alkyne-NHS group (BCN-NHS) first. This formed a NHS functionalised cyclic peptide-dye conjugate which could be reacted with the amine functionalised PEG polymer. After the conjugation, no lower molecular weight distribution associated with the cyclic peptide-dye was observed. This suggested the all the CP-dye was reacted with polymer.

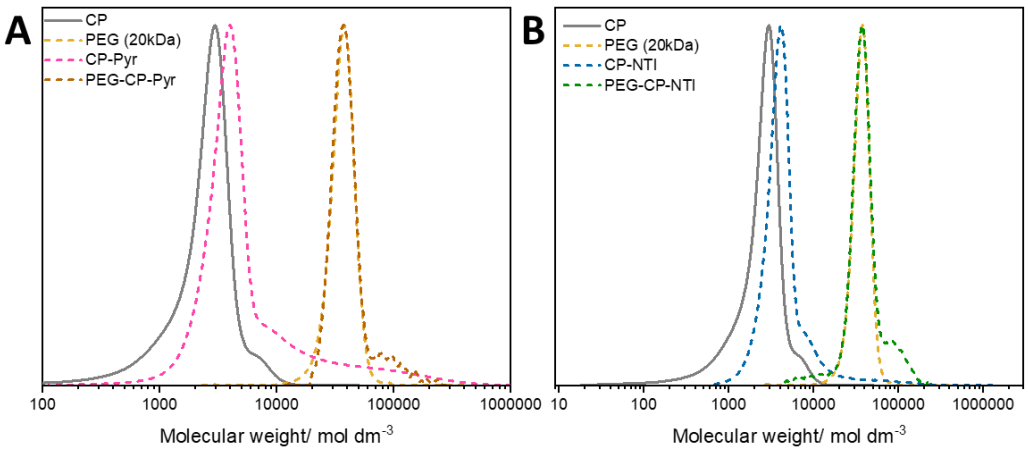

Figure 2.6 SEC chromatograph comparing the cyclic peptide (CP), polymer (PEG-NH_2 20kDa), cyclic peptide-dye conjugate and the reaction mixture of CP-NTI and PEG using the second approach (post-functionalisation).

The attachment of the hydrophilic polymer lead to a substantial improvement in the solubility of the CP conjugates. As the cyclic peptides assemble in H_2O a significant amount of the polymer conjugates could be recovered while removing any free polymer or residual small molecules *via* dialysis. Also, the improved hydrophilicity of the conjugates meant it was possible run them in a reverse-phase HPLC. The UV detector on the HPLC was set to the 280 nm which corresponds to the tryptophan on the cyclic peptide. The fluorescence detector was set to the relative excitation and emission maxima of the dye (pyrene or napthalimide). Strong fluorescence and UV signals were detected from the compounds with one clear major compound and some minor impurity, see Figure 2.7.

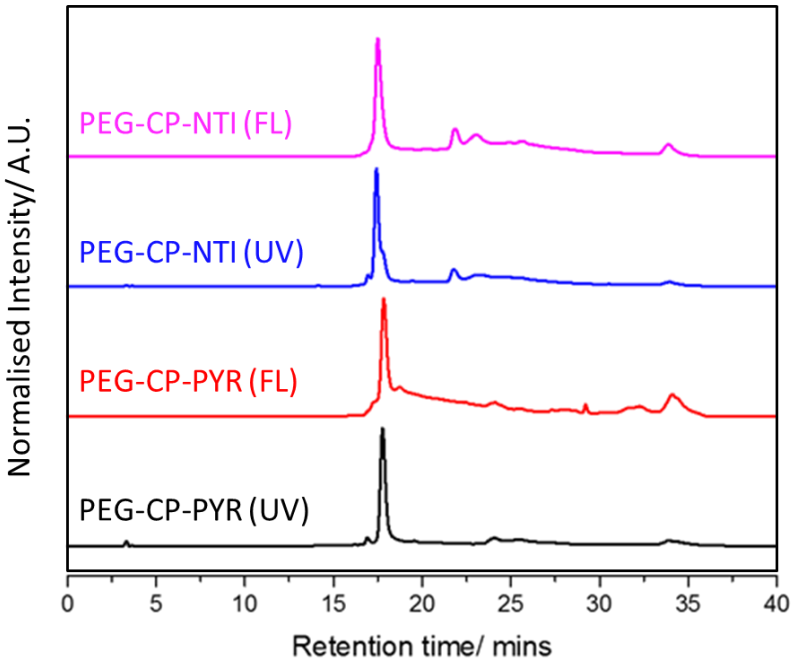

Figure 2.7 Normalised HPLC of PEG-cyclic peptide-dyes (PEG-CP-NTI). UV detector set to 280nm (tryptophan in the CP) and the fluorescence set to emission of the dyes.

2.5.4 Dynamics of the cyclic peptide-pyrene/napthalimide-polymer conjugates

Pyrene has two distinctive qualities; firstly it has an exceptionally long excited state lifetime and, secondly, it can form excimers with itself.[11] The formation of this excimer can be observed when two pyrene molecules are stacked on top of each other. This arrangement enables the energy transfer between the excited pyrene and a ground-state pyrene to take place leading to a characteristic emission band around 475 nm. Excimer formation has been utilised to observe the dynamic behaviour of phospholipids in membrane bilayers.[5] Pyrene can also behave as a donor for Förster resonance energy transfer (FRET) with napthalimide as an acceptor. This use of fluorescence energy transfer has been widely adopted to look at intermolecular interactions on the molecular or cellular levels. FRET utilises its proximity dependent mechanism to investigate the distance from two molecules.[12] For this energy transfer to take place two prerequisites must be met. Firstly, the emission band of the donor must overlap with the excitation of the acceptor molecule. Second, for an efficient energy transfer the donor and acceptor molecules must be within 1-10 nm of each

other. Granja *et al.* previously synthesised N-methylated dimeric cyclic peptides with pyrene (electron donor) and dapoxyl (electron acceptor) FRET pairs.[7] Nevertheless, for cyclic peptides, which form self-assembling nanotubes, these dynamics have not been studied so far. Especially, in the case of cyclic peptide-polymer conjugates, this knowledge is crucial to fully understand their self-assembly behaviour.

In this FRET system, pyrene was used as the donor and napthalimide (NTI) was used as the acceptor. Figure 2.8b clearly shows the emission band of the pyrene conjugate and excitation band of the napthalimide conjugate overlaps, fulfilling our first requirement for FRET to take place. Next, using the second requirement which is the proximity, we can relate the FRET behaviour to the conjugates being close to each other, i.e. in the same nanotube (Figure 2.8a). The distance between two cyclic peptides is4.5 Å, so if the dyes are with a few units of an assembled nanotube FRET should be observed.

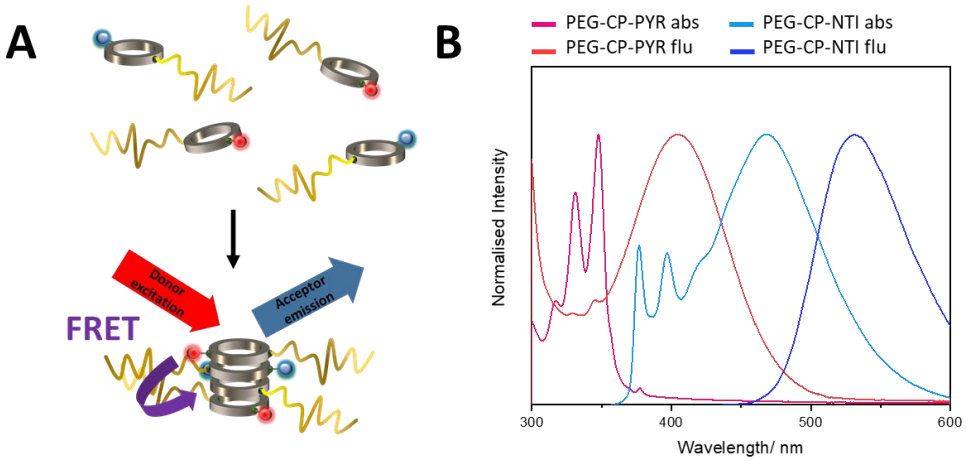

Figure 2.8 Normalised absorption and fluorescence spectra of the pyrene and napthalimide conjugate (PEG-CP-PYR, **6** and PEG-CP-NTI, **7**). The emission spectra of the donor (PEG-CP-PYR) overlaps with the excitation of the acceptor (PEG-CP-NTI).

Pyrene and napthalimide are inexpensive dyes compared to other commercial FRET dyes; this was the main reason for why they were used during the optimisation of the synthesis. However it is worth noting they have some limitations as a FRET pair. The excimer band (~ 475 nm) overlaps with the emission spectra of the napthalimide (~ 525 nm) this makes it difficult to observe the emission of the acceptor directly. Also, there is some direct excitation of the acceptor at the absorption maxima of donor (λ

$_{max}$ ~ 350 nm) which can artificially increase the FRET emission, therefore leading to some acceptor emission not due to the energy transfer. In an ideal FRET system, upon excitation of the donor the resulting emission of the donor can excite the acceptor and therefore an emission of the acceptor is observed. The extent of FRET is often quantified as the following ratio,

$$FRET\ ratio = \frac{emission\ of\ acceptor^*}{emission\ of\ acceptor * + emission\ of\ donor^*} \qquad (1)$$

* upon excitation of donor.

For this reason, once the synthetic procedure of these dyes were optimised, the conjugates were remade using the Cyanine 3 and 5 (Cy3 and Cy5). This well-studied commercial FRET pair was able to circumvent the key spectral issues surrounding the pyrene and napthalimide dyes.

2.5.5 Synthesis of Cyclic Peptide-Cyanine Dye-Polymer Conjugates

In order to investigate the dynamic kinetics of self-assembled cyclic peptide–polymer nanotubes, a new library of dye-conjugated peptides was synthesized. To infer information about the kinetic exchange of these systems, Cyanine 3 and 5 dyes were conjugated to peptide as a FRET donor and acceptor pair.

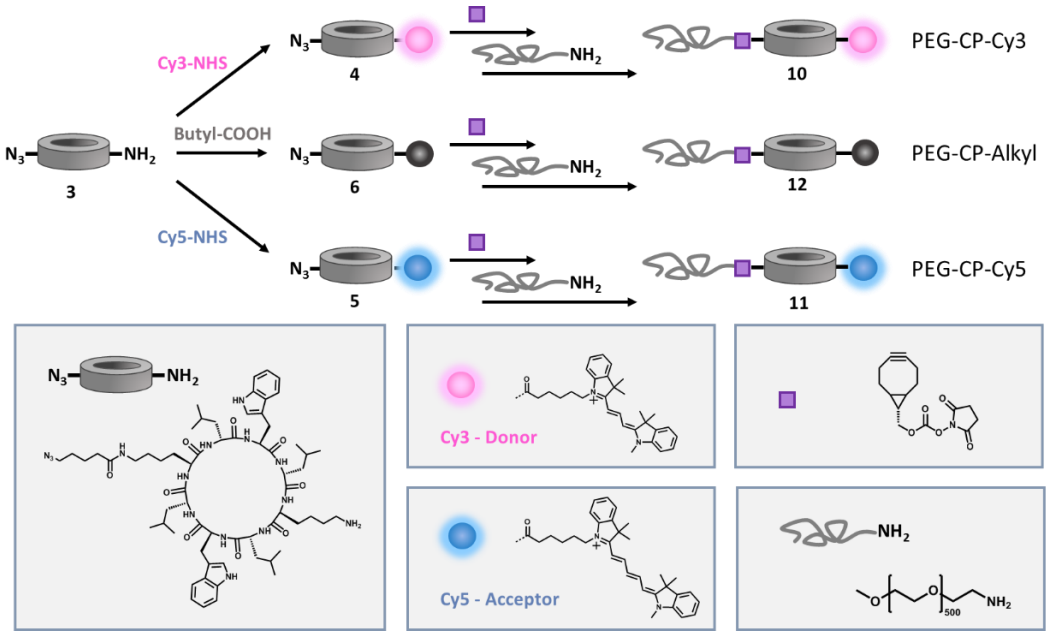

Scheme 2.5 Schematic representation of the synthesis of cyclic peptide-dye-polymer conjugates.

Using the attachment chemistry previously developed, the FRET dyes were conjugated onto the cyclic peptide *via N*-hydroxysuccinimide (NHS)–amine coupling. The efficiency of this step was assessed using high pressure liquid chromatography (HPLC) and was shown to be quantitative, enabling the FRET emission to directly inform us of the exchange kinetics of the supramolecular system. Cyanine FRET dyes Cy3 and Cy5 were also chosen as the FRET pair as their high extinction coefficients enable the detection of FRET at very low concentrations. Additionally, the spectral overlap of these dyes is ideal to avoid undesirable excitation of the acceptor. Unlike the pyrene and napthalimide dyes which were used previously, there is little to no direct excitation of the acceptor at the absorption maxima of the donor. Moreover, the absence of the excimer band makes it easier to quantify the emission from the acceptor.

The Cyanine dyes and their equivalent conjugates were significantly less hydrophobic than those with pyrene and napthalimide, therefore, could be dissolved in a range of different polar solvents. This made it possible to characterize the dye-functionalization of the conjugates *via* electrospray ionization time-of-flight (ESI-ToF) mass spectrometry (Figures 2.10) and HPLC equipped with ultraviolet (UV) and fluorescence detection (Figures 2.9). This method to characterise these compounds qualitatively (ESI-ToF) and quantitatively (HPLC) was particularly valuable, as these techniques do not require large sacrificially amounts of these expensive compounds.

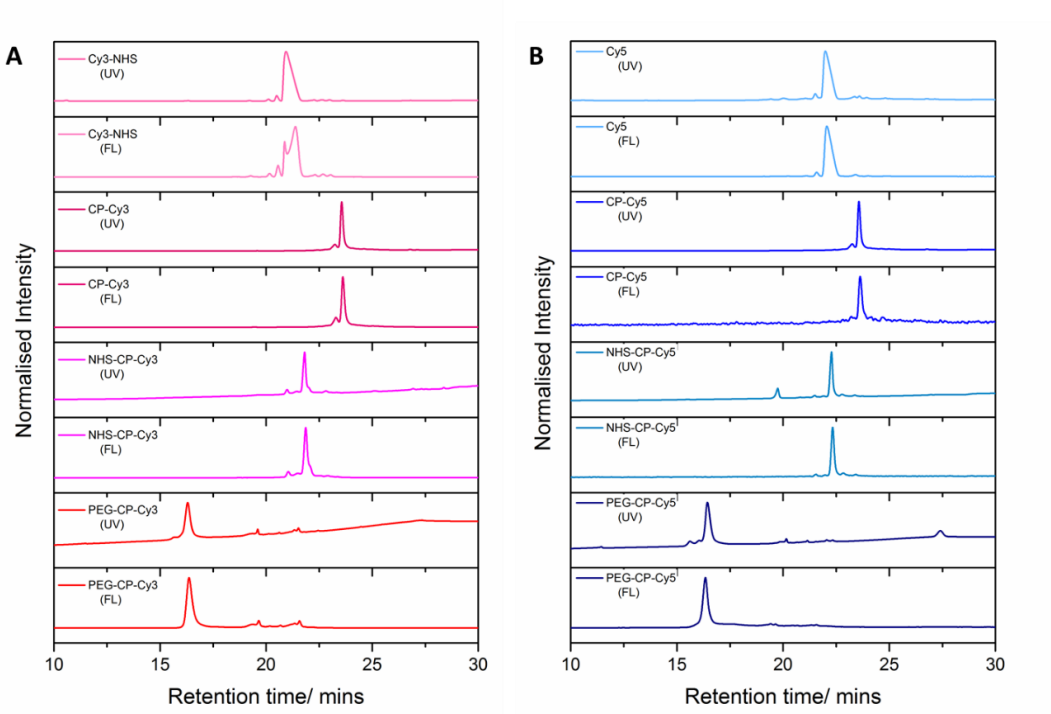

Figure 2.9 High performance liquid chromatographs (HPLC) of the a) donor conjugates and b) acceptor conjugates. Cyanine 3 and 5 were also measured to compare the polarity of the conjugates to the free dyes.

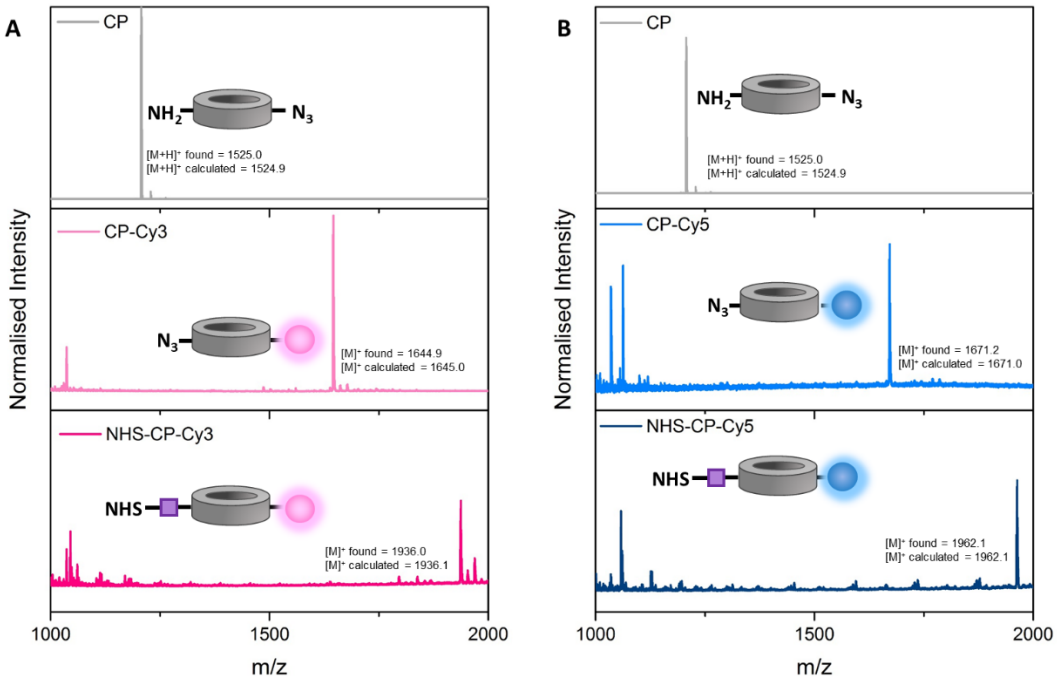

Figure 2.10 Electron spray – Time of Flight (ESI-ToF) mass spectra of the a) asymmetric cyclic peptide, cyclic peptide-Cy3 conjugate (CP-Cy3) and NHS-

functionalised cyclic peptide-Cy3 conjugate (NHS-CP-Cy3). b) ESI-ToF spectra of the equivalent Cy5 conjugates.

A non-fluorescent conjugate was also synthesized as a control. For this conjugate to best mimic the self-assembly of the dye-functionalized conjugates, the free amine of the lysine residue was converted to an amide group, by conjugation with valeric acid using the peptide coupling agent 1-[Bis(dimethylamino) methylene] -1H-1,2,3-triazolo [4,5-b] pyridinium 3-oxid hexa fluoro phosphate (HATU) (Scheme 3.1). The alkyl chain on the valeric acid replicates the alkyl linker on the NHS-functionalized dyes. Once again, ESI-ToF was used to qualitatively confirm the cyclic peptide with the alkyl chain, Figure 2.11.

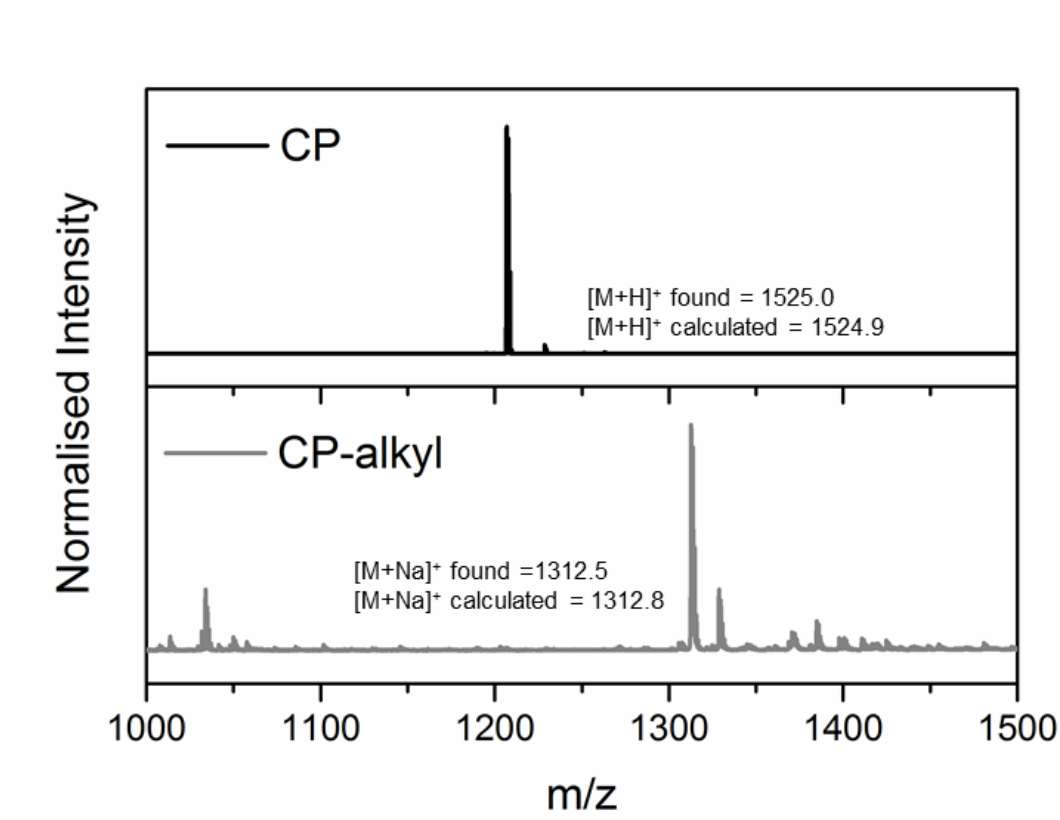

Figure 2.11 Electron spray ionisation – Time of Flight (ESI-ToF) mass spectrometry of the asymmetric cyclic peptide and cyclic peptide with the control alkyl chain without the dye (CP-Alkyl). The NHS-functionalised CP-Alkyl conjugate was not soluble to perform ESI-ToF.

Using the same synthetic protocol developed previously, the post-functionalisation method was used to conjugate the water-soluble polymer to the cyclic peptide to

control the length of the tubular assembly and prevent lateral aggregation. The ESI-ToF was used to confirm the NHS-functionalisation of the CP conjugates, see Figure 2.10.

This time, the NHS-functionalisation could be quantified using HPLC due to the solubility and clear shift in hydrophilicity between the CP-dye and NHS-CP-dye compounds (Figure 2.9). Upon conjugation of the PEG polymer to the cyclic peptide a large shift to lower retention time in the reverse-phase HPLC was observed. This shows the conjugation of the hydrophilic polymer significantly increased the hydrophilicity of the cyclic peptide containing conjugate.

The change in polarity in the HPLC was also used to confirm the conjugation and purity of the control CP-polymer conjugate. Due to the absence of a fluorescent dye to follow in the HPLC, for the PEG-CP-alkyl conjugate, multiple UV absorption detectors were used to follow the polymer at 220 nm and the tryptophan on the cyclic peptide at 280 nm. As expected the cyclic peptide can be seen in both the 220 nm and 280 nm wavelength detector; the PEG polymer only shows very weak absorption at 220 and no signal at 280 nm. Upon PEG conjugation a clear shift between the unfunctionalised cyclic peptide, free polymer and conjugate (PEG-CP-Alkyl) can be observed. Notably, the PEG-CP-Alkyl compound shows strong absorption at the same retention time in both 220 nm and 280 nm UV-HPLC spectra.

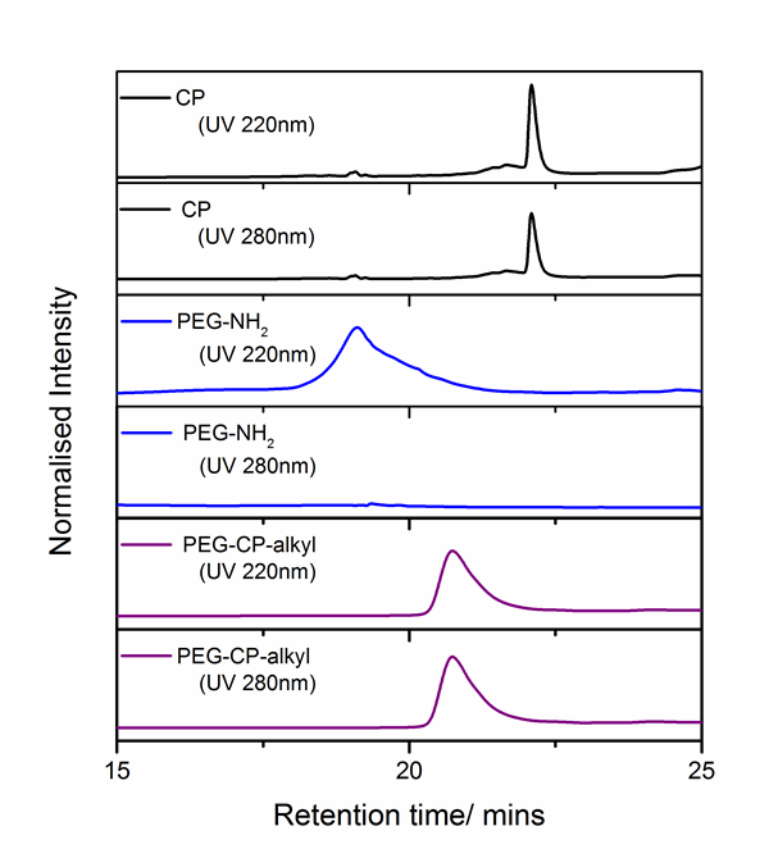

Figure 2.12 High performance liquid chromatographs (HPLC) of the asymmetric cyclic peptide, poly (ethylene glycol) (PEG 20kDa) polymer and the control conjugate with the absence of a FRET dye.

2.6 Conclusion

In this chapter, a new class of self-assembling cyclic peptides were developed to study their dynamic behaviour. Using FRET dyes on the periphery, which are proximity-dependent, the mixing of dye conjugates could be used to directly inform us of the exchanging CPs between the supramolecular assemblies. The focus on developing these systems for biological applications has given rise to a variety of water-soluble nanotubular structures, by attaching hydrophilic polymers to the peptide. As both the dye and polymer are essential to the monitoring and composition, a 'bottom up' approach was used to synthesise an asymmetric self-assembling peptide, with two different conjugation sites. The orthogonality of the azide and amine on the cyclic peptide enabled us to selectively attach both a dye and polymer to the periphery.

The dyes used here were carefully selected for the spectral properties as FRET pairs. Using the conjugates developed here, the next chapter will delve into the effect of environment can have on the exchange of unimers in a supramolecular system. More importantly, the design and synthesis of these orthogonal conjugates are not limited to cyclic peptide; this method can be used to measure the dynamics of a host of supramolecular polymers.

2.7 Experimental

2.7.1 Material

Fmoc-protected amino acids and coupling agents were purchased from Iris Biotech GmbH. Napthalimide carboxylic acid was gifted from Dr Benjamin M Long in the Jolliffe group at the University of Sydney. The amine functionalized PEG was purchased from Rapp Polymere. All other chemicals stated were purchased from Sigma-Aldrich, (Gillingham, UK) unless otherwise stated. Solvents were purchased from several departmental suppliers— Honeywell, Fisher and Sigma-Aldrich.

2.7.2 Characterisation

2.7.2.1 Nuclear magnetic resonance spectroscopy (NMR)

^{1}H NMR spectrum were measured using a Bruker DPX-300 or DPX-400 NMR spectrometer which operated at 300.13 and 400.05 MHz respectively. The residual solvent peaks were used as internal references. Deuterated trifluoroacetic acid (*d*-TFA) (δ_H = 11.5 ppm) was used to measure the peptides.

2.7.2.2 Size-exclusion chromatography (SEC) / Gel permeation chromatography (GPC)

The size-exclusion chromatograms (GPC) were measured using an Agilent PL50 instrument with a differential refractive index (DRI) detector. The instrument contained two PolarGel D columns (linear MW operating range: 200 to 400,000 g/mol (PS equivalent)) and a PolarGel 5μm guard column. DMF with 0.1% LiBr additive was used as the eluent. The system ran at 1 mg/min (50ºC), with an injection volume of 100 μL. The samples were prepared by filtering them through 0.22 μm pore size membranes, before injection. Agilent EasyVial poly (methyl methacrylate) standards were used to calibrate the instrument and output data was analysed using Agilent GPC/SEC software.

2.7.2.3 Vibrational spectroscopy - Infrared Spectra

Attenuated total refection (ATR) Fourier transform infrared (FTIR) spectra was measured using a Bruker Vector 22 FT-IR spectrometer.

2.7.2.4 Ultraviolet/visible (UV-vis) absorption spectroscopy

UV-vis absorption spectra was measured using an Agilent Technologies Cary 60 UV-Vis spectrometer. The total concentration of the samples were kept to 35 μM.

2.7.2.5 Fluorescence emission spectroscopy

Fluorescence emission spectra was measured using an Agilent Technologies Cary Eclipse Fluorescence spectrometer. The total concentration of the samples were kept to 35 µM.

Mixing study (PEG-CP-PYR and PEG-CP-NTI): First, 35 µM stock solutions of PEG-CP-PYR and PEG-CP-NTI were prepared in the water. The emission spectra of the PEG-CP-PYR was measured before the addition of the PEG-CP-NTI conjugate. Upon mixing, the fluorescence emission spectra was taken using the Agilent Kinetic software. The excitation of the donor was set to 345 nm.

2.7.2.6 High performance liquid chromatography (HPLC)

High performance liquid chromatograms (HPLC) was measured using an Agilent Technologies 1200 Series, equipped with a Luna 5u C18 100 Å, 250 x 4.6 mm column. Solvent mixtures of Methanol/Water and Acetonitrile/Water were used. All solvents contained 0.05 vol% TFA.

Method

Time/ mins	Water + 0.05% TFA	Acetonitrile + 0.05% TFA
0	5	95
5	5	95
25	95	5
30-35	95	5
35	5	95

2.7.2.7 Mass spectrometry (ESI-TOF)

Electronspray ionisation (ESI) – time of flight (TOF) mass spectra (MS) was measured using a Bruker MicroTOF to characterise the peptides (linear and cyclic). Samples were dissolved in methanol. The instrument can achieve less than 5 ppm mass accuracy.

2.7.3 Peptide Synthesis

2.7.3.1 Solid phase peptide synthesis – linear peptide

A linear octapeptide was sequenced *via* solid phase peptide synthesis (SPPS).

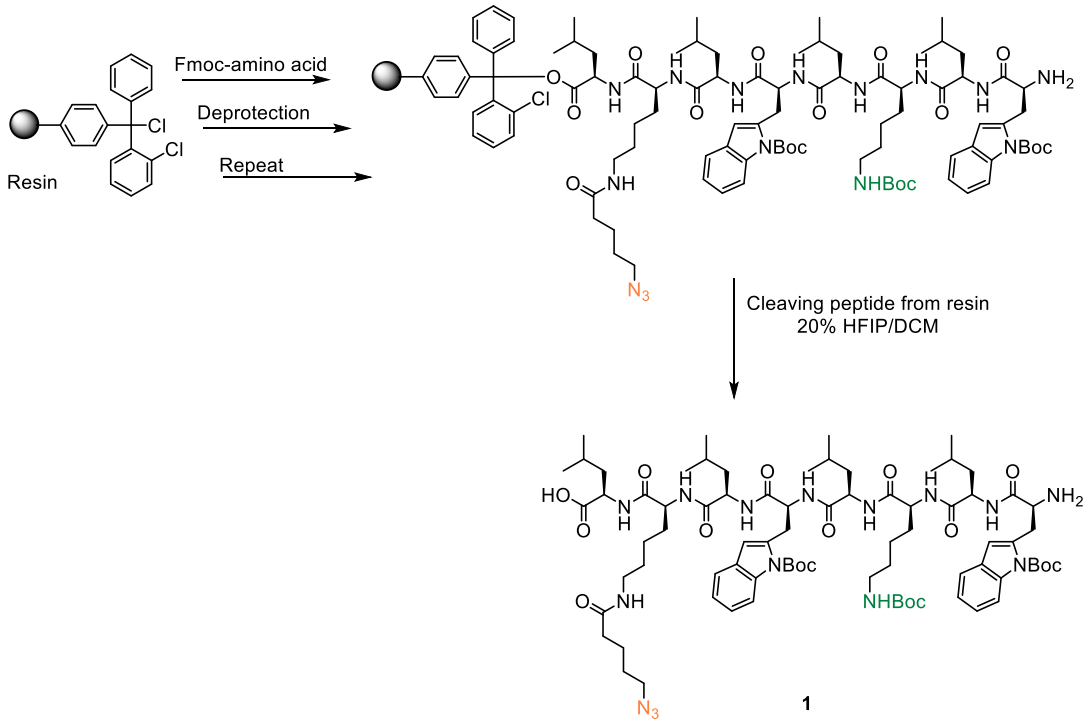

Scheme 2.6 Simplified scheme to make alternating D- and L- linear octa-peptide using solid phase peptide synthesis (SPPS).

This method has been adapted from similar procedures to synthesis other cyclic peptides with different amino acid sequences.[2]

In order to obtain an accurate amino acid sequence Fmoc protected amino acids were used. 2-chlorotrityl chloride resin (0.7 g, 0.77 mmol, 1.0 eq) was weighed into a sintered syringe. The resin was swollen for more than 30 minutes in DCM with constant agitation. The amino acid solution was prepared using Fmoc-D-Leu-OH (0.554g, 1.54 mmol, 2 eq), DIPEA (0.796 g, 6.16 mmol, 8 eq) in DCM (3 mL). The solution was bubbled with N_2 for 15 minutes. The DCM used to swell the solution was drained and then the amino acid solution was added to the resin, this suspension was shaken for 2 hours. The loaded resin was then washed with a solution of MeOH/DIPEA/DCM (2:1:17, 3 x 8 mL) followed by DCM (3 x 8 mL), DMF (3 x 8 mL) and DCM (3 x 8 mL) washes. A negligible sample of the resin was then transferred to a vial, dried under vacuum and then weighed. The loading of the resin

was calculated by deprotecting the sample of the resin, this was done by agitating the sample in a piperidine/DMF (1:4 vol, 1mL) solution for 20 minutes.

The deprotected sample was then diluted in DMF by a factor of 100 in order to obtain the exact absorption value *via* a UV-Vis spectrometer. The absorption value was used to calculate the concentration of loaded resin using the Fmoc peak at $\lambda = 301$ nm with $\varepsilon = 7800\ M^{-1}\ cm^{-1}$. The remaining resin in the sintered syringe and swollen using DCM (8 mL) for 30 minutes. After draining the DCM, the resin was washed with DMF (3 x 8mL). The Fmoc groups were cleaved using a piperidine/DMF solution 2 x (1:4 vol, 8mL, 5 minutes) and agitation. After Fmoc deprotection the resin was washed with DMF (5 x (8 mL, 30 seconds)), DCM (5 x (8 mL, 30 seconds)) and DMF (5 x (8 mL, 30 seconds)). Next the second amino acid was coupled. A solution containing the Fmoc-L-Lys (N_3)-OH (synthesised in the group by Tobias Klein) (0.568 g, 1.15 mmol, 1.5 eq), HATU (0.437 g, 1.15 mmol, 1.5eq), DIPEA (0.299 g, 2.31 mmol, 3 eq) and DMF (3 mL) was bubbled under N_2 gas for 10 minutes. The solution was then drawn into the syringe containing the resin. The solution and resin mixture was agitated overnight. The solution was then drained and the resin was washed in DMF (5 x (8 mL, 30 seconds)), DCM (3 x (8 mL, 30 seconds)) and DMF (3 x (8 mL, 30 seconds)) after which the deprotection and washing steps were repeated. Subsequent amino acids were coupled using Fmoc-amino acid (2.31 mmol, 3eq), HBTU (0.905g, 2.39 mmol, 3.1 eq) and DIPEA (0.597 g, 4.62 mmol, 6 eq). Addition and deprotection steps were repeated for each amino acid until the sequence was completed. After the final amino acid was added, deprotected and washed the linear peptide was cleaved from resin using a cleaving solution composed of HFIP/DCM (1:4 vol, 3 x (8 mL, 10 minutes)). To obtain the linear peptide remaining in the syringe further DCM (3 x (8mL, 30 seconds)) washes were completed. The filtrates containing the linear peptide were concentrated *in vacuo* to obtain an off-white powder.

Linear peptide **(1)**

Yield: 71%

^{1}H NMR: (500MHz, TFA-*d*) δ ppm, 8.11-8.14 (m, 2H, Trp aromatic), 7.28-7.57 (m, 8H, Trp aromatic), 5.17 (m, 2H, Trp-α-*H*), 4.55-4.69 (m, 5H, Leu-α-*H* + Lys-α-*H*), 4.25 (t, *J* = 8Hz, 1H, Lys-α-NH-*H*), 3.13-3.49 (m, 8H, Trp CH_2 + Lys CH_2), 2.67 (m, 2H, Lys(N_3) CH_2), 1.13-2.06 (m, 53H, Leu aliphatic CH CH_2, Lys(N_3) aliphatic CH_2, Boc CH_3, 0.76-0.95 (m, 28H, Leu aliphatic CH_3, Lys(N_3) aliphatic CH_2)

MS (ESI-ToF): $[M+H]^+$ calculated 1524.9 and found 1525.0, $[M+Na]^+$ calculated 1546.9 and found 1546.9.

2.7.4 Cyclisation

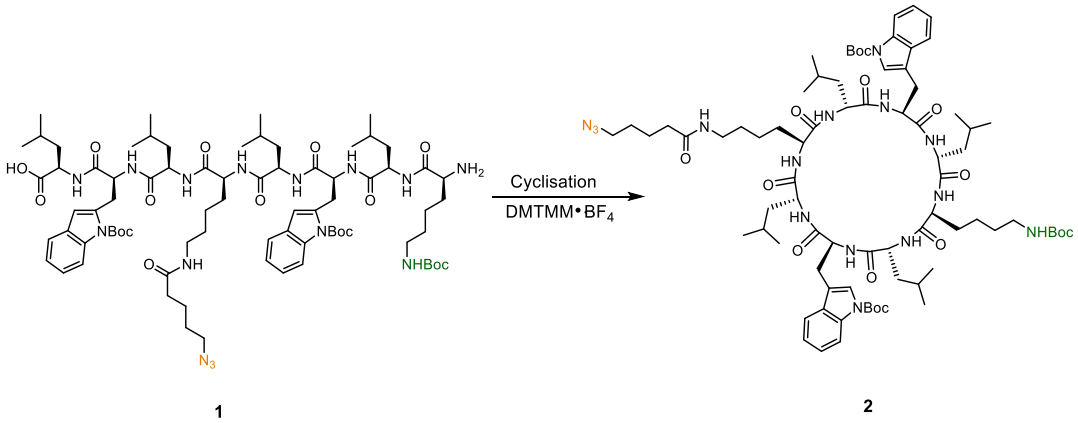

Scheme 2.7 Cyclisation of linear octa-peptide (**1**) to form protected cyclic peptide (**2**).

The linear peptide (**1**) (1.442 g, 0.946 mmol, 1.0 eq) was dissolved in DMF (100 mL) using sonication till the solution was clear. The solution was bubbled with N_2 (g) at room temperature then put into an ice bath until cooled. DMTMM $\cdot BF_4$ (0.466 g, 1.420 mmol 1.5 eq) in DMF (10 mL) was purged with N_2 (g) then added to the cooled linear peptide solution dropwise. The solution was stirred constantly for 91 hours under N_2 (g) at room temperature. DMF was removed *in vacuo*. Purification of the cyclic peptide was done using ice-cold methanol 3 x (20 mL) *via* centrifugation in 50 mL centrifuge tubes (7000 rpm, 5 mins). The cyclic peptide which formed a solid precipitate, at the bottom of the centrifuge tubes, was collected, transferred and dried under vacuum.

Cyclic peptide Boc protected (2)

Yield: 41%, 0.592g

^{1}H NMR: (500MHz, TFA-*d*) δ ppm, 8.09-8.11 (d, 2H, Trp aromatic), 8.09-8.11 (d, 2H, Trp aromatic), 7.61-7.62 (d, 2H, Trp aromatic), 7.51 (s, 2H, Trp aromatic), 7.29-7.37 (dt, 4H, Trp aromatic), 5.19 (t, 2H, Trp-α-*H*), 4.76 (m, 2H, Lys-α-*H*), 4.68-4.71 (m, 4H, Leu-α-*H*), 3.37-3.49 (m, 4H, Trp CH_2 + Lys CH_2), 3.07-3.26 (m, 4H, Lys CH_2,

Lys(N_3) CH_2), 2.70 (t, 2H, Lys(N_3) CH_2), 1.04-1.82 (m, 53H, Leu aliphatic CH CH_2, Lys(N_3) aliphatic CH_2, Boc CH_3, 0.75-0.84 (m, 28H, Leu aliphatic CH_3, Lys(N_3) aliphatic CH_2)

MS (ESI-ToF): $[M+Na]^+$ calculated 1528.9 and found 1528.9.

2.7.5 Deprotection of the cyclic peptide

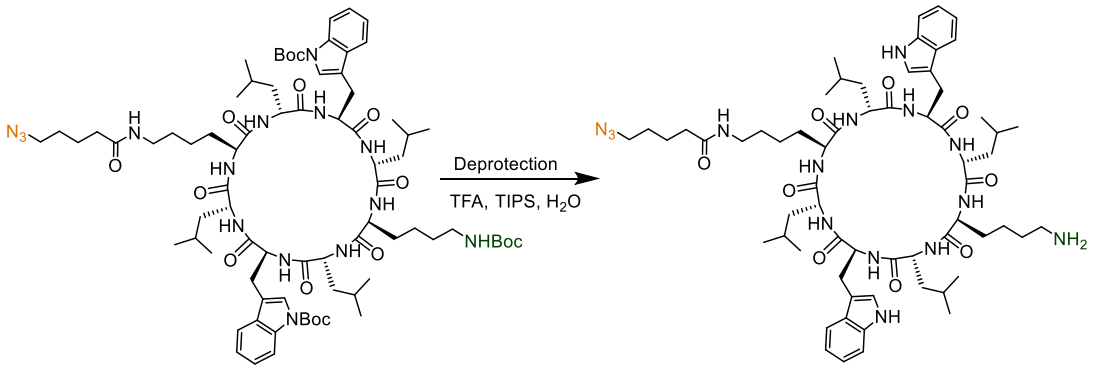

2 3

Scheme 2.8 Boc deprotection of cyclic peptide.

Boc groups were removed in using a deprotection solution of TFA/TIPS/H_2O (18:1:1 vol, 5 mL). The protected cyclic peptide (**2**) was agitated for 3 hours in the deprotection solution, then triturated using ice-cold diethyl ether and washed twice more with ice-cold diethyl ether. The off-white powder was collected and dried under vacuum.

Cyclic peptide Boc deprotected (3)

Yield: 93%, 0.2084 g

^{1}H NMR: (500MHz, TFA-*d*) δ ppm, 6.70-7.56 (m, 10H, Trp aromatic), 5.11 (t, 2H, Trp-α-*H*), 4.76 (m, 6H, Leu-α-*H*, Lys-α-*H*), 3.07-3.49 (m, 4H, Trp CH_2 + Lys CH_2), 3.07-3.26 (m, 4H, Lys CH_2, Lys(N_3) CH_2), 2.70 (t, 2H, Lys(N_3) CH_2), 1.04-1.82 (m, 26H, Leu aliphatic CH CH_2, Lys(N_3) aliphatic CH_2, 0.74-0.79 (m, 28H, Leu aliphatic CH_3, Lys(N_3) aliphatic CH_2)

MS (ESI-ToF): $[M+Na]^+$ calculated 1206.8 and found 1206.8.

2.7.6 *N*-hydroxysuccinimide (NHS) functionalisation of the napthalimide (NTI) dye

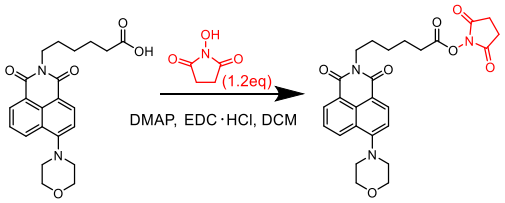

Figure 2.13 Synthetic route to NHS-functionalised napthalimide (NTI) dye.

The napthalimide dye, 6 - (6-morpholino - 1,3-dioxo - 1H - benzo [de] isoquinolin -2 (3H) - yl) hexanoic acid (0.2066 g, 0.521 mmol, 1.0 eq), NHS (0.072g, 0.626 mmol, 1.2 eq) and DMAP (6.4 mg, 0.052 mmol, 0.1 eq) were dissolved in DCM (35 mL) and left stirring in an ice bath until cooled. In a separate vial, 1-ethyl-3-(3-dimethylaminopropyl) carbodiimide hydrogen chloride (EDC·HCl) (0.120 g, 0.626mmol, 1.2 eq) was dissolved in DCM (15 mL). The EDC solution was added dropwise to the dye mixture. After the solution was stirred for 1 hour in the ice bath, the solution was left to stir for 16 hours at room temperature. The solution was washed using deionised water (2 x 40 mL), brine (2 x 40 mL) and dried with magnesium sulfate. The remaining solvent was removed *in vacuo* to obtain a yellow/orange solid. The crude product was purified by flash column chromatography, using a gradient from DCM to DCM with 5% methanol. Fractions containing the pure product were collected using the UV detector set to the dye at 398 nm.

NTI *

Yield: 67%

^{1}H NMR: (300 MHz, $CDCl_3$-*d*) δ ppm, 8.63 (d, 1H, C*H* aromatic), 8.56 (d, 1H, C*H* aromatic), 8.44 (d, 1H, C*H* aromatic), 7.73 (t, 1H, C*H* aromatic), 7.25 (d, 1H, C*H* aromatic), 4.21 (t, 2H, -N-C**H**$_2$-CH_2-CH_2), 4.04 (t, 4H, -N-C**H**$_2$-CH_2-O-), 3.29 (t, 4H, -N-CH_2-C**H**$_2$-O-, 2.84 (br s, 4H, N-Hydroxysuccinimidyl- C**H**$_2$-C**H**$_2$), 2.65 (t, 2H, -N-O-CO-C**H**$_2$-), 1.83 (m, 4H, -N-CH_2-C**H**$_2$-CH_2-C**H**$_2$-CH_2-), 1.56 (m, 2H, N-CH_2-CH_2-C**H**$_2$-CH_2-CH_2-).

2.7.7 Dye conjugation

2.7.7.1 Conjugation of the pyrene dye to the cyclic peptide (4)

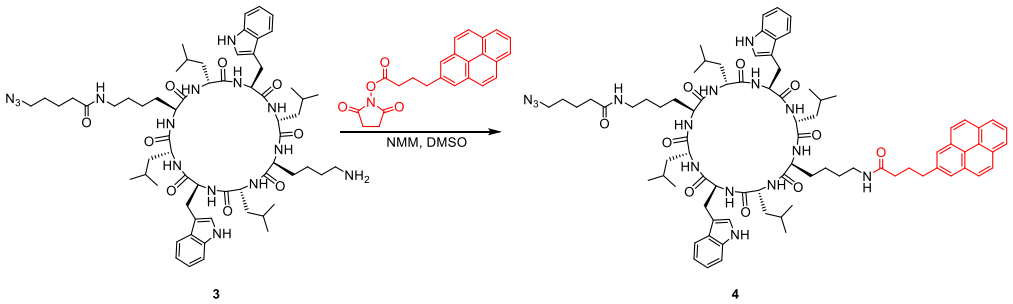

Scheme 2.9 Synthetic route to the cyclic peptide-pyrene conjugate (CP-PYR)

The deprotected cyclic peptide (**3**) (50 mg, 0.041 mmol, 1.0eq) was dissolved in DMF (300 µL). *N*,*N*-Diisopropylethylamine (DIPEA) (0.016 g, 0.124 mmol, 3.0 eq) was then added to the cyclic peptide solution and agitated for 30 minutes. 1-Pyrenebutyric acid *N*-hydroxysuccinimide ester (PYR) (0.019 g, 0.050 mmol, 1.2 eq) was then added to the CP base solution. The conjugation was reacted for 3 days at room temperature. The reaction was protected from light using aluminium foil. The solutions were purified *via* precipitation in ice-cold toluene. This was repeated three times. The remaining solvent was removed *in vacuo.*

CP-PYR†

Yield: 68%

^{1}H NMR: (500 MHz, TFA-*d*) δ ppm, 7.87-8.35 (m, 9H, Pyr aromatic CH), 7.68 (m, 2H, Trp aromatic), 7.19-7.44 (m, 8H, Trp aromatic), 5.23 (m, 2H, Trp-α-*H*), 4.65-4.83 (m, 6H, Leu-α-*H*, Lys-α-*H*), 3.50-3.72 (m, 6H, Trp CH_2 + Lys CH_2), 3.02-3.18 (m, 4H, Lys(N_3) CH_2), 2.83-2.90 (m, 4H, Lys CH_2, Lys(N_3) CH_2), 2.50 (m, 2H, Lys(N_3) CH_2), 1.70-2.01 (m, 28H, Lys(N_3) CH_2, Lys CH_2, Leu aliphatic -CH -CH_2), 0.83-0.94 (m, 24H, Leu aliphatic CH_3)

MS (ESI-ToF): $[M+Na]^+$ calculated 1498.84 and found 1498.75

†Full analytics could not be completed due precious amount of compound.

2.7.7.2 Conjugation of the napthalimide dye to the cyclic peptide (5)

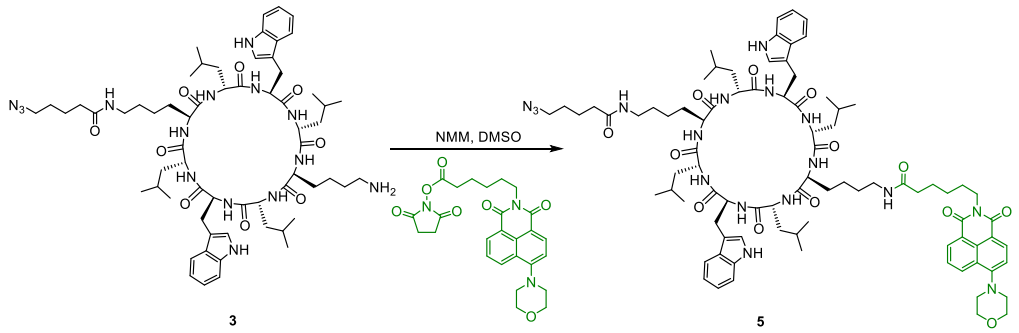

Scheme 2.10 Synthetic route to the cyclic peptide-napthalimide conjugate (**5**).

The cyclic peptide-napthalimide (**CP-NTI, 5**) was synthesised using the same procedure as the cyclic peptide-pyrene (**CP-PYR, 4**).

CP-NTI†

Yield: 77%

^{1}H NMR: (500 MHz, TFA-*d*) δ ppm, 8.85 (t, 2H, NTI aromatic CH), 8.73 (d, 1H, NTI aromatic CH), 8.23 (d, 1H, NTI aromatic CH), 8.10 (t, 1H, NTI aromatic CH), 7.05-7.56 (m, 10H, Trp aromatic), 5.13 (m, 2H, Trp-α-*H*), 4.65-4.72 (m, 6H, Leu-α-*H*, Lys-α-*H*), 4.55 (m, 4H, NTI - N-CH_2-C**H**$_2$-O-), 4.03 (t, 2H, NTI -N-C**H**$_2$-CH_2-CH_2-), 4.19 (m, 4H, NTI - N-C**H**$_2$-CH_2-O-), 3.37-3.57 (m, 6H, Lys CH_2, Trp CH_2), 3.15-3.34 (m, 4H, Lys(N_3) CH_2), 2.75 (m, 4H, Lys CH_2, Lys(N_3) CH_2), 1.13-1.56 (m, 24H, Lys(N_3) CH_2, Lys CH_2), 1.15-1.50, (m, 12H, Leu aliphatic -CH -CH_2), 0.76-0.81 (m, 24H, Leu aliphatic CH_3)

MS (ESI-ToF): $[M+Na]^+$ calculated 1606.89 and found 1606.83

†Full analytics could not be completed due precious amount of compound.

2.7.8 Polymer conjugation

2.7.8.1 Conjugation of the polymer to the cyclic peptide-dye via the pre-functionalisation strategy

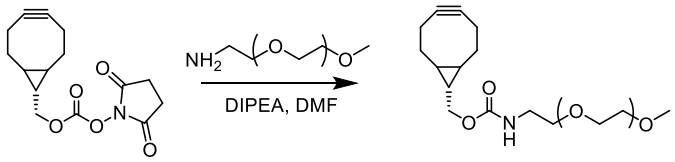

Scheme 2.11 NHS-coupling of the strained alkyne (BCN-NHS) and linear PEG-amine (PEG-NH_2) to form linear PEG with strained alkyne (PEG-BCN).

The α-Methoxy-ω-amino PEG 20kDa (50 mg, 2.25 µmol, 1.0 eq) was dissolved in DMF (300µL). *N*,*N*-Diisopropylethylamine (DIPEA) (0.870 mg, 6.74 µmol, 3.0 eq) was then added to the PEG solution and agitated for 30 minutes. (1R,8S,9s)-Bicyclo[6.1.0]non-4-yn-9-ylmethyl N-succinimidyl carbonate (BCN-NHS) (7.85 mg, 2.69 µmol, 1.2 eq) was then added to the solution. The conjugation was stirred overnight at room temperature. The reaction mixture was diluted with water, purified *via* dialysis (3 times) using centrifuge filter tubes and isolated *via* lyophilisation. This synthesis was repeated on a larger scale to obtain enough PEG - BCN for the polymer conjugation step.

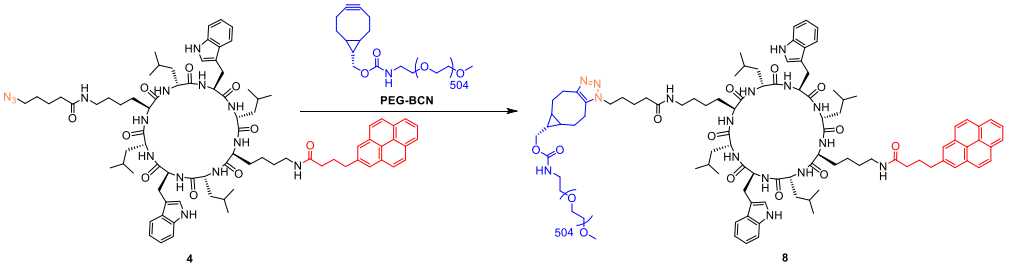

Scheme 2.12 Strained alkyne-azide coupling reaction to form the PEG-CP-PYR via the pre-functionalisation strategy

The cyclic peptide-pyrene conjugate (**CP-PYR, 4**) (10 mg, 8.29 µmmol, 1 eq) was dissolved in DMSO (1.5 mL). *N*,*N*-Diisopropylethylamine (DIPEA) (3.22 mg, 0.025 mmol, 3.0 eq) was then added to the CP-dye solution and agitated for 30 minutes. The strained alkyne modified PEG (**PEG-BCN**) (0.223 g, 9.95 µmol, 1.2 eq) was then added to the solution. The conjugation was reacted for 3 days at room temperature. The reaction was protected from light using aluminium foil. The reaction mixture was

diluted with water, purified *via* dialysis (3 times) using centrifuge filter tubes and isolated *via* lyophilisation.

The PEG-cyclic peptide-napthalimide (**PEG-CP-NTI, 9**) was also synthesised using the same procedure.

Due to the inefficient coupling of the polymer to the cyclic peptide a negligible amount of compound was recovered. Characterisation of these compounds *via* the pre-functionalisation polymer conjugation method was therefore not possible.

2.7.8.2 Conjugation of the polymer to the cyclic peptide-dye via the post-functionalisation strategy

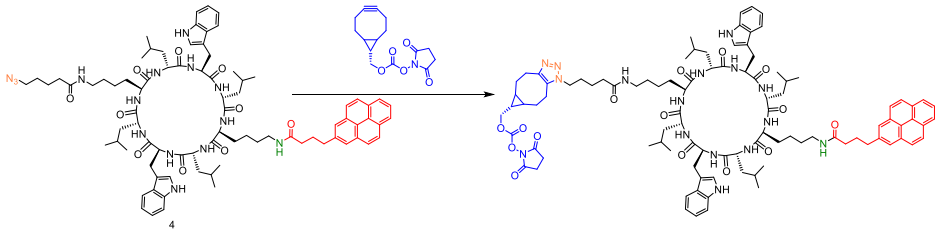

Scheme 2.13 Strained alkyne-azide coupling to form the NHS-functionalised cyclic peptide-pyrene conjugate (NHS-CP-PYR).

The cyclic peptide-pyrene conjugate (**CP-PYR**) (30 mg, 0.020 mmol, 1 eq) was dissolved in DMSO (1.5 mL). *N*,*N*-Diisopropylethylamine (DIPEA) (7.88 mg, 0.061 mmol, 3.0 eq) was then added to the CP-dye solution and agitated for 30 minutes. The strained alkyne-NHS compound (**BCN-NHS**) (7.12 mg, 0.024 mmol, 1.2 eq) was then added to the solution. The conjugation was reacted for 3 days at room temperature. The reaction was protected from light using aluminium foil. The solutions were purified *via* precipitation in ice-cold diethyl ether. The remaining solvent was removed *in vacuo*.

Due to the limited amount of the NHS-CP-Dyes synthesised, characterisation of these compounds was extremely difficult. Therefore the presence of this intermediary compound was only confirmed *via* ESI-ToF mass spectrum. Attempts to check the purity of this compound *via* HPLC were not successful.

NHS-CP-PYR (6)‡

MS (ESI-ToF): $[M+Na]^+$ calculated 1789.9 and found 1789.9.

NHS-CP-NTI(7)‡

MS (ESI-ToF): $[M+Na]^+$ calculated 1898.8 and found 1898.8 .

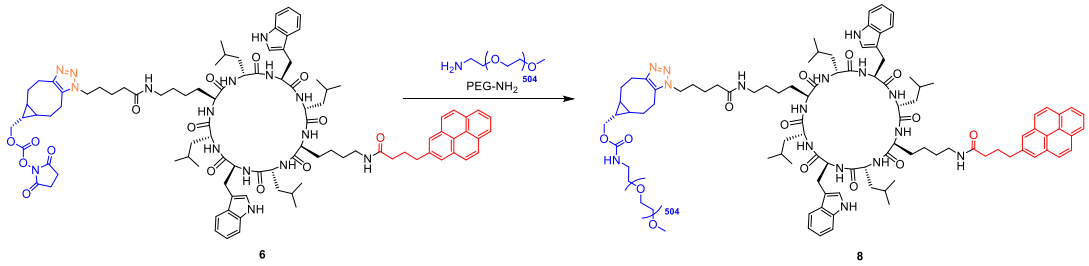

Scheme 2.14 NHS-amine coupling reaction to form the cyclic peptide-polymer-dye conjugate (**PEG-CP-PYR, 6**).

The α-Methoxy-ω-amino PEG 20kDa (PEG) (0.302 g, 0.014 mmol, 1.2eq) was dissolved in DMF. *N*,*N*-Diisopropylethylamine (DIPEA) (7.88 mg, 0.061 mmol, 3.0 eq) was then added to the PEG solution and agitated for 30 minutes. The NHS-functionalised cyclic peptide-pyrene conjugate (NHS-CP-PYR) (20 mg, 0.011 mmol, 1.0 eq) was then added to the solution. The conjugation was reacted for 3 days at room temperature. The reaction was protected from light using aluminium foil. The reaction mixture was diluted with water, purified *via* dialysis (3 times) using centrifuge filter tubes (50 kDa) and isolated *via* lyophilisation.

The PEG-cyclic peptide-napthalimide (**PEG-CP-NTI, 9**) was also synthesised using the same procedure.

PEG-CP-PYR (8)

Yield: 55% yield (assuming 100% yield of **NHS-CP-PYR** in the previous step)

^{1}H NMR: (500 MHz, DMF-*d*) was obtained (see appendix), some aromatic peaks can be observed, however assignment of this polymer conjugate was not possible due to the high molecular (20kDa) polymer attached to the CP.

HPLC: see Figure 2.9 – shows one major peak and some minor impurities. Notably the conjugates were observed, using UV and fluorescence detectors, in the HPLC due to the improvement of their solubility after the conjugation of the PEG polymer.

PEG-CP-NTI(9)†

Yield: 59% yield (assuming 100% yield of NHS-CP-PYR after conjugation and purification)

^{1}H NMR: see PEG-CP-PYR – spectra in the appendix

HPLC: see PEG-CP-PYR – spectra in Figure 2.9.

2.7.8.3 Dye conjugation of Cyanine dyes

CP-Cy3 (4): The cyclic peptide **4** (20.0 mg, 1.66 x 10^{-5} mol, 1 eq.) was dissolved in DMF (0.5 mL) with the aid of sonication. To make certain the amine on the cyclic peptide was deprotected N,N-Diisopropylethylamine (DIPEA) (10 $mgmL^{-1}$ stock solution in DMF, 0.64ml of stock solution, 6.4 mg, 4.98 x 10^{-5} mol, 3 eq.) was added. The solution was shaken for 30 minutes. The Cyanine3 NHS ester (11.6 mg, 1.99 x 10^{-5} mol, 1.2 eq.) was then added to the solution and shaken overnight. The product was purified *via* precipitation using THF. Yield: 67% (18.5mg, 1.12 x 10^{-5} mol). ESI-ToF, m/z (found) = 1644.9, (calculated) = 1645.0 ($[M]^+$), see figure 2.10. HPLC (t_R= 24 mins) using Acetonitrile/Water gradient. Spectra can be found in Figure 2.9.

CP-Cy5 (5): CP-Cy5 (**5**) was synthesised using the same protocol as CP-Cy3 (**4**). Cyanine5 NHS ester was used instead of Cyanine3 NHS ester to synthesise **5**. Yield: 29% (8.2 mg, 4.9 x 10^{-6} mol). ESI-ToF, m/z (found) = 1671.2, (calculated) = 1671.0 ($[M]^+$), see figure 2.10. HPLC (t_R= 24 mins) using Acetonitrile/Water gradient. Spectra can be found in Figure 2.9.

2.7.8.4 Conjugation of pentanoic acid to the cyclic peptide

CP-Alkyl (6): Pentanoic acid (2.7 µL, 2.49 x 10^{-5} mol, 3 eq.), HCTU (10.3mg, 2.49 x 10^{-5} mol, 3 eq.) and N,N-Diisopropylethylamine (DIPEA) (6.43 mg, 4.97 x 10^{-5} mol, 6 eq.) were dissolved together in DMF (1 mL) and shaken for 10 minutes. The cyclic peptide **4** (10.0 mg, 8.29 x 10^{-6} mol, 1 eq.) was separately dissolved in DMF (0.5 mL) with the aid of sonication. The pentanoic acid mixture was then added to the cyclic peptide solution. The resultant solution was shaken for 3 hours. The product was purified *via* precipitation using ice-cold diethyl ether. Yield: 61% (4.68 mg, 1.12 x 10^{-5} mol). ESI-ToF, m/z (found) = 1312.5, (calculated) = 1312.8 ($[M+Na]^+$), see figure 2.11. Due to the insolubility of this compound HPLC was not possible.

2.7.8.5 NHS functionalisation of the cyclic peptide conjugates (CP-Cy3, CP-Cy5 and CP-alkyl)

NHS-CP-Cy3 (7): The CP-Cy3 (**4**) (18.5 mg) was dissolved in DMF (0.5 mL) with the aid of sonication. (1R,8S,9s)-Bicyclo[6.1.0]non-4-yn-9-ylmethyl N-succinimidyl carbonate (BCN-NHS) was added to the cyclic peptide solution. The resultant solution was shaken overnight. The product was purified *via* precipitation using ice-cold diethyl ether. Yield: 73% (17.8 mg, 9.19 x 10^{-6} mol). ESI-ToF, m/z (found) =1936.0, (calculated) = 1936.1 ($[M]^+$), see figure 2.10. HPLC (t_R= 22 mins) using Acetonitrile/Water gradient. Spectra can be found in Figure 2.9.

NHS-CP-Cy5 (8): NHS-CP-Cy5 (**8**) was synthesised using CP-Cy5 (**5**) and the same protocol as NHS-CP-Cy3 (**7**). Yield: 78% (7.9 mg, 4.0 x 10^{-6} mol). ESI-ToF, m/z (found) =1962.1, (calculated) = 1962.1 ($[M]^+$), see figure 2.9. HPLC (t_R= 22 mins) using Acetonitrile/Water gradient. Spectra can be found in the figure 2.10.

NHS-CP-Alkyl (9): NHS-CP-Alkyl (**6**) was synthesised using CP-Alkyl (**6**) and the same protocol as NHS-CP-Cy3 (**7**). Yield: 74% (4.1 mg, 2.6 x 10^{-6} mol). Due to the insolubility of this compound ESI-ToF and HPLC was not possible.

2.7.8.6 Conjugation of the polymer to the cyclic peptide

PEG-CP-Cy3 (10): NHS-CP-Cy3 (**7**) (14mg) was dissolved in DMF (0.5mL) with the aid of sonication. α-Methoxy-ω-amino PEG 20 kDa (0.247 g, 1.08 x 10^{-5} mol, 1.5 eq.) was added to the cyclic peptide solution. To make certain the amine on the polymer was deprotected N,N-Diisopropylethylamine (DIPEA) (10mg/mL stock solution in DMF, 0.24 ml of stock solution, 2.4 mg, 1.4 x 10^{-5} mol, 2 eq.) was added. The solution was shaken overnight. The product was purified using centrifuge dialysis tubes with a molecular weight cut-off of 50kDa. Yield: 58% (101 mg, 4.21 x 10^{-6} mol). HPLC (t_R= 16 mins) using Acetonitrile/Water gradient. Spectra can be found in the Figure 2.9.

PEG-CP-Cy5 (11): PEG-CP-Cy5 (**11**) was synthesised using NHS-CP-Cy5 (**8**) and the same protocol as PEG-CP-Cy3 (**10**). Yield: 67% (59.9 mg, 2.48 x 10^{-6} mol). HPLC (t_R= 16 mins) using Acetonitrile/Water gradient. Spectra can be found in Figure 2.9.

PEG-CP-Alkyl (12): PEG-CP-Cy5 (**12**) was synthesised using NHS-CP-Alkyl (**9**) and the same protocol as PEG-CP-Cy3 (**10**). Yield: 56% (34.4 mg, 1.45 x 10^{-6} mol). HPLC (t_R= 21 mins) using Acetonitrile/Water gradient. Spectra can be found in Figure 2.9.

2.7.8.7 Reactions schemes for the dye and polymer conjugations steps.

Synthesis of PEG-CP-Cy3

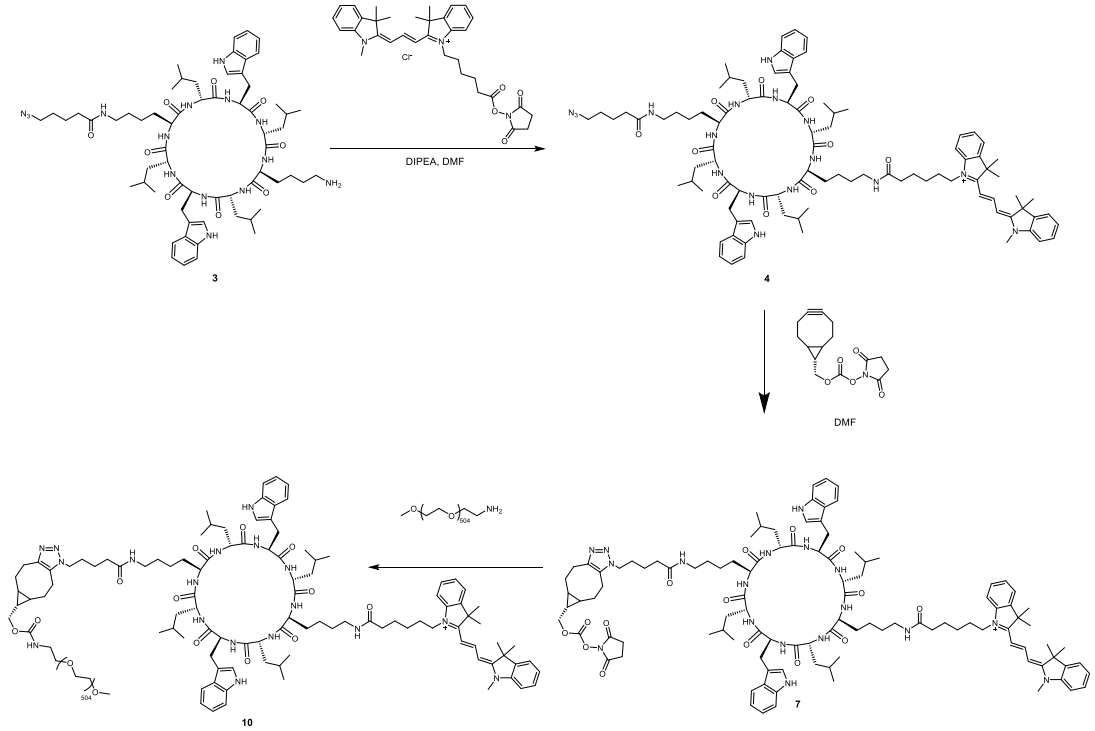

Synthesis of PEG-CP-Cy5

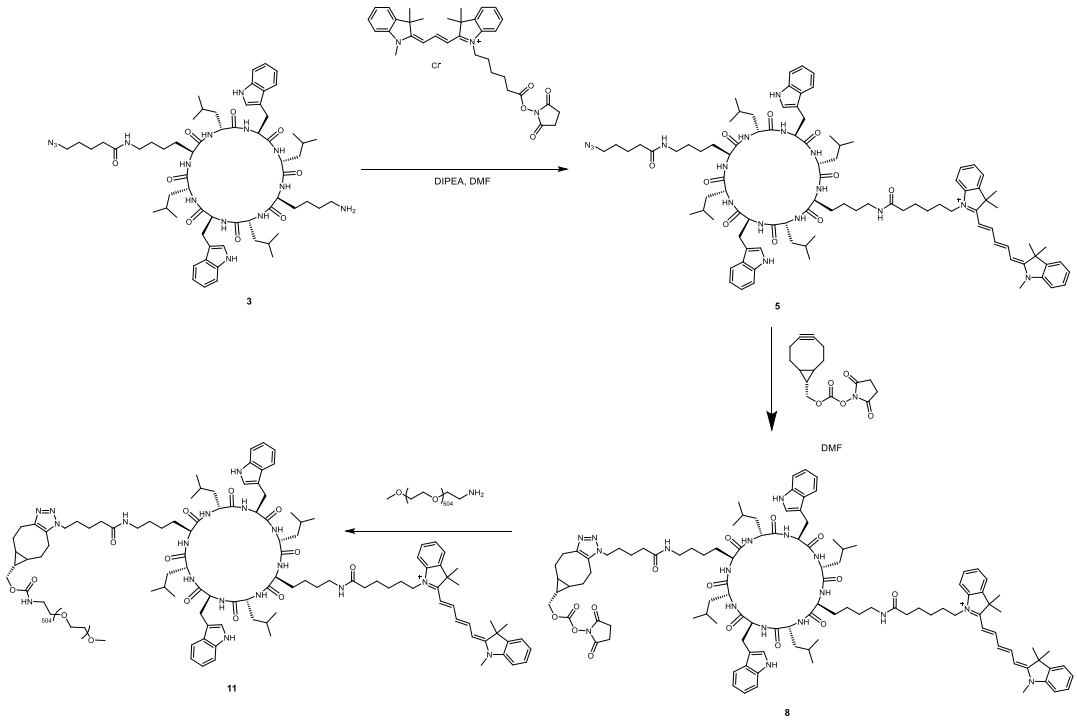

Synthesis of PEG-CP-Alkyl

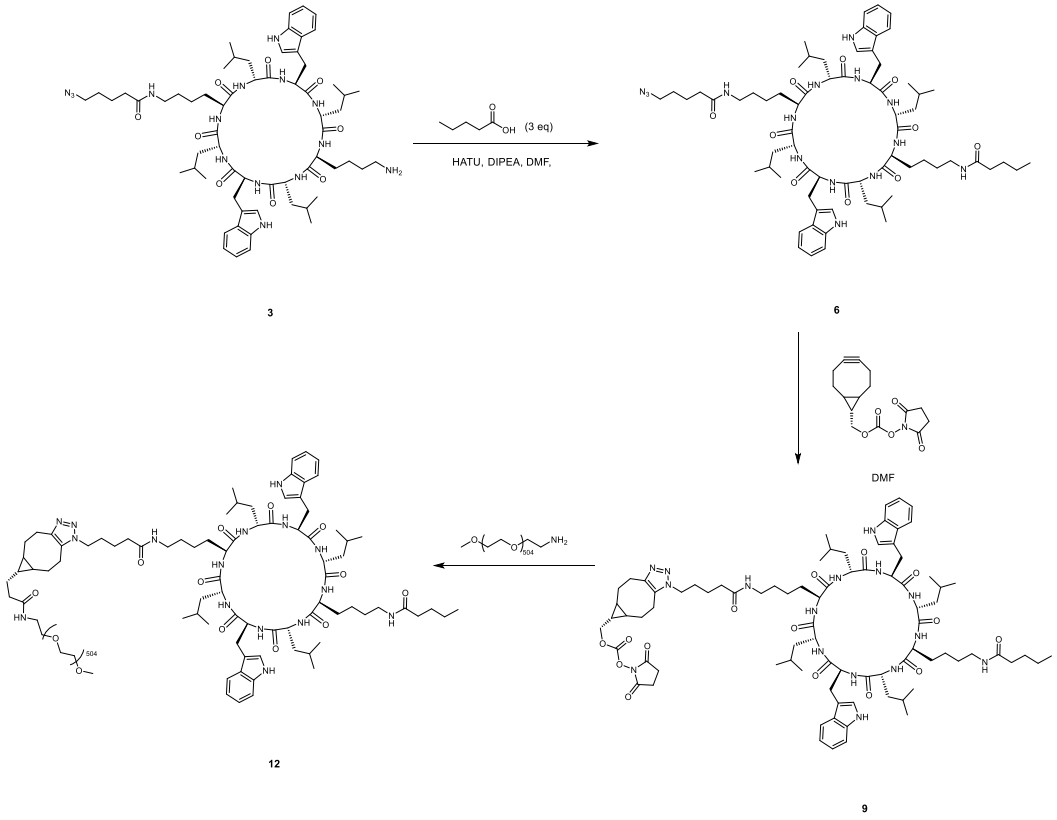

2.8 Appendix

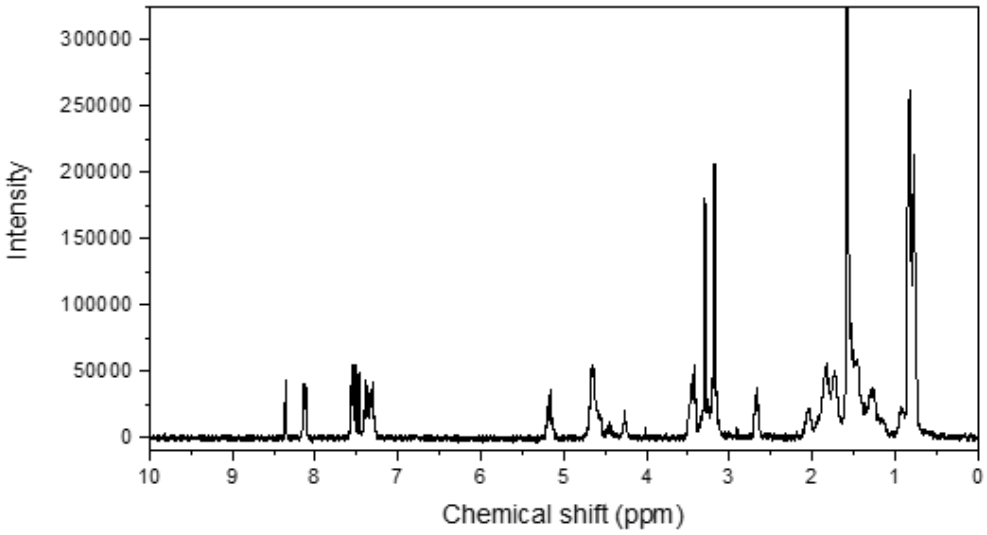

Figure 2.14 ^{1}H NMR of linear peptide (**1**). See experimental for assignment.

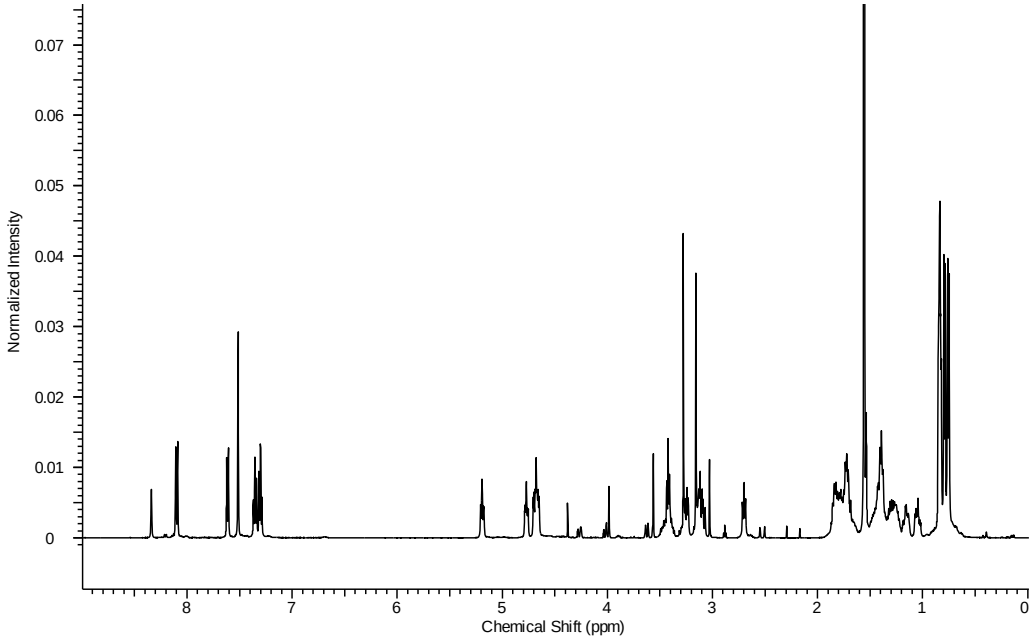

Figure 2.15 ^{1}H NMR of protected cyclic peptide (**2**). See experimental for assignment.

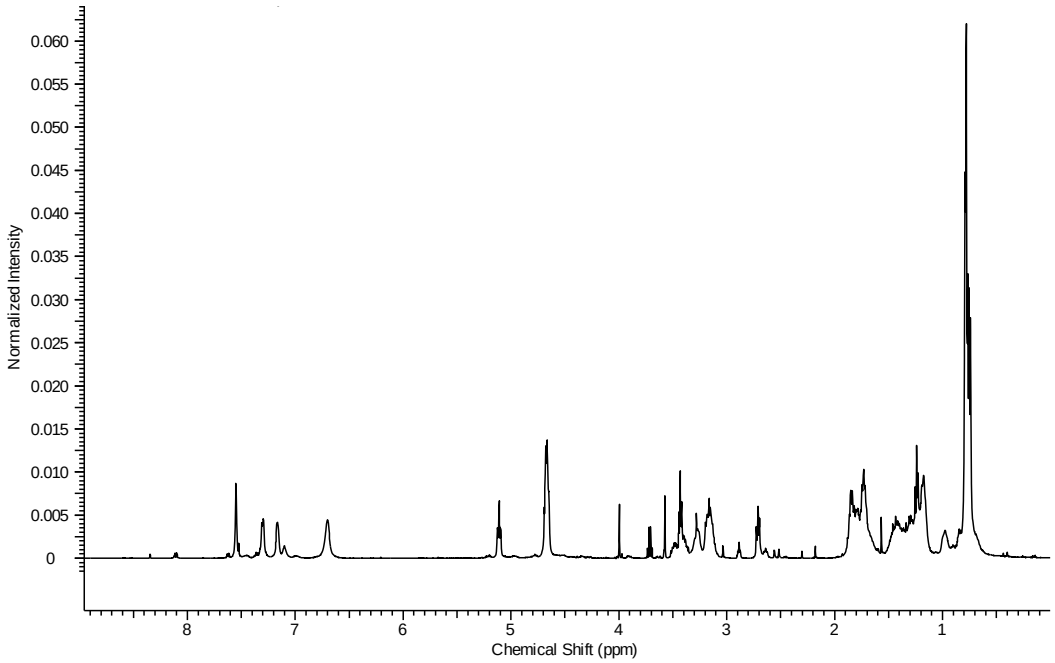

Figure 2.16 ^{1}H NMR of deprotected cyclic peptide (**3**). See experimental for assignment.

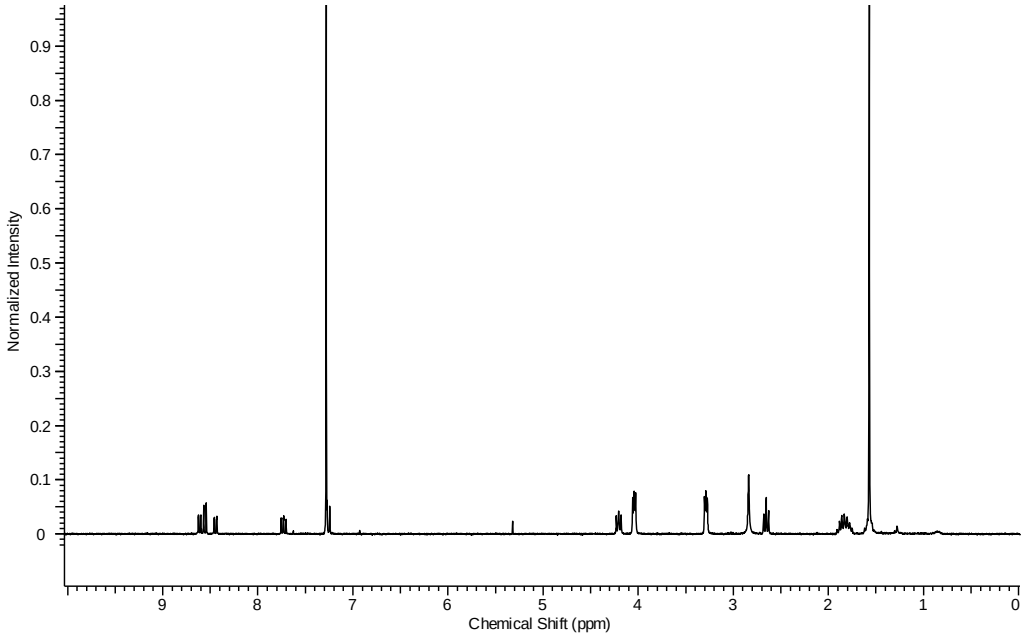

Figure 2.17 ^{1}H NMR of NHS-functionalised NTI dye (NTI). See experimental for assignment.

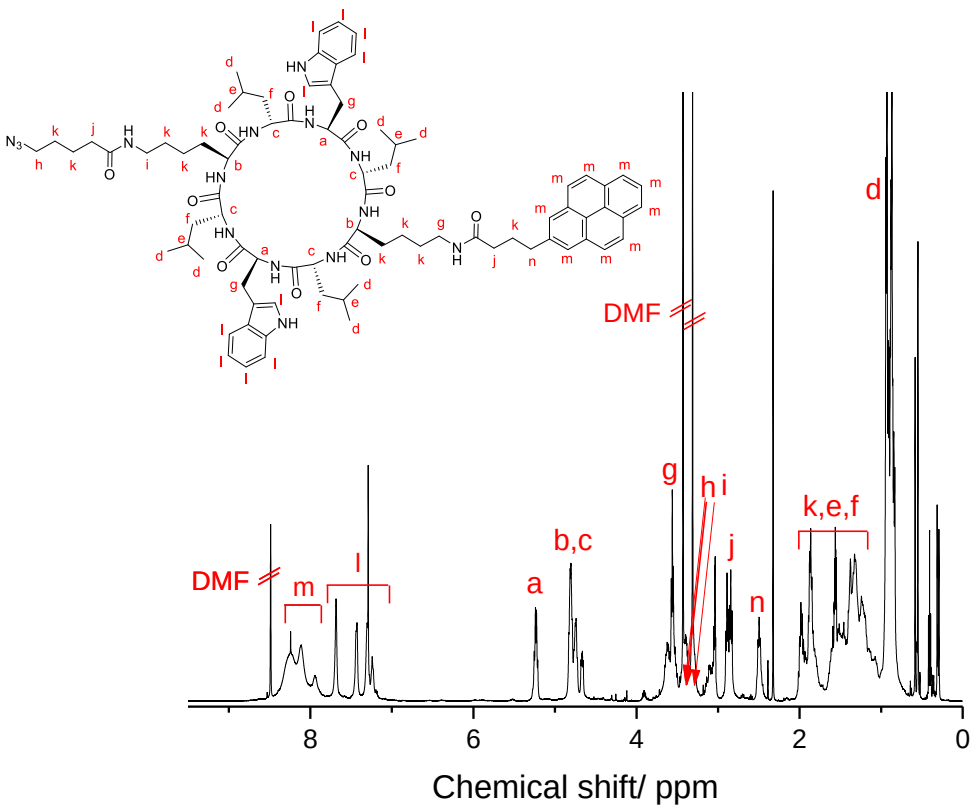

Figure 2.18 ^{1}H NMR of cyclic peptide-pyrene (**CP-PYR, 4**).

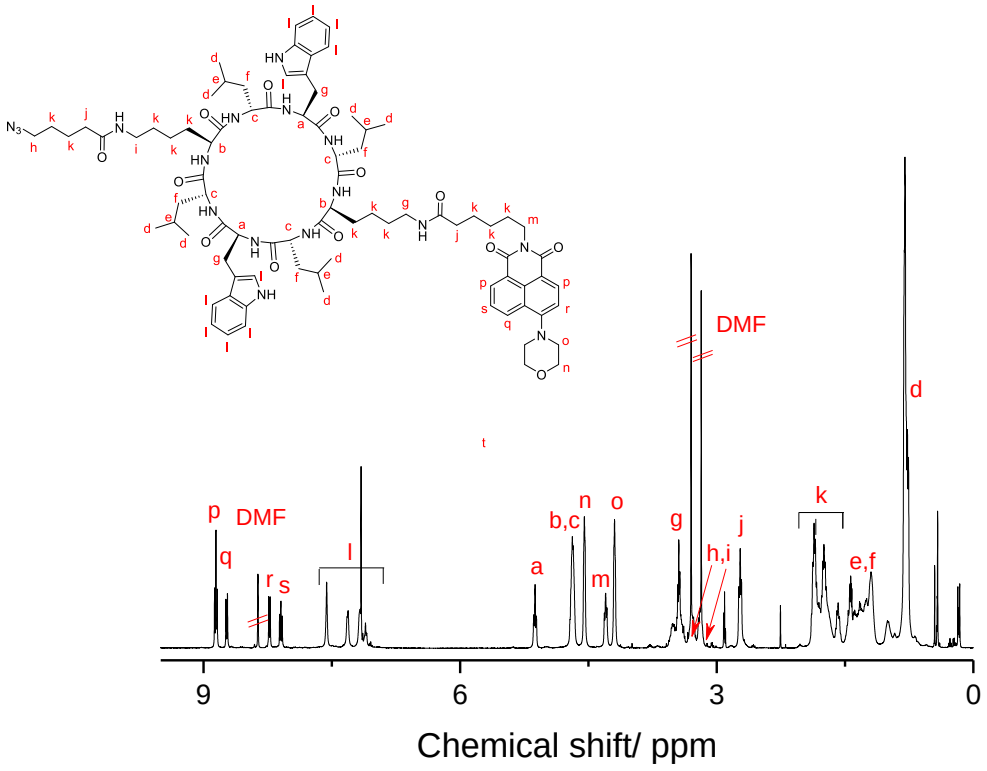

Figure 2.19 ^{1}H NMR of cyclic peptide-napthalimide (**CP-NTI, 5**).

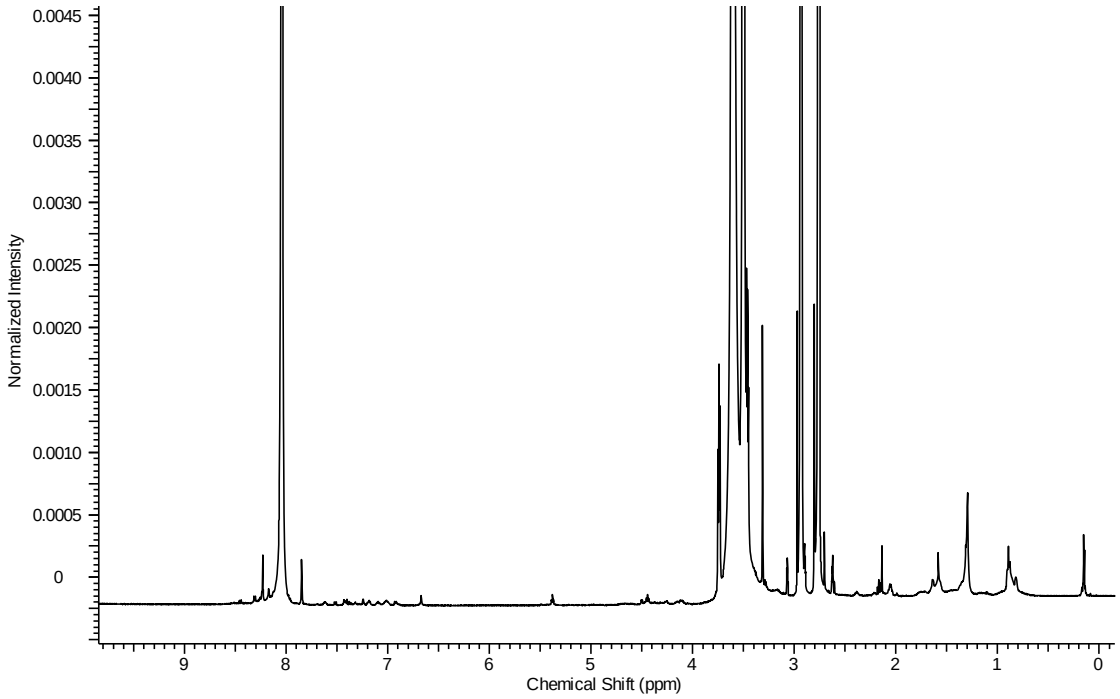

Figure 2.20 ^{1}H NMR of PEG-cyclic peptide-pyrene (**PEG-CP-PYR, 6**). Due to the size of the PEG (20kDa) assignment of peak was not possible.

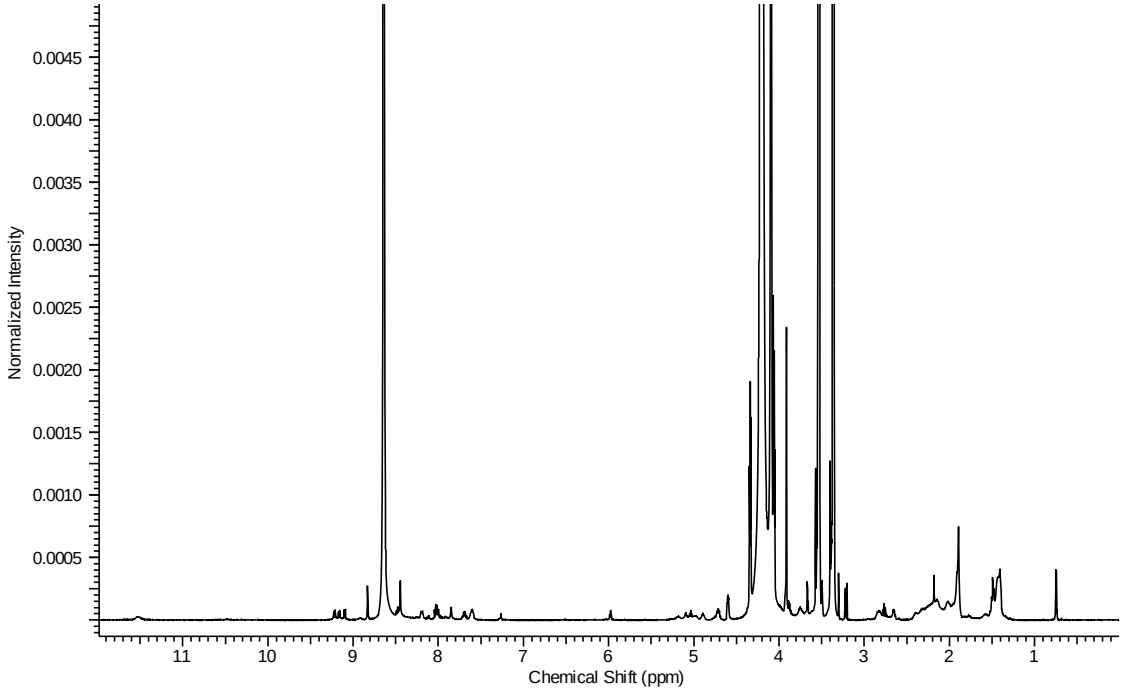

Figure 2.21 ^{1}H NMR of PEG-cyclic peptide-napthalimide (**PEG-CP-NTI, 7**). Due to the size of the PEG (20kDa) assignment of peak was not possible.

2.9 References

1. E. D. Spoerke, S. G. Anthony and S. I. Stupp, *Adv. Mater.*, 2009, **21**, 425-430.
2. R. Chapman, M. Danial, M. L. Koh, K. A. Jolliffe and S. Perrier, *Chem. Soc. Rev.*, 2012, **41**, 6023-6041.
3. A. M. Sanders, T. J. Magnanelli, A. E. Bragg and J. D. Tovar, *J. Am. Chem. Soc.*, 2016, **138**, 3362-3370.
4. S. C. Larnaudie, J. C. Brendel, K. A. Jolliffe and S. Perrier, *J. Polym. Sci., Part A: Polym. Chem.*, 2016, **54**, 1003-1011.
5. P. Somerharju, *Chemistry and Physics of Lipids*, 2002, **116**, 57-74.
6. F. Wurthner, *Chem. Commun.*, 2004, 1564-1579.
7. R. J. Brea, M. E. Vázquez, M. Mosquera, L. Castedo and J. R. Granja, *J. Am. Chem. Soc.*, 2007, **129**, 1653-1657.
8. J. C. Brendel, G. Gody and S. Perrier, *Polym. Chem.*, 2016, **7**, 5536-5543.
9. S. J. Butler and K. A. Jolliffe, *Organic & Biomolecular Chemistry*, 2011, **9**, 3471-3483.
10. E. D. H. Mansfield, M. Hartlieb, S. Catrouillet, J. Y. Rho, S. C. Larnaudie, S. E. Rogers, J. Sanchis, J. C. Brendel and S. Perrier, *Soft Matter*, 2018, **14**, 6320-6326.
11. T. Förster, *Ann. Phys.*, 1948, **437**, 55-75.
12. S. S. Vogel, C. Thaler and S. V. Koushik, *Science's STKE*, 2006, **331**.

Chapter 3 Investigating the Dynamic Behaviour of Self-Assembling Cyclic Peptide - Polymer Nanotubes in Solution and in Mammalian Cells

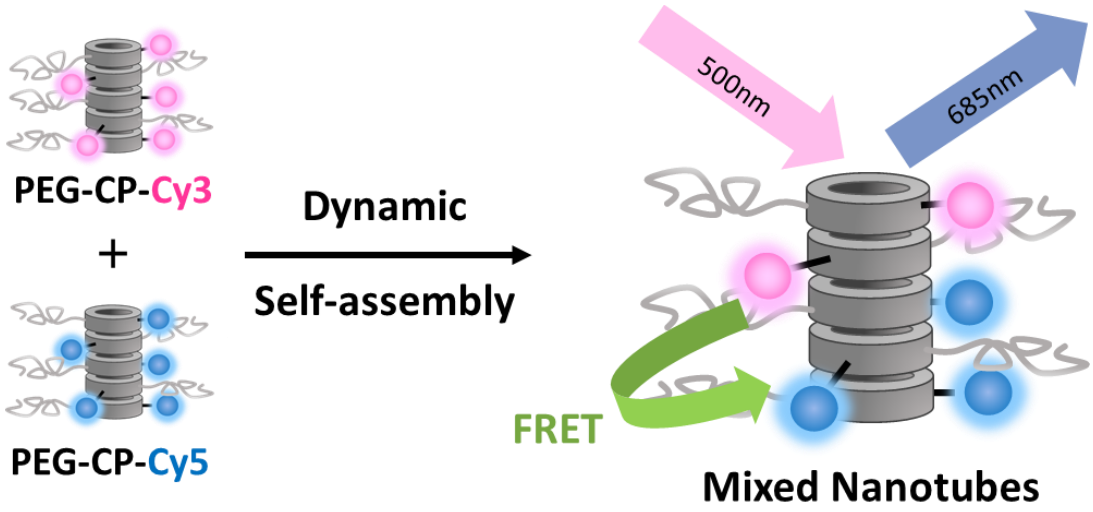

3.4 Introduction

A key advantage of self-assembling cyclic peptides is their highly adaptable design. In the previous chapter, using a 'bottom up' approach, the synthesis and characterisation of asymmetric model conjugates to monitor the dynamic behaviour of these supramolecular systems were developed. These conjugates were designed to contain both a FRET dye and polymer on the periphery in order to directly infer the exchange of cyclic peptides between the nanotubular assemblies, see figure 3.1.

In the following chapter, these systems will be used to prove the supramolecular nanotubes are dynamic - not kinetically trapped. Secondly, to gain a detailed understanding of what role the environment plays in the dynamics of these self-assembling systems, key parameters such as solvent and concentration were also varied. Finally, the use of FRET allowed us to observe the behaviour of these nanotubes in mammalian cells *in vitro*, thus providing essential information about their dynamics in a complex biological environment.

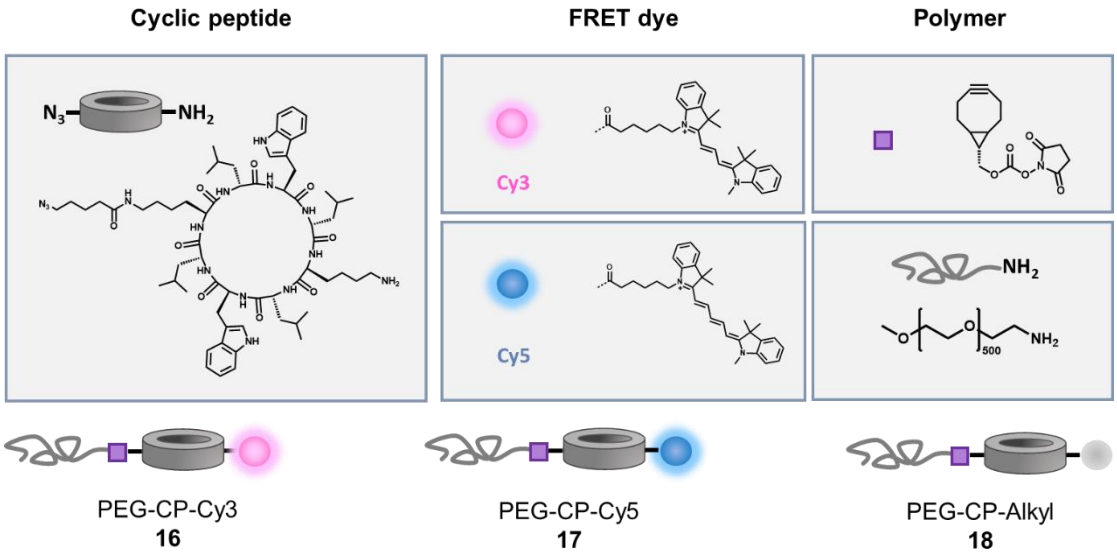

Figure 3.1 Schematic representation of the cyclic peptide-dye-polymer conjugates.

3.5 Results and Discussion

3.5.1 Characterisation of the self-assembling cyclic peptide conjugates

Hydrogen bonding between the amide bonds is known to drive the self-assembly of the CPNTs. However, the length of the formed nanotube can be influenced by number of different factors such as composition and position of the amino acids, as well as polymer grafting.[1] Before the dynamics of these supramolecular systems could be inferred, it was important to fully characterise the nanotubular assembly of these peptides. Herein, the morphology of the resulting CP-polymer conjugates were analysed using small angle neutron scattering (SANS), Static Light Scattering (SLS) and Transmission Electron Microscopy (TEM).

SANS is a powerful technique to characterise complex systems in order to understand any structural parameters, interactions, and changes due to environmental stimuli occurring in solution.[2] Previously, our group has used SANS to analyse a wide-range of CPNTs in different solvents, polymer conjugations, and in response to different stimuli (pH and temperature).[3-5] Here, SANS was used to confirm the formation of nanotubes for a mixture of conjugates PEG-CP-Cy3 **16** and PEG-CP-Cy5 **17**, and to analyse how the presence of a fluorophore affected their stacking potential compared to the non-dye conjugated control (PEG-CP-Alkyl, **18**).

Figure 3.5a shows the reduced, corrected SANS scattering data for the control and the dye conjugated peptide system. From the fit, the length of each nanotube could be obtained. The data were initially fitted with either a cylinder or a core-shell cylinder model form factors, however, a statistically reliable fit was not obtained. As a result, a hairy-cylinder model was used that combines the form factors for a micelle with a rod-like core and attached flexible polymer chains, with a high degree of accuracy in both cases (Experimental section 3.4.2.3).

The core-radius has been shown to be 0.34 nm in previous studies and was used as a fixed parameter in the fitting process.[3] From the values obtained, the number of aggregation (N_{agg}) can be determined by dividing the length of the tube by the distance between two single cyclic peptide unimers (0.47 nm), shown in Table 1.[3, 6] Visually analysing the scattering profiles reveals a major difference in the Guinier region (q = 0.00416 - 0.01). Given that the Guinier region provides information on larger structures within the system, deviations here indicate nanotubes of different lengths.

The control has a higher intensity at q^{-1}, suggesting the formation of longer nanotubes, which is demonstrated in the fits. The dye-conjugated peptide however, turns over, suggesting tubes of a finite length exist. The length of the tubes was found to be 117 nm, compared to 89 nm for the control and mixed system, respectively.

In addition to SANS, SLS experiments were used to determine the N_{agg} for the non-dye conjugated system in a range of concentrations (Experimental section 3.4.2.8). The dye conjugates could not be measured directly as the wavelength of the laser used for SLS (633nm) overlaps with the dye excitations (570 nm and 646 nm for Cy3 and Cy5, respectively). The N_{agg} of non-dye conjugated system was then used as a floating variable in the fitting process.

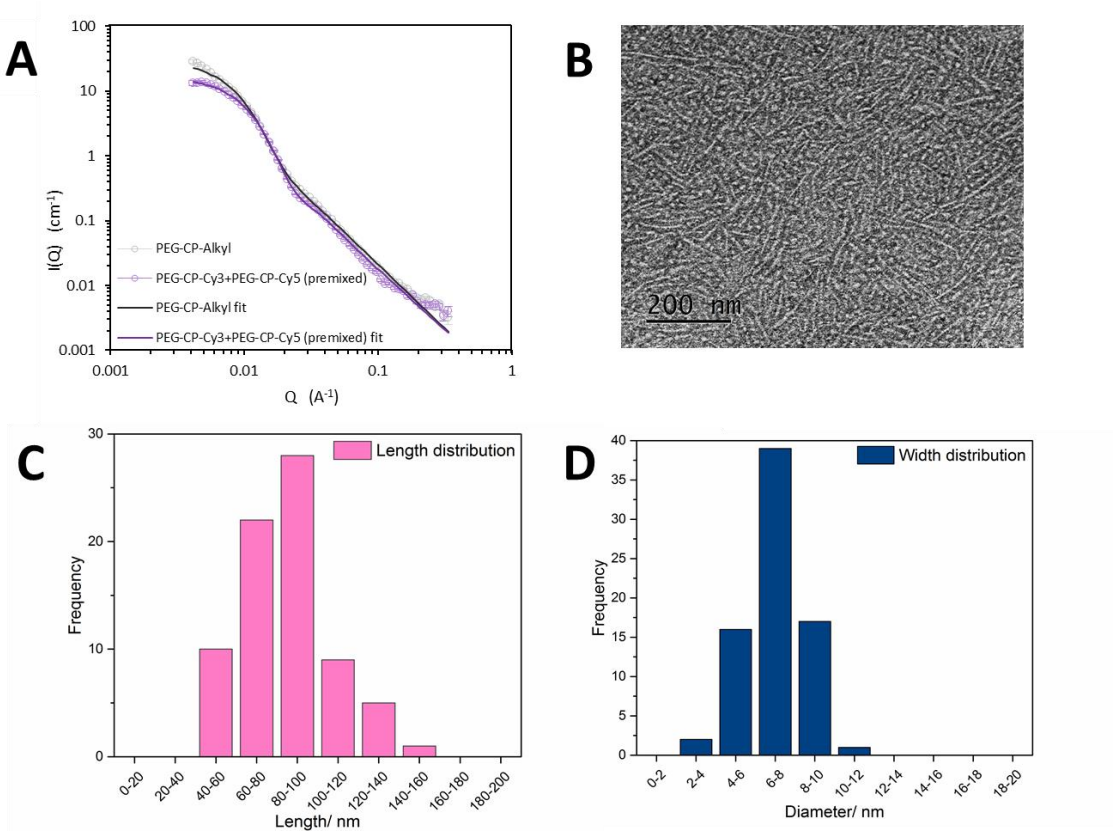

Figure 3.2 a) Reduced SANS scattering data for the PEG-CP-Alkyl (Control) and (Premixed) PEG-CP-Cy3 and PEG-CP-Cy5 system. The lines correspond to a fit to the hairy cylinder model. b) TEM image of cyclic peptide-polymer-dye conjugate (PEG-CP-Cy3) stained with UOAc. Distribution of nanotubular c) lengths and d) diameters extracted from TEM.

The data presented here clearly confirms that both the control (PEG-CP-Alkyl) and mixed systems (PEG-CP-Cy3 and PEG-CP-Cy5) form long nanotubular aggregates of similar size *in situ*. Discrepancy in the sizes can be attributed to the presence of the bulky and charged dye (Cy3 or Cy5). Yet, the variation remains minor, possibly due to the distance between the dye and the cyclic peptide created by the linker.

Table 3.1 Summary on the characterisation of CPNTs using SANS and TEM. TEM values are represented as mean lengths and diameters ± standard deviation of 37 individual nanotubes.

Sample	**Length (SANS)/ nm**	**N_{agg} (SANS)**	**Length (TEM)/ nm**	**N_{agg} (TEM)**	**Diameter (TEM)/ nm**
PEG-CP-Cy3	-	-	85.0 (± 22.3)	180.9	7.1 (± 1.5)
PEG-CP-Cy5	-	-	81.8 (± 14.1)	174.0	8.4 (± 2.2)
Premixed*	89.0	189.3	-	-	-
PEG-CP-Alkyl	116.9	248.8	117.7 (± 32.0)	250.4	15.5 (± 3.7)

*Premixed – PEG-CP-Cy3 and PEG-CP-Cy5

Using TEM the nanotubular morphology observed in SANS was independently confirmed. Samples were prepared from pure water (1 mg/mL) using the drop casting method. The low electron density of the peptide-dye-polymer conjugates made obtaining TEM images of these compounds very challenging, thus negative staining of samples dropcast on thin (4 nm) carbon-coated copper grids was used. Images are presented in Fig 3.2b. The TEM images were kindly obtained by Liam R MacFarlane at the University of Bristol.

The formation of one-dimensional structures can be seen for all three presented cyclic peptides (Figure 3.2B). Upon statistical analysis of the TEM images using ImageJ, a very narrow distribution with a mean diameter of 7.1 nm was determined for PEG-CP-Cy3 (Figure 1D). This finding is consistent with the formation of single conjugated nanotubes. The diameter of the PEG-CP-Cy5 was relatively similar (mean diameter = 8.4 nm), however a larger value was obtained for PEG-CP-Alkyl (mean diameter = 15.5 nm). This could be associated to lateral aggregation upon removal of the solvent. The distribution of nanotube lengths was found to be wider (mean length = 85.0 nm for PEG-CP-Cy3, and 81.8 nm for PEG-CP-Cy5), which is to be expected in a self-

assembled system (Figure 3.5c). Distribution for PEG-CP-Cy5 and PEG-CP-Alkyl and can be found in Experimental section 3.4.2.10.

3.5.2 Spectrochemical properties of dye conjugated cyclic peptides

Following synthesis and characterisation, FRET was used to probe the dynamic nature of these supramolecular systems. The FRET emission of the acceptor dye (PEG-CP-Cy5) only occurs when specific requirements are met. Firstly, the emission spectra of the donor (PEG-CP-Cy3) should overlap with the absorption spectra of the acceptor enabling the fluorescence of the donor to excite the acceptor. Unlike the pyrene and napthalimide dyes in Chapter 1, the Cyanine dye FRET pair Cy3 and Cy5 have an ideal spectral overlap and have been extensively used due to their high excitation coefficients and biocompatibility.[7] The absorption and emission spectra of PEG-CP-Cy3 and PEG-CP-Cy5 show that the conjugates conserve these properties (Appendix Figure 3.14 and 3.15, respectively). Direct excitation of the acceptor dye in the subsequent FRET studies, which could also lead to acceptor emission, was circumvented by exciting the donor at 500 nm instead of its absorption maxima. Secondly, FRET will only take place if the donor and acceptor (Cy3 and Cy5 respectively) are close enough in space for the energy transfer to take place, typically 10-100 Å. The average distance between two CPs has previously been reported to be 4.7 Å and the pore diameter of the CP around 7.5 Å.[1, 8, 9] Therefore, an energy transfer for the presented system is expected if both dyes are incorporated into the same nanotube upon mixing. When these conditions are fulfilled, the energy transfer translates into a decrease in donor emission and an increase in the acceptor emission, see Figure 3.3.

Here, FRET studies were carried out by comparing a mixture of PEG-CP-Cy3 and PEG-CP-Cy5, and a mixture of the free dyes in solution (Cy3 and Cy5) as a control. Mixing the dyes alone resulted in no change in the emission spectra over 30 minutes, which can be attributed to the dyes being too far from one another in solution (Figure 3.3b). In comparison, the emission of PEG-CP-Cy5 increased and the emission of PEG-CP-Cy3 decreased over time upon mixing (Figure 3.3b). This behaviour is indicative of the formation of FRET pairs, resulting from the exchange of monomer units or small segments of peptide between the formed nanotubes. The increase over time indicates that CPs dynamically exchange between different nanotubes to form increasingly mixed nanotubes, as no self-assembly and exchange would result in no

FRET occurring. A schematic depiction of mixed cyclic peptide-polymer-dye conjugates can be found in Figure 3.4a.

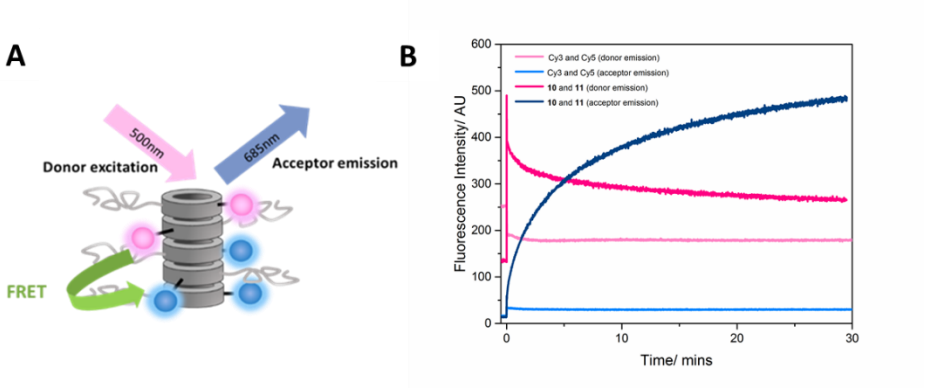

Figure 3.3 a) Schematic depiction of the FRET occurring in cyclic peptide nanotubes containing donor (Cy3) as well as acceptor (Cy5) dye molecules. b) Fluorescence donor and acceptor emission upon mixing the free dyes (Cy3 and Cy5) and the self-assembling dye conjugates (PEG-CP-Cy3 and PEG-CP-Cy5) in water.

3.5.3 Solvent dependent dynamic unimer exchange of CPNT

Using the FRET system outlined above we can further probe the dynamics of the dye conjugates (PEG-CP-Cy3 and PEG-CP-Cy5) in a range of different solvent environments. Our group has previously shown that cyclic peptides form shorter nanotubes in more hydrogen bond competitive solvents.[10] This is due to the solvent molecules competitively binding to the hydrogen bonding sites on the cyclic peptide required for stacking.

In order to investigate these dynamics, stock solutions of PEG-CP-Cy3 (**16**) and PEG-CP-Cy5 (**17**) were made in DMF, water and toluene which have a range of different properties. Emission spectra, upon mixing the dye conjugates (PEG-CP-Cy3 and PEG-CP-Cy5) in a 1:1 volume ratio were taken at several different time intervals (Figure 3.4b) until a plateau was reached. Emission was then expressed as a FRET ratio, calculated using equation 1.[11, 12]

$$E_{rel.} = \frac{I_A}{I_D + I_A} \quad (1)$$

Where I_A and I_D are the total acceptor and donor fluorescence intensities respectively.

Again, the change in emission associated with FRET (i.e. decrease in the donor and increase in the acceptor emission) was observed, with the exception of DMF, whereas

in water and toluene a clear increase can be observed, showing FRET is occurring. Interestingly, the rate at which FRET occurs appears to be different for both water and toluene (Fig 3.4c). In both solvents where conjugates are expected to assemble, the FRET ratio increases as a function of time, and therefore show the cyclic peptides dynamically exchanging to form progressively mixed nanotubes. This increase in FRET ratio eventually reaches a plateau whereby no further net mixing was observed and an equilibrium is maintained. The final FRET ratio of the equilibrium in different solvents clearly varies, and is postulated to be a result of the solvatochromic effects of the solvent, and/or the different lengths the nanotube assemblies. In addition, an insufficient exchange of CPs can lead to a lower final FRET ratio. The solvent dependent exchange kinetics were determined by modelling the increase in FRET ratio to a bi-exponential decay function, using OriginPro, providing two rate constants. A single exponential function yielded poor fits (R^2 <0.9). Other FRET ratio kinetics in literature have also reported to require bi-functional models.[11] This suggests that there are two different mixing processes occurring, an initial fast rate of mixing (k_1) followed by a slower gradual exchange between assemblies (k_2) until an equilibrium is reached. No rate constants could be determined for DMF as no increase over time was observed as the FRET ratio of < 0.l was reached instantaneously after mixing.

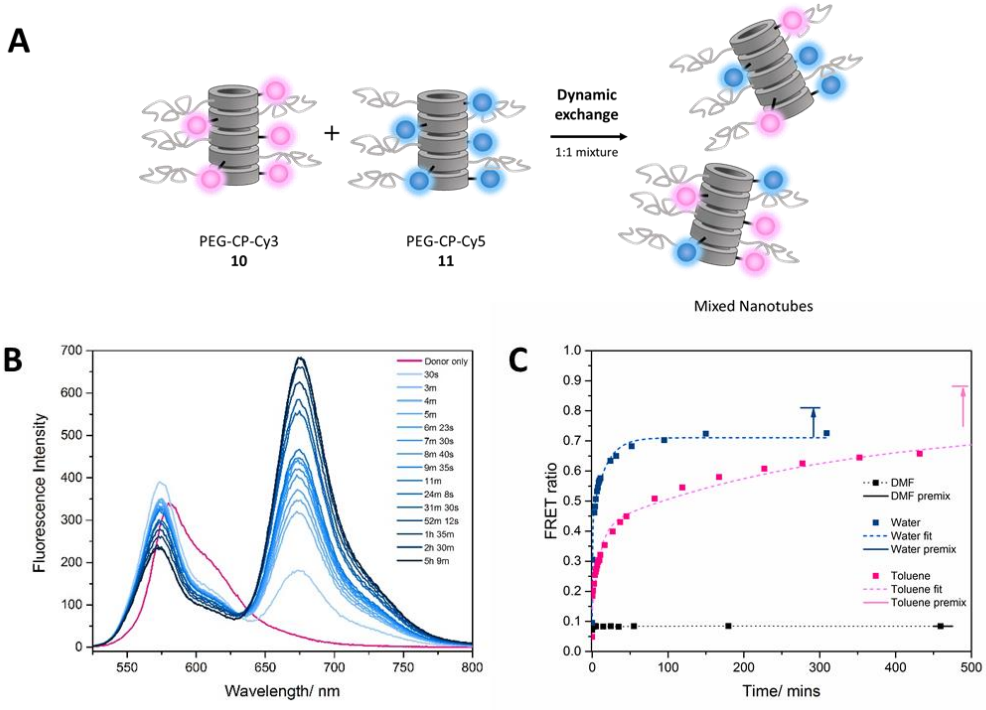

Figure 3.4 a) Schematic depiction of the FRET studies. Preassembled individual cyclic peptide-dye-polymer conjugates in water (left) and a 1:1 mixture of both

conjugates after the assemblies are left to dynamically exchange (right). b) Fluorescence emission spectra of PEG-CP-Cy3 and PEG-CP-Cy5 upon mixing in water and c) Normalised FRET ratio of the mixed system in DMF, water and toluene. Toluene plateau was reached after 6 days (see Appendix Figure 3.17).

In a highly hydrogen competitive solvent such as dimethylformamide (DMF), mainly unimeric species or small aggregates were expected,[10] which is corroborated by the lack of change in FRET ratio upon mixing (Figure 3.4c), as they behave similarly to the non-assembling free dyes. The fluorescence emission of the donor stays obviously greater than the emission of the acceptor, lending itself to a low FRET ratio. In a disassembled/fully dynamic system the FRET ratio would not be expected to change. The FRET ratio observed remains constant, however it is not at zero due a small proportion of formed conjugates.

In water, which is less hydrogen bond competitive than DMF, the solvent molecules can still compete with peptide-peptide hydrogen bonding, however to a far lesser extent than in DMF. The increase in FRET ratio (Figure 3.4c) shows that the dye conjugates are dynamically exchanging to form increasingly mixed tubular aggregates. The plateau reached after 3 hours shows that no further net mixing occurs after this point (Figure 3.4c).

Surprisingly, this dynamic behaviour was also observed in toluene where the solvent is not expected to compete with the hydrogen bond stacking sites of the CP. As expected, the rate at which they exchange is far slower than in water (7 days (figure 3.17) compared to 3 hours). In non-polar solvents the solvent molecules do not interact with the hydrogen bond sites on the cyclic peptide. For this reason, a slow rate of dynamics in toluene can be seen in both the kinetic rate constants (Table 3.2). A possible mechanism for this is that the nanotubes are breaking at different positions and reform instead of the exchange of unimers.[13]

The maximum FRET ratio was determined by measuring a premixed system. This was prepared by first separately dissolving each dye conjugate in DMF and then mixing them in a 1:1 volume ratio. The solvent was then evaporated and the residual CP conjugates were re-dissolved in water or toluene (Max FRET ratio, in Table 3.2). This ensured that the nanotubes formed in solution would be random supramolecular copolymers of both compounds. The minor difference observed between the

maximum and final FRET ratio could be associated to the presence of small homogenous regions within the nanotubes.

Table 3.2 The rate kinetics of the exchanging donor and acceptor conjugated cyclic peptide-polymer nanotubes. The final FRET ratio was the value at which the plateaux was reached.

Solvent	k_1/ s^{-1}	k_2/ s^{-1}	Final FRET ratio	Max FRET ratio*	Degree of mixing/ %
DMF	-	-	0.084	0.084	(100%)
Water	96.12	3.80	0.729	0.810	90%
Toluene	1.10	0.06	0.780	0.882	88%

* The maximum FRET ratio was determined using a premixed sample dissolve in the respective solvent. See experimental section for details.
In DMF, no emission change over time and a low FRET ratio indicates these conjugates resemble the free dyes which do not aggregate.

A theoretical FRET ratio of 1 would be expected if the dye conjugates formed statically mixed tubes of infinite length. Shown in Table 3.2, the final FRET ratios observed do not reach 1, therefore, suggesting the length of the aggregates formed or the presence of unimers in solutions prevents a quantitative exchange.

3.5.4 Concentration dependency of CPNT self-assembly

The described FRET system was also used to study the effect of concentration on the assembly of the CPNTs. Using the premixed system in water, *vide supra*, the solution was systematically diluted to observe the influence of concentration on the nanotube assembly. The fluorescence acceptor emission of this solution was measured upon excitation at 500 nm (donor) and 677 nm (acceptor) independently. The FRET intensity was normalised against the maximum emission determined by direct excitation of the acceptor. As expected, the normalised FRET intensity decreased upon dilution (Figure 3.5b). Interestingly, at low concentrations, a plateau was reached, after which further dilution of the system showed no change in normalised FRET emission.

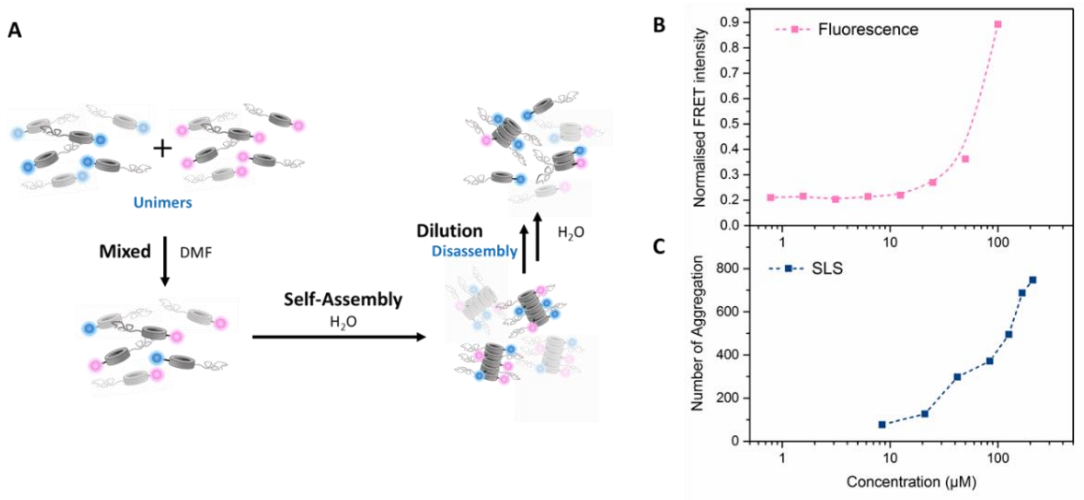

Figure 3.5 a) Fluorescence emission concentration dependent study of the mixed nanotubes. The concentration dependence on the cyclic peptide (premixed PEG-CP-Cy3 and PEG-CP-Cy5) stacking measured *via* b) fluorescence emission of the premixed dye conjugates and c) SLS of the control conjugates.

Using static light scattering (SLS) the average molecular weight and N_{agg} of non-dye conjugates were studied in a similar concentration regime as the FRET study with the dye conjugates (Experimental section 3.4.2.8). This is corroborated by SANS which showed similar nanotubular lengths for the premixed dye and non-dye conjugates. A trend, whereby at lower concentrations a decrease in the number of aggregation, was observed in the SLS. It should be noted that these scattering experiments only yield relative information about these systems, as these values may be an effect of interactions between tubes at higher concentrations. Nevertheless, the relative observations of the polymerization process as observed from SLS supports the trend as obtained by FRET, whereby at lower concentrations smaller aggregates were formed (Figure 3.5c). Aggregation of the conjugates at lower concentrations could not be studied accurately using SLS due to insufficient intensity of scattered light using the instrument set-up.

3.5.5 *In vitro* dynamic of cyclic peptide nanotubes

Having characterised the dynamics of these model cyclic peptide-polymer conjugates in a controlled environment (i.e. pure water), we turned to studying their behaviour in a more complex setting, namely living biological systems. This biological study was completed by Raoul Peltier in our group at the University of Warwick. The peptides PEG-CP-Cy3 and PEG-CP-Cy5 were incubated in the presence of MDA-231 cells

(human breast adenocarcinoma) and fluorescence, including FRET-associated fluorescence, was observed using fluorescent confocal microscopy. PEG-CP-Cy3 was used in a higher concentration (12 μM) than PEG-CP-Cy5 (4 μM) to account for the lower intensity as a result of not exciting the dye at its absorption maximum, resulting in a total concentration of 16 μM peptide. Negative controls whereby the cells were incubated individually with either PEG-CP-Cy3 or PEG-CP-Cy5 for 150 minutes clearly showed intracellular fluorescence when excited at their respective dye absorption and observed at their respective dye emission (Figure 3.6). The vast majority of the fluorescence can be observed in the intracellular region close to the nucleus, in a punctuated design which indicates that the compounds have not diffused in the cytosol but remain trapped within the lysosomes instead. Endosomal uptake and subsequent localisation in the lysosomes is expected for such nanosized objects and has been demonstrated for similar structures.[14]

When both PEG-CP-Cy3 **16** and PEG-CP-Cy5 **17** were co-injected and co-incubated in the presence of cells, allowing cyclic peptide-polymers to form mixed conjugates before or during cell entry, fluorescence associated with FRET could be observed within the cells. A similar result was observed when PEG-CP-Cy3 and PEG-CP-Cy5 where premixed in DMF, dried, re-dissolved in water, and injected in the cell culture. These results indicate that synthesised nanotubes of mixed conjugates can enter cells *via* endocytosis and remain intact within the harsh environment of the lysosomes for the time of the study.

Next, we wanted to test whether individual CPs could form mixed conjugates within the complex environment of living cells. We hypothesized that PEG-CP-Cy3 and PEG-CP-Cy5 nanotubes incubated separately with the cells could, given enough time, mix within the restricted environment of the lysosomes. By incubating PEG-CP-Cy5 for 30 minutes, washing the cells thoroughly and further incubating with PEG-CP-Cy3 for 120 minutes, a significant increase in the intracellular fluorescence associated with FRET as compared to the control was observed (Figure 3.6-3.7). This result clearly indicates that not only some of the nanotubes are transported into the same cell compartment but that the nanotubes are still able to exchange and re-organise themselves into mixed self-assembled systems within the cells. Taken together, the data demonstrate that this self-assembling system is robust enough to maintain its shape within a biological environment whereas the dynamic character is preserved

enabling different species of nanotubes to communicate with each other *via* the exchange of unimers. The compatibility of these nanostructures with living cells highlights the potential of these compounds for future biological and biomedical applications.

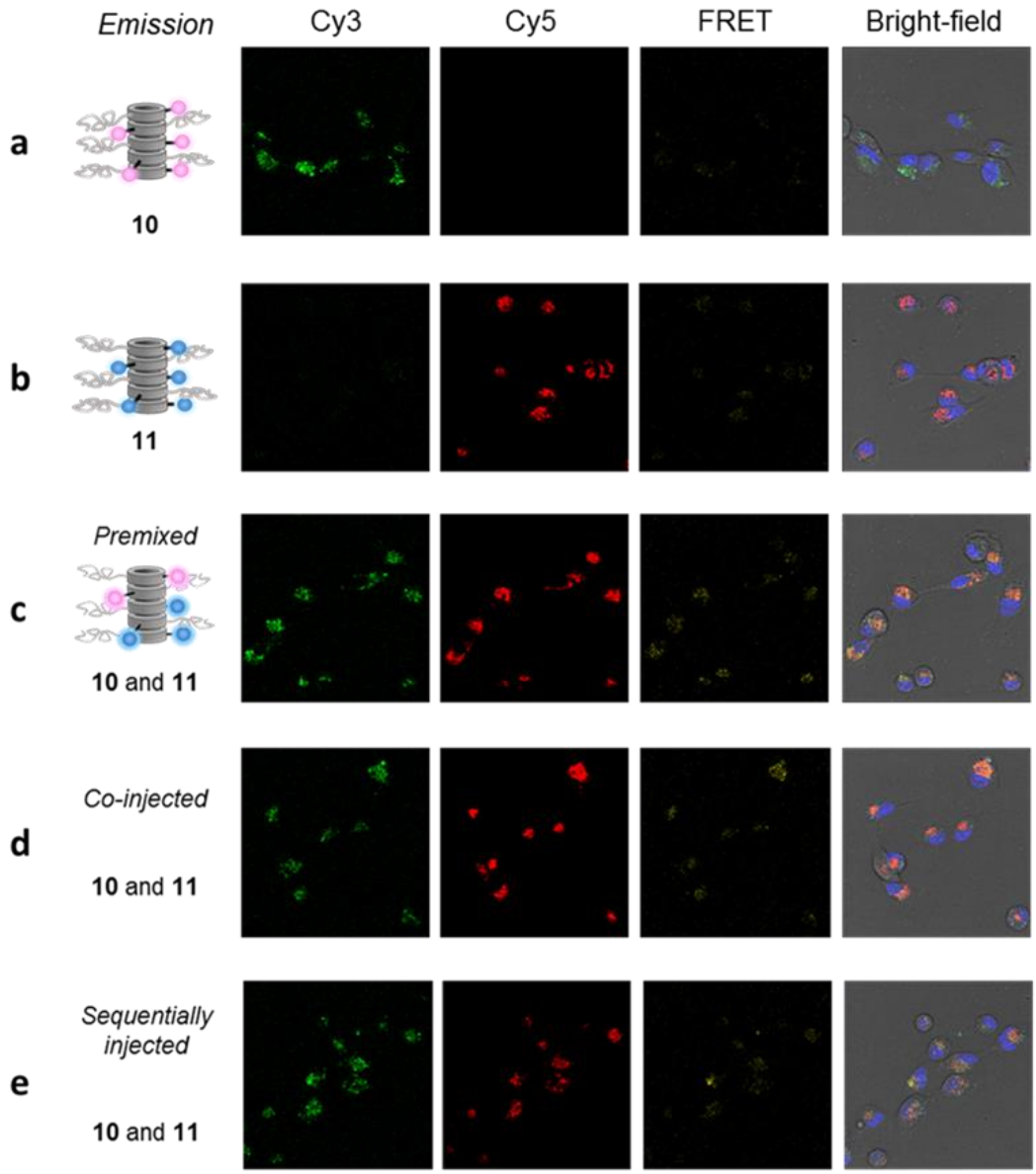

Figure 3.6 Confocal microscopy imaging of MDA-231 cells incubated in the presence of either A) PEG-CP-Cy5 alone (4 µM); B) PEG-CP-Cy3 alone (12 µM); C) premixed PEG-CP-Cy5 (4 µM) and PEG-CP-Cy3 (12 µM); D) co-injected PEG-CP-Cy5 (4 µM) and PEG-CP-Cy3 (12 µM); E) PEG-CP-Cy5 (4 µM) for 30 minutes, washed and PEG-CP-Cy3 (12 µM) for 120 minutes. Unless indicated otherwise, incubation proceeded for 150 min. Nucleus fluorescence was obtained using Hoechst 33342. Excitation/Emission used for measurement are as follow, nucleus channel (405 / 406-

459 nm), donor channel (517 / 540-577 nm), acceptor channel (633 / 670-724 nm), FRET (496 / 675-800 nm).

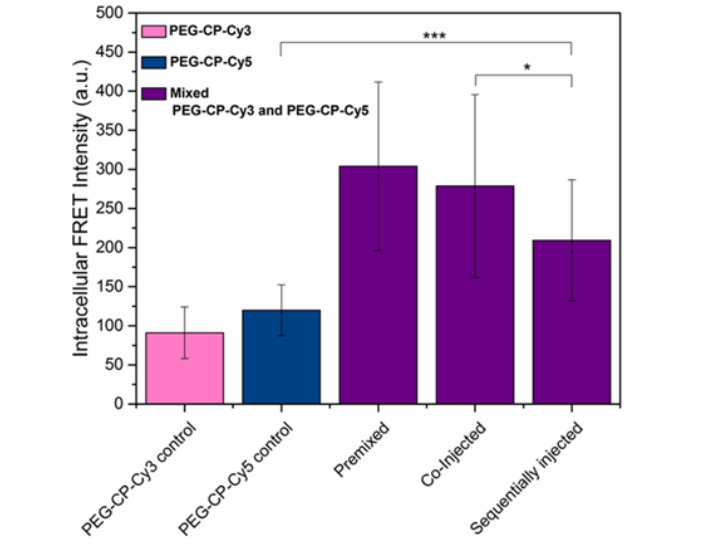

Figure 3.7 Average intensity of intracellular fluorescence associated with FRET, as calculated using the mean of fluorescence in each cells for a minimum of 15 cells.

3.6 Conclusion

The FRET dyes on the periphery of self-assembling cyclic peptide nanotubes have enabled us to directly monitor the dynamic behaviour of these supramolecular polymers in a range of different environments. The change in fluorescence emission was used to not only prove that the self-assemblies were rapidly disassembling and reassembling but also infer their rate of exchange and extent of mixing. Previously the hydrogen bond competitivity of the solvent was shown to directly affect the aggregation number here we show this was also extremely important in governing the rate of exchange between nanotubes. Although in all cases near quantitative mixing is observed in comparison to premixed samples; the kinetics are much faster in aqueous solutions as compared to toluene - with the nanotubes almost fully mixing after 3 hours.

Further studies showed that upon dilution the fluorescence associated with the FRET decreased, which is related to a steady decrease in size of the aggregates, a trend confirmed *via* static light scattering. In complex environments such as living cells, the combination of FRET and confocal microscopy showed that the different nanotubes were independently transported into the same cell compartments addition of the individual FRET-dye conjugates. This ability to recombine even under such conditions as present in living cells makes these materials attractive as a basic system for tracking of transport pathways, especially as further ligands can easily be attached to the polymer chain.

Overall, the obtained results provide the first fundamental information about the dynamic nature of these promising supramolecular systems in a range of different environments. From this understanding, the next chapter will focus on how we can improve the stability of these dynamic self-assemblies. This process of understanding and designing plays an integral part to realising the potential biological applications of these, and other, supramolecular polymers.

3.7 Experimental

3.7.1 Materials

Fmoc-protected amino acids and coupling agents were purchased from Iris Biotech GmbH. Cyanine3 NHS ester and Cyanine5 NHS ester were obtained from Lumiprobe GmbH, Germany. The amine functionalised PEG was purchased from Rapp Polymere. Pentanoic acid was purchased from Alfa Aesar (UK).

All other chemicals stated were purchased from Sigma-Aldrich, (Gillingham, UK) unless otherwise stated. Solvents were purchased from several departmental suppliers – Honeywell, Fisher and Sigma Aldrich.

3.7.2 Characterisation

3.7.2.1 Nuclear magnetic resonance spectroscopy (NMR)

^{1}H NMR spectrum were measured using a Bruker DPX-300 or DPX-400 NMR spectrometer which operated at 300.13 and 400.05 MHz respectively. The residual solvent peaks were used as internal references. Deuterated trifluoroacetic acid (*d*-TFA) (δ_H = 11.5 ppm) was used to measure the peptides.

3.7.2.2 Size-exclusion chromatography (SEC) / Gel permeation chromatography (GPC)

GPC was measured using an Agilent PL50 instrument with a differential refractive index (DRI) detector. The instrument contained two PolarGel D columns (linear MW operating range: 200 to 400,000 g/mol (PS equivalent)) and a PolarGel 5μm guard column. DMF with 0.1% LiBr additive was used as the eluent. The system ran at 1mg min^{-1} (50ºC), with an injection volume of 100 μL. The samples were prepared by filtering them through 0.22 μm pore size membranes, before injection. Agilent EasyVial poly (methyl methacrylate) standards were used to calibrate the instrument and output data was analysed using Agilent GPC/SEC software.

3.7.2.3 Small Angle Neutron Scattering (SANS)

SANS was carried out on the Sans2d small-angle diffractometer at the ISIS Pulsed Neutron Source (STFC Rutherford Appleton Laboratory, Didcot, U.K.).[15, 16] A simultaneous Q-range of 0.0045 – 0.7 Å^{-1} was achieved utilizing an incident wavelength range of 1.75 – 16.5 Å and employing an instrument set up of L1=L2=4m, with the 1 m^2 detector offset vertically 60 mm and sideways 100 mm. Q is defined as:

$$Q = \frac{4\pi \sin\frac{\theta}{2}}{\lambda} \qquad (2)$$

where θ is the scattered angle and λ is the incident neutron wavelength. The beam diameter was 8 mm. Each raw scattering data set was corrected for the detector efficiencies, sample transmission and background scattering and converted to scattering cross-section data ($\partial\Sigma/\partial\Omega$ vs. Q) using the instrument-specific software.[17] These data were placed on an absolute scale (cm^{-1}) using the scattering from a standard sample (a solid blend of hydrogenous and perdeuterated polystyrene) in accordance with established procedures.[18]

Following data acquisition, the SASfit software programme was used to model the data. In all cases several fixed parameters were used; concentration, the radius of the core, and SLD values (for the solvent, core peptide, and polymer shell).

Values for SLD were calculated using the following equation;

$$SLD = \frac{\rho N_a \sum_{i=1}^{N} b_i}{\sum_{i=1}^{N} M_i}$$

Where ρ is the bulk density of the material, N_a is Avogadro's constant, b_i is the scattering length contributions from the N atoms within the unit cell, and M is the atomic mass of N atoms. Values for individual atomic scattering lengths and atomic weights were taken from the NIST database.[19, 20] SLD parameters were calculated for the solvent, polymer, and peptide and used as fixed values in the fitting analysis. The use of data from previous SANS experiments provided the vale for cylinder radius of 0.4 nm.

The hairy-cylinder model, is a combination model adapted from the form factor of a micelle, with a rod-like core as an additionally structure factor. The form factor can be described as;

$$P(q) = N^2\beta_s^2 F_{s(q)} + N\beta_c^2 F_{c(q)} + 2N^2\beta_s\beta_c S_{sc(q)} + N(N-1)\beta_c^2 S_{cc(q)}$$

Where N is the aggregation number, and $\beta_s = V_s\,(\rho_s - \rho_{solv})$ / $\beta_c = V_c\,(\rho_c - \rho_{solv})$ is the total excess scattering lengths of the cylindrical core and in the corona, respectively. V_s and V_c are the volumes of the core and in the corona, respectively. ρ_s and ρ_c are the corresponding scattering length densities and ρ_{solv} is the scattering

length density of the surrounding solvent, calculated as previously discussed. Table 3.3 provides a summary of the fitting parameters. Columns marked * were fixed variables.

Table 3.3 Parameters and results from fitting the SANS scattering data to a hairy-cylinder model.

Sample	**Length of nanotube (nm)**	**N_{agg}**	**R_g (nm)**	***Core radius (nm)**	***SLD peptide (cm^{-1})**	***SLD polymer (cm^{-1})**
Cy3/Cy5 mixed	88.98	189.32	93.43	0.34	$5.09E^{-7}$	$6.78E^{-7}$
PEG-conjugated control	116.93	248.79	113.12	0.34	$5.09E^{-7}$	$6.78E^{-7}$

The individual fits (Fig 3.8 and 3.9) were considered statistically reliable when a Chi^2 of <30 was achieved.

Following data acquisition, the SASfit software programme was used to model the data. In all cases several fixed parameters were used; concentration, the radius of the core, and SLD values (for the solvent, core peptide, and polymer shell).

Values for SLD were calculated using the following equation;

$$SLD = \frac{\rho N_a \sum_{i=1}^{N} b_i}{\sum_{i=1}^{N} M_i}$$

Where ρ is the bulk density of the material, N_a is Avogadro's constant, b_i is the scattering length contributions from the N atoms within the unit cell, and M is the atomic mass of N atoms. Values for individual atomic scattering lengths and atomic weights were taken from the NIST database.[19, 20] SLD parameters were calculated for the solvent, polymer, and peptide and used as fixed values in the fitting analysis. The use of data from previous SANS experiments provided the vale for cylinder radius of 0.4 nm.

The hairy-cylinder model, is a combination model adapted from the form factor of a micelle, with a rod-like core as an additionally structure factor. The form factor can be described as;

$$P(q) = N^2\beta_s^2 F_{s(q)} + N\beta_c^2 F_{c(q)} + 2N^2\beta_s\beta_c S_{sc(q)} + N(N-1)\beta_c^2 S_{cc(q)}$$

Where N is the aggregation number, and $\beta_s = V_s\,(\rho_s - \rho_{solv})$ / $\beta_c = V_c\,(\rho_c - \rho_{solv})$ is the total excess scattering lengths of the cylindrical core and in the corona, respectively. V_s and V_c are the volumes of the core and in the corona, respectively. ρ_s and ρ_c are the corresponding scattering length densities and ρ_{solv} is the scattering length density of the surrounding solvent, calculated as previously discussed.

The individual fits (Fig 3.8 and 3.9) were considered statistically reliable when a Chi^2 of <30 was achieved.

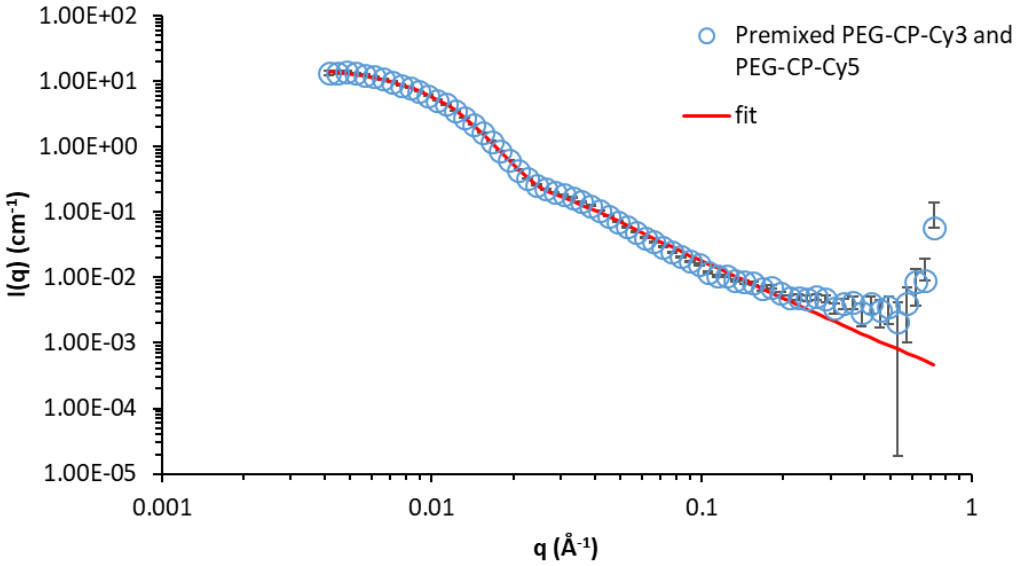

Figure 3.8 Reduced scattering data and fit to a hairy cylinder model for the premixed PEG-CP-Cy3 and PEG-CP-Cy5.

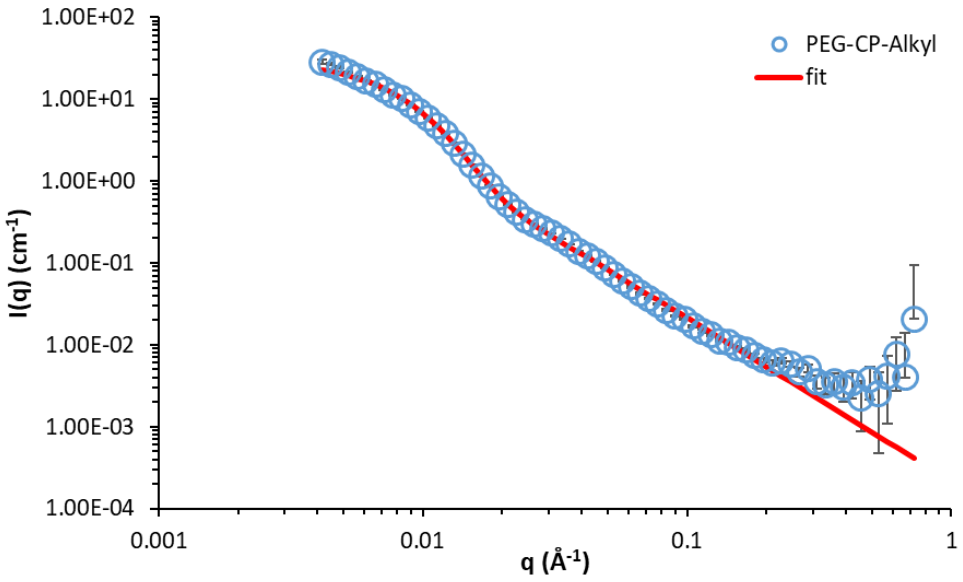

Figure 3.9 Reduced scattering data and fit to a hairy cylinder model for the control PEG conjugated cyclic peptide (PEG-CP-Alkyl).

3.7.2.4 Ultraviolet/visible (UV-Vis) absorption spectroscopy

UV-Vis absorption spectra was measured using an Agilent Technologies Cary 60 UV-Vis spectrometer. The UV spectra of PEG-CP-Cy3 (**16**) and PEG-CP-Cy5 (**17**) were obtained in each solvent (water, DMF, toluene). The solution were all made to the same concentration (35 µM). Spectra can be found in Appendix Figure 3.14.

3.7.2.5 Fluorescence emission spectroscopy

Fluorescence emission spectra was measured using an Agilent Technologies Cary Eclipse Fluorescence spectrometer. The FRET studies were performed using an excitation wavelength of 500 nm. This was done to significantly reduce the direct excitation of the acceptor in the FRET studies. The acceptor emission upon excitation at 500 nm was considerably smaller than at 548nm (absorption maxima of the donor). See Appendix Figure 3.15 for the emission spectra of the conjugates **16** and **17**.

Dynamics in self-assembled systems: First, 35 µM stock solutions of PEG-CP-Cy3 and PEG-CP-Cy5 were prepared in the water. The emission spectra of the PEG-CP-Cy3 was measured before the addition of the PEG-CP-Cy5 conjugate. The fluorescence emission spectra were taken using the Agilent Kinetic software. Excitation of the donor was set to 500 nm, donor emission (detected) to 565 nm and

acceptor emission (detected) at 662 nm. The mixing of the dyes Cy3-NHS and Cy5-NHS were also tested using the same conditions.

Solvent dependence study: First, 35 µM stock solutions of PEG-CP-Cy3 and PEG-CP-Cy5 were prepared in the relevant solvent. The emission spectra of the PEG-CP-Cy3 was measured before the addition of the PEG-CP-Cy5 conjugate. The fluorescence emission spectra were taken at several time points upon the addition of the PEG-CP-Cy5. The FRET ratio was obtained using the equation 1, the relative FRET intensities were calculated and fitted to a second order exponential function.

Concentration dependence study: First, 50 µM stock solutions of PEG-CP-Cy3 and PEG-CP-Cy5 in DMF were prepared. 1 mL of each stock solution was added to a vial and the solution was shaken for 30 minutes and the solvent was evaporated. The residual solid was then redissolved in a precise volume of water (around 1 mL) to create a dye conjugate solution with a concentration of 100 µM. 1 mL of this solution was transferred to measure the first concentration (100 µM). Next, 1 mL of water was added to the cuvette to yield the next dilution (50 µM). For subsequent concentrations the solution in the cuvette was transferred to another vial and further dilution concentrations were made up in a new vial using 1 mL of water and 1 mL of the transferred (previous) solution.

3.7.2.6 High performance liquid chromatography (HPLC)

High performance liquid chromatograms (HPLC) was measured using an Agilent Technologies 1200 Series, equipped with a Luna 5u C18 100 Å, 250 x 4.6mm column. Acetonitrile/Water were used. All solvents contained 0.04 vol% TFA. See table below for the method and gradients.

Table 3.4 HPLC gradient method

Time/ mins	**Acetonitrile/ %**	**Water/ %**
0-5	10	90
5-35	10 to 95	95 to 10
35-38	95	5

3.7.2.7 Mass spectrometry (ESI-TOF)

Electronspray ionisation (ESI) – time of flight (TOF) mass spectra (MS) was measured using a Bruker MicroTOF to characterise the peptides and peptide conjugates. The instrument can achieve less than 5 ppm mass accuracy.

3.7.2.8 Static Light Scattering (SLS)

The SLS data were obtained using the ALV/CGS-3 Compact Gonimeter System.

A range of different concentrations of non-dye conjugated CP-polymers measured using SLS. The compounds were first accurately measured in a vial and corresponding volumes of water were added to yield various different concentrations (5 mg mL^{-1} - 0.2 mg mL^{-1}). Before measuring, the solutions were filtered using 0.2 µM membrane PTFE lined filters to remove any large PEG crystalline aggregates.

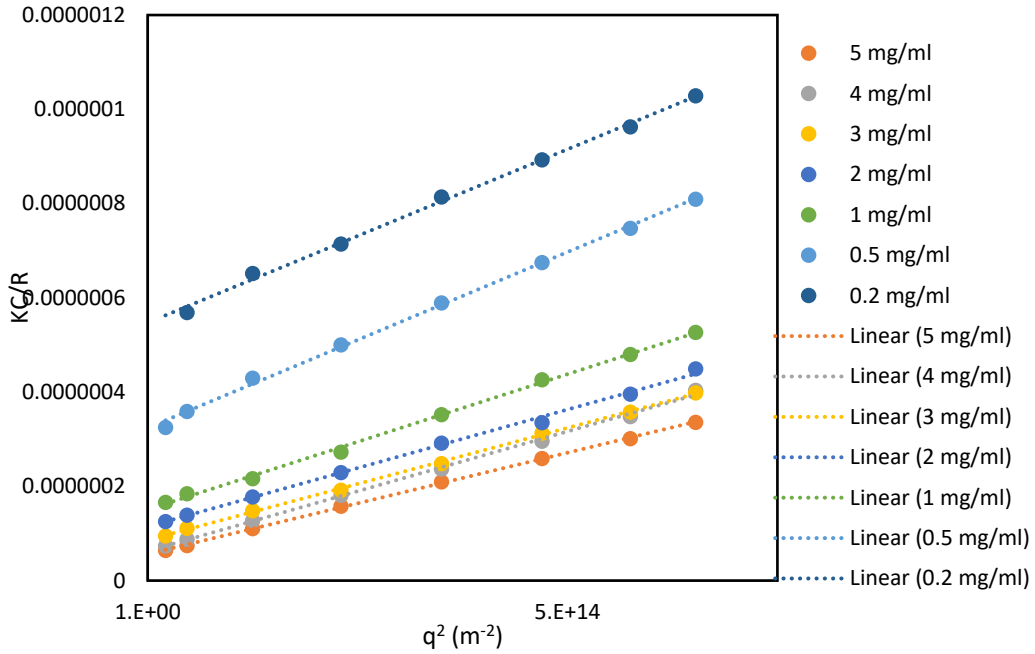

Figure 3.10 Evolution of KC/R of PEG-CP-Alkyl in water as a function of q^2 obtained by static light scattering.

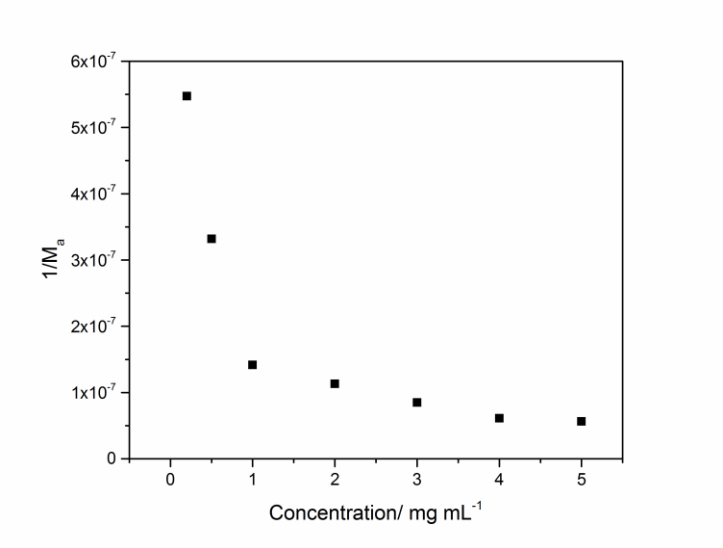

Figure 3.11 Evolution of $1/M_a$ of PEG-CP-Alkyl in water as a function of concentration obtained by static light scattering.

3.7.2.9 Confocal microscopy

MDA-231 (human breast adenocarcinoma) cells were cultured in High Glucose DMEM medium supplemented with 10% fetal bovine serum. For confocal microscopy, MDA-231 cells were seeded in an 8-well ibidi plate at a density of 10 000 cells per well and allowed to grow for 48 hours prior to the experiment. Cells medium was then replaced by fresh medium and supplemented with PEG-CP-Cy5 (4 µM), PEG-CP-Cy5 (12 µM), or both, from stock solutions at 200 µM in water. For the premixed sample, stock solutions of PEG-CP-Cy5 (200 µM) and PEG-CP-Cy5 (600 µM) were prepared in DMF, sonicated, DMF evaporated with N_2 flow and re-dissolved in water. Cells were incubated with conjugates for 135 minutes. In the case of sequential incubation, PEG-CP-Cy5 (4 µM) was incubated first for 30 minutes, the cells washed thoroughly with PBS, then incubated with fresh media and PEG-CP-Cy5 (12 µM) for 105 minutes. For all sample, Hoechst 33342 was then added and incubation proceeded for another 15 minutes before cells were washed with warm media twice. Confocal microscopy images were taken on a Leica TCS SP5 (Carl Zeiss, Germany) at a temperature of 37°C, using sequential scanning for each channel. Excitation/Emission used for measurement are used as follow: nucleus channel (405 / 406-459 nm), donor channel (517 / 540-577 nm), acceptor channel (633 / 670-724 nm), FRET (496 / 675-800 nm). Average of fluorescence for each sample was measured using ImageJ software by isolating single cells as region of interest and averaging the mean of fluorescence in each cells, on a minimum of 15 cells by samples.

3.7.2.10 Transmission Electron Microscopy (TEM)

Carbon films (4 nm) were prepared on freshly cleaved mica sheets using a Quorum Q150T Turbo carbon coater. These films were deposited on copper TEM girds (mesh 400 – Agar Scientific) by flotation water. Solutions of PEG-CP-dye/alkyl conjugates in water at 1 mg mL^{-1} were prepared by direct dissolution of the solid in filtered ultra-pure water. Samples were left to age for 24h at room temperature then filtered through PTFE syringe filters (0.45 μm pore size). 10 μL of each solution was drop-cast on freshly glow-discharged carbon-coated grids placed on filter paper. After drying, 10 μL of a 2% uranyl acetate solution in ethanol was dropped onto the grids on filter paper and left to dry. Bright field TEM micrographs were obtained with a JEOL 1400 microscope operating at 120 kV, equipped with a Gatan digital camera.

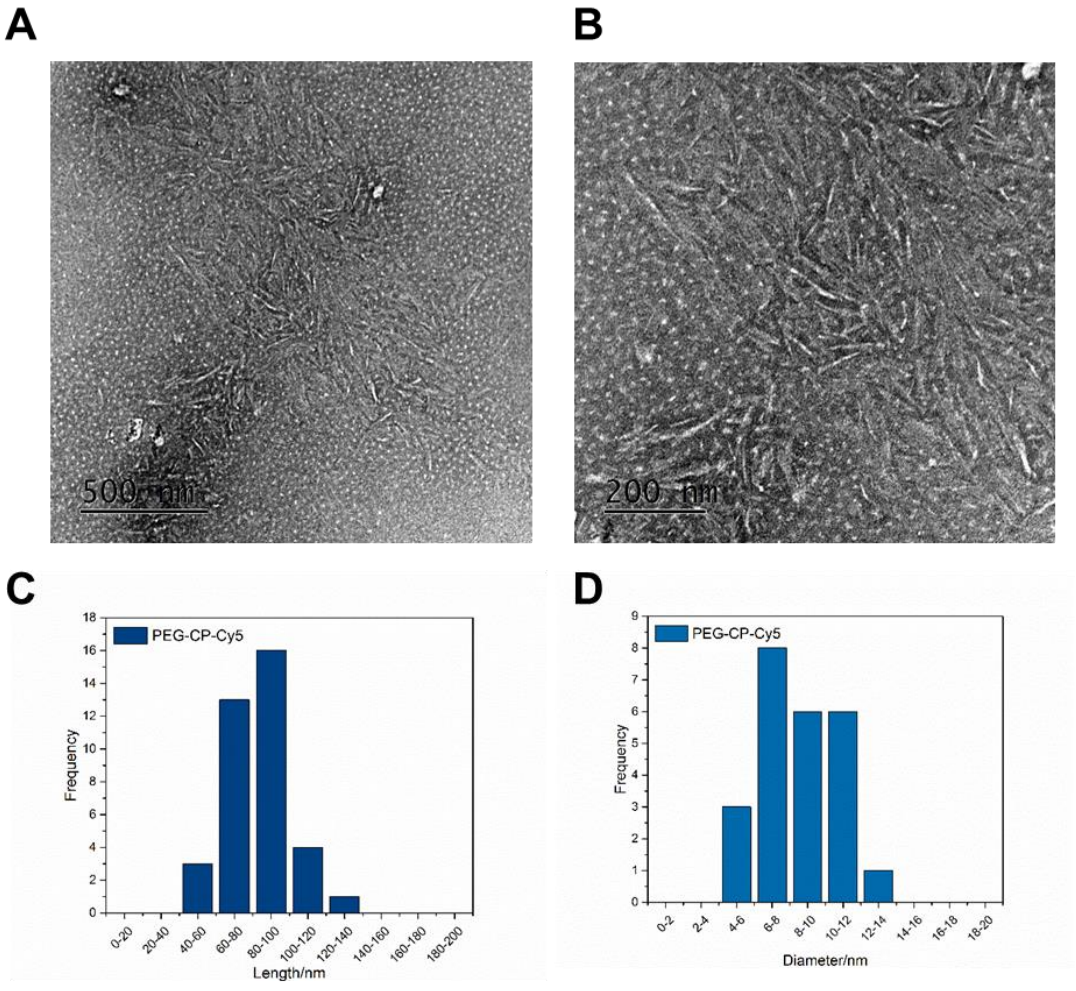

Note. TEM distributions obtained from image above (right)

Figure 3.12 TEM images of PEG-CP-Cy5 (**17**).

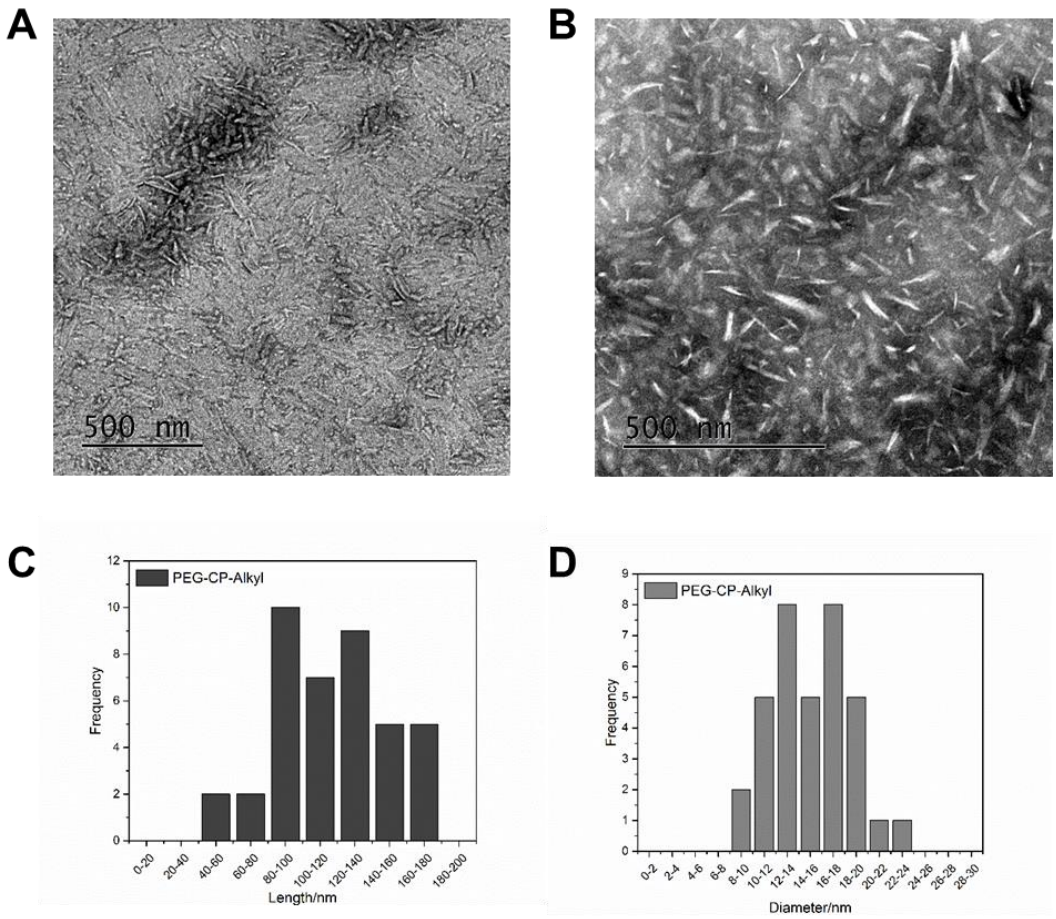

Note. TEM distributions obtained from image above (right)

Figure 3.13 TEM of PEG-CP-Alkyl (**18**).

TEM of the PEC-CP-Cy3 conjugates in Figure 3.2b.

Using ImageJ software the following length and diameter distributions were calculated.

Due to the effect of drying and low contrast in these pictures it was difficult to determine exact diameter and length values.

3.8 Appendix

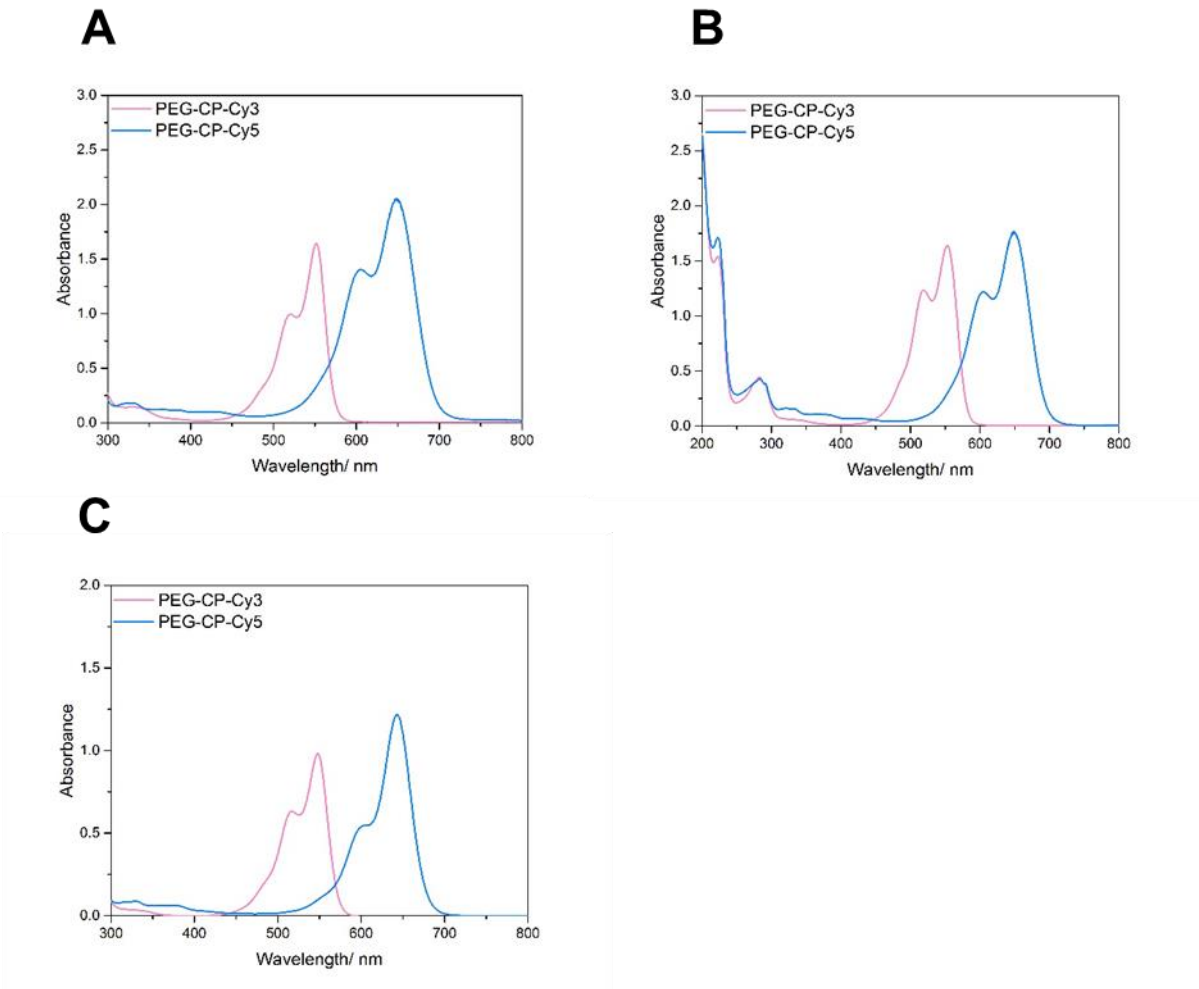

Figure 3.14 Ultraviolet (UV) spectra of PEG-CP-Cy3 and PEG-CP-Cy5 in a) dimethylformamide, b) water and c) toluene at 17.5µM.

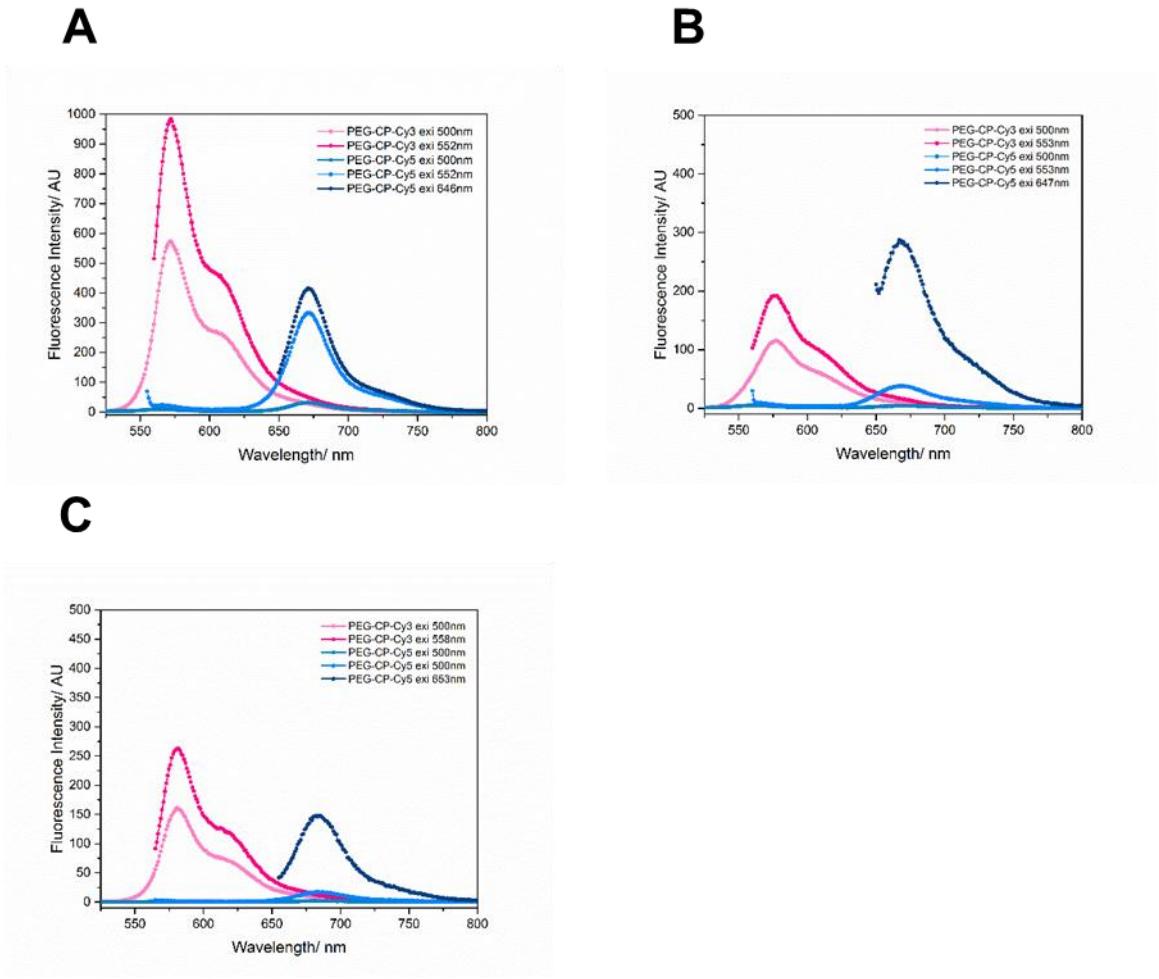

Figure 3.15 Fluorescence emission spectra of PEG-CP-Cy3 and PEG-CP-Cy5 in a) dimethylformamide, b) water and c) toluene at 17.5µM.

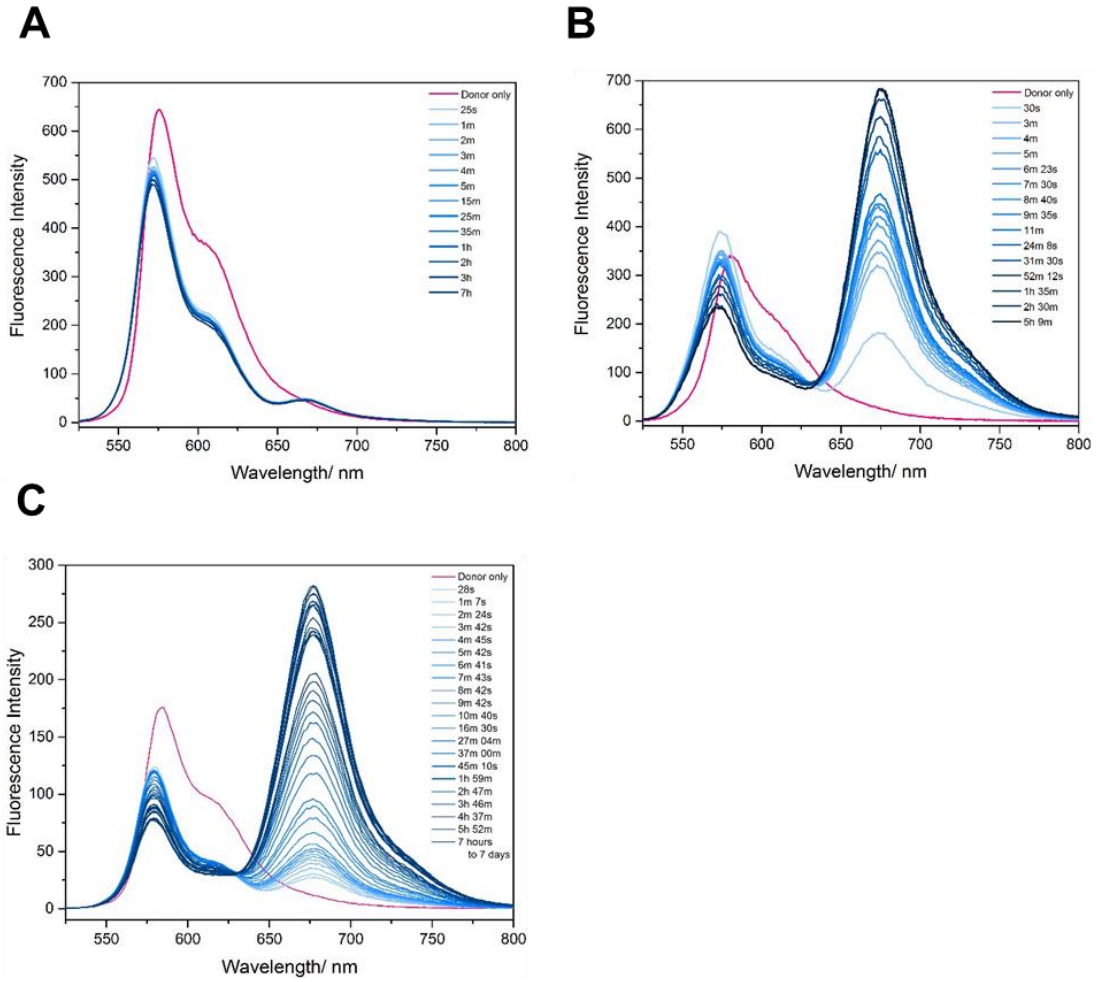

Figure 3.16 Fluorescence emission spectra of the FRET mixing study in a) dimethylformamide, b) water and c) toluene.

The fluorescence emission spectra of the mixed PEG-CP-Cy3 (17.5 µM) and PEG-CP-Cy5 (17.5 µM) were together taken at different times.

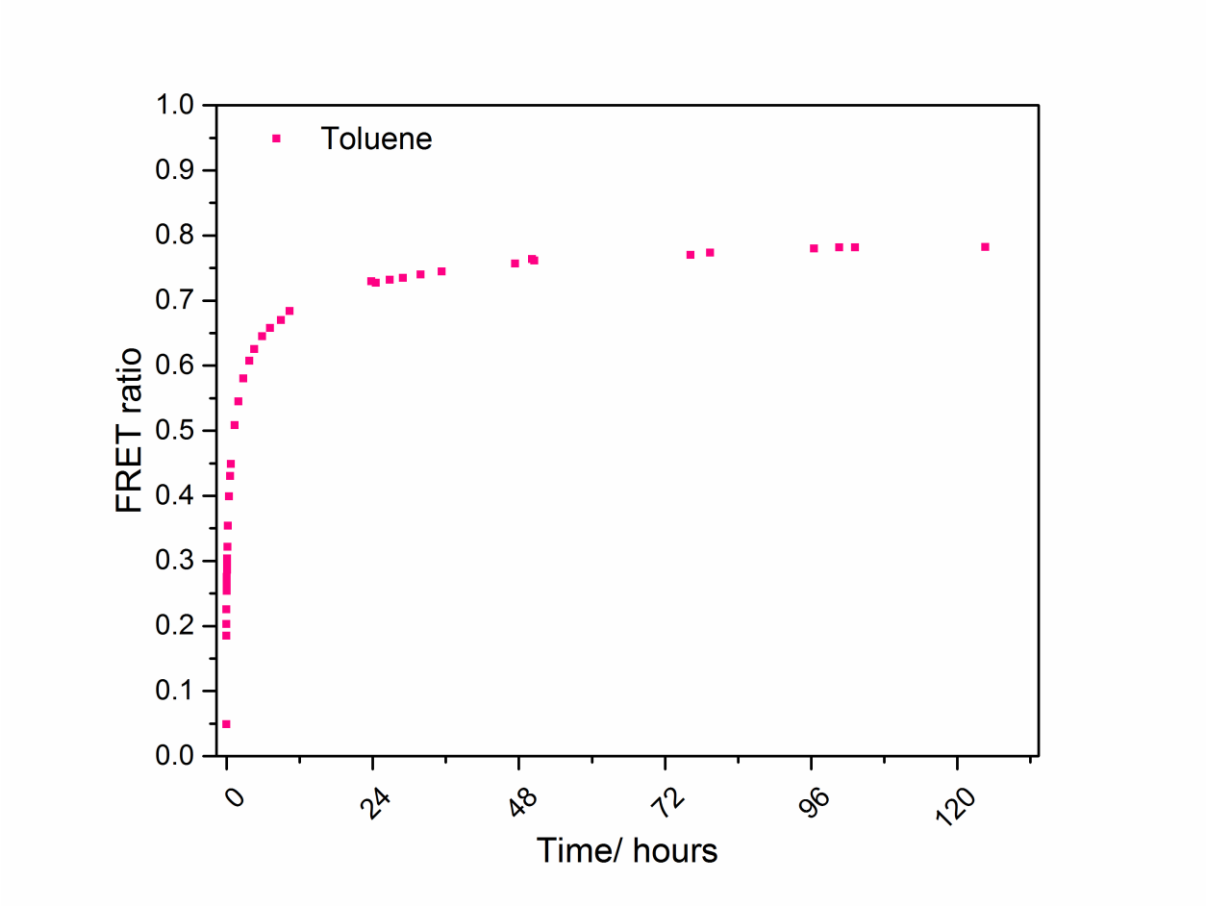

Figure 3.17 The kinetic exchange of PEG-CP-Cy3 and PEG-CP-Cy5 upon mixing in toluene.

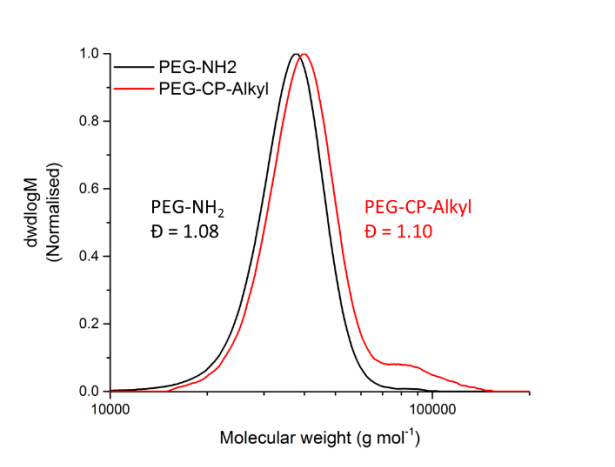

Figure 3.18 Normalised SEC trace of the initial PEG polymer before conjugation and the fully functionalised PEG-CP-Alkyl control conjugate.

Note. Deconvolution of the higher molecular distribution was attempted however was not possible.

(SEC: DMF +0.1% LiBr).

3.9 References

1. R. Chapman, M. Danial, M. L. Koh, K. A. Jolliffe and S. Perrier, *Chemical Society Reviews*, 2012, **41**, 6023-6041.
2. M. J. Hollamby, *Physical Chemistry Chemical Physics*, 2013, **15**, 10566-10579.
3. M. L. Koh, P. A. FitzGerald, G. G. Warr, K. A. Jolliffe and S. Perrier, *Chemistry – A European Journal*, 2016, **22**, 18419-18428.
4. R. Chapman, G. G. Warr, S. Perrier and K. A. Jolliffe, *Chem. Eur. J.*, 2013, **19**, 1955-1961.
5. S. Catrouillet, J. C. Brendel, S. Larnaudie, T. Barlow, K. A. Jolliffe and S. Perrier, *ACS Macro Letters*, 2016, **5**, 1119-1123.
6. M. Engels, D. Bashford and M. R. Ghadiri, *Journal of the American Chemical Society*, 1995, **117**, 9151-9158.
7. E. A. Jares-Erijman and T. M. Jovin, *Nat Biotech*, 2003, **21**, 1387-1395.
8. M. R. Ghadiri, J. R. Granja and L. K. Buehler, *Nature*, 1994, **369**, 301.
9. J. D. Hartgerink, J. R. Granja, R. A. Milligan and M. R. Ghadiri, *Journal of the American Chemical Society*, 1996, **118**, 43-50.
10. R. Chapman, M. L. Koh, G. G. Warr, K. A. Jolliffe and S. Perrier, *Chemical Science*, 2013, **4**, 2581-2589.
11. S. I. S. Hendrikse, S. P. W. Wijnands, R. P. M. Lafleur, M. J. Pouderoijen, H. M. Janssen, P. Y. W. Dankers and E. W. Meijer, *Chemical Communications*, 2017, **53**, 2279-2282.
12. C. Pietsch, U. S. Schubert and R. Hoogenboom, *Chemical Communications*, 2011, **47**, 8750-8765.
13. L. Albertazzi, D. van der Zwaag, C. M. Leenders, R. Fitzner, R. W. van der Hofstad and E. Meijer, *Science*, 2014, **344**, 491-495.
14. M. Chemerovski-Glikman, E. Rozentur-Shkop, M. Richman, A. Grupi, A. Getler, H. Y. Cohen, H. Shaked, C. Wallin, S. K. T. S. Wärmländer, E. Haas, A. Gräslund, J. H. Chill and S. Rahimipour, *Chemistry – A European Journal*, 2016, **22**, 14236-14246.
15. R. Heenan, S. Rogers, D. Turner, A. Terry, J. Treadgold and S. King, *Neutron News*, 2011, **22**, 19-21.

16. ISIS Science & Technology Facilities Council, http://www.isis.stfc.ac.uk).
17. Mantid Project, http://www.mantidproject.org).
18. G. T. Wignall and F. Bates, *Journal of applied crystallography*, 1987, **20**, 28-40.
19. F. S. VARLEY, *Neutron News*, 1992, **3**.
20. NIST, https://www.ncnr.nist.gov/resources/n-lengths/).

Chapter 4 Dual self-assembly of cyclic peptide nanotubes to provide stabilisation in water

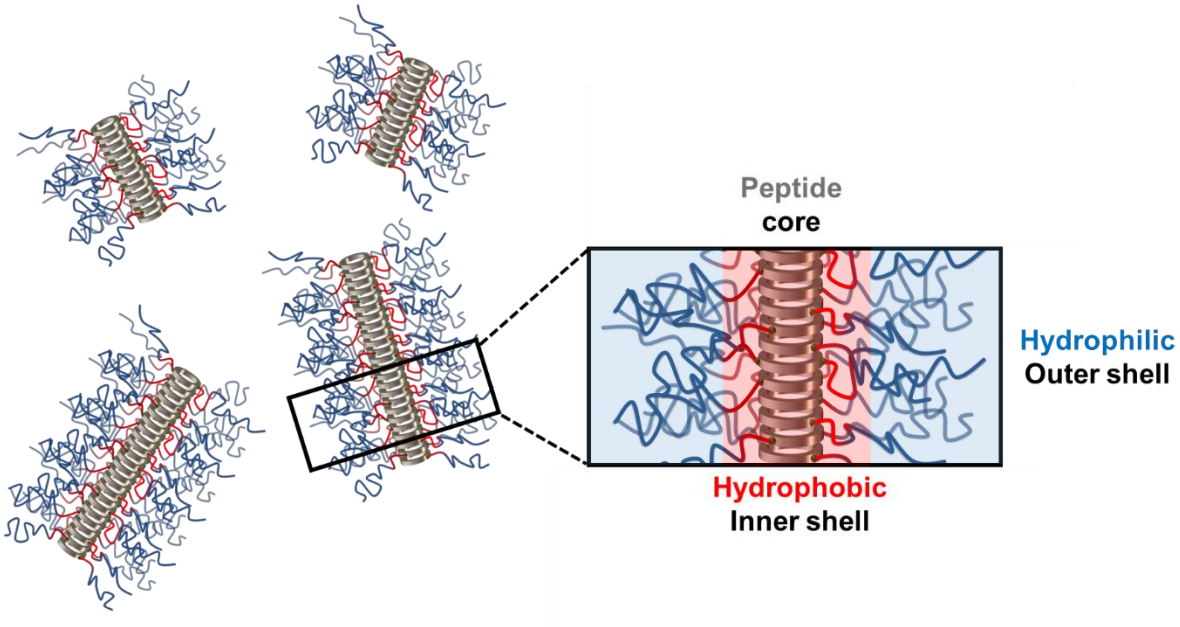

4.1 Introduction

Proteins play a vital role in all living systems, from the catalysis of metabolic reactions to providing structure of our cells. Since the hierarchical self-assembly of proteins was elucidated, these fascinating molecules have been the subject of a host of biological applications. The amino acid building blocks of the peptide (primary structure) determine how the sequence will non-covalently fold and interact with itself (secondary and tertiary structure) and other peptides (quaternary structure). Nucleases, tubular proteins such as the tobacco mosaic virus and the collagen of our connective tissues all use this hierarchical assembly to form their impressive complex and defined nanostructures. Although synthetically reproducing the complexity of these systems is still a far prospect, the advent of supramolecular polymers has brought us a step closer by providing us with a powerful tool to synthesise a range of different morphologies on the nanoscale, such as nanofibers,[1] nanoribbons[2] and nanotubes.[3, 4]

The transfer of supramolecular materials into applications requires a good understanding of their dynamic behaviour to avoid unexpected de-polymerization or aggregation. In the previous chapters the exchange behaviour of CPNT in water and *in vitro* showed the peptide unimers rapidly exchange between the self-assembled nanotubes.[5] The highly dynamic nature of these supramolecular assemblies explains why many of these systems are very short in length, typically around 10 nm.[6, 7] The hydrophilic polymer arms decorating the peptide nanotube provide a steric barrier to prevent lateral aggregation and in turn improve their solubility in water, however dramatically lower their aggregation number.[8, 9]

The next generation of bio-inspired nanomaterials aims to encompass multiple design features, including controlled size, stability, bio-compatibility and high functionality. There are only a few examples of stabilised elongated uniform self-assembled nanostructures using the concept of 'living' supramolecular polymerization, discussed in detail in Chapter 1 (Introduction). Despite these incredible advances, designing controlled self-assembly systems for biological relevant systems in aqueous conditions has been much more challenging.

Inspired by the hierarchical design and structure of proteins, a two-fold self-assembly approach was developed to help stabilise the elongated peptide nanostructure. The hydrogen bond stacking of the cyclic peptides provides the primary structure and

overall cylindrical morphology of the self-assembled aggregates. Here we introduce a secondary structural driving force in the form of a hydrophobic region around the peptide to stabilise the single cyclic peptide nanotubes. The individual nanotubes remain independent due to the hydrophilic corona stabilising the nanostructures in water. This hierarchical approach offers a method to stabilise, not only cyclic peptides, but other β-sheet forming self-assembled architectures. The increasing complexity of these systems is the next step to realising the biological applications of these promising synthetic supramolecular polymers.

4.2 Synthesis and Characterisation.

4.2.1 Design and synthesis of CP-diblock polymer conjugates.

In order to stabilise and improve the self-assembly of cyclic peptide–polymer nanotubes, an amphiphilic diblock co-polymer was attached to the periphery of the CP. As sterically demanding polymers have been shown to dramatically destabilise the nanotubes[8] less bulky monomers such as butyl acrylate (BA) and *N*,*N*-dimethylacrylamide (DMA) were chosen to form the hydrophobic and hydrophilic blocks, respectively. In order to form discrete regions around the cyclic peptide core (Figure 4.1), reversible addition fragmentation chain-transfer (RAFT) polymerisation was employed to generate narrow dispersity ($Đ < 1.15$) diblock co-polymers.[10, 11] A homopolymer of the hydrophilic monomer of the same chain length (i.e. degree of polymerisation) lacking the hydrophobic region was also synthesised as a control. See Figure 4.2

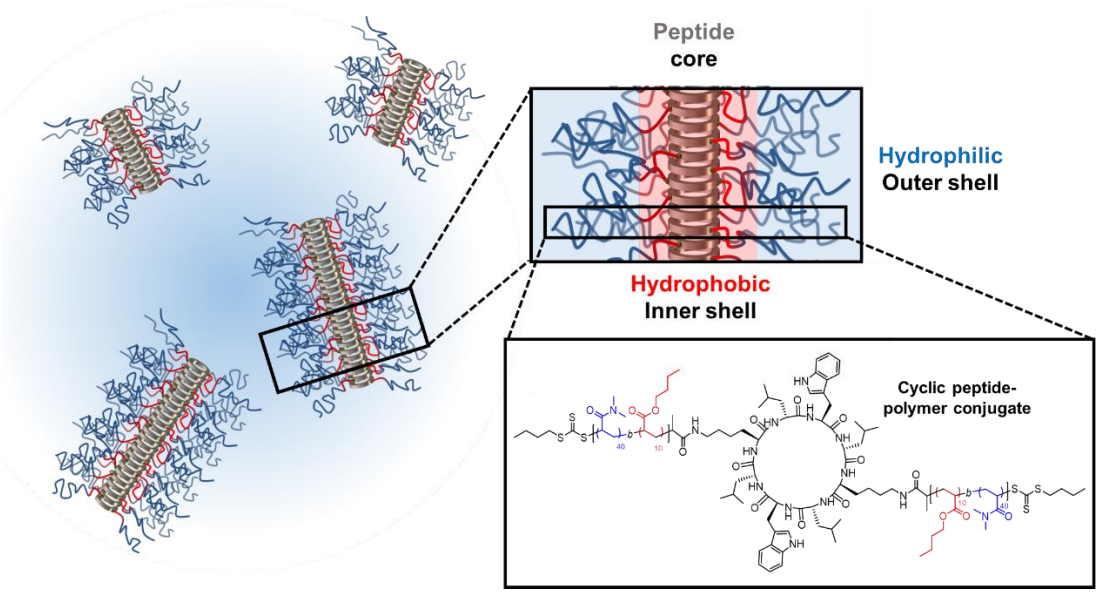

Figure 4.1 Self-assembling cyclic peptide-diblock polymer conjugates. In aqueous conditions, the diblock copolymers conjugated onto the cyclic peptide (CP-(pBA-*b*-pDMA)$_2$) self-assembles to form a hydrophobic region around the peptide and a hydrophilic corona.

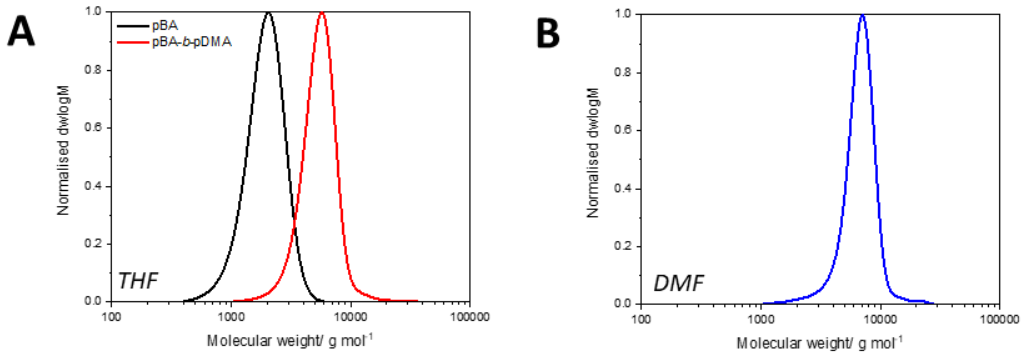

pBA
$Đ$ = 1.15
$M_{w,GPC}$= 2,000 g mol^{-1}
$M_{w,NMR}$= 1,520 g mol^{-1}

pBA-*b*-pDMA
$Đ$ = 1.13
$M_{w,GPC}$= 5,700 g mol^{-1}
$M_{w,NMR}$= 5,590g mol^{-1}

pDMA
$Đ$ = 1.14
$M_{w,GPC}$= 7,000 g mol^{-1}
$M_{w,NMR}$= 5,690 g mol^{-1}

Figure 4.2 SEC traces of the polymers: a) pBA and pBA-block-pDMA in THF and b) pDMA in DMF + 0.1% NH_4BF_4.

A CP with two conjugation sites was chosen to provide a dense hydrophobic core region around the peptide to better exclude water molecules competing with the hydrogen bond stacking of the nanotubes. The amine units of lysine were used to provide the handles for post-reaction modification of the peptide with the desired polymers. In the size exclusion chromatography (SEC) trace, a clear double molecular weight shift between the free polymer and the two-arm cyclic peptide-polymer conjugate was observed (see Figure 4.3). In the reaction mixture, containing both the conjugate and excess polymer, two distributions are visible. After purification *via* precipitation the lower molecular weight distribution associated with unconjugated polymer is removed. A conjugate with a similar degree of polymerisation, but without a hydrophobic region, was also synthesised as a control. The detailed synthetic procedure is given in experimental 4.6.3. For ease, the CP-(pBA-*b*-pDMA)$_2$ and CP-(pDMA)$_2$ are referred to as the diblock or control conjugate, respectively.

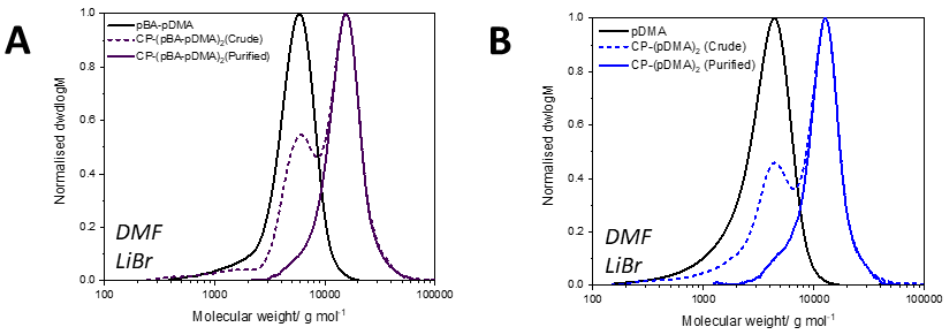

Diblock conjugate

pBA-*b*-pDMA
$Đ$ = 1.34
$M_{w,GPC}$= 5,600 g mol^{-1}

CP-(pBA-*b*-pDMA)$_2$
$Đ$ = 1.21
$M_{w,GPC}$= 15,800 g mol^{-1}
$M_{w,\ Theory}$= 12,200 g mol^{-1}

Control conjugate

pDMA
$Đ$ = 1.58
$M_{w,GPC}$= 4,400 g mol^{-1}

CP-(pDMA)$_2$
$Đ$ = 1.21
$M_{w,GPC}$= 13,000 g mol^{-1}

Figure 4.3 SEC traces of the polymer before conjugation and after conjugation. a) pBA-*b*-pDMA and CP-(pBA-*b*-pDMA)$_2$ and b) pDMA and CP-(pDMA)$_2$ in DMF +0.1% LiBr.

4.2.2 Characterisation of the diblock and control conjugates

Next, the morphology, dimensions, toxicity and self-assembly mechanism of these self-assembling cyclic peptide-polymer nanotubes were investigated. In transmission electron microscopy (TEM), we observed the elongated morphology of diblock conjugated CP, with an average length of 210 nm calculated for diblock conjugates prepared in water at 1 mg mL^{-1}.

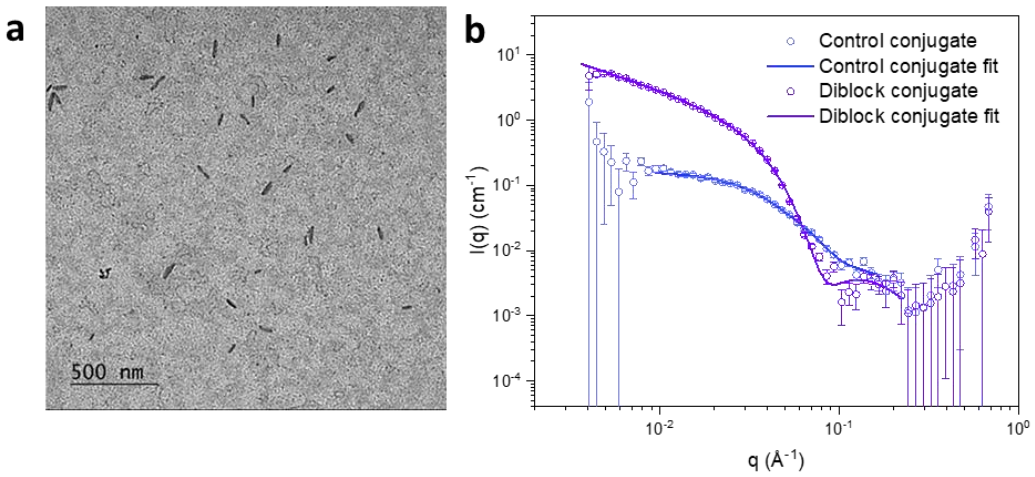

c

Conjugate	Length $_{TEM}$ / nm	Length $_{SANS}$ / nm	Length $_{SLS}$ / nm
Diblock conjugate	182	>100	273
Control conjugate	n.a	10	12

Figure 4.4 Characterisation of cyclic peptide-polymer nanotubes. a) TEM image of the diblock conjugates prepared in water. b) SANS profiles of the diblock and control conjugates fitted to a cylindrical micelle model using SASfit software. c) Table of the average length of the nanotubes measured *via* TEM, SANS and SLS respectively.

As expected, it was not possible to observe the self-assemblies of the fully hydrophilic control conjugate in TEM due to their size (around 12 nm in SLS, *vide infra*).[6-8] Small angle neutron scattering (SANS) was used to corroborate the nanotubular morphology of the peptide nanotubes in solution. Using SASfit software, the scattering profile of the diblock and control conjugates in D_2O were best fitted to a cylindrical micellar model. The resulting fits showed the average length to be over 100 nm (the size window available to SANS analysis) for the diblock conjugate, and 10 nm for the

control conjugates (Figure 4.4c). A detailed analysis of the SANS fitting and experimental is given in experimental 4.6.6.

The aggregate length and the number of participating unimers of the control conjugate were determined using static light scattering (SLS) as 12 nm and 25 respectively. The aggregation number (N_{agg}) was calculated by dividing the average molecular weight of the aggregate, obtained by SLS, with the molecular weight of the unimer. The theoretical spacing of 0.5 nm between the cyclic peptides[12] in the nanotubes was used to extrapolate the average length of the nanotubes (i.e. $N_{agg} \times 0.5$ nm). The nanotubular length of the diblock conjugate solutions prepared at 1 mg mL^{-1} were consistently higher than the control conjugates - see Figure 4.4c and 4.6.5 for details.

The fluorescent dye, 1,6-diphenylhexatriene (DPH),[13] which is quenched in water, was employed to confirm the hydrophobic region at the core of the nanotubes. Figure 4.8, depicted in section 4.6.4, shows the fluorescence of the DPH observed for the diblock conjugate, but not for the control conjugate, which does not have a hydrophobic region.

The diblock and control conjugates were tested for bio-compatibility using the 2,3-bis-(2-methoxy-4-nitro-5-sulfophenyl)-2H-tetrazolium-5-carboxanilide (XTT) assay. PC-3 cells (epithelial prostate cancer cells) were treated over 24 hours with the conjugates. The assay was used to examine the viability of the cells in the presence of the nanotubes. Both diblock and control conjugate showed no toxicity (0.1 – 100 μM, see experimental Figure 4.12). This XTT assay was carried out by Sean Ellacott in the Perrier group at the University of Warwick.

4.3 Dynamics of diblock conjugated cyclic peptide nanotubes

To study the stability of these nanotubes we determined their average size *via* SLS, after subjecting them to sonication for 1 hour. The samples were then left to stand and SLS was remeasured both after 1 hour and after 3 days. In a dynamic system, the reduction of N_{agg}, caused by the sonication will be corrected if the systems is left to equilibrate. This would result in a return to the original, and most thermodynamically stable, aggregation number. In a kinetically trapped, non-dynamic system, any decrease in the N_{agg} due to sonication will remain relatively unchanged over time, due to the high stability of the assemblies. Therefore, the difference in tubular length

between the original assemblies and the sonicated structures can be used as a measure for kinetic lability of CPNT-polymer conjugates.

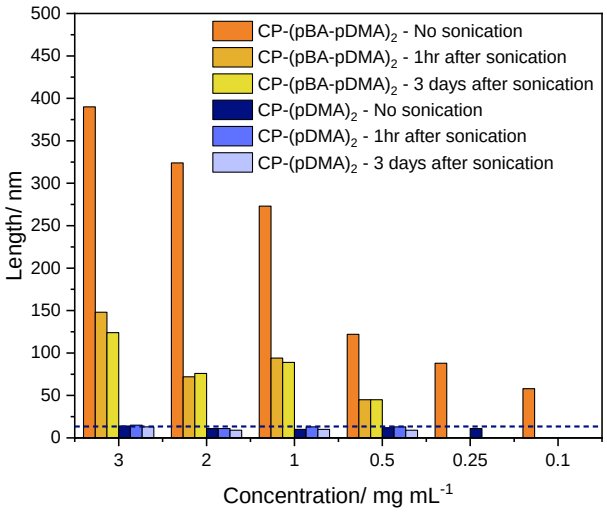

Figure 4.5 Dynamics of cyclic peptide-polymer nanotubes. The calculated length of the nanotubes from SLS over a range of concentrations (0.1 – 3.0 mg mL^{-1}) before and after sonication.

As shown in Figure 4.5, the aggregation number of the diblock conjugates was significantly reduced after sonication across all concentrations. Indeed, at 1 mg mL^{-1}, the average length of the original nanotubes was found to be 273 nm while, after sonication, values of 94 nm and 89 nm were measured after being left to stand for 1 hour and 3 days respectively. Conversely, no change was observed for the control conjugates, which were 11, 14, 10 nm before and after sonication (1 hour and 3 days after they were left to stand) – Table 4.2. This corroborates our hypothesis that the hydrophobic region helps to stabilise the peptide self-assembly and reduces the dynamic nature of these systems.[14] In contrast, the hydrophilic control conjugates which are highly dynamic are able to equilibrate rapidly to their original thermodynamically favourable state, explaining why no net change in N_{agg} is observed.

To provide further insight into the dynamic behaviour of these supramolecular assemblies, Förster resonance energy transfer (FRET) dyes were conjugated to the periphery of the cyclic peptide-polymer nanotubes, to probe the rates of exchange of these systems. Using orthogonal amine protecting groups, selective deprotection of

the amine was used to first attach the dye, then polymers to the peptide.[5] A detailed synthetic protocol and characterisation are given in experimental section 4.6.3.

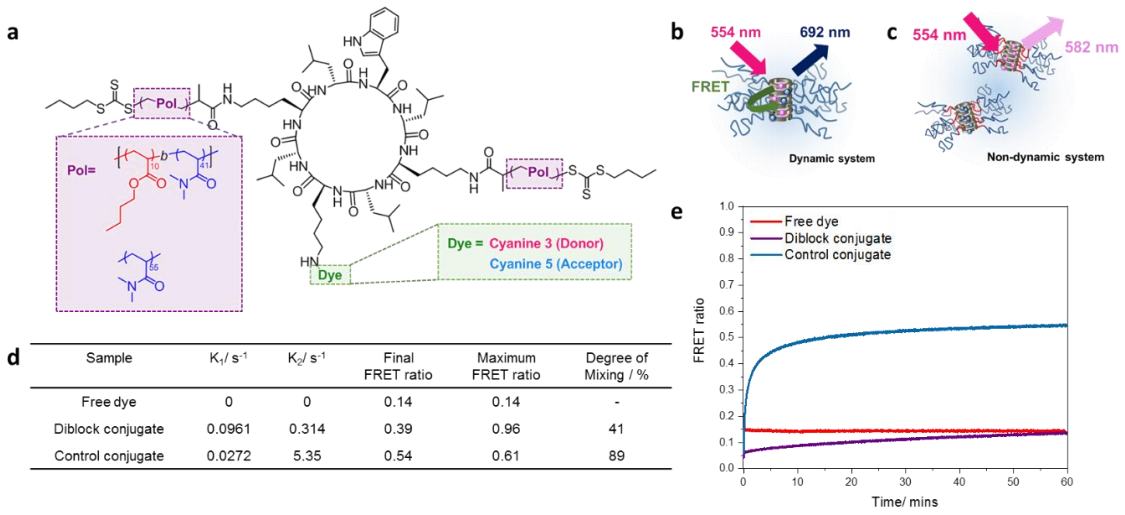

d

Sample	K_1/ s^{-1}	K_2/ s^{-1}	Final FRET ratio	Maximum FRET ratio	Degree of Mixing / %
Free dye	0	0	0.14	0.14	-
Diblock conjugate	0.0961	0.314	0.39	0.96	41
Control conjugate	0.0272	5.35	0.54	0.61	89

Figure 4.6 Kinetics of cyclic peptide-polymer nanotubes. a) The orthogonal functionalization of cyclic peptide (CP) with two polymer arms and a donor or acceptor FRET dye. b) Schematic of stable non-exchanging CP-polymer nanotubes. c) Scheme of dynamically exchanging mixed CP-polymer nanotubes. d) Rate constants for FRET exchange, final and maximum FRET ratio and degree of mixing for the free dye, diblock and control conjugates. Rate constants were determined by fitting to a second order decay function, see experimental section 4.6.11. Final FRET ratio was reached for the diblock and control conjugates after 7 days and 60 minutes respectively e) Graph to show the change in FRET ratio over time measured using fluorescence spectroscopy.

Cyanine (Cy) 3 (FRET donor) and Cy5 (FRET acceptor) were chosen as the FRET pair to detect the mixing of cyclic peptide conjugate unimers between nanotubes, see Figure 4.6a. If the Cy3 and Cy5 dyes are in close in proximity to one another, upon excitation of the donor dye, we should observe the emission of the acceptor dye due to energy transfer between the FRET pair.[15] This proximity-dependent energy transfer can only take place when two different dye conjugates are assembled together in the same nanotube (each cyclic peptide is around 7.5 Å in diameter and the distance between the two peptides is 4.5 Å; the FRET range is between 10 to 100 Å), see Figure 4.6b.[16, 17] A control study with free dyes shows a constant FRET ratio (0.14) and no change in donor or acceptor emission over time is observed (Figure 4.6e).

Each unimer contains one dye molecule (either Cy3 or Cy5). Independently, Cy3 and Cy5 conjugates were pre-assembled in water and then co-injected together. If the cyclic peptides are highly dynamic, *i.e.* they disassemble and re-assemble readily, they form progressively mixed nanotubes. As donor and acceptor dyes come in closer proximity with every exchange, the FRET emission increases over time. This process should eventually lead to a statistically mixed nanotube where the Cy3 and Cy5 modified peptide should be randomly distributed throughout the aggregate and a constant final FRET ratio is reached.

Notably, in the control conjugate the increase in FRET ratio was very fast and the plateau (no net change in FRET ratio) was reached within 60 minutes – as expected for a highly dynamic system. In contrast, the change in FRET ratio is extremely slow, when the diblock conjugates are co-injected. To elucidate a maximum for the FRET ratio for both systems, another control experiment was set up. The conjugates were premixed in DMF, where they primarily exist as unimers. The DMF was removed and the conjugates were resuspended in water to measure the maximum FRET ratio of statistically mixed nanotubes, see Figure 4.6d. A percentage degree of mixing was calculated by comparing the final FRET ratio (at the plateau) to the maximum FRET ratio from statistically mixed nanotubes. The degree of mixing for the control conjugates, as with previous hydrophilic CP-polymers without a stabilising hydrophobic core block, was around 90% or higher, indicating dynamic exchange of subunits to form statically mixed nanotubes.[5] Also the diblock conjugate after 7 days reached a final degree of mixing of only 41%, which suggests that the nanotubes are not fully mixing and discrete sections in the supramolecular assembly remain unchanged. The significant retardation in the rate of exchange (K_1 and K_2), provides further evidence the hydrophobic pBA core-block stabilises the hydrogen bonded peptide self-assembly; affording a much less dynamic system.

4.4 Composition of supramolecular diblock conjugates

To directly visualise the assembled peptide aggregates and any exchange between aggregates we imaged the nanotubes using super-resolution fluorescence microscopy, specifically direct stochastic optical reconstruction microscopy (STORM)[18]. Representative STORM images are shown in Figure 4.7 and also in the experimental section 4.6.13. In general the aggregates were well suited to imaging using STORM and the resolution of the final images were approximately 10 – 20 nm as calculated

using the Fourier ring correlation method.[19] The co-injected and premixed conjugates were prepared using the same method as the FRET ratio study (*vide supra*). The general size and shape of the aggregates seemed similar. In the premixed samples the Cy3 and Cy5 dyes were significantly co-localised, suggesting the aggregates were all formed from combinations of Cy3 and Cy5 labelled peptides. In contrast, the co-injected Cy3 and Cy5 diblock conjugates, left to mix after 1 day, featured much more aggregates which were just a single colour, showing that the Cy3 and Cy5 dyes were not as well mixed as in the premixed sample.

The stability of the hydrophobic core prevents the free exchange of CP-conjugates between nanotubes, explaining why the Cy3 and Cy5 cannot be seen randomly distributed throughout the nanotubes as is the case for the premixed sample. Moreover, in several cases block-like structures can be observed where two conjugates with different colours were attached to each other. These observations demonstrate that the ends of the nanotubes are still able to assemble, to form supramolecular block co-polymers. As a result some degree of FRET exchange was observed, but the degree of mixing remains still below 50% even after 7 days. Meijer and co-workers recently showed a similar phenomenon in organic solvents.[20]

Due to the wavelength of the SLS laser overlapping with the dye on the FRET conjugates, another method was required to observe the average size of the aggregates. Multiple particle tracking was performed to work out an average hydrodynamic volume of the different dye conjugates and their mixtures. Most importantly, the co-injected and premixed mixtures showed similar hydrodynamic radii (approx. 50 nm), see Table 4.3. It is worth noting that this is not a nanotube length, as the model assumes a spherical structure. The results nevertheless show that there are no significant differences in the average size between the aggregates.

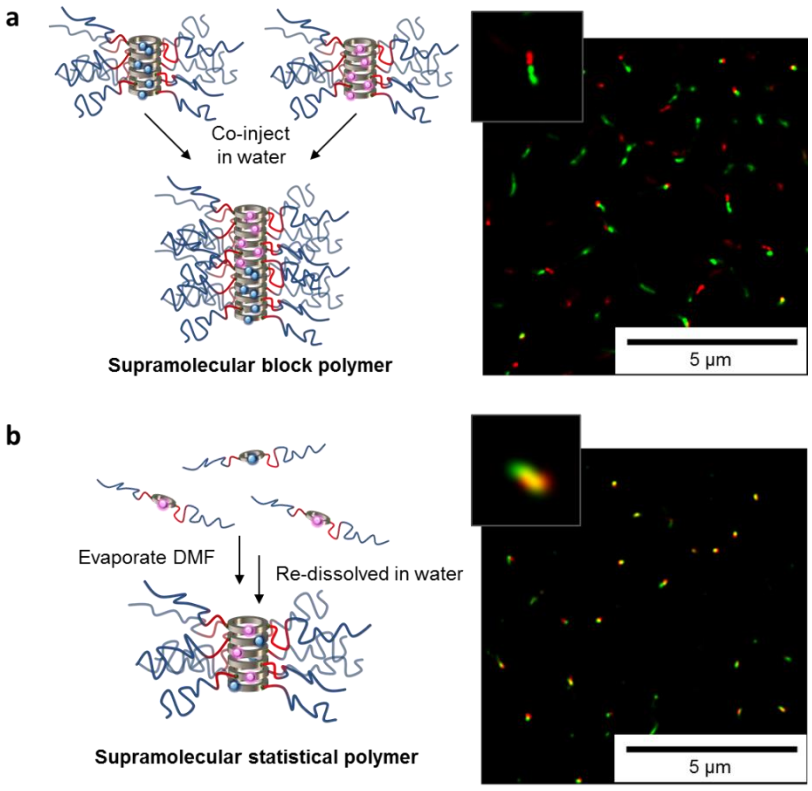

Figure 4.7 Composition of cyclic peptide-polymer nanotubes. Schematic and stochastic optical reconstruction microscopy (STORM) of a) co-injected and b) premixed cyclic peptide-polymer-dye conjugates.

4.5 Conclusion

A new generation of supramolecular cylindrical nanostructures which are stable, bio-compatible and easily functionalised have been reported. Unlike previous hydrophilic cyclic peptide conjugates which show fast dynamics and a low aspect ratio, by introducing a secondary hydrophobic driving force to stabilise the peptide assembly we observe the formation of a stable supramolecular polymer with a length above 100 nm. Furthermore, controlling the dynamic behaviour using additional hydrophobic interactions enables the formation of supramolecular block co-polymer structures. With these experiments we prove that these highly functional supramolecular polymer brushes are able to form defined nanostructures similar to previously reported CDSA materials but, importantly for biological applications, in aqueous conditions.

4.6 Experimental

4.6.1 Materials

Fmoc-protected amino acids and coupling agents were purchased from Iris Biotech GmbH. Cyanine3 NHS ester and Cyanine5 NHS ester were obtained from Lumiprobe GmbH, Germany. The RAFT agent, (propanoic acid)yl butyl trithiocarbonate (PABTC), was synthesised in our group using literature protocol.[50] The initiator V-601 was purchased from Fujifilm Wako Pure Chemical Corporation. N-N-Dimethylacryliamide (DMA, Sigma-Aldrich, 99%) and butyl acrylate (BA) were filtered through a basic aluminium oxide (Fisher Scientific) column to remove the radical inhibitor before polymerisation reactions.

All other chemicals stated were purchased from Sigma-Aldrich now Merck, (Gillingham, UK) unless otherwise stated. Solvents were purchased from several departmental suppliers—Honeywell, Fisher and Sigma-Aldrich.

4.6.2 Methods

4.6.2.1 Nuclear Magnetic Resonance (NMR) spectroscopy

^{1}H NMR spectra were measured using a Bruker DPX-300 or DPX-400 NMR spectrometer, which operated at 300.13 and 400.05 MHz, respectively. The residual solvent peaks were used as internal references. The following deuterated solvents were used: chloroform-d ($CDCl_3$), dimethyl sulfoxide-d6, deuterium oxide (D_2O). Chemical shift values (δ) are reported in ppm.

4.6.2.2 Size Exclusion Chromatography (SEC)

Molar mass distributions were obtained using size exclusion chromatography (SEC). The polymers and conjugates were measured using the Agilent 390-LC MDS instrument which measured differential refractive index (DRI). Samples were prepared around 1-3 mg mL^{-1} and filtered using 0.2 µM PTFE filters before auto-sampler injections.

PC	Agilent 1260 Infinity II-MDS	Agilent 1260 Infinity II-MDS	Agilent PL50
Eluent	THF with 2% TEA + 0.01 % BHT	DMF with 5mM NH_4BF_4	DMF + 0.1 % LiBr
Detectors	RI, Viscometer, LS, MWD	RI, Viscometer, VWD, LS	DRi, UV
Columns	2 x PLgel Mixed-C	2 x PLgel Mixed-D	2xPolargel M Columns
Calibration range	200 to 2,000,000 g/mol (PS equivalent)	200 to 400,000 g/mol (PS equivalent)	1,000 to 500,000 g/mol

(http://www.chem.agilent.com/Library/brochures/5990-7994-GPCorganics-Apr11-9lo.pdf)

4.6.2.3 High-Performance Liquid Chromatography (HPLC)

High-performance liquid chromatograms were measured using an Agilent Technologies 1200 Series, equipped with a Luna 5u C18 100 Å, 250 mm × 4.6 mm column. Acetonitrile/water was used. All solvents contained 0.04 vol% TFA. The following method was used: 0-5 mins 5:95 (Acetonitrile: Water), 5-35 mins gradient from 5:95 to 95:5 (Acetonitrile: Water), 35-38 mins gradient from 95:5 to 5:95 (Acetonitrile: Water).

4.6.2.4 Mass Spectrometry (MS)

The peptides and conjugates before polymer attachment were analysed using electrospray ionisation (ESI) - Mass spectrometry (MS) on the either the Agilent 6130B single Quad or Bruker MicroToF instruments.

4.6.2.5 Ultraviolet–Visible (UV–Vis) Absorption Spectroscopy

Spectroscopy: UV–vis absorption spectra were measured using an Agilent Technologies Cary 60 UV–vis spectrometer. The solutions were all made to the same concentration (35 μM).

4.6.2.6 Fluorescence Emission Spectroscopy

Fluorescence emission spectra were measured using an Agilent Technologies Cary Eclipse Fluorescence spectrometer. The FRET studies were performed using an absorption maxima of the donor conjugate (measured in using UV-Vis spectroscopy).

4.6.3 Synthesis and Characterisation

4.6.3.1 Polymer synthesis

4.6.3.1.1 pBA polymerisation

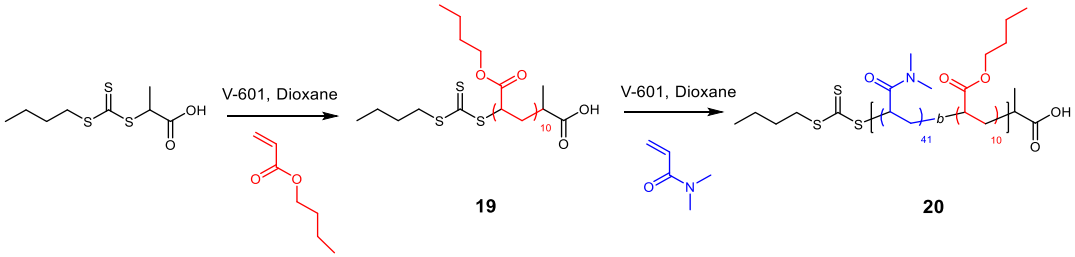

Scheme 4.1 Preparation of diblock co-polymer of butyl acrylate (BA) and dimethyl acrylamide (DMA).

pBA (**19**): For the synthesis of the first block, PABTC (0.214 g, 0.900 mmol, 1 eq.), butyl acrylate (1.153 g, 9.00 mmol, 10 eq.), V601 azo-initiator (4.14 mg, 0.018 mmol, 0.02 eq.) and 1,4-dioxane (0.901 g) were all weighed into a vial with a magnetic stirrer and sealed with a rubber septum. The solution was mixed thoroughly and deoxygenated by bubbling nitrogen for *ca.* 10 min. The vial was then placed in an oil bath set at 70°C for 20 hours. Samples conversion, calculated from ^{1}H NMR, during the polymerisation were taken using a degassed syringe. After the polymerisation, the mixture was cooled and opened to air. ^{1}H NMR and GPC of these polymers were taken to determined, conversion and molecular weight.

Yield was not calculated as the solution containing the macroCTA was used directly to synthesis the following diblock. ^{1}H NMR ($CDCl_3$, 300 MHz, δ ppm): 0.94 (3H, **H$_3$C**-CH$_2$-RAFT agent + 3H, **H$_3$C**-CH$_2$-BA monomer), 1.39 (2H, H$_3$C-**CH$_2$**-BA monomer), 1.61 (2H, H$_3$C-CH$_2$-**CH$_2$**-BA monomer), 3.35 (-**CH$_2$**-S- RAFT agent), 4.05 (2H, -**CH$_2$**-O-C(O)-BA monomer). M_n = 1,760 g mol^{-1}, $Đ$ = 1.15 (THF SEC, Agilent EasyVial PMMA calibration). ^{1}H NMR spectrum in Appendix Figure 4.19 and SEC chromatogram in Figure 4.2.

4.6.3.1.2 pDMA chain extension (pBA-b-pDMA)

pBA-*b*-pDMA (**20**): An exact aliquot of the mixture containing the first block (pBA) was taken by calculating the moles of MacroCTA (pBA-block) from the known concentration of your pBA polymerisation. In a new vial, the aliquot containing your pBA-block (900 mg, 0.254 mmol, 1 eq.), *N*,*N*-Dimethylacrylamide (DMA) (1.134g,

11.43 mmol, 45 eq.), V-601 (0.84 mg, 0.0143 eq.) and 1,4-Dioxane (1.382 g) were added together. The solution was mixed thoroughly and deoxygenated by bubbling nitrogen for ca. 10 min. The vial was then placed in an oil bath set at 70°C for 20 hours. The solution was precipitated in diethyl ether and dried in a vacuum oven. The product was a yellow solid.

Yield = 85% (1.2292 g); ^{1}H NMR ($CDCl_3$, 300 MHz, ppm): 0.94 (3H, **H$_3$C**-CH$_2$-RAFT agent + 3H, **H$_3$C**-CH$_2$-BA monomer), 1.37 (2H, H$_3$C-**CH$_2$**-BA monomer), 1.61 (2H, H$_3$C-CH$_2$-**CH$_2$**-BA monomer), 2.91 (6H, -N-(**CH$_3$**)$_2$), 3.34 (-**CH$_2$**-S- RAFT agent), 4.03 (2H, -**CH$_2$**-O-C(O)-BA monomer). M_n = 5,000 g mol^{-1}, $Đ$ = 1.13 (THF SEC, Agilent EasyVial PMMA calibration). ^{1}H NMR spectrum in Appendix Figure 4.20 and SEC chromatogram in Figure 4.2.

4.6.3.1.3 pDMA polymerisation

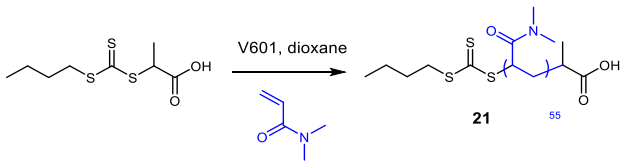

Scheme 4.2 Preparation of homopolymer of dimethylacrylamide (DMA).

pDMA (**21**): For the synthesis of the pDMA homopolymer, PABTC (50.06 mg, 0.210 mmol, 1 eq.), DMA (1.041 g, 10.50 mmol, 50 eq.), VA-044 azo-initiator (1.49 mg, 4.60 µmol, 0.0219 eq.) and a 1:4 co-solvent of 1,4-dioxane (0.421 mL)and deionised water (1.264 mL) respectively were all weighed into a vial with a magnetic stirrer and sealed with a rubber septum. The solution was mixed thoroughly and deoxygenated by bubbling nitrogen for *ca.* 10 min. The vial was then placed in an oil bath set at 70°C for 20 hours. Samples conversion, calculated from ^{1}H NMR, during the polymerisation were taken using a degassed syringe. After the polymerisation, the mixture was cooled and opened to air. ^{1}H NMR and GPC of these polymers were taken to determined, conversion and molecular weight. The solvent was evaporated using the aid of nitrogen flow, then the polymer was resuspended in dioxane and precipitated in hexane (repeat 3 times) and dried in a vacuum oven. The product was a yellow solid.

Yield = 88% (1.0483 g); ^{1}H NMR ($CDCl_3$, 300 MHz, ppm): 0.89 (3H, **H$_3$C**-CH$_2$-RAFT agent), 1.08 (3H, **H$_3$C**-(C(O)-OH)-RAFT agent), 1.85-1.46 (4H, H$_3$C-**CH$_2$**-**CH$_2$**-RAFT agent + 2H, -CH-**CH$_2$**- polymer backbone), 2.62 (-**CH**-CH$_2$- polymer

backbone), 2.80-3.25 (6H, -N-(**CH**$_3$)$_2$) M_n = 5,000 g mol^{-1}, $Đ$ = 1.13 (THF SEC, Agilent EasyVial PMMA and PS calibration). ^{1}H NMR spectrum in Appendix Figure 4.21 and SEC chromatogram in Figure 4.2.

4.6.3.2 Conjugation of the polymer to cyclic peptide

4.6.3.2.1 CP-(pBA-pDMA)$_2$ – Diblock conjugate

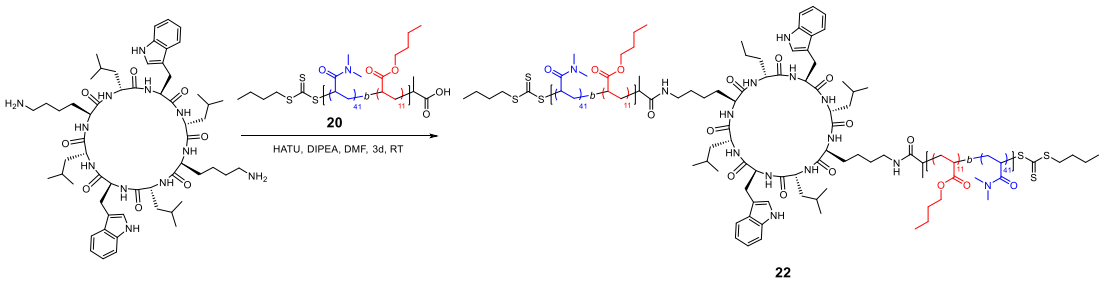

Scheme 4.3 Preparation of cyclic peptide-diblock conjugates

CP-(pBA-pDMA)$_2$ (**22**): The cyclic peptide (**2**), cyclo(D-Leu-Lys-D-Leu-Trp)$_2$, was synthesised using literature protocol.[21] CP (15 mg, 13.88 µmol, 2.2 eq.) was dissolved in DMF (0.5 mL) with the aid of sonication. In a separate vial, pBA-pDMA (**20**) (0.171 g, 30.54 µmol, 2.2 eq.), HATU (0.0116 g, 30.54 µmol, 2.2 eq.) and DIPEA (0.0108 g, 83.28 µmol, 6 eq.) were dissolved in 0.5mL DMF and shaken for 30 minutes then added to the CP solution. The combined solution was shaken for 2 days at room temperature. The product then precipitated in diethyl ether five times. To ensure the polymer stays in solution and is removed with the supernatant during the precipitation procedure a small amount of methanol used to redissolved both polymer and conjugate before precipitation solvent, diethyl ether, was reintroduced. A minimum amount of diethyl ether was used to precipitate the conjugate. The purification of the excess polymer can be monitored *via* SEC traces in Figure 4.3. Yield = 47% (84.5 mg).

4.6.3.2.2 CP-(pDMA)$_2$ – Control conjugate

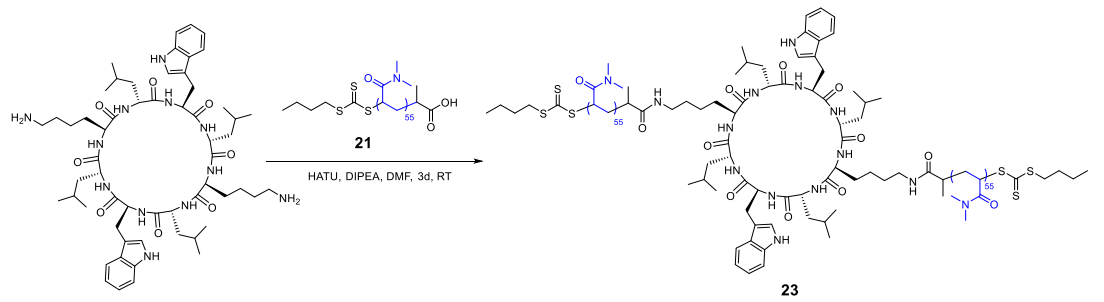

Scheme 4.4 Preparation of cyclic peptide-pDMA conjugates

CP-(pDMA)$_2$ (**23**): CP (15 mg, 13.88 µmol, 2.2 eq.) was dissolved in DMF (0.5 mL) with the aid of sonication. In a separate vial, pDMA (**21**) (0.174 g, 30.54 µmol, 2.2 eq.), HATU (0.0116 g, 30.54 µmol, 2.2 eq.) and DIPEA (0.0108 g, 83.28 µmol, 6 eq.) were dissolved in 0.5mL DMF and shaken for 30 minutes then added to the CP solution. The combined solution was shaken for 2 days at room temperature. The solvent was evaporated with the aid of a nitrogen flow. The product then purified using centrifuge dialysis tubes with a molecular weight cut-off of 10 kDa (Merck Millipore). The purification of the excess polymer can be monitored *via* SEC traces in Figure 4.3.Yield = 41% (71.5 mg).

4.6.3.3 Synthesis of cyclic peptide-dye conjugates

4.6.3.3.1 Dye conjugation to the cyclic peptide

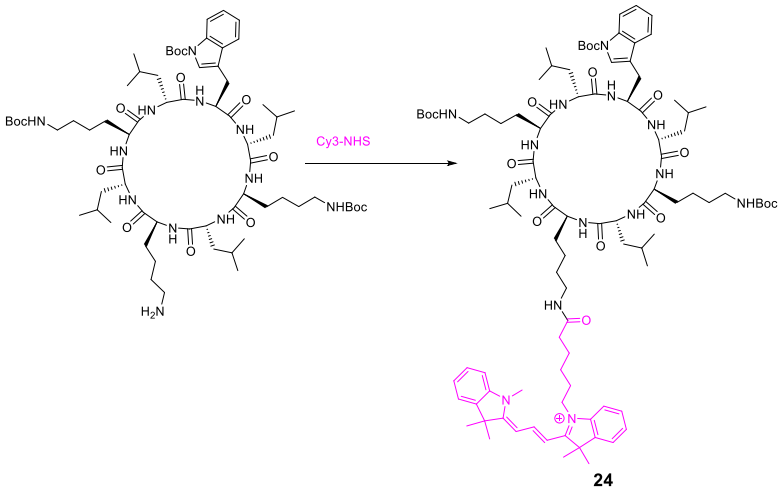

Scheme 4.5. Preparation of Cyannine3 conjugated cyclic peptide-polymer conjugates

Cy3-CP-protected (**24**): The partially deprotected cyclic peptide was synthesised according literature protocol.[3] This cyclic peptide was dissolved in 0.5 mL of DMF with the aid of sonication. *N*,*N*-Diisopropylethylamine (DIPEA) (0.0117 g, 90.7 µmol, 6 eq.) was added to the CP solution and mixed. Cyanine3 NHS ester (purchased from Lumiprobe GmbH) (0.011g, 17.4 µmol, 1.15 eq.) was added to the CP solution and stirred for 3 days. The reaction was followed *via* HPLC, in Appendix Figure 4.22. The purified peptides were characterized by mass spectrometry (electrospray ionization, ESI) (Table 4.1). Yield: 78% (20.6 mg).

4.6.3.4 Deprotection of the dye conjugated cyclic peptide

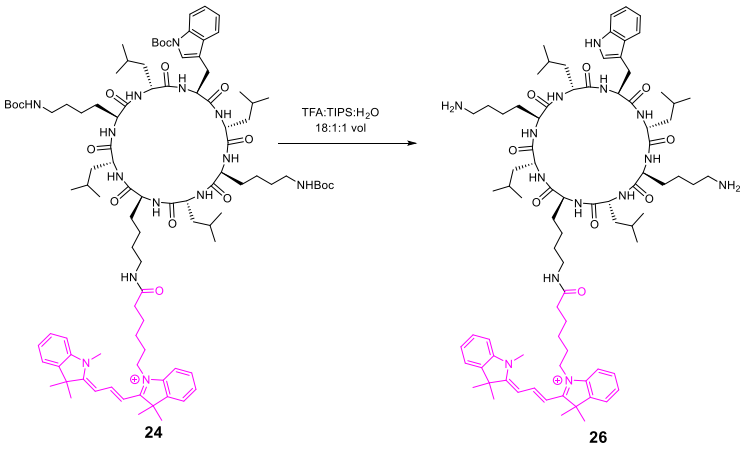

Scheme 4.6 Deprotection of Boc groups on the cyclic peptide-dye conjugates

Cy3-CP-deprotected (**26**): Boc groups were removed in using a deprotection solution of TFA/TIPS/H2O (18:1:1 vol, 5 mL). The dye conjugated Boc protected CP (**24**) (20.632 mg) was agitated for 3 hours in the deprotection solution, then triturated using ice-cold diethyl ether and washed twice more with ice-cold diethyl ether. The pink precipitate was collected and dried under vacuum. The reaction was followed *via* HPLC, Appendix Figure 4.22. Mass spectra attributions can be found in Table 4.1. Yield: 94% (25.7 mg).

Cy5 conjugates

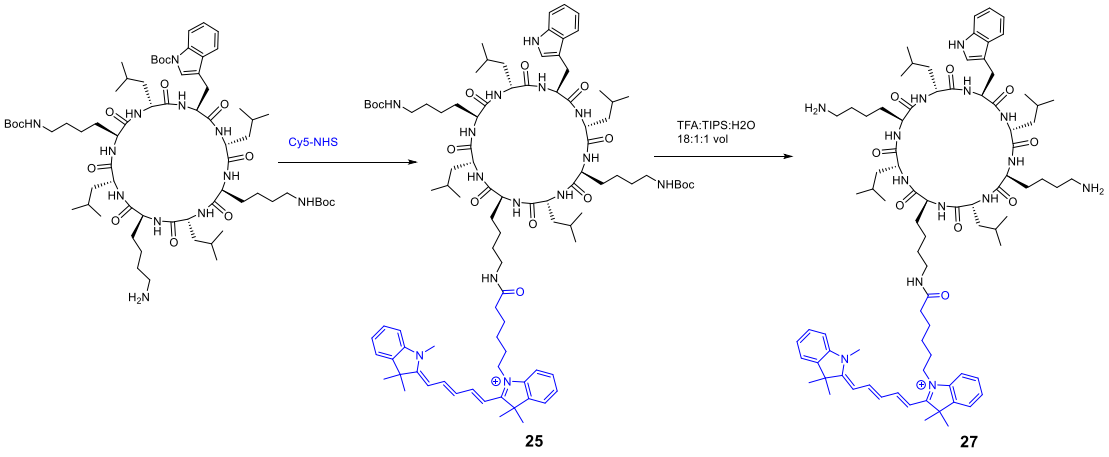

Scheme 4.7 Preparation of Cy5 conjugated cyclic peptides.

The Cyannine5 conjugates (**25** and **27**) (Scheme 4.7) were synthesised using the same procedure to synthesise Cyannine3 conjugates. The reaction was followed *via* HPLC,

Appendix Figure 4.23. Mass spectra attributions can be found in Table 4.1. Cy5-CP-Protected (**7**): Yield: 92% (25.4 mg). Cy5-CP-Deprotected (**27**): Yield: 65% (13.7 mg).

4.6.3.5 Conjugation of the polymers to the cyclic peptide-dye conjugates

4.6.3.5.1 Cy3-CP-(pBA-pDMA)$_2$ – Diblock dye conjugate

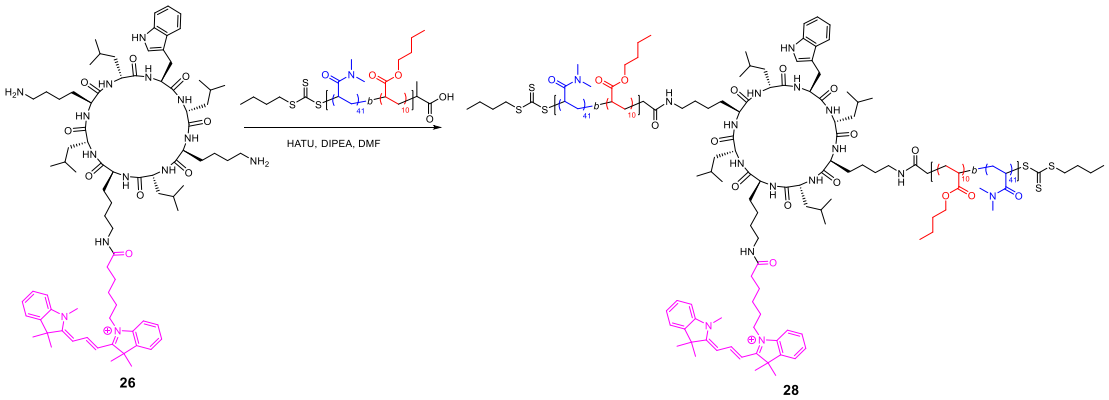

Scheme 4.8 Preparation of cyclic peptide-dye-diblock polymer conjugates

Cy3-CP-(pBA-pDMA)$_2$ (**28**): Cyclic peptide-dye conjugate (Cy3-CP-dep, **26**) (16 mg, 10.9 µmol, 1 eq.) was dissolved in DMF (0.5 mL) with the aid of sonication. In a separate vial, pBA-pDMA (**22**) (0.138 g, 24.1 µmol, 2.2 eq.), HATU (9.2 mg, 24.1 µmol, 2.2 eq.) and DIPEA (8.5 mg, 65.7 µmol, 6 eq.) were dissolved in 0.5 mL DMF and shaken for 30 minutes then added to the CP solution. The combined solution was shaken for 3 days at room temperature. The product then precipitated in diethyl ether five times. To ensure the polymer stays in solution and is removed with the supernatant during the precipitation procedure a small amount of methanol used to redissolved both polymer and conjugate before precipitation solvent, diethyl ether, was reintroduced. A minimum amount of diethyl ether was used to precipitate the conjugate. The purification of the excess polymer can be monitored *via* SEC traces (see Appendix 4.24). Yield = 43% (58.3 mg).

4.6.3.5.2 Cy3-CP-(pDMA)$_2$ – Control dye conjugate

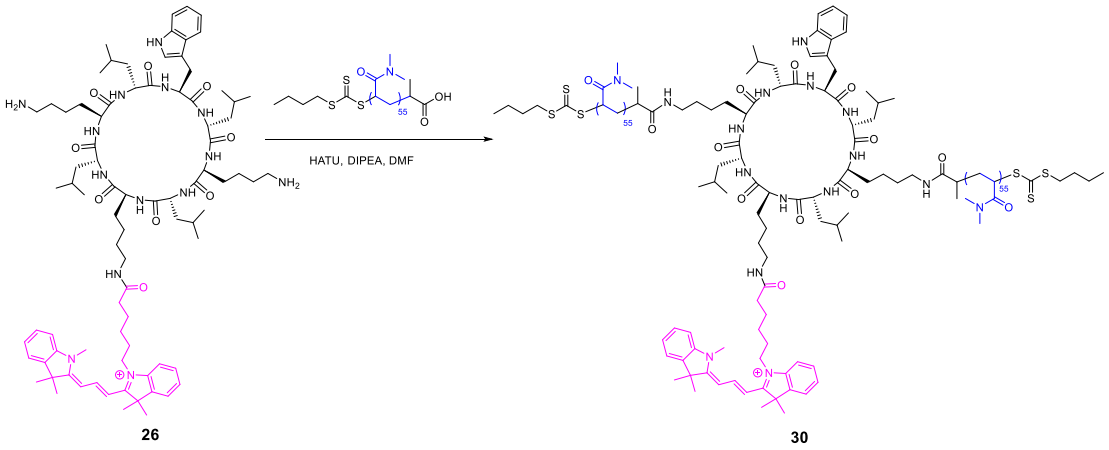

Scheme 4.9 Preparation of cyclic peptide-dye-homopolymer conjugates

Cy3-CP-(pDMA)$_2$ (**30**): Cyclic peptide-dye conjugate (Cy3-CP-dep, **26**) (6.2 mg, 4.17 µmol, 1 eq.) was dissolved in DMF (0.5 mL) with the aid of sonication. In a separate vial, pDMA (**21**) (51.2 mg, 9.16 µmol, 2.2 eq.), HATU (3.48 mg, 9.16 µmol, 2.2 eq.) and DIPEA (3.23 mg, 25.0 µmol, 6 eq.) were dissolved in 0.5mL DMF and shaken for 30 minutes then added to the CP solution. The combined solution was shaken for 3 days at room temperature. The solvent was evaporated with the aid of a nitrogen flow. The product then purified using centrifuge dialysis tubes with a molecular weight cut-off of 10 kDa (Merck Millipore). The purification of the excess polymer can be monitored *via* SEC traces (see Appendix Figure 4.24). Yield = 7% (3.174 mg).

The Cyannine5 conjugates (**29** and **31**) were synthesised using the same procedure to synthesise Cyannine3 conjugates. The purification of the excess polymer can be monitored *via* SEC traces (see Appendix 4.24). Cy5-CP-(pBA-pDMA)$_2$ (**29**): Yield: 49% (34.1 mg). Cy5-CP-(pDMA)$_2$ (**31**): Yield: 8% (4.390 mg).

Table 4.1 Electrospray ionisation (ESI) - Mass spectrometry (MS) characterisation of cyclic peptide and dye conjugates carried out on the Agilent 6130B single Quad.

Sample No.	Compound [a]	ESI (g mol^{-1})		
		Calculated	Found	Attribution
	Linear peptide (LP) - standard	1499.7	1499.9	$[M+H]^+$
	Cyclic peptide (CP) - standard	1081.7	1081.7	$[M+H]^+$
	CP-Dde protected	1509.9	1509.94	$[M+Na]^+$
	CP-Dde deprotected	1323.9	1323.8	$[M+H]^+$
24	Cy3-CP-Boc protected	892.6	892.9	$[M+Na]^{2+}$
25	Cy5-CP-Boc protected	905.6	905.9	$[M+Na]^{2+}$
26	Cy3-CP-Boc deprotected	731.5	731.8	$[M+H]^{2+}$
27	Cy5-CP-Boc deprotected	744.5	744.8	$[M+H]^{2+}$

4.6.4 1,6-diphenylhexatriene (DPH) dye experiment

1,6-diphenylhexatriene (DPH) was dissolved to make a 1 mg mL^{-1} solution in DMSO. Under the UV lamp (365 nm) the dye fluorescence was clearly observed. In separate vials, accurately prepared 1 mg mL^{-1} solutions of the diblock and control conjugates solutions were made up in de-ionized water. The solutions were left on a shaker overnight to full dissolve and equilibrate. Before dye addition the fluorescence of the de-ionised water and DMSO (solvent only) and the conjugates in solution were checked. Using a micro-pipette exactly 5% vol ratio of the dye solution in DMSO was added to the conjugates.

The fluorescence of DPH quenches in the presence of water. As the DPH dye enters a hydrophobic region where it can shield itself from the water, fluorescence can once again be observed. When the dye enters the hydrophobic pBA core around the cyclic peptide, the dye fluorescence can be observed. Clear fluorescence emission in the diblock conjugate solution was observed after 10 mins. No fluorescence was observed in the solvent or the control conjugate solution after 3 days.

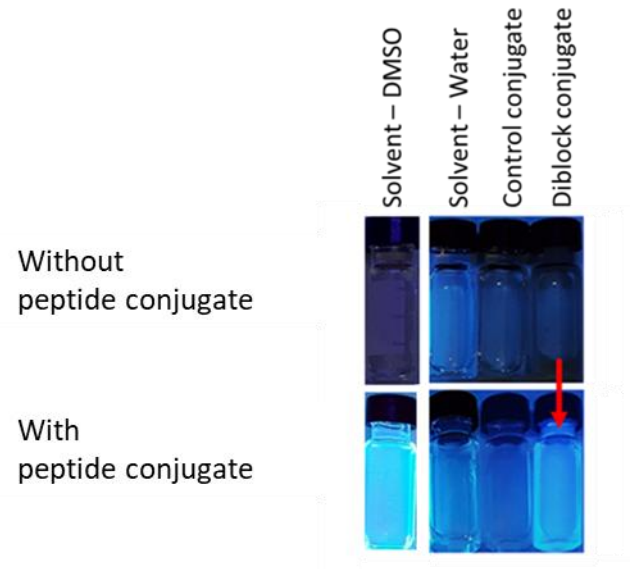

Figure 4.8 Images of cyclic peptide polymer conjugates with the addition of DPH dye. Upon dye addition, fluorescence was observed in the case of the diblock conjugate solution. No visible fluorescence was observed for the control conjugate, absence of the hydrophobic core.

4.6.5 Static Light Scattering (SLS)

The SLS data were obtained using the ALV/CGS-3 Compact Gonimeter System. A range of different concentrations of the diblock and control conjugates were measured using SLS, before and after sonication. The compounds were first accurately measured in a vial and corresponding volumes of water were added to yield various different concentrations (0.5–3 mg mL^{-1}). Before measuring, the solutions were filtered using 0.45×10^{-6} m membrane PTFE lined filters to remove any large aggregates.

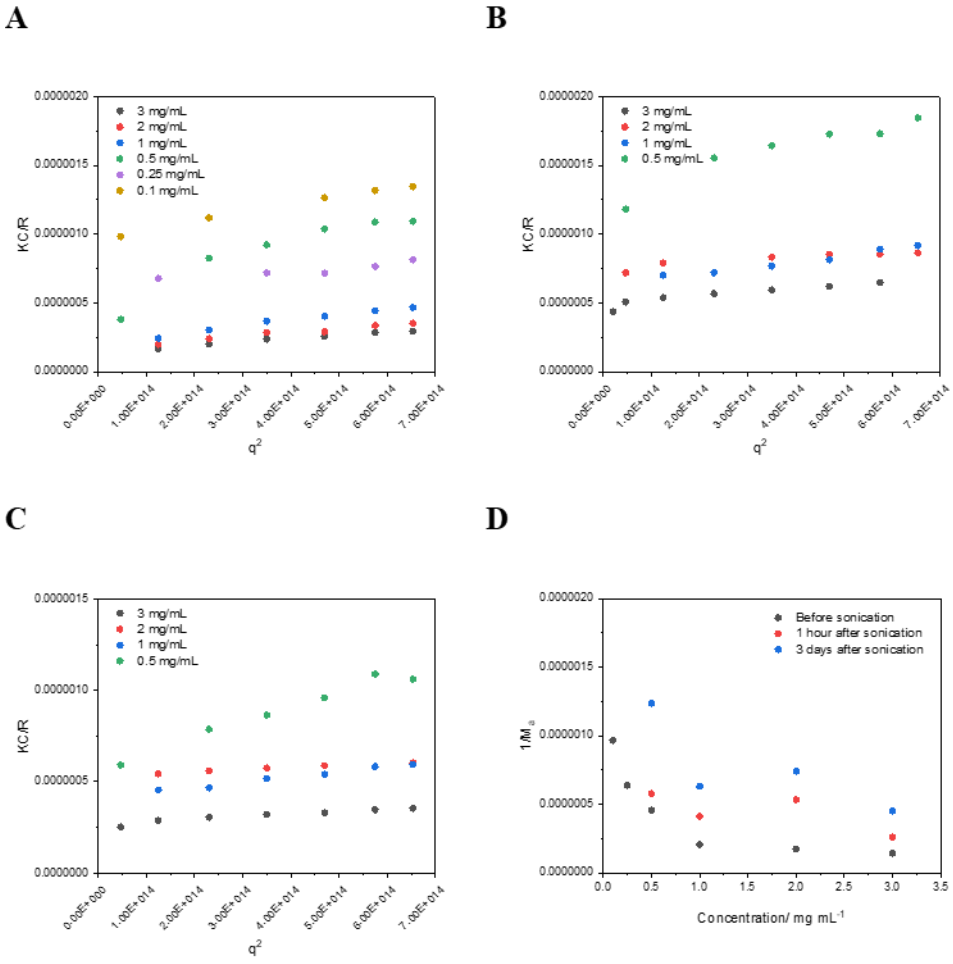

Figure 4.9 Evolution of KC/R of diblock conjugate (CP-(pBA-pDMA)$_2$) in water as a function of q² obtained by static light scattering. a) Before sonication, b) 1 hour after sonication and c) 3 days after sonication. d) Evolution of $1/M_a$ of diblock conjugate in water as a function of concentration before sonication, 1 hour after and 3 days after sonication obtained by static light scattering.

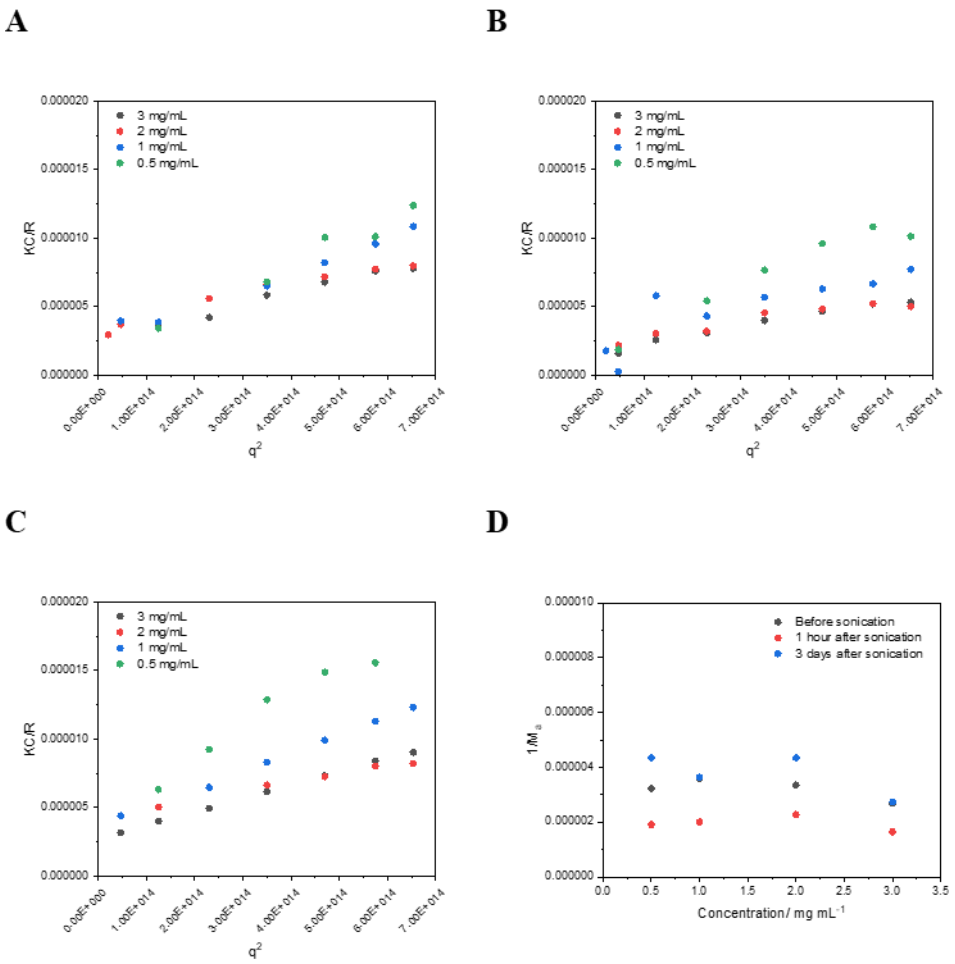

Figure 4.10 Evolution of KC/R of control conjugate (CP-(pDMA)$_2$) in water as a function of q² obtained by static light scattering. a) Before sonication, b) 1 hour after sonication and c) 3 days after sonication. d) Evolution of 1/M_a of control conjugate in water as a function of concentration before sonication, 1 hour after and 3 days after sonication obtained by static light scattering.

Table 4.2 Length of the nanotubes calculated from static light scattering over a range of concentrations (0.1 – 3.0 mg mL^{-1}) before and after sonication.

	Before Sonication				1 Hour After Sonication				3 Days After Sonication			
Conc/ mg ml^{-1}	Control conjugate		Diblock conjugate		Control conjugate		Diblock conjugate		Control conjugate		Diblock conjugate	
	N_{agg}	Length/nm	N_{agg}	Length/nm	N_{agg}	Length/nm	N_{agg}	Length/nm	N_{agg}	Length/nm	N_{agg}	Length/nm
3.0	30	14	830	390	32	15	314	148	29	13	263	124
2.0	24	11	690	324	23	11	154	72	19	9	161	76
1.0	22	10	581	273	27	13	199	94	22	10	189	89
0.5	25	12	260	122	28	13	95	45	19	9	96	45
0.25	23	11	187	88	-	-	-	-	-	-	-	-
0.10	-	-	123	58	-	-	-	-	-	-	-	-
Average	25	11	-	-	28	14	-	-	22	10	-	-

4.6.6 Single-Angle Neutron Scattering (SANS)

SANS was carried out on the LARMOR small-angle diffractometer at the ISIS Pulsed Neutron Source (STFC Rutherford Appleton Laboratory, Didcot, UK). Prior to measurement, each sample was dissolved in D_2O and placed in a 2 mm quartz cuvette. The scattering cross-section was measured over a Q-range of 0.004 - 0.5 $Å^{-1}$ where Q is defined as:

$$Q = \frac{4\pi \sin\frac{\theta}{2}}{\lambda} \qquad (1)$$

Here, θ is the scattered angle, and λ is the incident neutron wavelength. A Q-range of 0.004 - 0.5 $Å^{-1}$ was achieved utilizing an incident wavelength range of 0.9 - 13.3 Å. The detector is located 4.1 m from the sample and is 664 mm wide * 664 mm high with the beam in the centre of the detector. The beam size is 6 mm wide and 8 mm high. Each raw scattering data set was corrected for the detector efficiencies, sample transmission and background scattering and converted to scattering cross-section data ($\partial\Sigma/\partial\Omega$ vs. Q) using the instrument-specific software. These data were placed on an absolute scale (cm^{-1}) using the scattering from a standard sample (a solid blend of hydrogenous and perdeuterated polystyrene) in accordance with established procedures.

Following data acquisition, the SASfit software programme was used to model the data. In all cases several fixed parameters were used; concentration, the radius of the core, and SLD values (for the solvent, core peptide, and polymer shell).

Values for SLD were calculated using the following equation;

$$SLD = \frac{\rho N_a \sum_{i=1}^{N} b_i}{\sum_{i=1}^{N} M_i} \qquad (2)$$

Where ρ is the bulk density of the material, N_a is Avogadro's constant, b_i is the scattering length contributions from the N atoms within the unit cell, and M is the atomic mass of N atoms. Values for individual atomic scattering lengths and atomic weights were taken from the NIST database.[22, 23] SLD parameters were calculated for the solvent, polymer, and peptide and used as fixed values in the fitting analysis. The use of data from previous SANS experiments provided the vale for cylinder radius of 0.4 nm.

The hairy-cylinder model, is a combination model adapted from the form factor of a micelle, with a rod-like core as an additionally structure factor. The form factor can be described as;

$$P(q) = N^2\beta_s^2 F_{s(q)} + N\beta_c^2 F_{c(q)} + 2N^2\beta_s\beta_c S_{sc(q)} + N(N-1)\beta_c^2 S_{cc(q)}$$

Where N is the aggregation number, and $\beta_s = V_s\,(\rho_s - \rho_{solv})$ / $\beta_c = V_c\,(\rho_c - \rho_{solv})$ is the total excess scattering lengths of the cylindrical core and in the corona, respectively. V_s and V_c are the volumes of the core and in the corona, respectively. ρ_s and ρ_c are the corresponding scattering length densities and ρ_{solv} is the scattering length density of the surrounding solvent, calculated as previously discussed. The solutions were prepared by dissolving the conjugates in 1 mg mL^{-1} of D_2O.

Fixed variables

V_{brush} - the molecular volume of the polymer arms - *Calculated as the M_w of the polymer divided by Avogadro's constant (N_a) and multiplied by the density*

R_core = 5 Å fixed as the radius of the CP

d – fixed at 1 – non penetration of chains into the cylindrical core of the CP

eta_core, eta_brush, eta_solv – SLD value calculated using molecular structures

Table 4.3 Parameters and results from fitting the SANS scattering data to a hairy-cylinder model

Diblock conjugate – Contribution 1 – CYL+Chains (RW)

Parameters	**Fit**	**Value**	**Units**
Delta	✓	2.45747e-5	
R_core		5	Å
n_agg	✓	0.0601087	
V_brush		14776	cm^3
eta_core		8.20995e-007	$Å^{-2}$
eta_brush		1.64e-006	$Å^{-2}$
eta_solv		6.33e-006	$Å^{-2}$
xsolv_core	✓	183.893	
Rg	✓	13.9993	Å

h		1	
H	✓	1000	Å

Diblock conjugate - Contribution 2 – extended Guinier law

Parameters	**Fit**	**Value**	**Units**
Delta	✓	0.133184	
I0	✓	0.133184	
a	✓	0.88974	
Ra	✓	41.9261	

chisqr: 256, red. chisqr: 6.57

Control conjugate - CYL+Chains (RW) - chisqr: 26.8, red. chisqr: 1.03

Parameters	**Fit**	**Value**	**Units**
Delta	✓	0.083845	
R_core		5	Å
n_agg	✓	0.00453034	
V_brush		15757	cm^3
eta_core		8.20995e-007	$Å^{-2}$
eta_brush		9.57751e-007	$Å^{-2}$
eta_solv		6.33e-006	$Å^{-2}$
xsolv_core	✓	0.572701	
Rg	✓	12.0219	Å
h		1	
H	✓	492.444	Å

4.6.7 Transmission Electron Microscopy (TEM)

Carbon coated grids, carbon film on copper 300 mesh, were purchased from EM Resolutions.

Solutions of CP-diblock conjugate in water at 1 mg mL−1 were prepared by direct dissolution of the solid in filtered ultra-pure water. 10μL of solution was dropcast on freshly glow-discharged carbon-coated grids placed on filter paper. Bright field TEM micrographs were obtained with a Jeol 2100Plus is operating at 200 kV, equipped with a Gatan OneView IS camera.

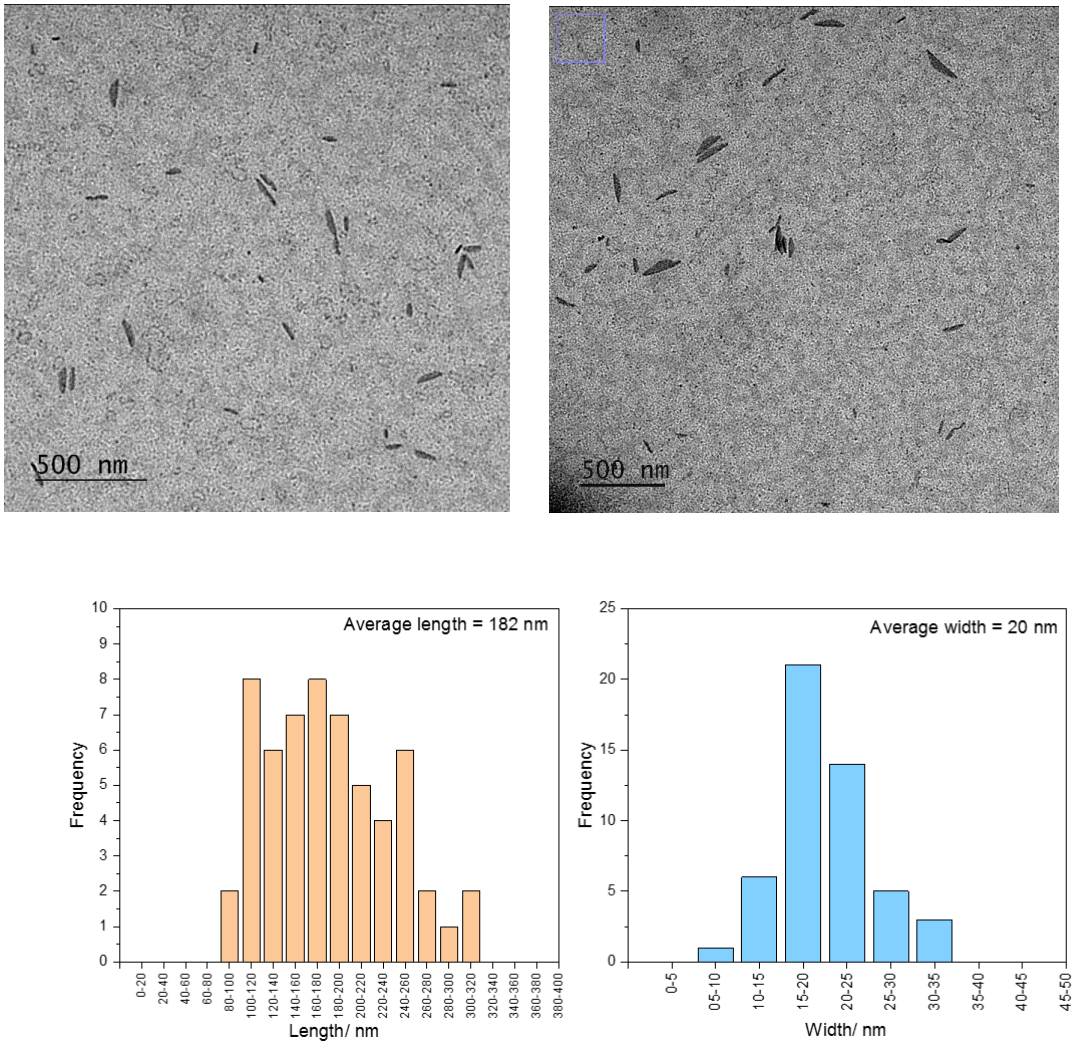

Figure 4.11 TEM images of diblock conjugated cyclic peptides (CP-(pBA-pDMA)$_2$) prepared in water (1 mg/mL).

4.6.8 Toxicity

4.6.8.1 Cell culture

PC-3 (epithelial prostate cancer cells) cells were grown in Dulbecco's modified Eagle's medium (DMEM) supplemented with 10% (v/v) fetal bovine serum (FBS) and 2 mM of L-glutamine and penicillin at 37°C in a humid 5% CO_2 environment. Cells were typically passaged at 80-90% confluence.

4.6.8.2 Cytotoxicity assay (XTT/PMS)

Toxicity of the conjugates was assessed using a standard XTT protocol. The CP conjugates to be tested were dissolved in water with 0.5% DMSO in order to obtain solutions at 500 μM. These solutions were used to prepare multiple dilutions in a mixture of supplemented culture media (DMEM) and PBS (50:50) at the following concentrations: 100, 50, 10, 1 and 0.1 μM. PC-3 cells were seeded in a transparent Greiner 96 well-plate at a density of 10,000 cells per well and incubated for 24 h. The culture media was then replaced by 100 μL of the prepared solutions. After 24 h incubation, the medium was removed, the cells were washed once with PBS buffer before adding fresh media supplemented with 25 μL of XTT solution (1 $mg \cdot mL^{-1}$) containing N-methyl dibenzopyrazine methyl sulfate (PMS) (25 $\mu mol.L^{-1}$). Cells were incubated for another 24 h. Absorbance was then directly measured using a BioTek™ Cytation™ 3 Cell Imaging Multi-Mode Reader at 450 nm and 650 nm (background). Two repeats of this experiment were performed; the error bars plotted are standard error of the mean.

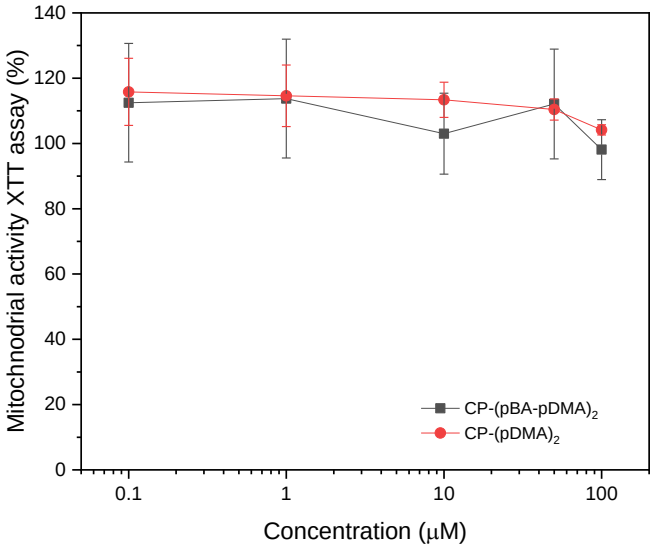

Figure 4.12 Toxicity profile for diblock (CP-(pBA-pDMA)$_2$) and control (CP-(pDMA)$_2$) conjugates.

4.6.10 UV-vis spectroscopy

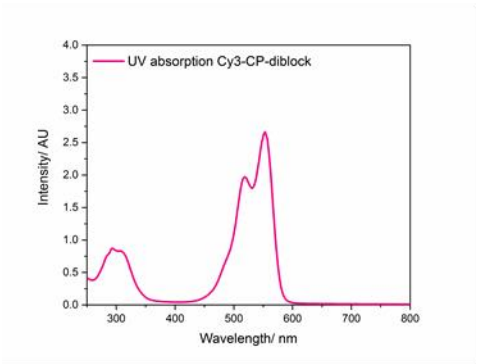

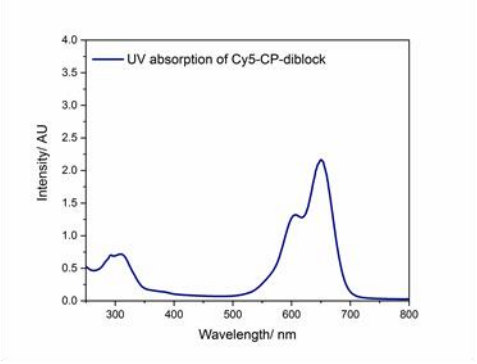

Figure 4.13 UV absorption spectra of Cy3-CP-Diblock and Cy5-CP-Diblock conjugates in water at 35 µM.

4.6.11 Fluorescence emission spectroscopy

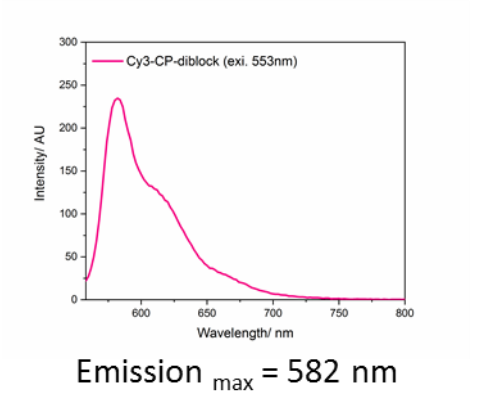

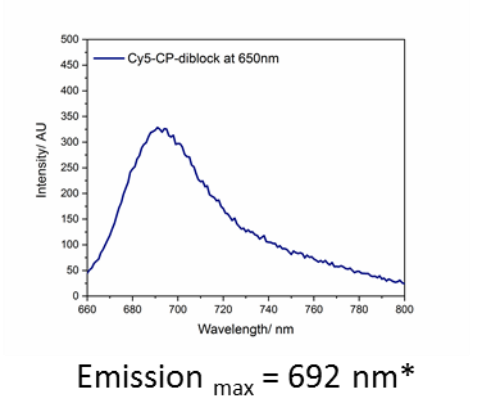

***N.B** Cy5 conjugate notably less fluorescent (Detector voltage set to high 800 V)

Figure 4.14 Fluorescence emission spectra of Cy3-CP-Diblock and Cy5-CP-Diblock conjugates in water at 35 µM.

4.6.12 FRET exchange study

Solutions of Cy3 and Cy5 conjugates were prepared in water at 35 µM. The FRET ratio over time was measured, after co-injection of the dye conjugate pair (1:1 vol ratio), by fluorescence emission microscopy. Upon excitation at the donor absorption maxima, the emission at donor and acceptor maxima of the dyes were used to calculate the FRET ratio (see main manuscript for definition). The energy transfer from the donor to the acceptor i.e. the FRET measured, can be related to the exchange of cyclic peptides between nanotubes in solution. Furthermore the change in FRET over time can be modelled to a second order decay function,[5, 24] to calculate the rate of exchange taking place. The fitting below was done using OriginPro software. Details of the fit can be found below.

A Cy3-CP-(pBA-pDMA)$_2$ and Cy5-CP-(pBA-pDMA)$_2$

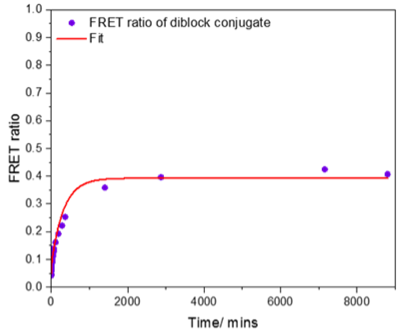

Model	ExpDec2
Equation	y = A1*exp(-x/t1) + A2*exp(-x/t2) + y0
Plot	B
y0	0.54954 ± 6.0585E-4
A1	-0.25226 ± 0.00167
t1	1.63271 ± 0.01406
A2	-0.11525 ± 9.98507E-4
t2	18.85467 ± 0.41719
Reduced Chi-Sqr	1.0082E-4
R-Square(COD)	0.98248
Adj. R-Square	0.98247

B Cy3-CP-(pDMA)$_2$ and Cy5-CP-(pDMA)$_2$

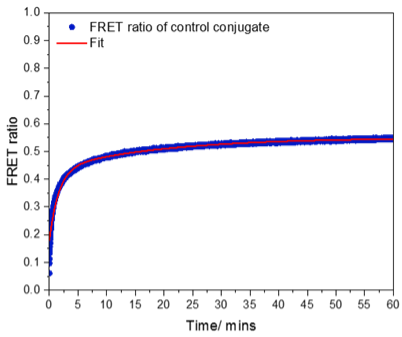

Model	ExpDec2
Equation	y = A1*exp(-x/t1) + A2*exp(-x/t2) + y0
Plot	B
y0	0.39297 ± 0.00118
A1	-0.02821 ± 2.11023E-4
t1	5.76864 ± 0.08967
A2	-0.30887 ± 0.00117
t2	321.12536 ± 2.00909
Reduced Chi-Sqr	5.46154E-6
R-Square(COD)	0.98931
Adj. R-Square	0.9893

Figure 4.15 FRET exchange study of cyclic peptide dye conjugates with two polymer arms of a) diblock copolymer pBA$_{10}$-*b*-pDMA$_{40}$ or b) homopolymer pDMA$_{50}$.

4.6.13 Particle tracking and Stochastic Optical Reconstruction Microscopy (STORM)

Particle tracking and Stochastic Optical Reconstruction Microscopy (STORM) experiments were performed with the sample at 1 mg/ml peptide concentration dissolved in de-ionised water (>18MΩ) and then filtered using a 0.45 μm cellulose acetate syringe filter (SupaTop). Images of the peptide aggregates were captured on our specially constructed STORM microscope and full details of the microscope is detailed in our previous work.[18] For both experiments circular imaging spacers (Thermo Scientific) were fixed to cleaned glass microscope slides to create wells for the sample. Then, for the particle tracking experiments, 7.5 μL of the peptide solution was deposited in the well formed by the spacer and the slide and a circular glass coverslip was used to seal the sample into the well. The sample was illuminated and the diffusion of aggregates through the solvent was videoed at 100 fps for 30 secs. Care was taken to ensure only aggregates at least 10 μm from the surface were recorded to eliminate the risk of hydrodynamic drag from the surfaces. Background subtraction was performed in ImageJ on the raw videos using the "rolling-ball" algorithm.[25] The position of particles in the processed videos were then tracked using our previously developed particle tracking software.[26]

For the STORM experiments, 3 μL of sample was placed directly onto a cleaned glass coverslip to allow adsorption of the aggregates to the glass. Then, 4 μL of OxEA STORM imaging buffer[27] was placed into the well on the microscope slide. The coverslip was then fixed over the well such that the imaging buffer and sample came into contact with each other and the total volume of liquid in the well was 7 μL. For the STORM images, at least 5,000 images of each aggregate were recorded at high laser intensity. To capture two colour images, two raw data sets were captured sequentially for each STORM image, one for the Cy5 dye (647 nm laser) and then another for the Cy3 dye (568 nm laser). Localisation of fluorophores in the raw data was then performed with the ImageJ plugin ThunderSTORM.[28] The two resulting single colour images (one for Cy5 dye and one for Cy3 dye) were then combined into a two colour image. We calculated and corrected for any drift of the sample between recording the two single colour images by calculating the 2D cross-correlation of the Cy3 and Cy5 images. The peak of the 2D cross-correlation gave us an estimation of the drift and this was typically between 0 and 50 nm, we could then translate either

the Cy3 or Cy5 image and recombine them to form the final two colour image with correct alignment between the colour channels.

To find the hydrodynamic radius of aggregates in the particle tracking experiments we calculated the ensemble averaged mean square displacement (MSD) of all the tracks output from our particle tracking software. In a purely viscous fluid, like the water used here, the MSD is linearly dependent upon time or lag time, τ, and

$$\langle r \rangle = 2nD\tau^{\alpha}, \quad (2)$$

where n is the number of dimensions, D is the diffusion co-efficient and α is the power law exponent (α=1 for purely viscous fluids).[29] To verify our data, we performed a power law fit to Equation 1 and the results are shown in Figure S8. In all cases the MSD was found to be linearly dependent on lag time with power law exponents of 1.0-1.1 in all cases, as expected. Using the gradient of each fit, the hydrodynamic radius, r_h, was found using the relation between it and the diffusion co-efficient,

$$D = \frac{kT}{6\pi\eta r_h}, \quad (3)$$

where η is the viscosity of water and kT is the thermal energy.[29] Particle tracking experiments were performed individually on the Cy3 and Cy5 labelled peptides as well as mixtures of the Cy3 and Cy5 peptides when mixed before assembly (Premixed) or when assembled and then mixed in solution (after co-injection). All the results were similar with a hydrodynamic radius of approximately 50 nm, except for the aggregates formed by just Cy5 labelled peptides which were slightly smaller at 33 ± 1 nm, as shown in

Table 4.4 Tabular results of the particle tracking experiments. The fit was performed on the ensemble averaged MSD which was calculated from the average of many MSDs calculated from each individual track and the number in each sample is greater than 1,000 as shown. The power law fit exponent is shown and is close to 1 as expected. A control experiment was also performed using fluorescent beads with a radius of 50 nm. Our results agreed with the manufactures specification of the size.

Sample	Number of tracks	Power law fit exponent	Hydrodynamic radius (nm)
Cy3-CP-Diblock	1704	1.04	52 ± 2
Cy5-CP-Diblock	1100	1.06	33 ± 1
1 day after co-injection	1996	1.03	50 ± 2
30 day after co-injection	2434	1.06	46 ± 2
Premixed	3480	1.06	49 ± 2
50 nm beads	18130	1.05	49 ± 2

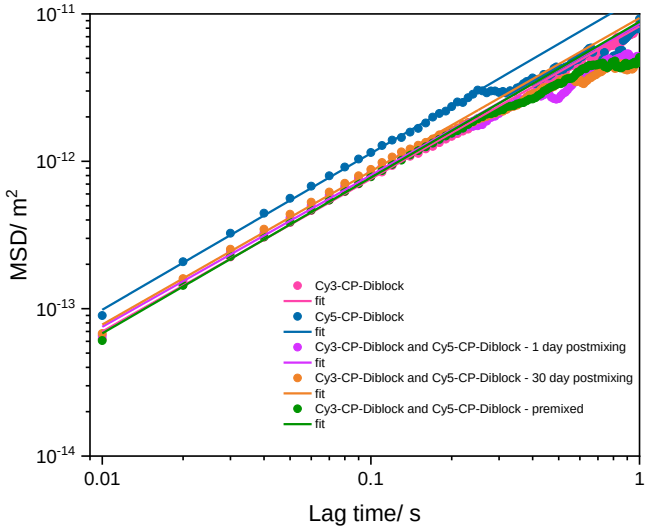

Figure 4.16 The MSD as a function of lag time for the experimental data (filled circles) and the fit to each data set (solid line). The Cy3-CP-Diblock, co-injected Cy3-CP-Diblock and Cy5-CP-Diblock conjugate and premixed samples all have similar hydrodynamic radii of about 50 nm and the Cy5 aggregates are slightly smaller with a hydrodynamic radius of 33 ± 1 nm. All MSDs were linearly dependent on lag time showing that the particles exhibited the expected Brownian motion and that the data was of high quality. Each MSD shown is the ensemble average from at least 1,000 individual particle MSDs.

4.6.14 Stochastic Optical Reconstruction Microscopy (STORM) Imaging

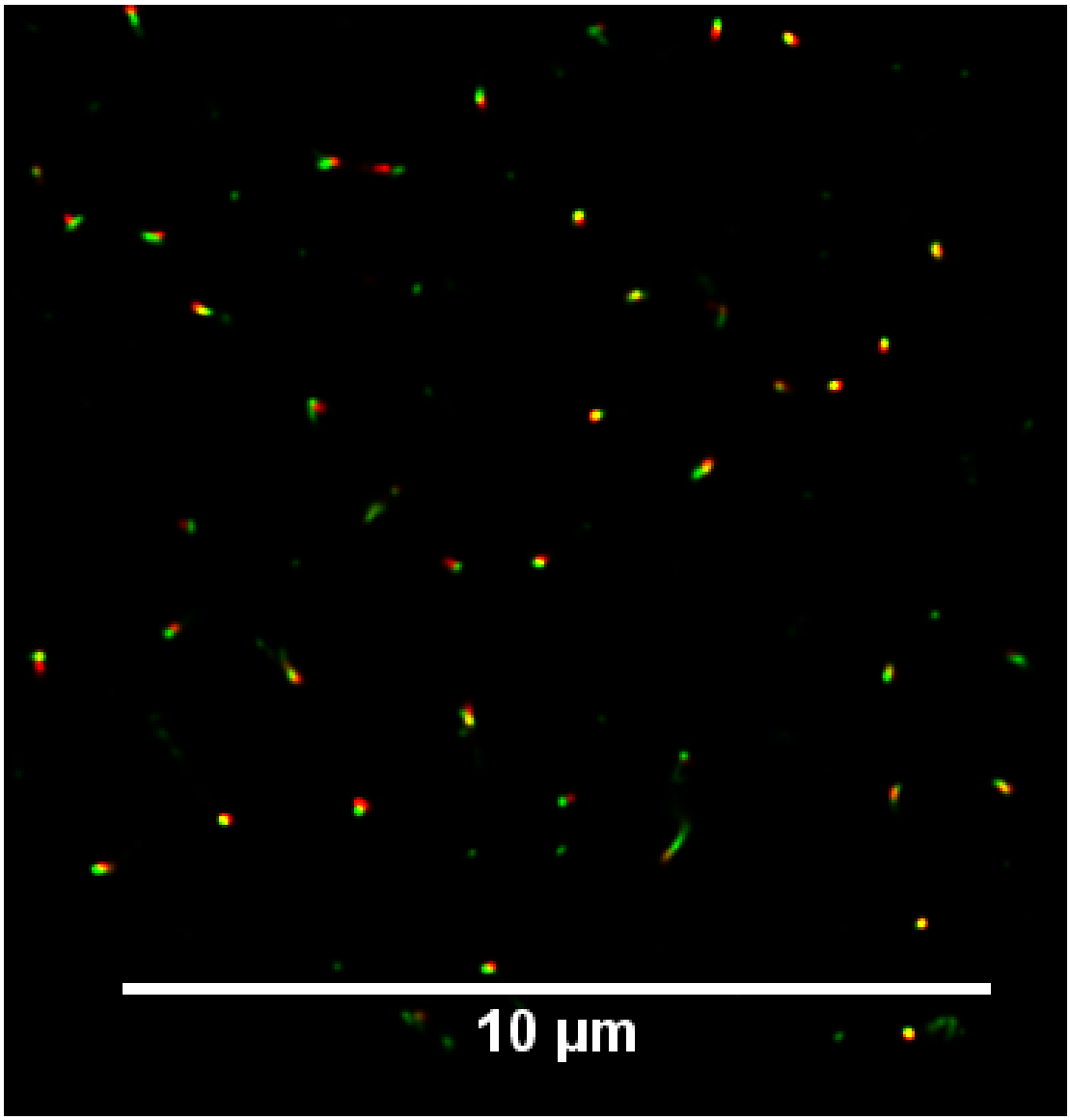

Figure 4.17 A STORM image of the premixed sample, the scale bar is 10 µm (left). This image further shows that almost all aggregates feature some degree of co-localisation and are therefore formed of a mixture of Cy3 and Cy5 labelled peptides.

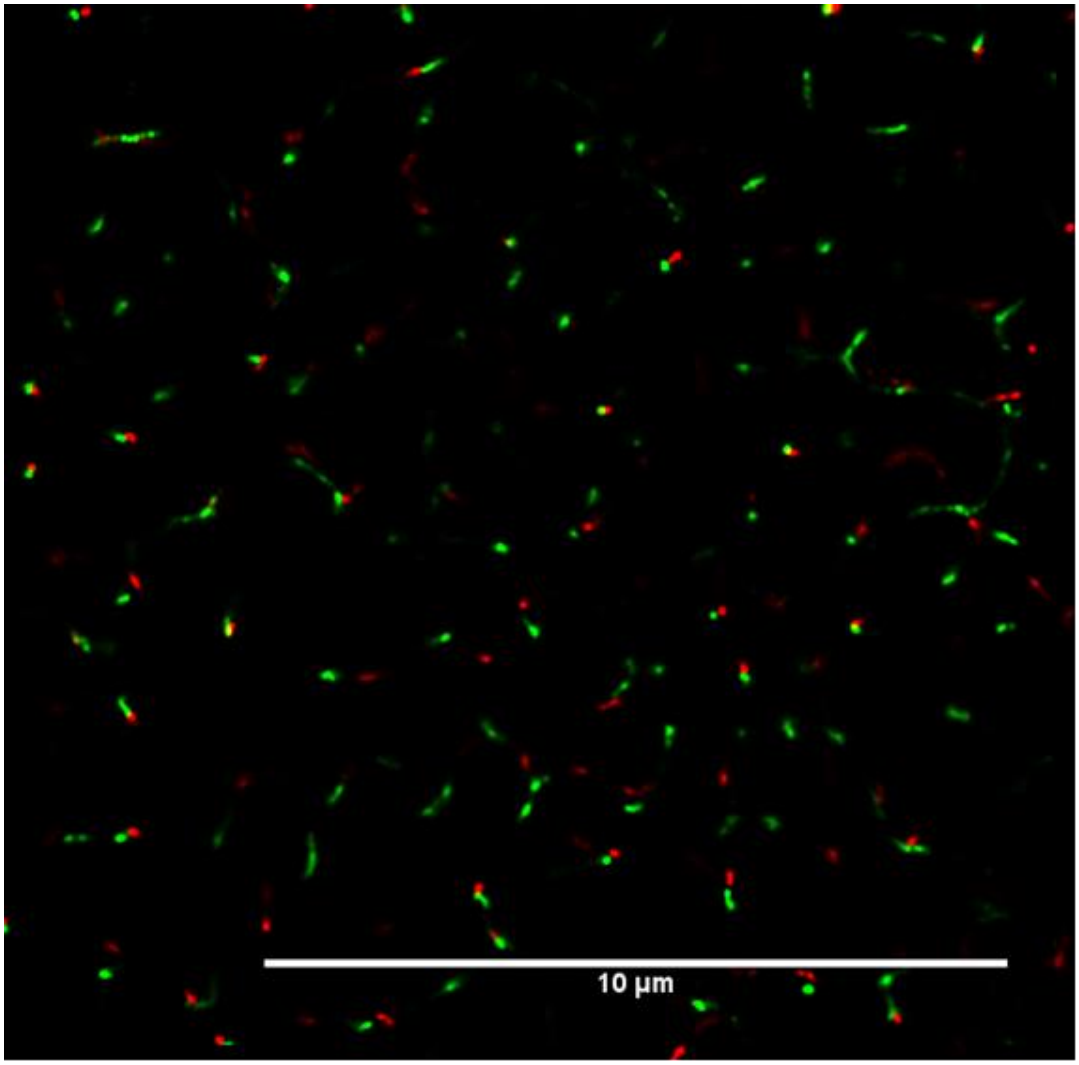

Figure 4.18 A STORM image of the sample 1 day after co-injection of Cy3 and Cy5 diblock conjugate, the scale bar is 5 µm long. After one day many of the aggregates are co-localised in the co-injected sample, however not to the same degree as in Figure 4.17. However, you can see how some of the aggregates have attached to each other at the ends, or potentially formed new multi-coloured aggregates since mixing.

4.7 Appendix

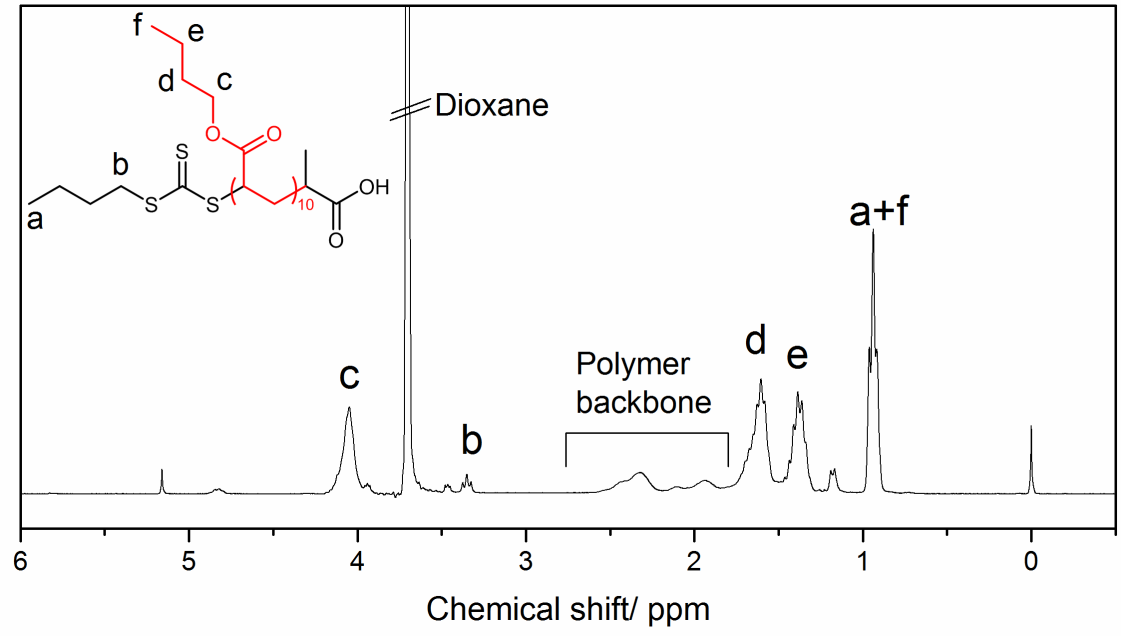

Figure 4.19 ^{1}H NMR of pBA (**19**) polymer

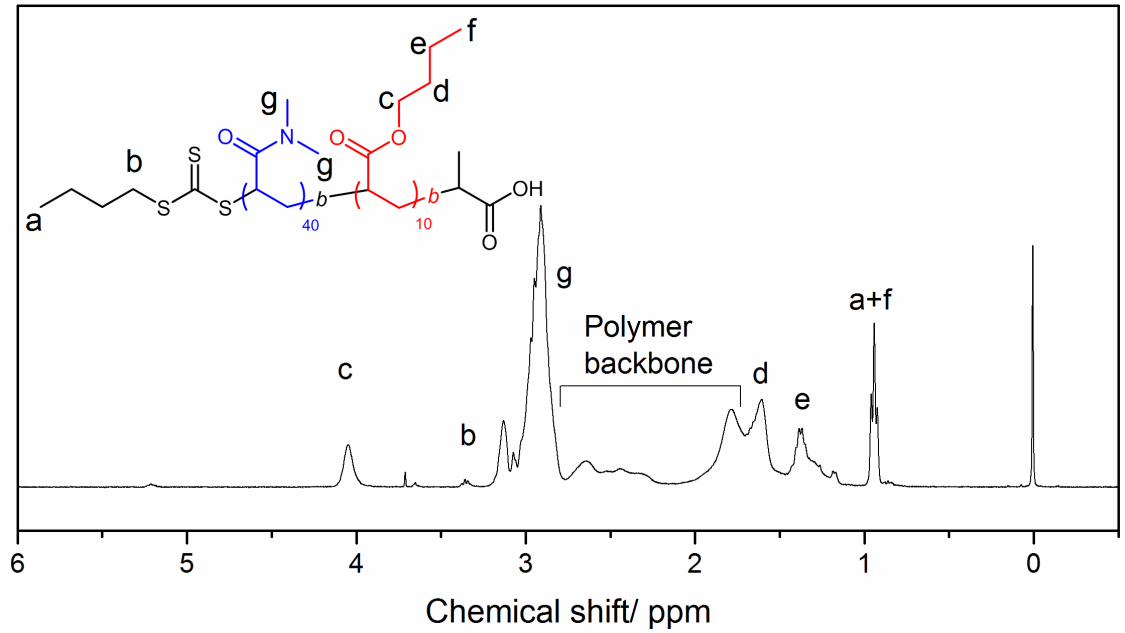

Figure 4.20 ^{1}H NMR of pBA-pDMA (**20**) polymer

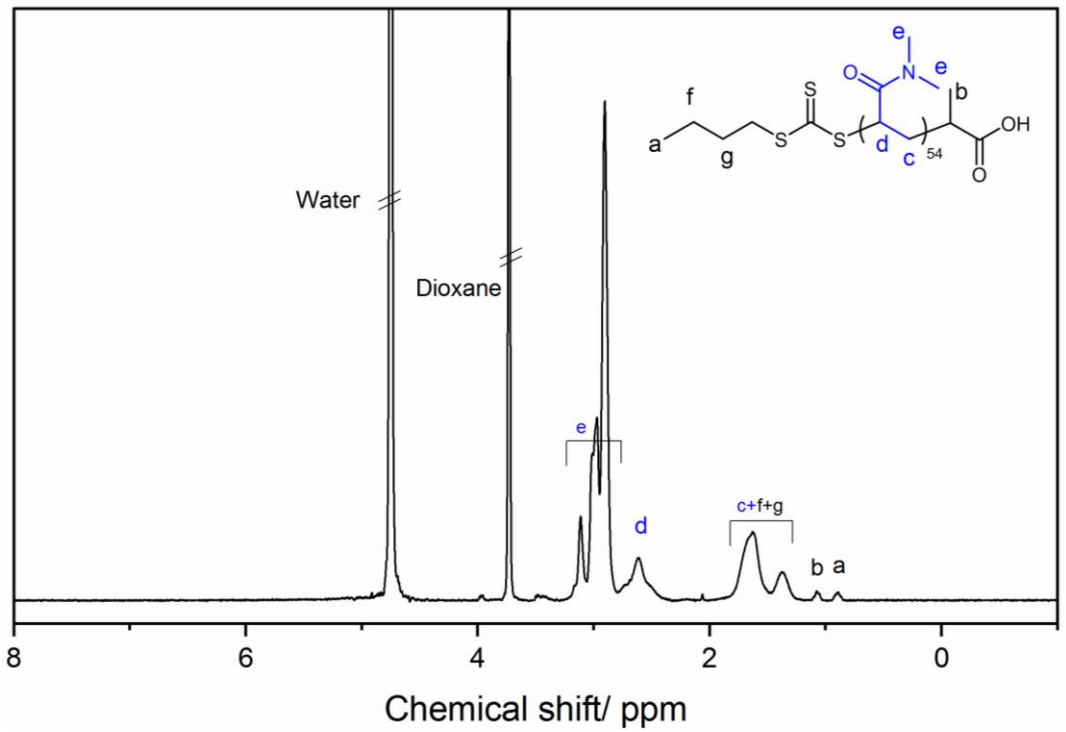

Figure 4.21 ^{1}H NMR of pDMA (**21**)

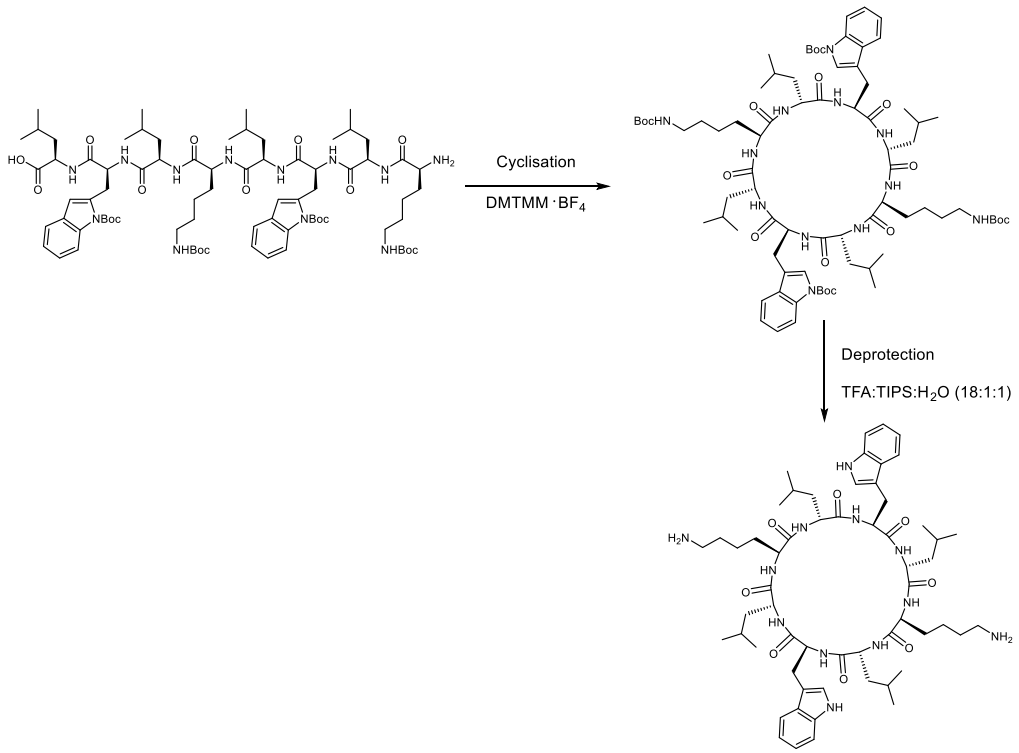

Scheme 4.10 Preparation of the linear and cyclic peptide. See literature procedure for details.[21]

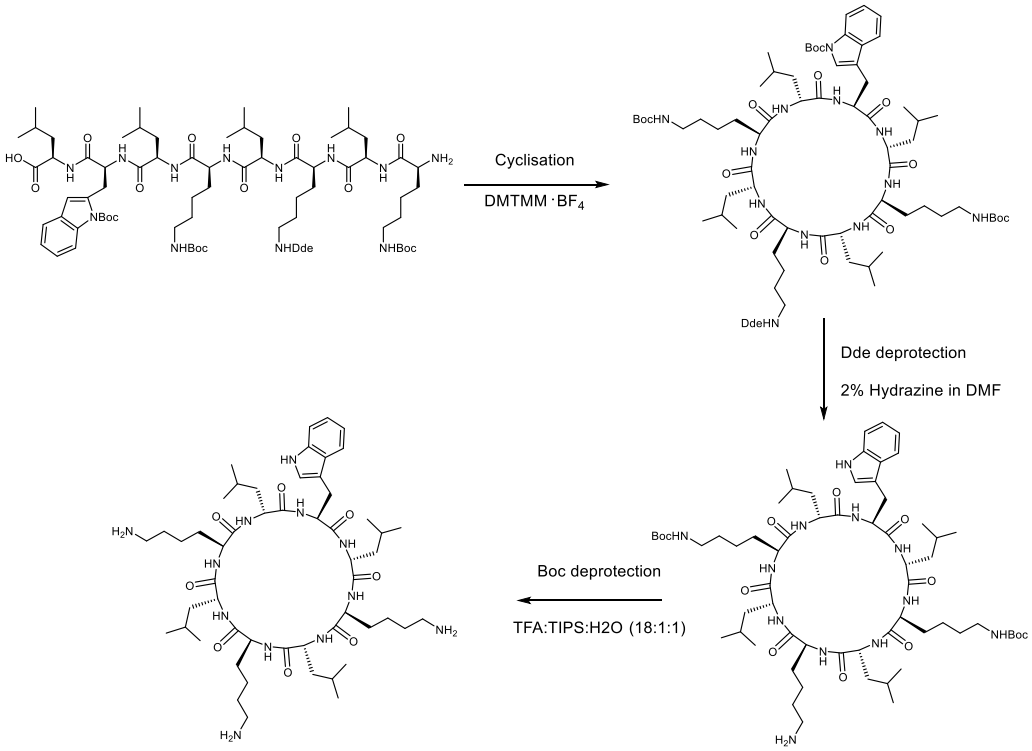

Scheme 4.11 Preparation of the linear and cyclic peptide with orthogonal amine protection chemistry. See literature procedure for details.[3]

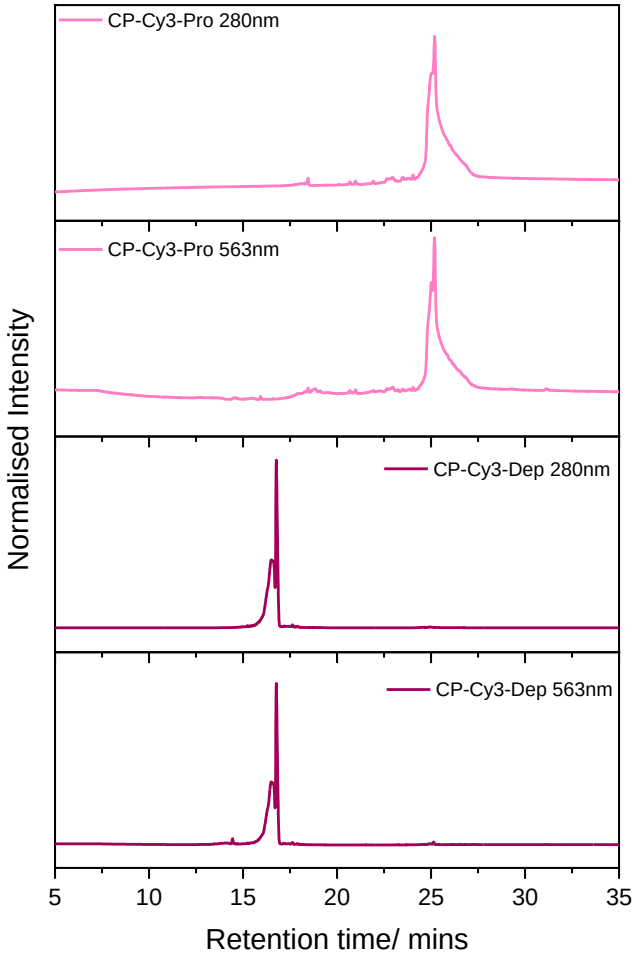

Figure 4.22 High Performance Liquid Chromatography (HPLC) spectra of the CP-Cy3-Protected (24) and CP-Cy3-Deprotected (26). Detector set to 280 nm (tryptophan of cyclic peptide) and 563 nm (Cyanine 3 emission).

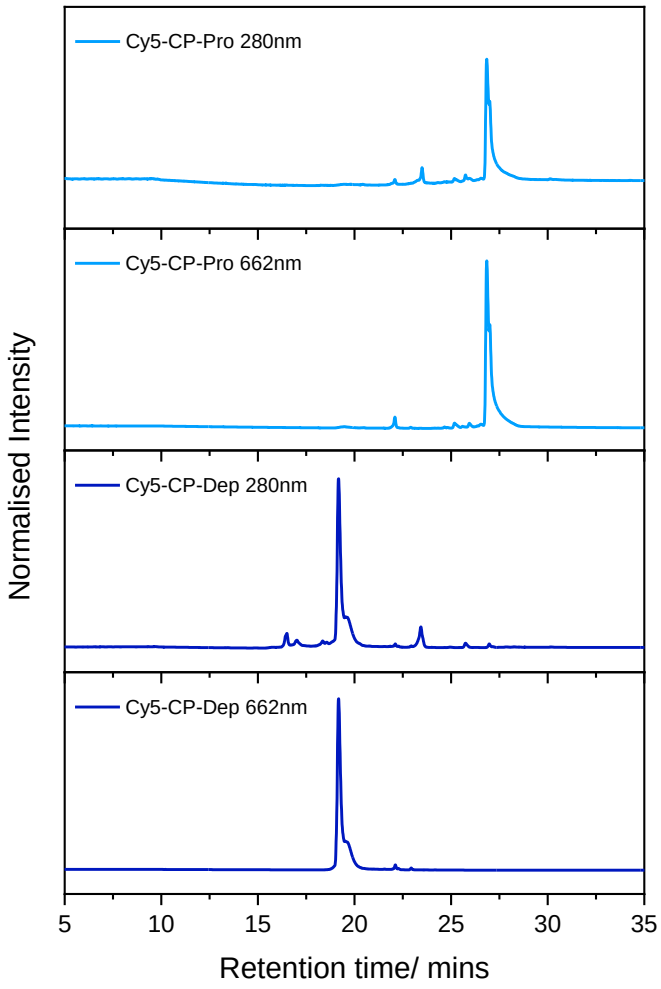

Figure 4.23 High Performance Liquid Chromatography (HPLC) spectra of the Cy5-CP-Boc Protected (25) and CP-Cy5-Boc Deprotected (27). Detector set to 280 nm (tryptophan of cyclic peptide) and 662 nm (Cyanine 5 emission).

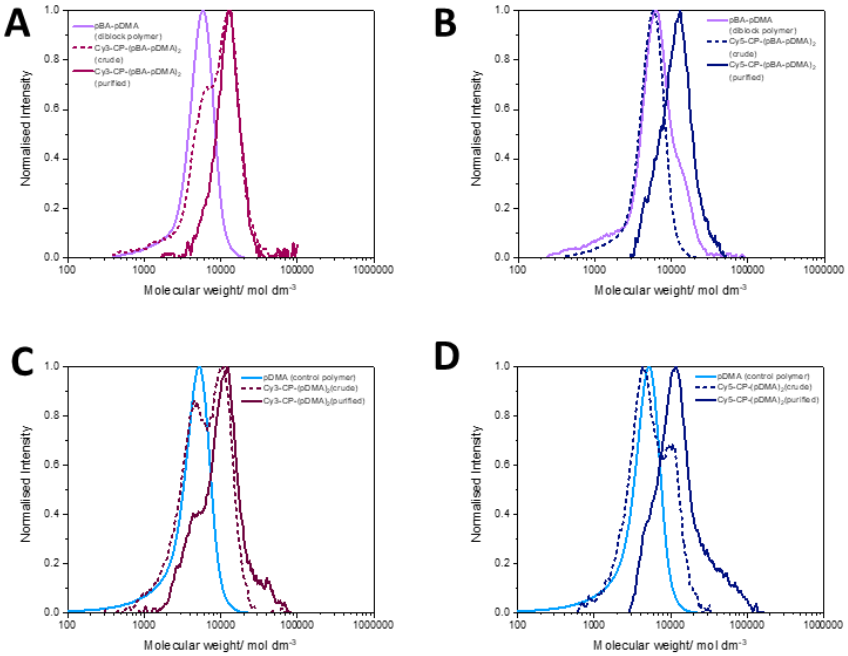

N.B. Due to the amounts and low yields obtained for these compounds, very dilute samples were measured and therefore a high signal to noise was observed.

Figure 4.24 Size exclusion chromatography of the free polymer and the cyclic peptide-polymer dye conjugates in DMF + 0.1% LiBr. a) Cy3-CP-(pBA-pDMA)$_2$ (**28**), b) Cy5-CP-(pBA-pDMA)$_2$ (**29**), c) Cy3-CP-(pDMA)$_2$ (**30**) and d) Cy5-CP-(pDMA)$_2$ (**31**).

4.9 References

1. S. Onogi, H. Shigemitsu, T. Yoshii, T. Tanida, M. Ikeda, R. Kubota and I. Hamachi, *Nat Chem*, 2016, **8**, 743-752.
2. S. Yagai, Y. Monma, N. Kawauchi, T. Karatsu and A. Kitamura, *Org. Lett.*, 2007, **9**, 1137-1140.
3. H. Shaikh, J. Y. Rho, L. J. Macdougall, P. Gurnani, A. M. Lunn, J. Yang, S. Huband, E. D. H. Mansfield, R. Peltier and S. Perrier, *Chem. - Eur. J.*, 2018, **24**, 19066-19074.
4. M. R. Ghadiri, J. R. Granja, R. A. Milligan, D. E. McRee and N. Khazanovich, *Nature*, 1993, **366**, 324-327.
5. J. Y. Rho, J. C. Brendel, L. R. MacFarlane, E. D. H. Mansfield, R. Peltier, S. Rogers, M. Hartlieb and S. Perrier, *Adv. Funct. Mater.*, 2018, **28**, 1704569.
6. S. C. Larnaudie, J. C. Brendel, K. A. Jolliffe and S. Perrier, *ACS Macro Letters*, 2017, DOI: 10.1021/acsmacrolett.7b00728, 1347-1351.
7. S. C. Larnaudie, J. Sanchis, T.-H. Nguyen, R. Peltier, S. Catrouillet, J. C. Brendel, C. J. H. Porter, K. A. Jolliffe and S. Perrier, *Biomaterials*, 2018, **178**, 570-582.
8. E. D. H. Mansfield, M. Hartlieb, S. Catrouillet, J. Y. Rho, S. C. Larnaudie, S. E. Rogers, J. Sanchis, J. C. Brendel and S. Perrier, *Soft Matter*, 2018, **14**, 6320-6326.
9. S. Catrouillet, J. C. Brendel, S. Larnaudie, T. Barlow, K. A. Jolliffe and S. Perrier, *ACS Macro Lett.*, 2016, **5**, 1119-1123.
10. J. Chiefari, Y. K. Chong, F. Ercole, J. Krstina, J. Jeffery, T. P. T. Le, R. T. A. Mayadunne, G. F. Meijs, C. L. Moad, G. Moad, E. Rizzardo and S. H. Thang, *Macromolecules*, 1998, **31**, 5559-5562.
11. D. J. Keddie, *Chem. Soc. Rev.*, 2014, **43**, 496-505.
12. J. D. Hartgerink, J. R. Granja, R. A. Milligan and M. R. Ghadiri, *J. Am. Chem. Soc.*, 1996, **118**, 43-50.
13. F. Thomas, W. M. Dawson, E. J. M. Lang, A. J. Burton, G. J. Bartlett, G. G. Rhys, A. J. Mulholland and D. N. Woolfson, *ACS Synth. Biol.*, 2018, **7**, 1808-1816.
14. J. B. Gilroy, T. Gädt, G. R. Whittell, L. Chabanne, J. M. Mitchels, R. M. Richardson, M. A. Winnik and I. Manners, *Nat. Chem.*, 2010, **2**, 566.
15. T. Förster, *Ann. Phys.*, 1948, **437**, 55-75.

16. R. Chapman, M. Danial, M. L. Koh, K. A. Jolliffe and S. Perrier, *Chem. Soc. Rev.*, 2012, **41**, 6023-6041.
17. S. S. Vogel, C. Thaler and S. V. Koushik, *Science's STKE*, 2006, **331**.
18. H. Cox, P. Georgiades, H. Xu, T. A. Waigh and J. R. Lu, *Biomacromolecules*, 2017, **18**, 3481-3491.
19. M. van Heel and M. Schatz, *J Struct Biol*, 2005, **151**, 250-262.
20. B. Adelizzi, A. Aloi, A. J. Markvoort, H. M. M. Ten Eikelder, I. K. Voets, A. R. A. Palmans and E. W. Meijer, *J. Am. Chem. Soc.*, 2018, **140**, 7168-7175.
21. S. C. Larnaudie, J. C. Brendel, K. A. Jolliffe and S. Perrier, *J. Polym. Sci., Part A: Polym. Chem.*, 2016, **54**, 1003-1011.
22. F. S. VARLEY, *Neutron News*, 1992, **3**.
23. NIST, https://www.ncnr.nist.gov/resources/n-lengths/).
24. S. I. S. Hendrikse, S. P. W. Wijnands, R. P. M. Lafleur, M. J. Pouderoijen, H. M. Janssen, P. Y. W. Dankers and E. W. Meijer, *Chem. Commun.*, 2017, **53**, 2279-2282.
25. Sternberg, *Computer*, 1983, **16**, 22-34.
26. S. R. Salman, A. W. Thomas, Z. Xiubo and R. L. Jian, *Phys. Biol.*, 2007, **4**, 220.
27. L. Nahidiazar, A. V. Agronskaia, J. Broertjes, B. van den Broek and K. Jalink, *PLOS ONE*, 2016, **11**, e0158884.
28. M. Ovesný, P. Křížek, J. Borkovec, Z. Švindrych and G. M. Hagen, *Adv. Bioinf.*, 2014, **30**, 2389-2390.
29. L. J Bonales, A. Maestro, R. Rubio and F. Ortega, *Microrheology of Complex Fluids*, 2011.

Chapter 5 Conclusion and Outlook

Since the conception of self-assembling cyclic peptide nanotubes, many have envisioned their promising use in bio-therapeutics. The advent of water-soluble cyclic peptide systems, made possible by the attachment of hydrophilic polymers, has enabled our group to work on realising their potential as drug delivery vectors. However, to explain the biological results and improve the design of these systems in the future, a better understanding of the self-assembly was needed. The foremost question was whether the cyclic peptide nanotubes were dynamic or non-dynamic assemblies.

In chapter 2, self-assembling cyclic peptides with FRET dyes were developed to study their dynamic behaviour. Using FRET dyes on the periphery, which are proximity-dependent, the mixing of dye conjugates could be used to directly inform us of the exchanging CPs between the supramolecular assemblies. As both the dye and polymer are essential to the monitoring and composition, a 'bottom up' approach was used to synthesise an asymmetric self-assembling peptide, with two different conjugation sites. The orthogonality of the azide and amine on the cyclic peptide enabled us to selectively attach both a dye and polymer to the periphery.

In the next chapter, the FRET pair conjugated on the cyclic peptide was used to directly monitor the dynamic behaviour of these supramolecular polymers in a range of different environments. The change in fluorescence emission was used to not only prove that the self-assemblies were rapidly disassembling and reassembling but also infer their rate of exchange and extent of mixing. Previously the hydrogen bond competitivity of the solvent was shown to directly affect the number of aggregation, here we showed this was also extremely important in governing the rate of exchange between nanotubes. Although in all cases near quantitative mixing is observed in comparison to premixed samples; the kinetics are much faster in aqueous solutions as compared to toluene - with the nanotubes almost fully mixed after 3 hours in water.

Further studies showed that upon dilution the fluorescence associated with the FRET decreased which is related to steady decrease in the size of aggregates, a trend confirmed *via* static light scattering. In complex environments such as living cells, the

combination of FRET and confocal microscopy showed that the different nanotubes were independently transported into the same cell compartments. This ability to recombine even under such conditions as present in living cells makes these materials attractive as a basis system for tracking of transport pathways, especially as further ligands can easily be attached to the polymer chain. These results gave us the first insights into the dynamic nature of these promising supramolecular systems.

For the final chapter, we reported a new generation of supramolecular cylindrical nanostructures which are stable, bio-compatible and easily functionalised. Unlike previous hydrophilic cyclic peptide conjugates which show fast dynamics and a low aspect ratio, by introducing a secondary hydrophobic driving force to stabilise the peptide assembly, we observed the formation of a stable supramolecular polymers with lengths above 100 nm. Furthermore, controlling the dynamic behaviour using additional hydrophobic interactions enables the formation of supramolecular block co-polymer structures. With these experiments we prove that these highly functional supramolecular polymer brushes are able to form defined nanostructures, importantly for biological applications, in aqueous conditions.

Building upon these systems, there are a number of avenues of interest to further this work in the future. First, would be to use the stabilising block in the design of future drug delivery vectors to prevent unwanted disassembly. Furthermore, installing a responsive polymer which could switch between hydrophobic and hydrophilic would enable us to control the stability of the supramolecular assembly.

The second would be to realise controlled nanotubular length for these self-assembling nanotubes. The hydrophobic inter-shell, inspired by the semi-crystalline core-forming blocks from CDSA, could be used to grow uniform nanotubes if the assemblies are kinetically trapped. Few attempts have been made but a systematic study of growth would be the next step to control the supramolecular assembly process.

To conclude, hopefully this thesis highlights the importance of understanding the supramolecular behaviour and how, using this information, we can better design future synthetic supramolecular polymers. The hope is that one day will be able to synthesis self-assemblies as complex as proteins to address a host of biological issues. For this, vast improvements in complexity and control will need to be achieved.

List of publications

1. Rho, J.Y.; Brendel, J.C.; MacFarlane, L.R.; Mansfield, E.D.H.; Peltier, R.; Rogers, S.; Hartlieb, M.; Perrier, S. Probing the Dynamic Nature of Self-Assembling Cyclic Peptide–Polymer Nanotubes in Solution and in Mammalian Cells, Adv. Funct. Mater. 2017, 1704569
2. Shaikh, H; Rho, J.Y.; MacDougall, L.J.; Gurnani P; Lunn, A.M.; Mansfield, E.D.H.; Hartlieb, M; Perrier, S and Peltier, R. Hydrogel and Organogel Formation by Hierarchical Self-Assembly of Cyclic Peptides Nanotubes, Chem. Eur. J. 2018, 24, 19066.
3. Mansfield, E.D.H.; Hartlieb, M; Catrouillet, S; Rho, J.Y.; Larnaudie, S.C.; Rogers, S.E.; Sanchis, J; Brendel, J.C.; Perrier, S, Systematic study of the structural parameters affecting the self-assembly of cyclic peptide–poly(ethylene glycol) conjugates, Soft Matter, 2018,14, 6320-6326.
4. Song, Q; Yang, J; Rho, J.Y.; Ellacott, S.H. and Perrier, S; Supramolecular switching the self-assembly of cyclic peptide – polymer conjugate via host−guest chemistry, Chem. Commun., 2019, 55, 5291-5294
5. Rho, J.Y.; Cox, H; Mansfield, E.D.H.; Ellacott, S.H.; Peltier, R.; Brendel J.C.; Hartlieb, M.; Waigh, T. and Perrier, S, Hierarchical self-assembly of supramolecular peptide nanotubes to provide stabilisation in water, Submitted, 2019.
6. Mansfield, E.D.H.; Ellacott, S.H.; Gurnani, P; Rho, J.Y.; Rogers, S and Perrier, S, Mechanisms of self-assembly for cyclic peptide-polymer conjugates and subsequent interaction to form statistical supramolecular copolymers, Submitted, 2019.
7. Rho, J.Y.; Gurnani P; Barlow, T.R.; Hartlieb, M and Perrier, S. RAFT emulsion polymerisation of self-assembled peptide amphiphile nanofibers, Manuscript in Preparation, 2019.
8. Yang, J; Song, J-I; Song, Q; Rho, J.Y.; Mansfield, E.D.H; Sambrook M; Huang F and Perrier, S; Hierarchical Self-assembled Supramolecular Tubisomes for Photo Triggered Drug Release, To be submitted, 2019.